NASA Contractor Report 185294

A Physical Model for the Acousto-Ultrasonic Method

Michael T. Kiernan and John C. Duke, Jr.
Virginia Polytechnic Institute and State University
Blacksburg, Virginia

October 1990

Prepared for
Lewis Research Center
Under Grant NAG3-172

National Aeronautics and
Space Administration

Table of Contents

A Physical Model for the Acousto-Ultrasonic Method

Michael T. Kiernan and John C. Duke, Jr.
Virginia Polytechnic Institute and State University
Department of Engineering Mechanics
Blacksburg, Virginia 24061

Introduction

The advancement of technology demands increased implementation and further development of advanced material systems such as composite materials. However, a sound engineering approach requires utilizing models of material behavior which can be used to predict ensuing behavior and to avert disatrous failures due to various sources of damage like fatigue. Utilizing models to predict future behavior for a material usually requires ascertaining information on the state of the material.

For example, fracture mechanics utilizes known material properties and measurement of crack length and orientation to predict the behavior of a cracked isotropic material such as aluminum. This may entail using a nondestructive testing (NDT) method, for instance radiography, to determine information on the crack. For an isotropic material, such as aluminum, this offers a plausible method for safe use in critical structures.

However, composite materials fail by much more complicated processes which can not be adequately modeled by the conventional theory of fracture mechanics. Future implementation of composite materials for the advancement of technology requires the synergistic development of NDT methods and models of material failure. Furthermore, it requires the unification of NDT with models of material failure to develop the ability to predict future material life and behavior based on NDT results, which is known as nondestructive evaluation (NDE).

Researchers are currently working to develop models that predict the strength of a material and its degradation due to fatigue. The following chapter will say more concerning fatigue models. In general, fatigue models require an input parameter or parameters which describe the present state of the material.

A number of NDT methods have been developed to help determine the material state, each with various advantages and disadvantages. Reviews and comments on most NDT methods may be found in references 21 and 26. Some NDT methods are more easily related to the mechanical state of the material, while some offer the advantage of being simpler and quicker to implement for practical application.

The fundamental aspects of the AU method entail introducing a mechanical excitation at one point on a material surface and sensing the resulting disturbance at another spot on the material surface. A general diagram (fig. 1) displays the basic idea of the method and the versatility of its implementation.

Much work has been directed at determining the best methods for creating the mechanical disturbance and how best to sense it (refs. 34, 87, 152, 155. 159, 160, and 161). Also, work has been directed at how to best analyze the signal produced by the sensing instrument (refs. 7, 49 ,8, 10, 99, 147, and 63) and some work to understand the physics of the wave propagation (refs. 54 and 97). However, no theory to date fully explains the nature of wave propagation in composite plates associated with the AU method.

The original implementation of the AU method involved using a piezoelectric transducer to simulate acoustic emissions and another ultrasonic piezoelectric transducer to monitor the resulting disturbance at another location. Initial analysis of the received electrical signal involved counting voltage excursions above a threshold voltage to gain an indication of the energy in the signal. The number of counts above the threshold voltage was multiplied by pulse rate and the sample interval to yield a value termed the Stress Wave Factor (SWF). If the electronics and the orientation of transducers are the same for two different sections of material, it was postulated that the region of

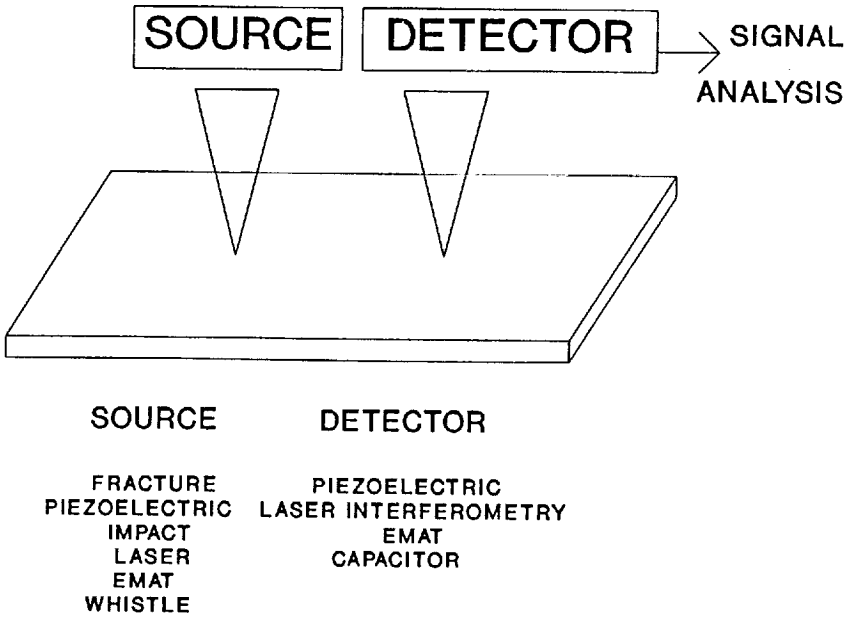

Figure 1. General diagram of AU method

material with the highest SWF value would be the strongest. The primary assumption is that a material that most efficiently transfers energy via stress wave propagation will better transfer service loading and hence be less prone to fracture. This was used by Vary and coworkers (ref. 36) to predict strength of small composite bend specimens. Also, this method was used to monitor progressive fatigue damage in composite specimens. Hence, early work on the AU method showed that the AU measurement (SWF) correlated to the material condition of the specimen and ensuing behavior, thus fulfilling one basic demand of an NDT method.

Additionally, the method shows other practical advantages. First, the direction of wave propagation is in the plane of the plate, which is often the plane of primary loading. Thus, the AU method offers the advantage of characterizing the material in the direction of loading. Secondly, the AU method offers the practical advantage that access to only one side is necessary.

A number of problems exist with application of the AU method and these are in fact defining the path of research on the AU method. First, the present experimental technique is tedious and rather difficult to reproduce. Methods of overcoming these problems involve using advances, such as laser technology, for creating disturbances and measuring disturbances. Secondly, the method has, prior to this work, had no sound theoretical basis for composite materials, so that connections could be made to other physical models of material behavior.

The purpose of this dissertation is to develop an understanding of the mechanics of the acousto-ultrasonic (AU) method and hence to pave the way for relating AU parameters to input parameters for fatigue models. In otherwords, mechanics is the common ground by which both NDT methods and fatigue models may be understood and eventually related to develop an NDE method. Using this philosophy, it is the goal of this dissertation to both forward an understanding of the mechanics of the AU method and to begin merging it with fatigue models.

The second chapter covers the unifying concepts of mechanics of composite materials, ultrasonic wave propagation theory, and experimental ultrasonics to help provide a basis for building an AU

model for use with predictive models. Lamb wave theory and through-thickness-transverse-resonance (TTTR), both used in later chapters, are covered in this chapter. Also, a more comprehensive review of AU research is covered in this chapter, with emphasis on theory and results utilized in this dissertation. This chapter also serves to motivate the direction taken in subsequent chapters.

The third chapter details the experimental set-up and procedure. This is very important in order to understand the limitations of this work and to best implement these results. Moreover, this chapter includes general statements concerned with practical application of the AU method. An understanding of the experimental set-up combined with the physical interpretation of results may also lead to improved experimental set-ups.

The fourth chapter provides results obtained using the experimental procedure described in the prior chapter, including both qualitative and quantitative descriptions of the signals used to understand the wave propagation. These results along with results from the literature search provide a basis for a physical understanding of the AU method. Additionally, results are given which are not totally understood at present, but will hopefully guide the way to further research and improved modeling.

The fifth chapter details a physical understanding of the AU method that has been obtained by comparing experimental results presented in the fourth chapter to the theory discussed in the second chapter. This involves using elasticity solutions, Lamb wave theory, and through thickness transverse resonance. Qualitative trends are noted and quantitative comparisons are made between experimental results and computer results from programming TTTR and Lamb wave equations. Specifically, results seen in the AU signal are identified as higher order Lamb waves. Discussion is also directed toward explaining the mechanism by which the transducer excites the Lamb waves seen in AU experiments.

The sixth chapter uses the physical understanding of the AU method, forwarded in the fifth chapter, to construct a model of the AU method. This model includes the use of computer codes which compute through the thickness transverse resonance frequencies and dispersion information on guided waves in composite materials. A large body of discussion is directed at how to model the mechanics between the input and the resulting Lamb waves. Additional comments are made on how the model may be improved and built upon for future use. This chapter also discusses how the AU model could be combined with fatigue models to yield NDE information.

The seventh and final chapter forwards an overview of the dissertation topic. Discussion here incorporates ideas for future research and practical considerations of applying the AU method.

In general, this dissertation develops a physical understanding of the AU method from experimental results, wave propagation theory, and understanding of composite materials. Additionally, an approach for modeling AU results is developed based on the physical understanding of the AU method. The major contribution of this work is the physical interpretation of experimental results and the application of this toward developing an NDE method.

Literature Review

The literature review starts with a basic coverage of composite materials and composite material damage models. This review is by no means comprehensive, but introduces notation and ideas for understanding following comments. Next, basic concepts of wave propagation are presented, including the behavior of plane waves in various media and the concept and analysis of a waveguide. Specifically, the use of Rayleigh/Lamb wave analysis to predict plate wave behavior and the phenomenon of through-thickness-transverse-resonance (TTTR) are the focal points of the discussion on waveguide theory. Basic wave propagation and wave guide theory can be used to develop models of the last two subjects to be covered in the literature review, these being analytical ultrasonics and the AU method. The literature review of the AU technique will show the need for AU models in composite materials and hence promote the usefulnesss of the dissertation topic.

Composite Materials

A great deal of work and research has been devoted to understanding composite material behavior. References 43-48,119,123,114,109 give a good general overview of some of the basic results of this

work. One major division in understanding the mechanics of composite materials is that of micromechanics and macromechanics. Micromechanics is concerned with understanding the behavior and interaction of the constituent materials in the composite. Obviously, this is of great importance in truly understanding the mechanics associated with composite material behavior. Generally, macromechanics models global mechanical behavior by treating each lamina as an anisotropic homogeneous material. A couple of pertinent comments will be made on both macromechanics and micromechanics. The discussion below starts by introducing the notation and coordinate system which is used throughout the paper. Next, a brief discussion is given on macromechanics and then micromechanics. Then, several points are made concerning the field of damage mechanics, which involves understanding both micromechanics and macromechanics. Lastly, a brief coverage of the critical element model is given, along with some comments on fatigue modeling of composites in general.

Basic Notation and Coordinate System

Figure 2 shows the basic coordinate system which will be used in the rest of the dissertation. Notice that b is half the plate thickness. Also, notice that the origin is located on the horizontal middle plane of the plate.

Figure 3 shows the definition of azimuthal angle which will be used throughout the remainder of the paper. Also, the relative direction of the fibers in a given lamina with respect to a chosen zero degree fiber direction will follow the same convention (i.e., positive for counter clockwise rotation). Hence, a laminate is described by writing ply fiber orientations with respect to the zero degree direction between brackets and separated by slashes, in the order they occur starting with the top ply and ending with the bottom ply. Also, a subscript s following a bracketed configuration means the laminate is composed of a top half of laminae described by what is in the brackets and a bottom half which is the mirror image. For example, [0, 90]$_s$ is pictured in figure 4.

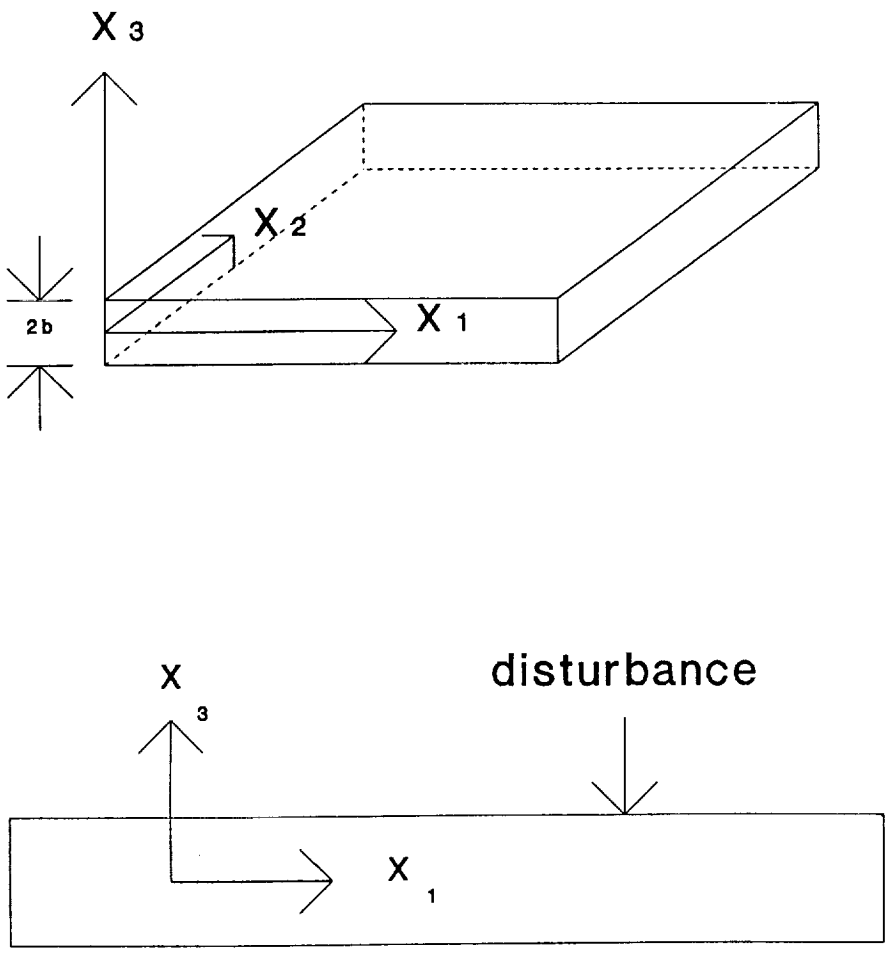

Figure 2. Definition of coordinate system

The standard notation will be used for the general 3-d linear elastic stress-strain relations. This involves using both the compliance matrix and the stiffness matrix defined below:

$$\sigma_i = C_{ij}\varepsilon_j$$

$$\varepsilon_i = S_{ij}\sigma_j$$

The reduced tensor notation utilizes the following reductions:

11---1, 22---2, 33---3, 23---4, 13---5, 12---6

where σ_{ij} and ε_{ij} are the stress and strain tensors, respectively. The rotation of stress and strain tensors to new coordinate systems is performed using concepts of tensor analysis. However, attention should be given to which definition of shear strain is used and correcting factors should be included. These concepts can be used to derive the equation for the rotation of the stiffness matrix, given in unreduced tensor notation:

$$\overline{C}_{ijkl} = a_{im}a_{jn}a_{ko}a_{lp}C_{mnop}$$

The a_{im} type terms are the direction cosines between the coordinate axes. Hence, $\overline{C}_{ijkl}$ shows how reorienting an anisotropic material, such as a fiber reinforced lamina, modifies the moduli relative to a given direction. Note that in the unreduced notation the subscripts only take values up to 3 and that certain mixed terms are half the value of the same term in the reduced notation (ref. 105). Thus, the value for the moduli of a fiber reinforced ply with fibers oriented in any direction can be easily obtained by transforming the stiffness matrix values for a coordinate system with one coordinate axis in the fiber direction and another perpendicular to the plane. The coordinate system aligned with the fiber and transverse fiber direction contains less terms in the stiffness matrix due to inherent symmetries. This transformation will prove important for the equations describing how wave propagation varies relative to fiber direction for composite materials. These transformed values for various layers can be averaged together in a laminate analysis scheme. A good coverage of the relationships between engineering properties and terms in the stiffness and compliance ma-

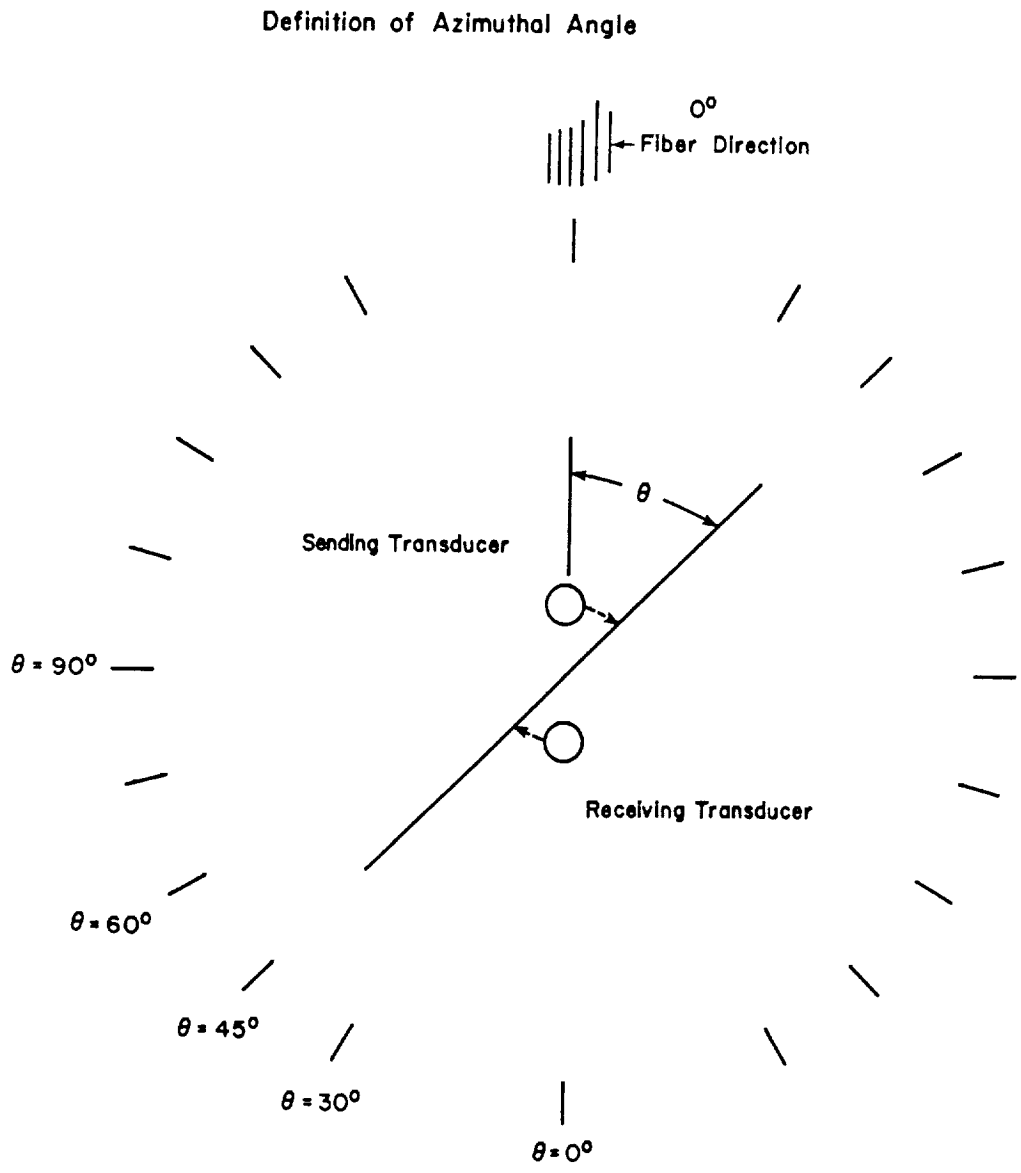

Figure 3. Definition of azimuthal angle

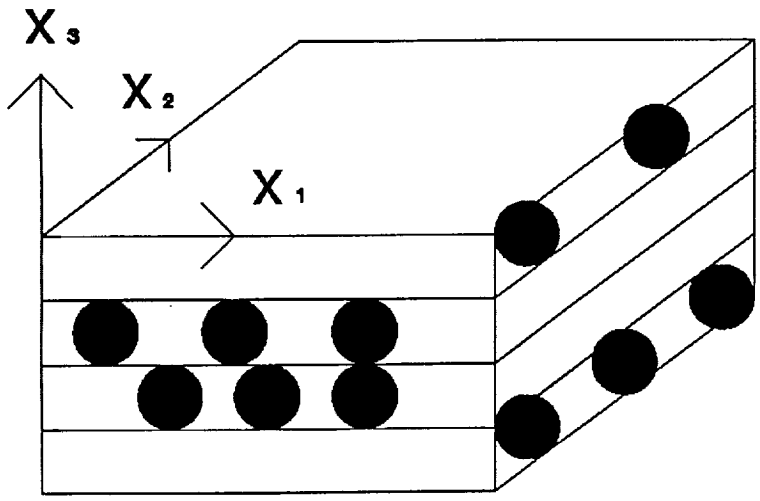

Figure 4. Laminate notation- $[0, 90]_s$

trices can be found in Jones' book (ref. 123). Also, the matrix Q_{ij} is used to represent the reduced plane stress matrix (ref.123). Finally, the following notation is utilized for engineering properties: Poisson's ratio

$$\nu_{ij} = -\varepsilon_j/\varepsilon_i$$

for

$$\sigma_i = \sigma$$

and coefficients of mutual influence

$$\eta_{i,ij} = \varepsilon_i/\gamma_{ij}$$

for

$$\tau_{ij} = \tau$$

and

$$\eta_{ij,i} = \gamma_{ij}/\varepsilon_i$$

for

$$\sigma_{ij} = \sigma$$

The other engineering constants are fairly self-explanatory and standard (see ref. 123).

A, B and D matrices are calculated by the following equations

$$A_{ij} = \sum_{k=1}^{n} (\overline{Q}_{ij})_k (z_k - z_{k-1})$$

$$B_{ij} = .5\sum_{k=1}^{n}(\overline{Q}_{ij})_k(z_k^2 - z_{k-1}^2)$$

$$D_{ij} = 1/3\sum_{k=1}^{n}(\overline{Q}_{ij})_k(z_k^3 - z_{k-1}^3)$$

where n is the number of plies and $\overline{Q}_{ij}$ are the values of the reduced stiffness matrix. These matrices can then be used to calculate displacements and curvatures due to in-plane loads and moments. This is an example of averaging layers to get laminate response. For unsymmetric laminates the B matrix is nonzero and in-plane loading can result in curvature.

Macromechanics

A good basic coverage of macromechanics can be found in references 123 and 124. Macromechanics uses ply level properties, assuming homogeneity, to determine laminate behavior. This includes analytically predicting how the laminate will deform under loading and predicting ply level failure. Laminate analysis can be used to predict deformations and ply level stresses by calculating the A, B, and D matrices. This type of analysis, encompasses assumming plane stress or that the material is sufficiently thin to ignore out of plane effects. A good coverage of laminate analysis can be found in reference 124. Failure theories can use the information on stresses and strains in various lamina to predict ply-level failures. Theories include the Maximum stress and Tensor Polynomial criteria. These theories and others can be found in Jones' book (ref. 123).

A variety of interesting phenomena occur due to the variation of material properties with azimuthal angle, caused by the fibers. First, even for a single ply this causes a coupling between shear and tension for directions other than in the fiber direction or transverse to the fiber. This type of be-

havior is quantified by the coefficient of mutual influence defined above. For instance, $\eta_{ij,i}$ indicates the amount of shear deformation which will result due to a tensile or compressive force. These type of basic mechanical properties should be kept in mind when trying to understand wave propagation phenomena in composite materials.

Differences in the mechanical behavior of various plies leads to interlaminar stresses at edge boundaries and can lead to delamination between plies. Herakovich has reported on the relations between engineering properties of neighboring plies and the propensity for delamination (ref. 119).

In general, Macromechanics considers the effects of fiber and matrix interaction to be smeared together, so that a ply may be treated as a homogeneous anisotropic material. Laminate analysis and plate theory can then be used to predict how the laminate will deform under load. This information can then be used in failure theories to predict when various plies will fail. Also, laminate analysis can be used to gain information on when a laminate may delaminate. Lastly, approximations for ply level effects of damage can be used with laminate analysis to show the effects of damage on the mechanical behavior of a composite material, as predicted by a macromechanical approach. For instance, laminates with cracked plies can be analyzed with the value of the modulus for the cracked plies lowered or reduced to zero. Determining exactly how damage, such as cracks, changes the moduli of composite materials is the domain of micromechanics.

Micromechanics

The area of micromechanics concerns trying to determine how stress and strain interaction will take place between the fiber and matrix materials. Also, micromechanics is concerned with the effects of damage on the distribution of stress and strain in specific areas such as in the fiber and matrix. This can then be used to predict failure or changes in stiffness. Furthermore, this type of approach is essential for understanding damage mechanics and the progression of damage leading to failure

in composite materials. Analysis of this type is used in failure models such as the Critical Element (ref. 43). Although present research on the AU method is not overly concerned with a micromechanics type of approach, various observed phenomena may ultimately be explained by using a micromechanics approach. This may especially be true when trying to explain the effects of damage on stiffness and damping. For instance, Nuismer's approach (ref. 111) may be used to predict stiffness reduction in a cracked ply. This effect may then be used with laminate analysis to predict reduction in stiffness. This may then be used with wave theory to predict changes in AU. Basically, micromechanical analysis involves defining a representative volume and setting up a boundary value problem based on this volume. This may include considering internal boundaries between fiber and matrix within the representative volume. Then mechanical properties of separate materials are used with governing equations to determine overall volume behavior.

Damage Mechanics

References 109, 111, and 114 survey the area of damage mechanics and document a variety of observations. In general, these observations concern damage due to fatigue, but references 70, 100, 116 and 117 concern damage incurred due to impact.

The first mode of damage encountered during unidirectional cyclic tensile loading is matrix cracking in plies with fibers oriented away from the loading direction. These cracks usually run between fibers in a direction parrallel to the fibers. Cracks usually appear first in plies with fibers oriented furtherest from the loading direction (i.e., in many cases 90 degrees). Also, the spacing of cracks can be predicted based on a shear lag model (ref. 109). The cracks reduce the stiffness of the laminate. Various models exist for predicting this reduced stiffness, some involving continuum based solutions.

Next, high stress regions associated with cracks near the ply interface cause fibers to break in neighboring plies. It has been reported that two-thirds of the total number of fiber breaks occur in the first one-third of the fatigue life (ref. 109).

Also, microcracks begin to form at primary crack tips located at ply interfaces. A large number of these cracks usually exist and they do not extend far from the primary cracks. Plunkett (ref. 125) has reported that these small microcracks cause an increase in the damping of the material. Hence, the microcracks may cause energy to be dissipated in these regions, leading to increased localization of damage in these areas. The damping effects of these microcracks may explain the fact that AU values decreased more at this stage than stiffness values. Many other factors, such as load rate (ref. 148), stress concentrators, and tension versus compression affect fatigue behavior and modes of failure. Understanding these effects is still a goal of research. Hopefully, an increased understanding of the mechanics controlling these effects can be combined with an increased understanding of the AU method. For instance, maybe damping of AU waves may be extrapolated analytically to predict what is going on mechanically at various loading rates and then related to damage modes.

Finally, areas of localized damage may grow, leading to delamination and local failure. The growth of delaminations has been treated analytically by O'Brien (ref. 114). Also, the mechanical effects of the delamination and matrix cracks may be calculated using micromechanics and put into macromechanics models to predict laminate properties for damaged materials (ref. 111). As mentioned, damage, such as matrix cracking, causes changes the example in material properties, for instance material stiffness. Hence, the material will behave differently on a global sense and also tend to distribute stress differently as a result of damage. The final effect of the damaged region may be to concentrate stress in plies with fibers in the direction of loading. This concentrated stress, whether caused by fatigue or applied stress, may, if large enough, eventually lead to laminate failure. Predicting the growth of this region and eventual composite failure is the goal of modeling efforts such as the critical element model. NDT methods attempt to assess the state of the damage process. A full NDE method for composite materials involves using damage models with the NDT methods

to predict the service life and future behavior of a composite material. This involves understanding the process by which material any regard properties change due to damage and how these changes proliferate and cause more damage. Hence, an increased understanding of damage mechanics provides information for constructing fatigue models, understanding NDT results, and hopefully for relating fatigue models to NDT methods.

Models

A number of approaches have been used to model the fatigue of composite materials. Most of these approaches are phenomenological. One early model consisted of a linear equation for residual strength as a function of fatigue cycles (ref. 44). More recent approaches are being developed which are more mechanistic and can be applied to variable blocks of loading (ref. 43 and 108).

First, Poursartip and Beaumont (ref. 108) have developed a simple model which involves integrating a differential equation for damage to give fatigue life. For example stiffness can be used as a damage parameter, since it decreases with damage. As pointed out in the reference, this parameter may be replaced by any other representative indicator of damage. In example, the AU value obtained in the direction of loading would perhaps serve as a good indicator of damage. In fact, the study comparing the SWF value to fatigue cycles showed the AU measurement to change more than stiffness (ref. 6). This may be due to the fact that the AU measurement is sensitive to both stiffness reduction and various sources of wave motion attenuation. This method only deals slightly with the mechanics of the matter, but has the advantage of simplicity. However, as with any current method some experimental data is necessary.

A more mechanistically based approach is the critical element model proposed by Reifsnider and coworkers (ref. 43). The major aspect of this method is that a critical element which controls the strength of the laminate is defined. In many applications this is the laminae with fibers in the di-

rection of load. Hence, the phenomenological characterization of the cyclic strength degradation of the critical element is essential for application of this model. This method accounts for various mechanical effects of damage which occur. This involves the redistribution of stress due to matrix cracks. Additionally, this approach accounts for the 3-dimensionality of the stress state and strength by introducing a failure theory type term ($F(n)$) for the applied stress over ultimate strength term in the residual strength equation. In any regard, this method uses information on the mechanics of the damage process to allow the prediction of fatigue for a given laminate based on knowledge of a single ply.

The purpose of pursuing these models is to help relate the mechanics of these models to the mechanics of the AU model. Presently, these models trace fatigue state by changes in stiffness, which most certainly affects AU results. Also, the directional dependence of the effect of damage shows up in the results of the AU method and is also of interest in applying the critical element. Additionally, the stress waves may interact with damage through scattering and damping mechanisms and be sensitive to more subtle mechanical effects of damage which are not evident in stiffness measurements. However, the relationship between these effects and fatigue behavior is probably beyond the present mechanical understanding of fatigue. As stated, the purpose of an NDE method is to help predict the mechanical behavior and life of an engineering component. The best way to do this is to find pertinent parameters to use in damage models. Hence, this coverage of damage models serves to show how the mechanics of the damage models and the proposed AU model are related, in hopes of finding how AU parameters may be combined with damage models to determine the engineering response and remaining life of a structure.

Wave Propagation

Wave propagation is concerned with how time and position dependent displacements change throughout a material. The conventional theory of wave propagation can be broken into the two basic categories of bounded and unbounded media. However, the theory of wave propagation in bounded media involves using much of the theory from wave propagation in unbounded media. In this section, a short review of the basics of unbounded wave propagtion is given and then a somewhat more comprehensive coverage of the Rayleigh/Lamb wave problem and TTTR is presented.

Unbounded Media

The equations for wave propagation in an unbounded continuous media are derived by applying Newton's second law to a rectangular parallelepiped (Ref. 24). This leads to the following continuum equation for motion:

$$\rho \ddot{u}_i = \sigma_{ij,j}$$

where $\sigma_{ij,j}$ is the gradient of the stress tensor, ρ is the density of the material, and $\ddot{u}$ is the particle acceleration.

Linear Elastic Homogeneous Isostropic (LEHI) Materials

For a LEHI material this equation shows two types of bulk plane waves, dilatational (P-wave) and distortional (S-waves), which can be propagated through the material. The (P-wave) has displacements in the direction of propagation and the (S-wave) has displacements perpendicular to the di-

rection of wave propagation. In general, this leads to 3 modes of wave propagation in a given direction, if the full 3-d eigenvalue problem is solved: one (P-wave) with displacements in the direction of propagation and two (S-waves) with displacements that are mutually perpendicular to the direction of wave propagation. The following phase velocities are easily derived for each of the modes of wave propagation:

$$(P-wave) \quad v_p = (E/\rho)^{.5}$$

$$(S-wave) \quad v_s = (G/\rho)^{.5}$$

where E and G are the tensile and shear modulus, respectively. These velocities are derived by assuming a harmonic plane wave is propagating through the material.

A description of the reflection and refraction of these waves at an interface is relatively straightforward and is covered in references 3 and 24. A simple case of this situation is that of a plane wave striking the surface of an infinite half space. The basic solution to these problems can be visualized by using "slowness surfaces" to view the reflection problem. This approach can be derived by using Snell's law (which says that the ratio of the sine of the angle of incidence over the velocity of the wave must be equal to the ratio of the sine of the angle of reflection over the velocity of the reflected wave) and by considering stress free boundary conditions.

The solution of the infinite half space problem shows that a reflected P-wave and a reflected S-wave are caused by an incident P-wave, where the S-wave is at a lesser angle to the vertical. An incident S-wave (where the shear motion is in the plane of motion) causes a reflected P-wave and S-wave, if the angle of incidence is less than the critical angle. The critical angle may be calculated by Snell's law. When the angle of incidence is greater than the critical angle, a Rayleigh surface wave and an S-wave are created. A Rayleigh wave travels parallel to a surface, causing an oval motion of particles. The disturbance decays in amplitude with distance from the top surface and no energy is transmitted from the surface into the half space of material below. Reference 142 considers the problem at the critical angle. Equilibrium conditions can then be used to determine relative values

of reflected waves. Figure 5 shows the dependence of reflected wave amplitude over incident wave amplitude (A_0) on angle of incidence, for the reflected shear wave (A_2) and the reflected P-wave (A_1). This type of behavior is related to mode coupling, which will be discussed later in regard to its effect on AU results.

Dispersion

For various reasons, the wave number k may depend on the frequency ω in a nonlinear manner. Hence, the phase velocity $v = \omega/k$ depends on frequency. This leads to a number of interesting phenomena. Plots of wave number versus frequency (dispersion curves) present this information in graphical form. If a curve is nondispersive, the curve is a straight line, where the slope of the line is the phase velocity. If the curve is nonlinear (dispersive), the phase velocity is the slope of a line from the origin to the point on the curve.

First, the separate harmonic components tend to separate in the wave train. Hence, various harmonic components tend to separate out, especially in cases where the component frequencies possess different phase velocities and group velocities.

The concepts of beat frequency and group velocity also help to explain dispersive wave motion. These concepts relate to each other and help to explain phenomena seen in the AU technique.

The concept of beat frequency is often utilized in vibration and wave motion analysis to determine the effect of two frequencies separated by a small frequency difference. Basically, the two harmonic wave components with wave number k_1 and k_2 and frequency ω_1 and ω_2, respectively, may be superimposed and trignometrically manipulated to produce the following equation:

$$u = 2a\cos\left(\frac{k_2 + k_1}{2}x - \frac{\omega_2 + \omega_1}{2}t\right)\cos\left(\frac{k_2 - k_1}{2}x - \frac{\omega_2 - \omega_1}{2}t\right)$$

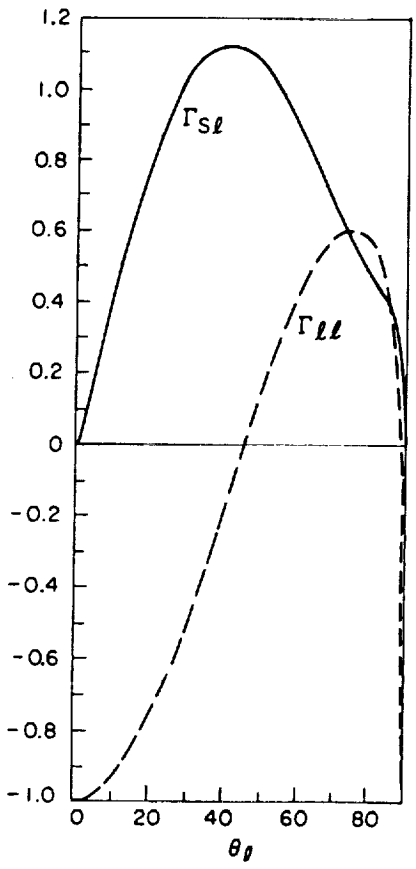

Figure 5. Reflected wave amplitudes for incident P-wave [ref. 147]

The first term represents the average of the motion characteristics of the two separate components and is close to the original motion, if the two values are comparable. The second term propagates more slowly and is a modulation or beat term.

Group velocity is used to describe the energy speed - the speed at which the modulating pulse travels. This describes the speed at which the pulse travels and can also be shown to be the speed of energy propagation. For the case of two frequencies this value is simply given by

$$v_{gr.} = (\omega_2 - \omega_1)/(k_2 - k_1)$$

However, if a number of frequencies are present the group velocity or pulse velocity is given by the equation

$$v_{gr.} = \frac{d\omega}{dk}$$

Graphically, the group velocity for a certain wave motion is the instantaneous slope of the dispersion curve.

These concepts have been united into a concept for analyzing a wave packet by utilizing a Gaussian exponential function (ref. 139). This theory gives the same values for phase and group velocities and predicts the extent of pulse spread. Adaptation of this type of theory may help to improve modelling of the AU method.

Dispersion is caused by a number of sources in materials. Authors have cited a number of these for composites:

Layering (ref. 32, 51, 69, and 106)

Different phases-fiber/matrix (ref. 51, 69, and 107)

Wave guide effects (ref. 12 and 13)

Inclusions and damage (ref. 66, 69, and 81)

Hence, a good deal of both experimental and theoretical work has been conducted to understand wave dispersion in composite materials.

Comments will be made later on how the dispersion caused by a wave guide may produce some of the above mentioned phenomena. This may help to shed light on signatures occurring with the AU technique.

Diffraction and Interference Effects

The fact that any real wave is generated from a source of finite size, that does not generate a plane wave with perfect phase, spawned the need for less idealized treatments of wave propagation. Much of the theory associated with these ideas is borrowed from optical theory, where observation of these effects are most obvious (e.g., Young's slit experiment). Basically, this theory is concerned with the manner in which waves of different phase interact with each other, in either a constructive or destructive manner. In the case of a finite source problem, this can be broken-up into two regimes- Fraunhafer and Fresnel.

Fraunhafer- region far away from the source, where plane waves considered to start at each separate point on the source have recombined to form a diffraction arc of constant phase (i.e., a plane type wave)

Fresnel- region close to the source requires a Huygens wavelet approach

Reference 139 presents a good overview of this theory as applied to slits with plane light incident. An area of interesting work may be to develop this type of work as it applies to the AU method. However, the situation is very complicated, because the effects of the reflected waves off the top

and bottom plate boundaries leads to a complicated system of different path lengths and hence phase differences.

Linear Elastic Homogeneous Anisotropic (LEHA) Materials

For anisotropic materials, the eigenvalue problem becomes somewhat more complicated and in general 3 separate modes of wave propagation exist. Also, the properties of these modes are dependent on the direction in which the waves are traveling.

Starting with the basic constitutive law for an anisotropic material and assuming infinitesimal strain, the equation of motion can be expressed as

$$C_{ijkl}u_{l,ik} = \rho\ddot{u}_j$$

where C_{ijkl} is the stiffness matrix, $u_{l,ik}$ is the gradient of the strain tensor, $\ddot{u}_j$ is the acceleration and ρ is the material density. An assumed plane wave solution can be expressed as

$$u_k = A_k e^{i(v_m x_m - \omega t)}$$

where t is time, u_k is the displacement vector, v_m is the wave vector, x_m is the position vector, and ω is the angular frequency. The phase velocity can be defined as

$$v = \omega / |v|$$

where

$$|v| = (v_1^2 + v_2^2 + v_3^2)^{.5}$$

Hence, these equations can be combined to arrive at the basic eigenvalue problem for a wave propagating in an infinite anisotropic linear material

$$A_k(\lambda_{ik} - \rho v^2 \delta_{ik}) = 0$$

where

$$\lambda_{ik} = C_{ijkl} v_j v_l$$

$$A_k = A\alpha_k$$

and

$$\alpha_k \alpha_k = 1$$

The determinant of the three by three matrix in the parentheses can be solved to obtain three values of phase velocity for an assigned direction $\xi_i / |\xi|$. For each phase velocity the displacement amplitudes can be determined to within an arbitrary constant. A program has been written to solve this equation for any direction in a composite plate and is listed in appendix G. These results help to understand the nature of wave propagation in composite materials and to derive dispersion curves for plate waves in composite materials. Also, a form of this equation is used later to determine phase velocities in the thickness direction, and in turn to predict the TTTR frequencies.

For anisotropic materials, such as composites, the variation of mechanical properties with azimuthal angle causes coupling between shear stresses and normal displacements and between normal stresses and shear displacements (ie. coefficients of mutual influence). For example, a wave launched in a general direction, with predominately normal displacement, will excite shear forces, thus force and displacement vectors are not aligned, leading to the energy flux deviation. Specifically, the energy flux deviation is the redirection of the energy in a stress wave from the direction it is launched. In the example the energy vector is obtained through the matrix multiplication of the stress matrix and velocity vector. For cases where there is coupling between shear and normal motions, the shear stress, caused by the imposed predominately normal (motion found by solving the Christoffel equation) motion, matrix multiplies the velocity vector (oriented in the direction of

propagation) and the shear stress acts to redirect the energy flux. For certain directions in anisotropic materials and for all directions in isotropic materials, there is no coupling between shear and normal motions/stresses (e.g. coefficients of mutual influence are zero). In these cases, the energy flux is in the direction of the motion, because no stresses arise that are not oriented with displacements. Hence, the unit vector normal to the plane of constant phase is not always aligned with the flow of energy. In particular, the energy flux vector can be expressed mathematically as:

$$E_i = -\sigma_{ij}\dot{u}_j = -C_{ijkl}u_{k,l}\dot{u}_j,$$

where the dot over the u_j denotes a time derivative.

The problem of a wave impinging on a stress free interface is greatly complicated by a number of effects associated with energy flux and the fact that 3 separate pseudo-waves (motions are not purely normal or shear) make up the wave motion. A number of authors have pursued this problem (refs. 22).

The first complication is that the critical angle (angle above which an incident shear wave can not excite a reflected normal wave) is dependent on the energy flux vector and not on the slowness surface (ref. 40).

The next complication is the existence of 3 non-circular slowness surfaces. This can lead to a variety of complications. For instance, for a stress free boundary this means any incident wave will cause 3 reflected waves with displacement vectors oriented with various components in and out of the plane associated with the wave vector. Additionally, as pointed out by Henneke (ref. 22), a wave impinging on the interface between two separate anisotropic materials may result in more than 3 waves being refracted, depending on the angular variation of material properties.

These types of problems create great difficulties in applying various wave tracing techniques and other similar approaches to understanding the AU method.

Other Constitutive Relations

Although the model which is forwarded in this work does not include the effects of other more complex constitutive relations, these effects are mentioned for the purposes of explaining effects seen experimentally and to promote further work.

First, any real material has mechanisms for dissipating energy or attenuating wave propagation. These include scattering, absorption, reflections, viscoelastic effects, and various other dissipative effects. As mentioned in Kolsky (ref. 24), understanding mechanisms for dissipating stress wave energy may lead to increased understanding of damage mechanisms occurring in materials. Developments in understanding this type of behavior also leads to more sophisticated ultrasonic methods. Christensen (ref. 126) gives a good treatment of stress wave propagation in a viscoelastic medium, with some notes on how this may be used to determine viscoelastic constitutive values. Kolsky (ref. 24) gives a good overview of sources of internal friction, their models and associated experimental work. Also, a number of authors have modelled scattering due to inhomogeneities that occur in composites and result due to imperfections (refs. 93, 94, 115, 81, and 66). Combining models that account for material inhomogeneities with AU models will allow for more detailed information to be obtained from the AU method.

Plastic and shock waves can occur in instances where high amplitude excitations (such as explosive type charges occur). Plastic waves occur much more often than shock waves in solid materials. However, reference 104 gives the theoretical formulation of shock wave propagation in composite materials.

Plastic waves occur when the amplitude of a stress excitation is above the proportional limit. The mathematical formulation for plastic waves can be found in reference 24. The wave speed of a plastic wave is less than that of an elastic wave, but the amplitude would be greater. Hence high impact excitations would produce a small amplitude elastic wave which would preceed a high am-

plitude plastic wave. One area of research might involve relating elastic wave propagation to plastic wave propagation, so that elastic wave propagation might be used to predict plastic wave propagation and damage.

The propagation of stress waves in inhomogeneous matter is of both practical and theoretical interest. In general, the propagation of stress waves in inhomogeneous material can lead to scatter (ref. 69), dispersion (ref. 51), and various waveguide effects such as Love and Stonely waves. Many of these phenomena depend on the relative dimensions of the inhomogeneity compared to the wavelength of the stress wave. This is an active area of both experimental and theoretical research.

Plate Wave Equations

Two basic approaches can be used to derive the equations for plate waves. The first is the more conventional Rayleigh/Lamb wave analysis. The other more recent approach is the method of partial waves or transverse resonance (ref. 127).

The Rayleigh/Lamb wave approach involves expressing the displacement vector u_i as a scalar and vector potential and then solving for the potentials in the equations of motion by the separation of variables method. Next, the potentials are combined in a proper manner to satisfy the boundary conditions (stress free) at the top and bottom surfaces of the plate.

In the partial wave method, exponential-type waves are reflected back and forth between the top and bottom surfaces of the plate. This leads to traveling waves in the direction of wave propagation and standing waves in the thickness direction of the plate. These waves are found by establishing the condition for transverse resonance through the thickness of the plate. For anisotropic materials, the method of partial waves leads to a solution much easier than the more classical approach. Also, as pointed out by Solie and Auld (ref. 127), this method highlights certain physical features of the nature of plate wave propagation.

Isotropic Plate Waves

As is the case with many areas in science, the origin of the plate problem was experimental observation. Specifically, the nodal patterns for a vibrating plate were noted in 1787. In 1815, Germain derived the equations for an isotropic plate vibrating with a bending motion. Additional contributions were made to this problem by a number of famous scholars, including: Lagrange, Legendre, Fourier, Poisson, Cauchy, and Euler (ref. 11). Lagrange's work expanded on that of Germain, leading to the Germain-Lagrange equation. This equation assumes a thin plate vibrating in a flexural motion to arrive at the equation

$$D\nabla_1^2\nabla_1^2 u_3 + 2\rho b\frac{\partial^2 u_3}{\partial t^2} = 0$$

where,

$$\nabla_1^2 \equiv \frac{\partial^2}{\partial x_1^2} + \frac{\partial^2}{\partial x_3^2}$$

and

$$D = 4\mu b^3/3(1-\nu)$$

and b, μ, ν and ρ are half the plate thickness, Lame's shear modulus, Poisson's ratio and the mass density, respectively. In 1850, Kirchoff published a paper in which he employed a variational method to derive the plate bending vibration equations, including a derivation of the proper boundary conditions and a comparison to original experimental results. It is this basic approach that Mindlin later utilized to obtain his higher order approximation method.

Although enjoying much less attention, it was at about this same time that Poisson derived the equations governing the motion for extensional waves in a thin plate. These equations are known simply as the Poisson extensional equations

$$(\bar{\lambda}+\mu)\frac{\partial}{\partial x_1}\left(\frac{\partial u_1}{\partial x_1}+\frac{\partial u_2}{\partial x_2}\right)+\mu\nabla_1^2 u_1=\rho\frac{\partial^2 u_1}{\partial t^2}$$

$$(\bar{\lambda}+\mu)\frac{\partial}{\partial x_2}\left(\frac{\partial u_1}{\partial x_1}+\frac{\partial u_2}{\partial x_2}\right)+\mu\nabla_1^2 u_2=\rho\frac{\partial^2 u_2}{\partial t^2}$$

where,

$$\bar{\lambda}=2\lambda\frac{\mu}{\lambda+\mu}$$

where λ is Lame's constant. The Germain-Lagrange equation and Poissons' extensional equations are only valid if the wavelength of the vibration is greater than the plate thickness and the waves are low frequency. Moreover, the solutions assume that there is no variation of displacement in the x_3 direction or what is the thickness coordinate.

In 1888, Rayleigh utilized the theory of linear elasticity to derive the equations for the general plate problem in an isotropic material, using the equation of motion stated above.

The equation of motion can be decoupled, revealing two independent modes of wave propagation by using the Poisson-Lame decomposition formula. Thus, a purely extensional wave (P-wave) with velocity given as

$$v_p^2=\frac{\lambda+2\mu}{\rho}$$

is found to propagate with irrotational motion. Additionally, shear waves (S-waves) are found to propagate with velocity

$$v_s^2=\frac{\mu}{\rho}$$

as equivoluminal waves. λ and μ are Lame's constants.

Hence, combining these basic equations derived from elasticity with the imposition of traction free boundaries at the top and bottom surfaces

$$\tau_{3i} = 0$$

at

$$x_3 = \pm b$$

Rayleigh set the stage for solving the problem for plates of arbitrary thickness. The solution to this problem, much of which was performed by Lamb (ref. 58), lead to a number of interesting results, including the prediction of an infinite number of higher order modes. Moreover, he showed that the fundamental mode solution converged to the elementary theory as the plate thickness was reduced to zero thickness and to Rayleigh surface waves in a half space as the wavelength converges to zero. Note, the boundary conditions are automatically satisfied in the elementary theory.

By introducing two horizontally polarized shear waves (SH-waves) along the x_1 which are reflected off the top and bottom surfaces, a plate wave is set-up to have displacement only in the x_2 direction. Specifically, this involves introducing the waves defined by

$$u_2 = E_1 \exp i(\xi x_1 + \beta x_3 - \omega t) + E_2 \exp i(\xi x_1 - \beta x_3 - \omega t)$$

where

$$\omega = v_s(\xi^2 + \beta^2)^{.5}$$

where u_1 and u_2 are equal to zero. Moreover, the angles of incidence and reflection are given by the equation

$$\theta_3 = \tan^{-1} \frac{\xi}{\beta}$$

Notice, the angle of the input wave defines the ratio of the wave numbers. Now, the basic form of the solution can be found to be a harmonic wave traveling in the x_1 direction, with x_2 displacement which varies sinusoidally through the thickness, where the frequency of the wave is given by

$$\omega^2 = v_s^2\left[\xi^2 + (\frac{n\pi}{2b})^2\right]$$

Hence, the solution is dispersive (nonlinear relationship between frequency and wave number in the propagation direction) for all orders higher than the zero mode. The wavelength of each of these solutions is given by $2\pi/\xi$ and the phase velocity by $v = \omega/\xi$. The lowest frequency is given by $\omega = v_s\pi/2b$, which is considerably lower than the corresponding lowest frequency for flexural vibrations. Basically, the input horizontally polarized shear waves (SH-waves) can be shown to dictate the plate waves. It should also be noticed that an earlier elementary solution did not exist for the SH waves.

Next, Lamb continued using Rayleigh's basic solution to derive the basic Rayleigh-Lamb waves, which are produced by the introduction of a pressure wave (P-wave) and a vertically polarized shear wave (SV-wave) to the plate. These can be expressed by the scalar potential for the pressure wave and the one vector potential for the SV-wave. Specifically, if consideration is given only to the propagation in the x_1 direction, then

$$\varphi = \varphi_0 \exp i(\xi x_1 \pm \alpha x_3 - \omega t)$$

$$\omega = v_p^2(\alpha^2 + \xi^2)$$

$$H_2 = H_0 \exp i(\xi x_1 \pm \alpha x_3 - \omega t)$$

$$\omega = v_s^2(\beta^2 + \xi^2)$$

where φ is the scalar potential for the P-wave and H_2 is the vector potential for the SV-wave. The wave normal for the P-wave can be found to make an angle $\theta_1 = \pm \tan^{-1}(\xi/\alpha)$ with the vertical axis and the SV-wave can be found to make an angle $\theta_3 = \pm \tan^{-1}(\xi/\beta)$ with the vertical axis. By

combining four of the SV-waves with four of the P-waves, each with proper amplitude and phase, the motion can be shown to be harmonic in the x_1 direction; the amplitudes vary sinusoidally through the thickness, the phase velocity is $v_p = \omega/\xi$ and the wavelength is $2\pi/\xi$. For a plate free of traction forces on the top and bottom surfaces, this can be described as motions which are symmetric and antisymmetric about the mid-plane of the plate. Hence combining the symmetry arguments with the traction free boundaries, equations for both the symmetric and antisymmetric motions can be found. This includes the displacements u_1 and u_3, the corresponding stresses which must exist, and the transcendental equations which describe the dispersion relations between the wave numbers. For the symmetric mode,

$$u_1 = i(B\xi \cos \alpha x_3 + C\beta \cos \beta x_3) \exp i(\xi x_1 - \omega t)$$

$$u_3 = (-B\alpha \sin \alpha x_3 + C\xi \sin \beta x_3) \exp i(\xi x_1 - \omega t)$$

$$F_1 = (\xi^2 - \beta^2)^2 \cos \alpha b \sin \beta b + 4\alpha\beta\xi^2 \sin \alpha b \cos \beta b = 0$$

where the stress components can easily be calculated using the constitutive relations (ref. 11). For the antisymmetric mode,

$$u_1 = i(A\xi \sin \alpha x_3 - D\beta \sin \beta x_3) \exp i(\xi x_1 - \omega t)$$

$$u_3 = (A\alpha \cos \alpha x_3 + D\xi \cos \beta x_3) \exp i(\xi x_1 - \omega t)$$

$$F_2 = (\xi^2 - \beta^2)^2 \sin \alpha b \cos \beta b + 4\alpha\beta\xi^2 \cos \alpha b \sin \beta b = 0$$

where the stress components can easily be calculated using the constitutive relations (ref. 11). The variables A, B, C and D are defined by

$$\varphi = (A \sin \alpha x_3 + B \cos \alpha x_3) \exp i(\xi x_1 - \omega t)$$

and

$$H_2 = i(C \sin \beta x_3 + D \cos \beta x_3) \exp i(\xi x_1 - \omega t)$$

Also, the slowness surface analysis produces the results

$$\alpha^2 + \xi^2 = \frac{\omega^2}{v_p^2}$$

and

$$\beta^2 + \xi^2 = \frac{\omega^2}{v_s^2}$$

So, the slowness surface analysis for both the SV-wave and P-wave can be added to the F_i equations (stress free boundary conditions) to obtain 3 equations which can be used to relate the variables α, β, ξ and ω. Thus, if one knows the mode of a Rayleigh-Lamb wave and either one of the wave numbers or the resonant frequency, then they can find the remaining variables, as well as the displacements and the stresses (up to a constant) as a function of time and space. Alternately, if any combination of two of the wave numbers and resonant frequency are known the the mode of propagation and the displacements can be determined up to a constant. For instance, the relationships between physical variables has been utilized in NDE to derive a basic equation relating the angle of incidence for the input wave in water to the ratio of the velocity of the input wave in the water to the phase velocity of the Lamb wave (ref. 21). This basic information can be presented in graphical form as a standard dispersion curve (see figure 6). A quick view of the dispersion curve provides basic information on the characteristics of the wave propagation. First, the higher the wave number the higher the angle is between the vertical (x_3) axis of the plate and the direction of the input wave vector. Hence, a general indication of the frequenies present for a general range of input angles for a given mode may be ascertained. The instantaneous slope of the curves gives the group velocity and the slope of an imagined line from the origin to the point for a particular mode of wave propagation gives the phase velocity.

It is interesting to note that the form of this solution for real values of ξ can be grouped into three sets depending on the relation between ω/ξ with the velocities of the vertically polarized shear wave (SV-wave) and P-wave. If ω/ξ is less than v_s then α and β are both imaginary. If ω/ξ is greater than

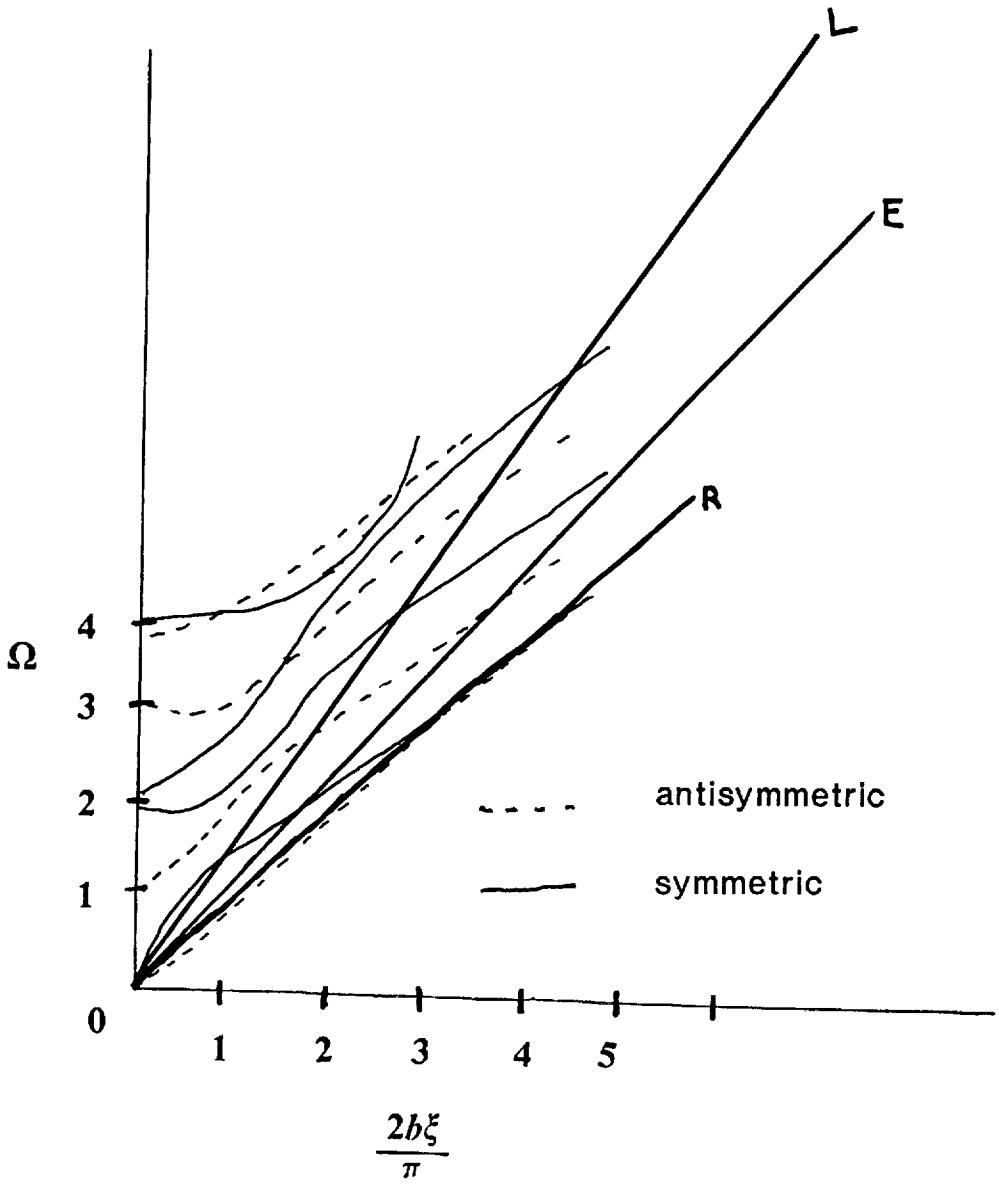

Figure 6. Dispersion curve for infinite isotropic plate [ref. 11]

v_s, but less than v_p , then α is imaginary and β is real. Finally, if ω/ξ is greater than v_p then both the wavenumbers become real. These three situations can be seen in the dispersion curve, below line OE where both α and β are imaginary, between line OE and OL where α is imaginary and β is real, and above line OL where both wave numbers are real (ref. 11). The values of the wave numbers dictate both the spatial variation of wave motion and the relative magnitude of various displacements.

If one looks at the limits of the dispersion curve a variety of interesting points can be made. In the region where $\Omega/\tilde{\xi}$ is less than 1 both α and β are imaginary, and $\tilde{\xi}$ goes to zero the solution for the antisymmetric modes converges to

$$\Omega = \tilde{\xi}^2 \pi (1/3(1 - 1/k^2))^{.5}$$

where

$$\Omega = \frac{\omega}{\omega_s}$$

$$\omega_s = \frac{\pi v_s}{2b}$$

$$k = \frac{v_p}{v_s}$$

$$\tilde{\xi} = \frac{2b\xi}{\pi}$$

and b is half the plate thickness. The symmetric mode does not have any solution for this limit in this section of the dispersion curve. This resonant mode corresponds to that of the zero order thin plate mode for flexural vibrations as predicted by elementary theory.

In region two, where α is imaginary and β is real, the symmetric mode is given as

$$\Omega = \tilde{\xi} 2(1 - 1/k^2)^{.5}$$

when $\tilde{\xi}$ becomes vanishing small. The phase speed of this mode shows up to be between that of the SV-wave and the P-wave. This is the same solution derived by the elementary theory for high wavelength extensional waves. Now, as $\tilde{\xi}$ increases the solution approaches the line OR. The symmetric branch crosses the line OE at $\beta = 0$ with the solution going to

$$\Omega = \tilde{\xi} = \frac{2b\alpha}{\pi(1 - 1/k^2)^{1/2}}$$

$$\tanh \alpha b = \frac{\alpha b}{4(1 - 1/k^2)}$$

This is related to the Goodier-Bishop wave, the waves produced at critical angles or grazing angles, namely either when the SV-wave is exactly at the angle where it can no longer produce reflected P waves or if a P-wave is incident at exactly zero degrees (ref. 142). Basically, these equations were derived by taking the reflection equations and writing the tangent term as a power series of exponential terms and dropping all higher terms.

As $\tilde{\xi}$ gets large, the fundamental symmetric and antisymmetric dispersion curves both approach the line OR. This is in the region where both α and β are imaginary. The basic dispersion relation reduces to

$$4\alpha\beta\xi^2 - (\xi^2 + \beta^2)^2 = 0$$

the phase speed of this wave is less than v_s. Since, both wavenumbers are imaginary, both displacement components vary hyperbolically across the thickness with maximum amplitude at the top and bottom surfaces. Actually, the solution reduces to that of a Rayleigh wave in a half space.

Hence, the symmetric mode goes through a transition from an extensional wave to a Goodier-Bishop wave to a Rayleigh wave. This shows that the nature of the wavenumber for the input wave governs the nature of the plate wave.

The Lame modes are found to exist if $\xi = \beta$. This causes the symmetric wave equation to become

$$\cos \beta b = 0$$

and the antisymmetric wave equation becomes

$$\sin \beta b = 0$$

This causes τ_{11} and τ_{13} to disappear at the top and bottom surfaces. This in fact corresponds to an equivoluminal wave, which is caused by the interference of pure SV-waves which are reflected and incident at $\theta_3 = 45°$.

Simple thickness modes occur when displacement components are only a function of the x_3 coordinate and time. In this special case, the three types of plane waves each can propagate between the top and bottom surface, independent of the other waves, setting up separate plate waves which can be derived from the standard plate wave equations by setting ξ equal to zero. Also, simple thickness modes are known as through the thickness transverse resonances (TTTR). These modes correspond to where the higher order modes cross the ordinate (ω-axis) on the dispersion curve (see figure 6). Since the phase velocity is defined as $v = \omega/\xi$, the phase velocity for the thickness modes is infinite.

The manner in which the phase velocities drop from infinity for the higher order modes, when ξ becomes nonzero, can be seen in figure 8. Also, note the slope of the dispersion curve for the higher order modes, near the thickness modes, are relatively low (figure 7), indicating that the group velocity or rate of energy flow is relatively low. Thus, these modes are characterized by rather high phase velocities and rather slow modulating (group) velocities. Moreover, the first order symmetric curve has a negative group velocity, indicating that energy should be flowing toward the source.

However as a general trend, these curves start with a very high phase velocity and a rather low group velocities and move to higher group velocities (ie. the curves turn upwards at larger slopes) with lower associated phase velocities. Additionally, the higher the mode the flatter the curves tend to become (in general) and hence the less the group velocity. Generally, the higher the mode, the higher the phase velocity and the slower the group velocity. Phase velocities and group velocities vary along each of these curves and vary from curve to curve; hence, a great deal of dispersion is associated with these higher order modes. It is again very important to note that for higher order modes the frequency of the resulting wave changes very little with ξ. Thus, many ray angles of input (θ_1) result in similar frequencies. Hence, a lot of energy may be created around these frequencies.

Another interesting facet of the analysis of the Rayleigh-Lamb wave problem is the consideration of imaginary and complex wavenumbers for ξ. Although, the existence of imaginary wave numbers was recognized earlier, it was not until the 1950's that they were actually included in the analysis and given physical significance. A great deal of this work was done by Mindlin, generating an interesting body of literature. The amplitude of the wave for imaginary values of ξ lead to the wave being attenuated as the wave travels in the x_1 direction. Physically, for a finite plate, the energy from this mode is channeled to edge waves on the side of the plate. Work by Mindlin shows that in some cases these edge modes can still show significant displacements up to 30 times the plate thickness from the edge (ref. 112). This type of phenomenon should be kept in mind for situations when ultrasonic work is done on finite specimens, such as small laboratory samples.

Another interesting discovery was the existence of a second edge mode which is very constrained to the edge, if the frequency of the propagating wave is greater than the first symmetric thickness shear mode. Also, Mindlin and Fox solved the problem of the real part of the solution for the antisymmetric mode of a plate bounded on a single side. However, in general a total solution has not been found for a fully bounded plate, which includes all edges and complex wave numbers.

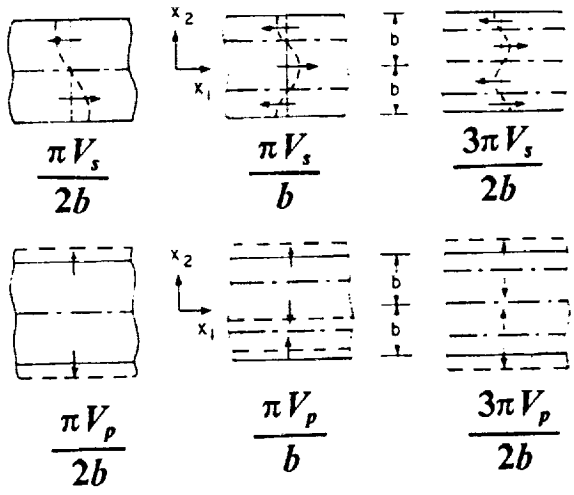

Figure 7. Simple thickness mode [ref. 11]

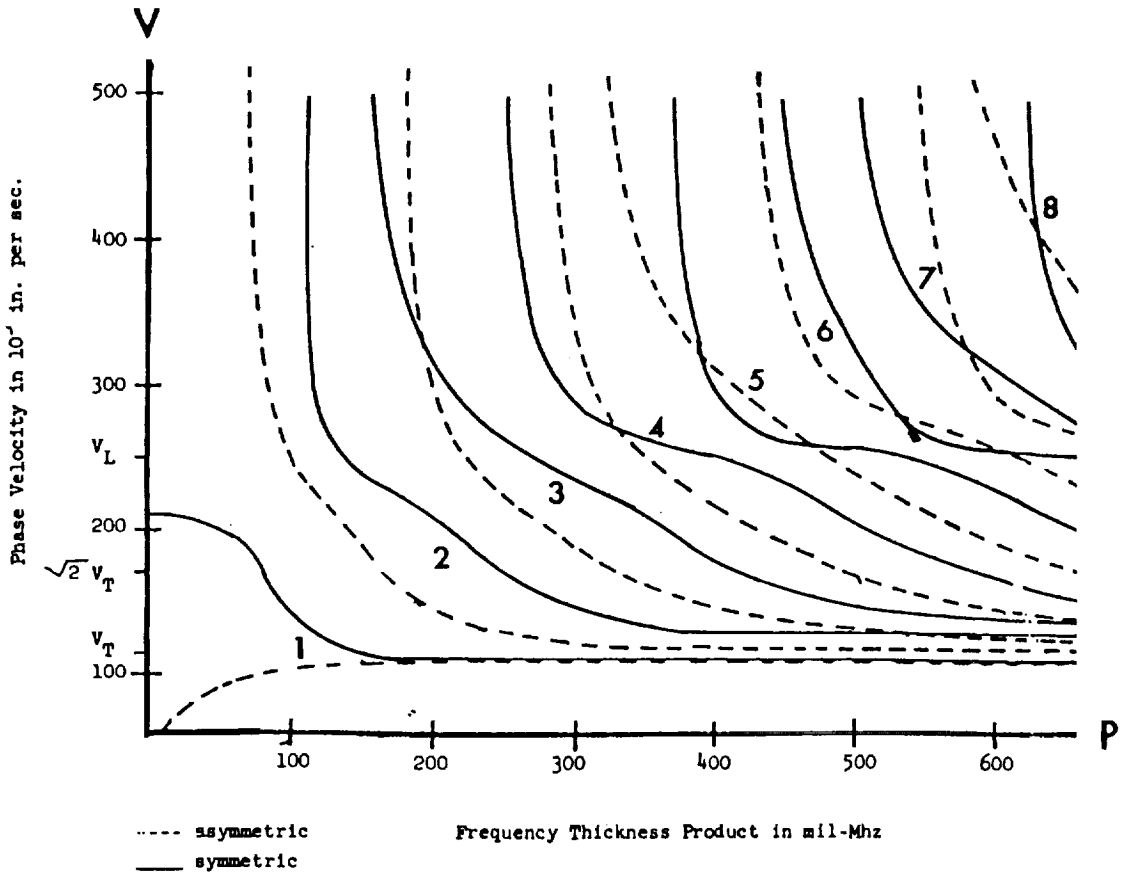

Figure 8. Velocity versus frequency [ref. 59]

The plate problem for an isotropic plate has a rich history, starting with experimental investigations, followed by elementary solutions from many of the great scientific minds of the time. Eventually, the general solution was obtained by Rayleigh and Lamb, showing that the elementary solutions are approached in the limit of low frequency. Furthermore, they showed the dependence which the output has on the input wave forms and how these relate to the actual plate modes. For example, simple thickness modes occur for an input of a zero wave number in the x_1 direction, a totally vertical input wave. Also, a Goodier-Bishop wave results if β is zero. Finally, it is interesting to note that the most general problem for all sides bounded is not as of yet solved, in general, however particular aspects of it have been solved, showing the physical relevance of complex wavenumbers.

Anisotropic Plate Waves

Several investigators have looked at the problem of plate waves in anisotropic materials. As might be expected, the anisotropic constitutive relation greatly complicates the analysis of the plate wave problem. A variety of extra plate wave modes are created due to the extra modes of plane waves which are possible. Also, the properties of the Lamb waves (ie. dispersion curves) depend on azimuthal angle. Further complications arise due to the fact that all modes are coupled into the same equations, hence vastly complicating numerical procedures. In fact, the full analysis of the anisotropic problem would be prohibitive without the use of the computer. However, Ekstein did formulate the full analytical solution to the problem for the case of orthotropic symmetry in 1945 (ref. 113). Detailed analysis of the dispersion relations of anisotropic materials were not developed until Mindlin and co-workers used a variational approach (ref. 52). More recently the method of transverse resonance or partial waves has been forwarded as a solution technique (ref. 127). Since, this method is the basis of the approach used here to solve the plate wave problem for composite plates, a short synopsis of this method will be provided for future reference.

In the method of partial waves, plate wave solutions are constructed from exponential waves that are reflecting back and forth between the bottom and top surfaces. This approach considers plate

waves to consist of traveling waves in the direction of propagation and standing waves through the thickness.

The exponential trial solution is expressed as

$$u_i = \alpha_i \exp[i(k_i x_i - \omega t)]$$

This is then substituted into the Christoffel matrix to obtain

$$(k_{iI} c_{IJ} k_{Jj} - \rho\omega^2 \delta_{ij}) u_j = 0$$

In this work, the subscript convention is as follows

$$i, j = 1, 2, 3 \quad I, J = 11, 22, 33, 23, 13, 12$$

The k_{iI} matrix is defined as follows

$$k_{iI} = \begin{bmatrix} k_x & 0 & 0 & 0 & k_z & k_y \\ 0 & k_y & 0 & k_z & 0 & k_x \\ 0 & 0 & k_z & k_y & k_x & 0 \end{bmatrix}$$

and k_{Jj} is the transpose matrix. The partial waves are coupled to each other by reflections at the surfaces in accordance with Snell's Law

$$k_1 = k = \omega / v$$

where v is the plate wave velocity. The particle displacement vector then becomes

$$u_j = \alpha_j \exp[ik(x_1 + l_2 x_2)]$$

where

$$l_2 = k_2 / k_1$$

for every partial wave solution.

The substitution of the equation for u_j into the Christoffel matrix results in a system of three homogeneous linear equations for the α_i values, with coefficients that are functions of density, frequency, and the stiffness matrix terms. This results in a 6th order polynomial for l_2 with six resulting roots

$$l_2^{(n)}$$

where

$$n = 1, ..., 6$$

Next, the displacement field may be taken as a linear combination of the six allowed partial waves. Mathematically, this may be expressed as

$$u_j = \sum_{n=1}^{6} C_n \alpha_j^{(n)} \exp[ik(x + l_2^{(n)} z)]$$

These expressions may be used with constitutive relations to yield stresses. These stresses may then be used in the boundary conditions

$$\tau_{12} = \tau_{32} = \sigma_{22} = 0$$

at $z = \pm h/2$. This leads to a system of six homogeneous linear equations where the coefficients of C_n are now functions of ρ , c_{ij}, $v = \omega/k$, and hk . Setting the determinant of the system of equations to zero results in the dispersion relations, which yields information on the dependence of velocity on frequency. These can be used to derive the commonly used dispersion curves with the infinite number of branches. Furthermore, the system can then be solved to find relative values for the C_n values. Thus, an indication can be obtained on the relative displacements occurring in the plate.

As mentioned, investigation of these relations results in a number interesting phenomena. These include a number of additional modes not seen in isotropic materials (ref. 11). The general character of the dispersion curves for anisotropic materials is similar, however the curves have more jumps and the extra modes lead to extra curves. Also, the dispersion curve is different for different azimuthal angles. Additionally, pseudosurface waves exist, which leak energy (ref. 127).

Applications

The theory of Lamb waves has been utilized for a number of applications. Mindlin and coworkers utilized the theory of Lamb waves to predict behavior of resonators for radio communications. Also, the theory of Lamb waves has been used to explain acoustic emission results (ref. 129) and for use in nondestructive testing (refs. 21).

Through Thickness Resonance

The through thickness resonance mode (simple thickness mode) corresponds to the constructive interference of either a P-wave or an S-wave reflecting back and forth perpendicularly between the top and bottom surface. This mode of plate wave corresponds to the intersection of the higher modes with the frequency axis. As mentioned, these modes have a theoretically infinite phase velocity. The frequencies and displacements of these modes are simple to calculate and are given, for an orthotropic material, by the following equations:

Symmetric Modes

$$(a) \quad u_3 = B' \sin(m\pi \frac{x_3}{2b}) \quad u_1 = 0 \quad m = 1, 3, \ldots$$

(b) $u_1 = C' \cos(n\pi \frac{x_3}{2b}) \quad u_3 = 0 \quad n = 2, 4, \ldots$

Antisymmetric Modes

(a) $u_1 = D' \sin(n\pi \frac{x_3}{2b}) \quad u_3 = 0 \quad n = 1, 3, \ldots$

(b) $u_3 = A' \cos(m\pi \frac{x_3}{2b}) \quad u_1 = 0 \quad m = 2, 4, \ldots$

Frequencies

$$f_p = \frac{nv_p}{2t} \qquad f_s = \frac{nv_s}{2t}$$

$$v_p = (\frac{C_{33}}{\rho})^{.5} \quad v_s = (\frac{C_{44}}{\rho})^{.5} \quad v_s = (\frac{C_{55}}{\rho})^{.5}$$

For Isotropic Materials

$$C_{33} = (1 - \nu) \frac{E}{(1 + \nu)(1 - 2\nu)}$$

$$C_{44} = C_{55} = \frac{E}{2(1 + \nu)}$$

where t is the plate thickness, $N = 1,2,3,\ldots$ and C_{ij} are stiffness matrix values expressed in reduced tensor notation (reference 13). Hence, if C_{44} does not equal C_{55}, extra resonances may occur through the thickness. Also, for materials in which the x_3-axis is not in a plane of orthotropic symmetry, the shear wave velocities are affected by coupling terms in the stiffness matrix.

Also, the shear wave resonances are polarized, for anisotropic materials, due to the polarization of the S-waves in the x_3 direction. This is suspected of contributing to experimental results presented in chapter 4.

The simple thickness vibrations described by these equations are for very idealized conditions, with infinite plane waves propagating absolutely normal to the top and bottom surfaces. However, understanding these results may be of some use in understanding AU results. First, although much of the AU wave disturbance is not due to plane waves resonating absolutely perpendicular to the top and bottom surface, the AU waves are thought to be a result of reinforcing of plane waves with very small angles from the normal. Hence, simple thickness modes may have many of the same properties of AU waves, and thus physical understanding of the AU waves may be gained by understanding simple thickness modes. Additionally, understanding how plane waves combine to meet boundary conditions and cause resonance may help to understand how the very early low frequency, low amplitude part of the AU signal is created. This problem may be better understood by relating Green's function results to Lamb wave equations. Although the early part of the signal is of very low amplitude, it may provide a great deal of information concerning the state of the material. Hence, understanding the simple thickness mode may be very useful in understanding the AU method.

Analytical Ultrasonics

Analytical ultrasonics entails measuring material microstructure and other variables which control the mechanical behavior of materials (refs. 20, 21 and 25). The ultimate goal of this approach is to be able to assess a material's strength, moduli, toughness, and other properties which can be used to predict future material behavior. The realization of this goal will depend on developing more advance models of wave/material interaction, better understanding of basic material behavior, better

understanding of excitation mechanics, better experimental equipment (transducers etc.), procedures, and more advanced signal processing techniques. Hence, advancement of analytical ultrasonics requires improvement in wave propagation models and better experimental tools. A few comments, concerning this area, is provided in this section to provide information which may be pertinent to the AU method.

Green (ref. 27) gives a good overview of the general state of technology in analytical ultrasonics. He discusses pertinent issues such as material behavior models, wave excitation sources, and measurement methods. Since the AU method and analytical ultrasonics are undeniably coupled, issues important to analytical ultrasonics are important to AU and vice-versa. In general, analytical ultrasonics uses wave propagation theory and experimental work to predict the future behavior of materials.

First, the attenuation of a wave can be used to obtain information on a material. The attenuation of a wave in a material may be caused by material dissipation mechanisms, scattering, reflection of the wave or more likely a combination of all of these. The measurement of stress wave attenuation is the method used to produce the often used ultrasonic C-scan. In many applications, the attenuation of a stress wave as a function of frequency is measured (ref. 36 and 74). This is especially useful for obtaining detailed information on microstructure. Models of this are discussed later.

Another source of information derived from stress wave propagation is the wavespeed. A simple application of this is the use of wavespeed to measure the moduli of a material. In fact, Kriz and Stinchcomb (ref. 128) used this approach to obtain the full stiffness matrix for a Gr/Ep composite. More recently, Kline and co-workers (ref. 17) have developed a method where obliquely incident waves are transmitted into a specimen and received at another point. This is performed during an ultrasonic C-scan at several orientations and then a numerical procedure is applied to the wavespeed measurements to determine stiffness matrix quanities. Other researchers have utilized the measurement of the phase velocity of Lamb waves as an NDE method (refs. 12, 13, and 89). Also, wavespeed measurement is used to determine residual stress. This is due to the inherent nonline-

arity of material moduli and changes in density do to changes in bulk volumes. Acousto-elasticity (ref. 38) is a specific subarea of elasticity devoted to the study of this phenomenon.

Dispersion is another phenomenon associated with wave propagation that can yield information on micro- (ref. 51,105, and 107) and macro-structure. Dispersion is when waves of different frequency travel at different speeds. This can result in sine waves of varying frequencies separating in the time domain (see experimental results). Dispersion can be caused by small particles or phases in a material that effect the acoustic velocity of waves for certain frequencies of wave propagation and by waveguide dispersion (e. g. note the nonlinearity of Lamb wave curves).

Also, of concern in analytical ultrasonics are developments in mathematical theories for analyzing waves. Equally important is the development of computational methods for making calculations based on the mathematical theory. One example of this type of work is that of Pao and co-workers with the generalized ray theory (ref. 122) for calculating transient plate responses. Also, the Green's function has been utilized to calculate transient plate responses (ref. 121). Also, Vasudevan and Mal (ref. 129) have used a transform integral technique to determine the transient response of an elastic plate to a buried source. This involves summing residues of the dispersion relations from the boundary conditions and transforming from the frequency domain to the time domain. The residues occur at the through-thickness-transverse-resonance frequencies and at the minima of the first order symmetric and third order antisymmetric mode. The procedure excludes the effects of the negative group velocity regions. Also, a small complex perturbation term was introduced into the FFT to account for attenuation. Their approach and results seem to show some correlation with the work in this dissertation.

Another area where wave modeling can be applied to ultrasonics is trying to understand the near field (Fresnel field) and the far field (Fraunhafer region). The Fresnel field is characterized by regions of alternating pressures. The Fraunhafer region has lobes of fairly constant pressure (described by $r-\theta$ plots (ref. 21).

Also, Claes (ref. 140) has outlined an interesting solution to the plate wave solution in an isotropic plate due to an axisymmetric source. The solution yields Bessel functions which account for the decrease in amplitude due to waves diffusing from the source. The solution degenerates to a basic plane wave solution at a large distance from the source.

Mathematical models of frequency dependent attenuation have been developed and have been used to explain ultrasonic data (ref. 74). A partial list of attenuation mechanisms and their mathematical effects are listed below:

Rayleigh scattering-$\alpha_r = c_r a^3 f^4$

Stochastic scattering-$\alpha_p = c_p a f^2$

Diffusion scattering-$\alpha_d = c_d a^{-1}$

Hysteresis losses-$\alpha_h = c_h f$

Thermoelastic losses-$\alpha_t = c_t f^2$

Viscous losses-show second order frequency dependence

Absorption losses (dislocation vibration, internal friction, and relaxation effects)-show second power down to first power effects on frequency

In the above expressions f is frequency and a is the grain size or discontinuity size. Various authors have attempted to relate these models to form single equations describing the frequency dependent attenuation of various materials (ref. 74).

An important facet of analytical ultrasonics is understanding the transducers. A number of papers have been published on various ultrasonic sources which may be utilized (ref. 68). These sources include:

Piezoelectric

Gas jet

EMAT

Laser

Spark gas discharge

High resistance metal sheets

Capacitance

The physics associated with each of these sources is a separate area of research.

The piezoelectric transducer itself is continually being refined and improved, resulting in a great number of different transducer properties. For instance, new products, such as KYNAR film (ref. 165) and dry couplant transducers (ref. 166), are adding to the possible choice of piezoelectric sources. Characterizing the properties of various transducers and understanding their effects is a heavily researched area of ultrasonics (refs. 133 and 110). The following are just a few of the concerns with characterizing piezoelectric transducers:

Relationship between voltage-current and force-displacement (Linear system response matrix) (ref. 133)

Transducer diameter (ref. 21)- see fig. 9

Phase cancellation effects (ref. 152)

Uniformity of displacement on transducer face

Frequency response of transducer (fig. 24, chapter 3)

Crystal type (longitudinal or shear)

Proper orientation of transducer in casing

Coupling mechanism and effects

These effects strongly influence all analytic ultrasonics methods and most assuredly results seen in the AU method.

Finally, advances in signal analysis are of great interest to researchers in analytical ultrasonics. For instance, a number of early papers on the AU technique (refs. 7 and 63) were concerned with signal analysis. These involve areas such as pattern recognition (ref. 143), Fourier analysis, analytic signal (ref. 16), and various fields of digital signal processing (ref. 2). Many of these concepts will be covered in the following section.

Acousto-ultrasonics

The acousto-ultrasonic technique involves exciting ultrasonic stress waves at one position on a material surface and sensing the wave at another position on the same material surface. In general, various excitations, sensors and analysis software can be used to perform the method as is shown in figure 1 (chap. 1). Most implementations of the method to date have involved using ultrasonic piezoelectric transducers for both sending and sensing the stress waves. However, the use of pulsed laser excitation of stress waves is currently under investigation by several investigators (ref. 161).

Two major advantages of the AU method over other commonly used methods are that:

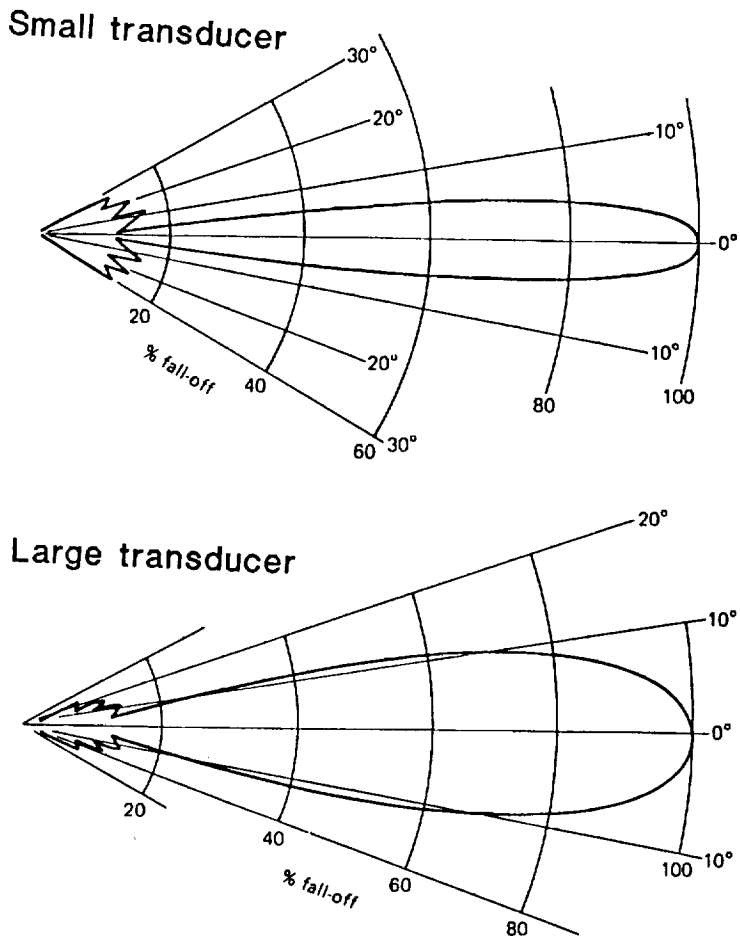

Figure 9. Effect of transducer diameter [ref. 21]

Access to only one material surface is required

Can propagate stress waves in direction of loading

Hence, although a number of methods exist for nondestructively testing a material, the AU method has the advantages of only requiring access to one surface and yielding information on in plane material properties.

The general contention of the AU method is that a section of material which adequately transmits stress waves will also properly transfer stress under loading and hence be less prone to fracture. Thus, one facet of the AU method is to simply make comparisons of the energy content of an ultrasonic signal that is propagated between two positions on a piece of a material. The idea is that if a high energy content signal is produced between two points, then the area of material between those points will be able to resist fracture more than a similar area of material between two points where a weak signal is obtained. For instance, a damaged area (delaminations, matrix splits, debonds etc.) will, in general, reflect and absorb energy in a stress wave and will also, in most cases, (except in certain instances where stress concentrations are lowered) result in areas where fracture may initiate.

Understanding the mechanics of how damaged areas interact with stress wave propagation encompasses areas of the theory of stress wave propagation and analytical ultrasonics. However, the first step in understanding any ultrasonic method is to develop a model for the idealized case where simple material constitutive relations govern the problem and the material is in perfect condition (defects and damage do not alter the material's response). Then, more complex material behavior may be accounted for by adding to the simple model or by using the simple model as a basis for developing more complex models.

Early Research

The name acousto-ultrasonic is derived from ultrasonic evaluation and acoustic emission monitoring; in fact Vary attributes the basic idea to acoustic emission work done by Egle and Brown (ref. 137). Egle and coworkers utilized what became the AU configuration to simulate acoustic emissions in order to better understand acoustic emission results (ref. 134).

It should also be noted that prior to the actual adoption of the AU method for composite materials, similar types of experimental configurations were being utilized for conventional materials (ref.74).

The pioneering work on the AU method was conducted by Vary and co-workers at NASA Lewis (Ref. 5). This work entailed introducing the term Stress Wave Factor (SWF) to quantify the energy in the AU signal. The SWF involves measuring discrete voltages in the signal at a selected sampling rate and counting the number of voltage peaks above a preselected threshold voltage. SWF measurements were made in the cross fiber direction on a number of unidirectional Graphite/Polyamide composite coupons which had been subjected to varying cure pressures. Next, the coupons where subjected to a three point bend test to determine interlaminar shear strengths. Results showed that the lower cure pressures resulted in lower SWF and lower material strength. It was also noted that the lower cure pressure resulted in a greater void content. In general, this early work showed that AU can be used to give a relative indication of interlaminar shear strength for unidirectional composites. Figure 10 shows the results obtained by Vary and coworkers.

The initial work by Vary and co-workers stimulated additional investigations by other researchers, that resulted in a number of observations and methods of signal quantification.

First, Govada et. al. supported Vary and coworker's results that SWF measurements taken at discrete locations along the length of a thin composite specimen could be used to predict failure location for uniaxial loading (ref. 88). The basic premise of this work was that the area of low SWF

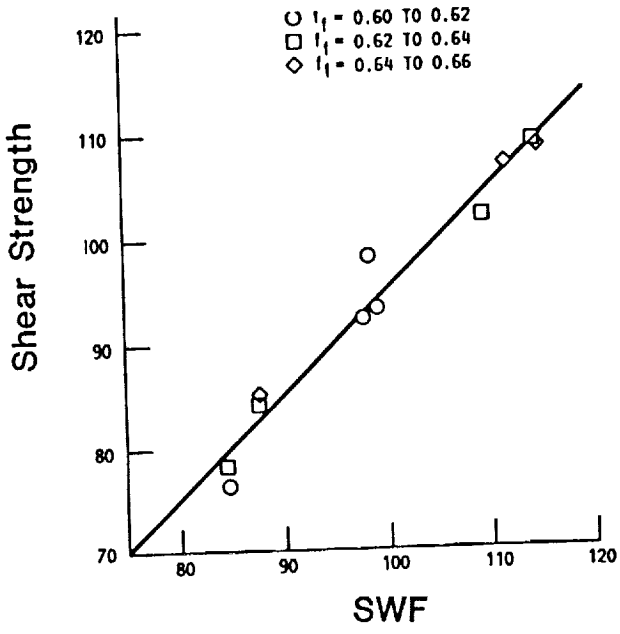

Figure 10. SWF as a function shear strength [ref. 137]

would be the area of failure during unidirectional loading. However, the work revealed that an averaging technique had to be used which accounted for the proximity of the sending transducer to the area being measured.

Further work at Virginia Polytechnic Institute (VPI) revealed that the SWF factor decreased with fatigue loading (ref. 6), hence, showing that the AU technique is a good quantifier of fatigue damage. In fact, figure 11 shows how the SWF factor (energy measurement) compares to stiffness measurement as a function of fatigue life. As mentioned, this indicates that the AU measurement might be a more sensitive measurement for use in fatigue models than stiffness degradation.

Early work by Williams and coworkers at Massachusetts Institute of Technology involved evaluating impact damage (ref. 56). Also, work was done using frequencies generated in the AU technique to determine the dispersion of composite materials at those frequencies (up to 5 MHz) (ref. 30). It was found that no material dispersion occurred at these frequencies. Further work by Karaguelle involved using ray tracing techniques to model the AU technique in an aluminum plate (ref. 49). This model assumed the transducer imported a uniform normal stress where the transducer contacted the specimen and treated the elasticity problem as a half space problem to calculate resulting wave propagation. The successive reflections of these waves are traced to determine the resulting behavior of an aluminum plate. However, the solution technique and certain assumptions cause numerical instabilities if $h/\lambda < 1.6$, where h is the plate thickness and λ is the wavelength of a P-wave. This causes problems in trying to apply this theory to experimental results found using the original AU set-up.

Williams and coworkers also discussed the possibility of exciting structural resonances in certain configurations (ref. 112), however, the frequencies of these resonances must be in the range of the input transducer and other experimental equipment. Generally, structural resonances are not excited with the conventional AU set-up in laboratory conditions, but depending on the equipment and structure, structural resonances may very well be set-up during field application of the AU

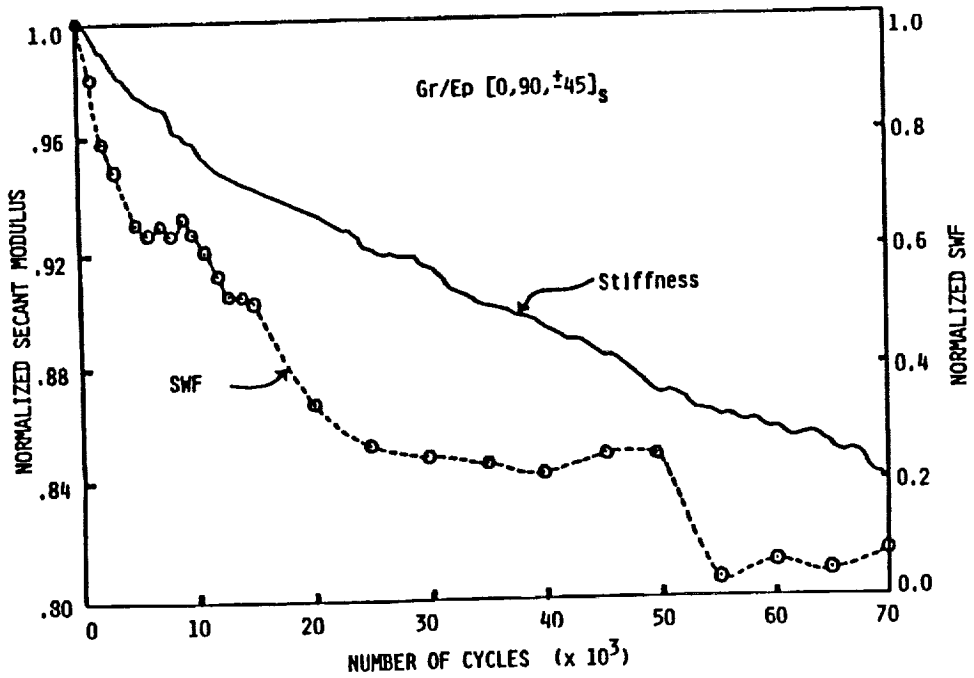

Figure 11. SWF and stiffness as a function of fatigue cycles

method. The matching of experimental equipment to the material and structural application should be considered separately for each application of the AU technique.

Subsequent advances involved the introduction of more advanced signal processing techniques. This helped to develop a more refined method and helped to start explaining the physics of the AU method.

Karaguelle and Williams applied "homomorphic signal processing" to the detection of flaws in an aluminum plate (ref. 63). This work involved picking out the signal from one particular reflection pattern, by deconvolving a short portion of the signal which may contain multiple reflections.

Talreja and Henneke introduced the use of theory from random noise involving moment calculations from the frequency domain to quantify information in the AU signal (ref. 7). Moment calculations were obtained by integrating the product of the AU signal's spectral density function (obtained by taking the FFT of the AU signal and squaring amplitude values) and the frequency over the frequency domain. Parameters can then be calculated, from these moments, that describe certain characteristics of the signal (e.g. energy content and centroid frequency). This approach marked the beginning of the evolutionary process which led to this dissertation. Hence, a more detailed description of the work done using this approach is provided. This includes a description of software, basic equations, and ensuing experimental results. The program described below is an earlier version of the program used to obtain results in chapter four; however, this program was used to generate results for this chapter. These results will be discussed in the chapter on physical understanding.

AU Analysis Software

In particular, a description is presented of a computer software package used to analyze the AU signal (ref. 10) and generate results. The intitial step in the computer analysis is to retrieve the

digital signal from the storage disk, where it has been stored during the AU data acquisition phase. This involves reading information on gating parameters and then the bit representation of each voltage. These bit representations are used to calculate actual voltages and time values. Next, voltage/time graphs can be generated for observation of general signal characteristics. Additional subroutines allow for the signal to be gated and for any DC bias to be removed from the signal. Estimates of wave arrival velocities are made by dividing the transducer separation distance by the time of wave train arrival (ie. first non-zero voltage reading) as measured from the instant of triggering. In addition, phase velocity estimates were made for certain cases by increasing the transducer separation distance and noting the translation in the time domain for a particular point in the wave pattern display, wave train. A peak in the time signal could be followed on the computer screen as the receiving transducer was moved away from the sending transducer. For certain signal content, the general shape of the signal changed very little as the receiving transducer was translated on the specimen. Hence, this procedure was applied to parts of the wave train which contained predominately a single frequency content in order to determine a wave speed to be associated with a particular frequency of wave motion.

A fast Fourier transform (FFT) algorithm was used to yield frequency domain information on the gated digital voltage/time data. The voltage/time data was gated from the first non-zero voltage reading to the end of the wave train. Using the FFT, amplitude/frequency and phase/frequency data were generated, the amplitude/frequency data were plotted and AU parameters were calculated. The equation describing the amplitude values calculated via the FFT is:

$$X_k = \frac{1}{n} \sum_{r=0}^{n-1} v_r e^{-i(2\pi kr/n)}$$

where v_r are voltages and $f_k = k/(n\Delta t)$ is the frequency corresponding to X_k.

The determination of AU parameters involves calculating various moments of the spectral density (the square of the amplitude values $S_k = X_k^2$) about the vertical axis, S_k axis (see figure 12). For instance if $S(f)$ is the continuous spectral density function, the n-th moment is defined as:

$$M_n = \int_0^{f_m} S(f) f^n df,$$

where f_m is the Nyquist frequency. In the case of digital data, the integration is replaced by a summation to yield:

$$M_n = \sum_{k=0}^{(m-1)} \frac{(S_k + S_{k+1})}{2} \Delta f (f_k + \Delta f/2)^n,$$

where S_k are the spectral density values, f_k are the corresponding frequency values and Δf is the frequency difference between f_k and f_{k+1}. For instance, the zeroeth moment (M_0) is defined as:

$$M_0 = \int_0^{f_m} S(f) df$$

or for the digital data obtained experimentally

$$M_0 = \sum_{k=0}^{(m-1)} \frac{(S_k + S_{k+1})}{2} \Delta f$$

M_0 is simply the area under the spectral density curve. This can be analytically related to the mean square of the voltage signal. For application to AU signal evaluation, M_0 is renamed A1. Therefore, A1 is an indication of the amount of energy in a received signal. A2 is defined as M_1/M_0 and is the central frequency of the signal. A signal with a higher A2 is transferring proportionally more energy at higher frequencies than lower frequencies when compared to a signal with a lower A2.

In addition, A4 is defined as $(M_4/M_2)^{.5}$ and A3 is defined as $(M_2/M_0)^{.5}$. A4 is the frequency of maxima and A3 is the frequency of zero voltage crossings (reference 5, page 92). The quantity A4/A3 is known as the distortion factor and is an indication of the amount of high frequency signal in a predominantly lower frequency signal. Figure 12 indicates how the moments are related to the spectral density function. Again, it should be kept in mind that the spectral density function is the square of the amplitude function for a given frequency value.

In order to obtain more specific information on the acousto-ultrasonic signal, filtering capabilities were included in the the digital signal software analysis (refs. 9 and 10). Basically, this involves calculating M_0 for a particular frequency range. Thus, the area under a specific portion of the spectral density curve can be obtained. Mathematically, this may be expressed as:

$$M_0 = \int_{f_l}^{f_h} S(f)df,$$

where $S(f)$ is the spectral density function, f_l is the low frequency end point and f_h is the high frequency end point. In the summation equation, this involves only summing for the values of k which correspond to the S_k values of interest (ie. corresponding to a peak). In particular, this feature is used to find the area under one frequency peak in the amplitude/frequency plot, yielding a parameter which is indicative of the amount of energy transferred at a particular vibrational frequency range. Initially, observation of amplitude/frequency plots revealed the occurrence of certain amplitude peaks at the same frequency for a given plate thickness, regardless of plate lay-up or azimuthal angle. The amplitude/frequency plots for different azimuthal angles were then examined to determine values for f_l and f_h. Next, the determined f_l and f_h values were used to calculate filtered moment values from the AU signals obtained at different azimuthal angles. Figure 12 displays how filtered A1 values are calculated and the nomenclature used for a particular calculation.

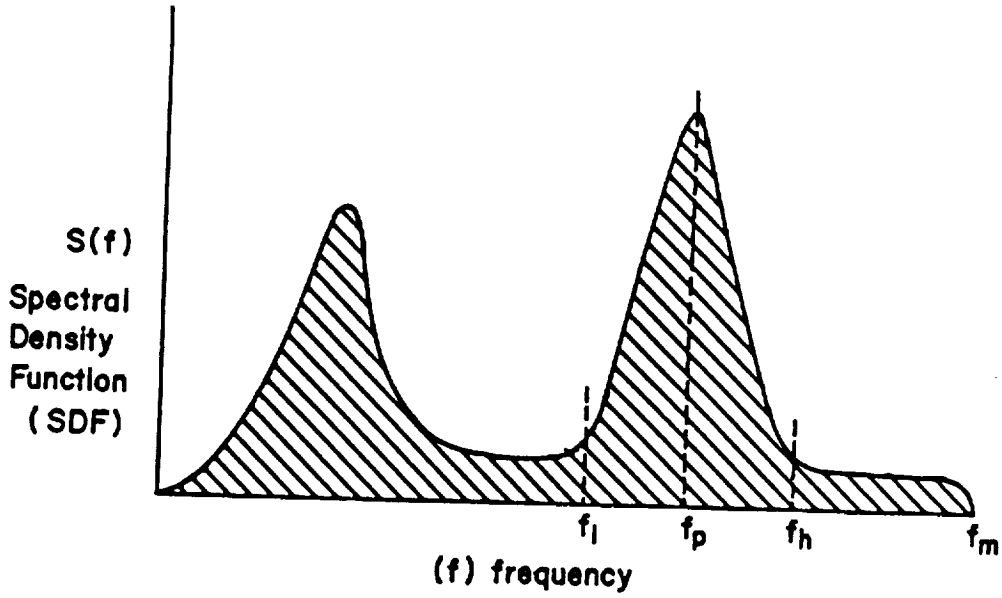

S(f) - Magnitude of spectral density (Amplitude squared)
f - Frequency

$$M_n = \int_0^{f_m} S(f) f^n df$$ n-th moment

$$M_o = \int_0^{f_m} S(f) df$$ O-th moment (Area under curve)

Definition of Filtered SWF Parameter

$$AI(f_l, f_h) = \int_{f_l}^{f_h} S(f) df$$

f_p - frequency of maximum SDF for peak
f_l - low frequency for chosen filter
f_h - high frequency for chosen filter

Figure 12. Calculation of filtered AI values

Results

The observation of time domain results and amplitude/frequency plots revealed basic information to be used in understanding the AU method as well as providing information to be used for both calculating and interpretating AU parameters. Figures 13 and 14 show some sample voltage/time (V/T) and amplitude/frequency (A/F) plots. Figure 13 shows the dominance of the 1 MHz and the 3.4 MHz frequency peaks in the spectrum for the signal obtained in the 0 degree direction of the 4-ply zero degree plate with no gate applied to the signal. Also, it should be noted that the 3.4 MHz peak is about 75 percent the amplitude of the 1 MHz peak. In contrast, the voltage/time plot in the 90 degree direction for the 4-ply zero degree plate (figure 14) revealed a signal with only the 1 MHz signal content and shows a steady amplitude throughout the signal, without the high signal content early in the signal. Observation of the corresponding amplitude/frequency plot reveals that the 3.4 MHz frequency content is still present, but comparatively less than the dominant 1 MHz content.

To gain insight into the influence of plate thickness on the observed AU behavior an 8-ply 0 degree laminate was examined and directly compared to results obtained on a 4-ply 0 degree laminate. A summary of observations made from voltage/time and amplitude/frequency plots in the 0 and 90 degree direction follows:

For 4-ply laminates amplitude peaks in the amplitude/frequency plots consistently occurred at 1 MHz and 3.4 MHz

For 8-ply laminates amplitude peaks in the amplitude/frequency plots consistently occurred at 500 kHz and 1.7 MHz

The experimental results for the variation of AU parameters with azimuthal angle for the [0,0,0,0] laminate can be seen in figures 15-18. Figures 15-16 show the variation of A1 and A2, respectively.

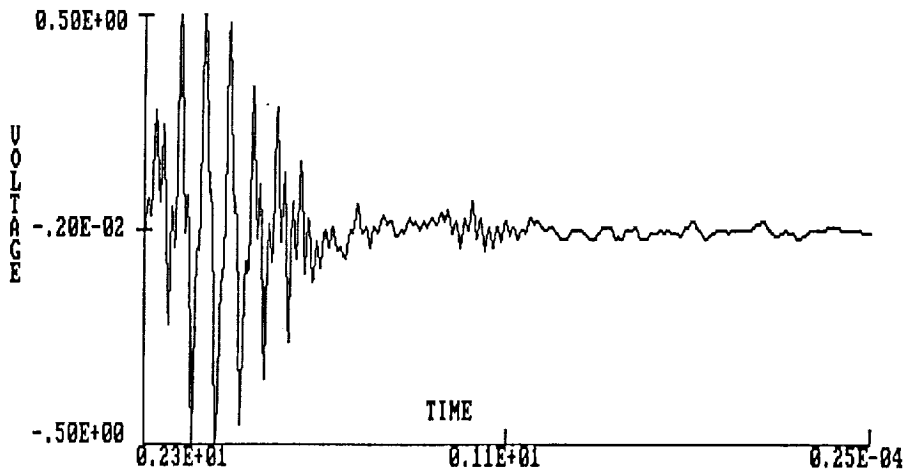

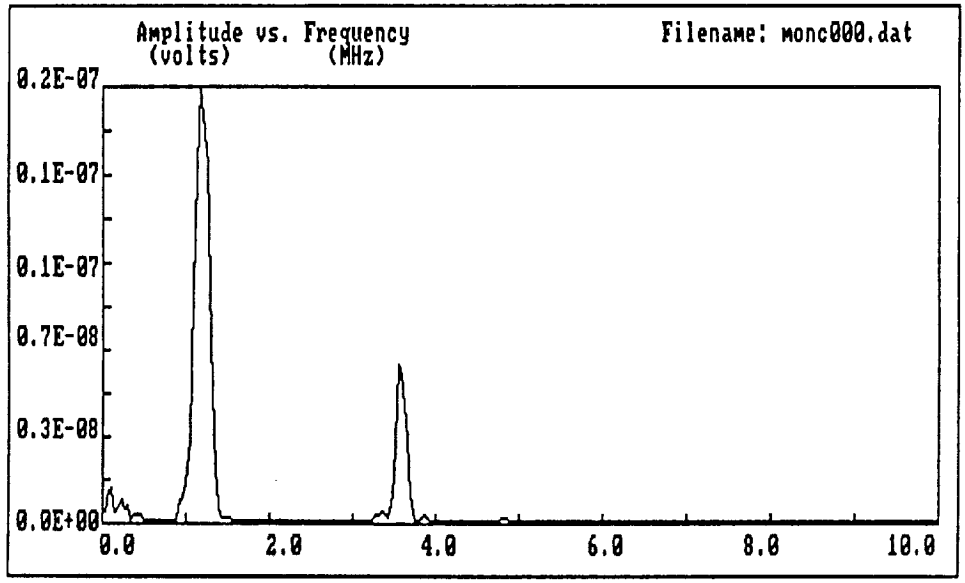

Figure 13. a)V/T b)A/F, in unidirectional panel-0 deg. dir.

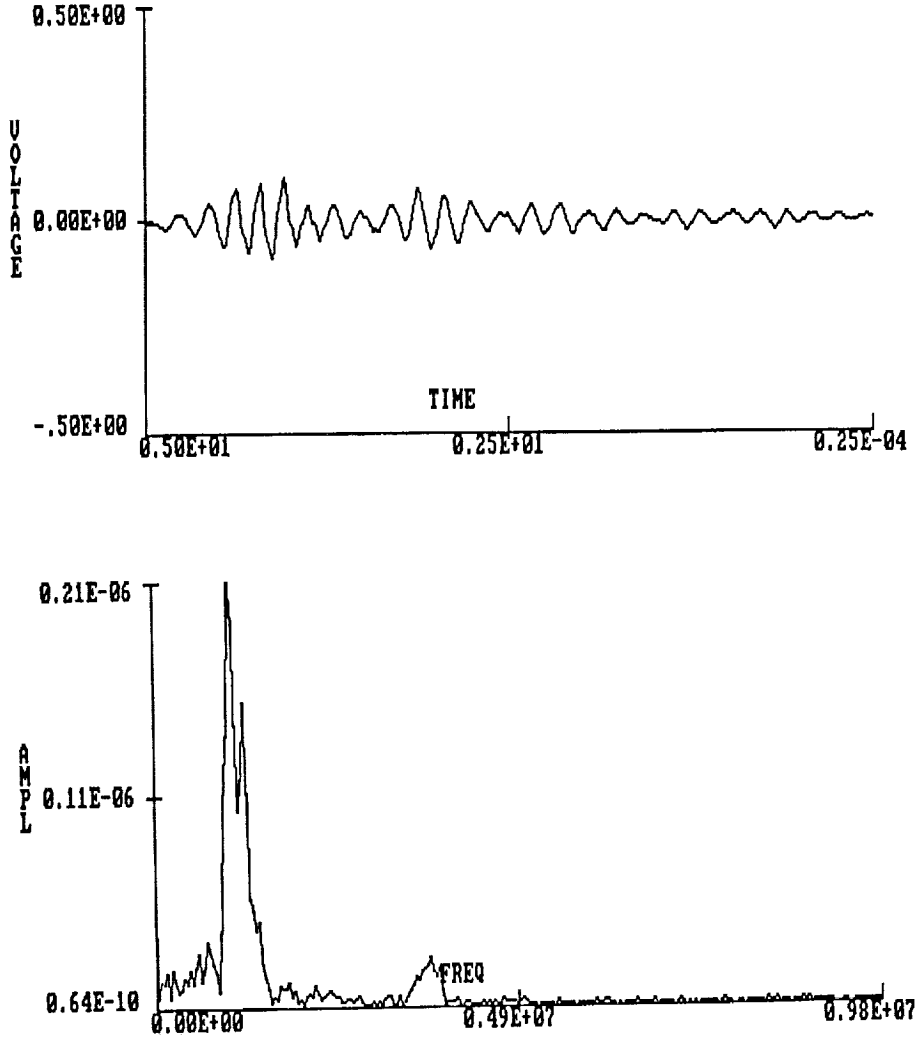

Figure 14. a)V/T b)A/F, in unidirectional panel-90 deg. dir.

The plot of A1 versus azimuthal angle for a 4-ply zero degree laminate (figure 15) shows the decrease in A1 with azimuthal angle up to 45 degrees and then the relatively constant value obtained between 45 and 90 degrees. The plot of A2 versus azimuthal angle (figure 16) shows a peak A2 value at 15 degrees. In general, unidirectional panels showed a peak A2 value between 10 and 20 degrees to the fiber direction (this same type of variation also occurred for the A4/A3 parameter). The variation of E_x with azimuthal angle is compared with the variation of A1 in figure 15. The behavior of A1 and A2 with azimuthal angle seen in this data has also been seen by another researcher (ref. 99). Figure 16 also shows the variation of the coefficient of influence with azimuthal angle and how it compares to A2. Hence, AU seems to mimic the variations in material properties. One purpose of AU modelling is to determine the exact relationship, so that AU may be used to make more exact evaluations on how material properties vary with azimuthal angle. Figures 17 and 18 show the variation in energy content for the resonant peaks at 1.0 MHz and 3.4 MHz, by displaying how A1(.8,1.2) and A1(3.2,3.6) are affected by change in azimuthal angle. The variation of A1(.8,1.2) with azimuthal angle is similar to that of A1. Also, notice that the behavior of A1(.8,1.2) seems to show the same behavior as E_x (figure 17), once again showing the relationship between AU response and mechanical properties. However, notice that the A1(.8,1.2) descends more rapidly and reaches a fairly constant value at approximately 30 degrees. The plot of A1(3.2,3.6) versus azimuthal angle reveals a much slower descent of A1(3.2,3.6) at angles under 20 degrees and then a quick descent to a fairly constant value between 20 degrees and 45 degrees, showing behavior more similar to the reduced stiffness matrix value $\overline{Q}_{11}$ (figure 18). The plot of A1 versus azimuthal angle (figure 19) for the [90,0,0,90] plate exhibits a quick descent from a relatively high value at an azimuthal angle of 0 degrees and a slower descent from a maximum value at 90 degrees, reaching a minimum value between 40 and 50 degrees. Also, the characteristic peaks at 15 degrees to fiber directions for the [90,0,0,90] laminate can be seen in figure 20.

Figure 21 displays a plot showing the rather extreme decrease in A1(3.2,3.6), especially in the fiber direction, for AU on a specimen with a delamination. Also, the value of A2 for the case of de-

lamination is shown to lose the characteristic peak at 15 degrees. Also, notice the plots compare AU parameters to the variation of material properties. This is also discussed in reference 9.

Current and Future State of AU Method

Currently, a number of investigators are working on various applications of the AU technique. For instance, Duke and Kiernan have looked at the use of the AU technique to predict the direction of damage development in impacted Gr/Ep panels (refs. 100). This includes understanding the effect fatigue damage has on AU results compared to the effect it has on impact damage. Hence, efforts are already underway to use the AU method to determine the effect damage has on future material response. Finally, this research has looked at how the variation of AU with azimuthal angle is altered by damage resulting from impact. In some instances, this has caused change in the location of high AU values. It may be that this gives some indication of how stress is redistributed for loading of impact damaged specimens (note the high AU measurement is not necessarily for right over the damage, but for close to the damage). Hence, this could be utilized to determine a stress concentration factor and suggest the direction in which damage may grow. This research has also shown which AU parameters are most sensitive to early fatigue damage. Other applications include the use of the AU technique to detect the density of trans-ply cracking in composites (ref. 102) and the application of the AU technique for predicting hygrothermal degradation (ref. 103). Other authors have utilized the statistical nature of AU measurements to quantify damage (ref. 146). The AU method has also found application to such diverse areas as adhesive joints, bones, and wood (ref. 144, 145 and 167).

Future work with the AU method may involve using the analytic signal to quantify the AU signal. This approach would allow measurements of energy rate and group velocities. Also, this may be combined with other advanced forms of digital filtering to gleen even more detailed information from the AU signal.

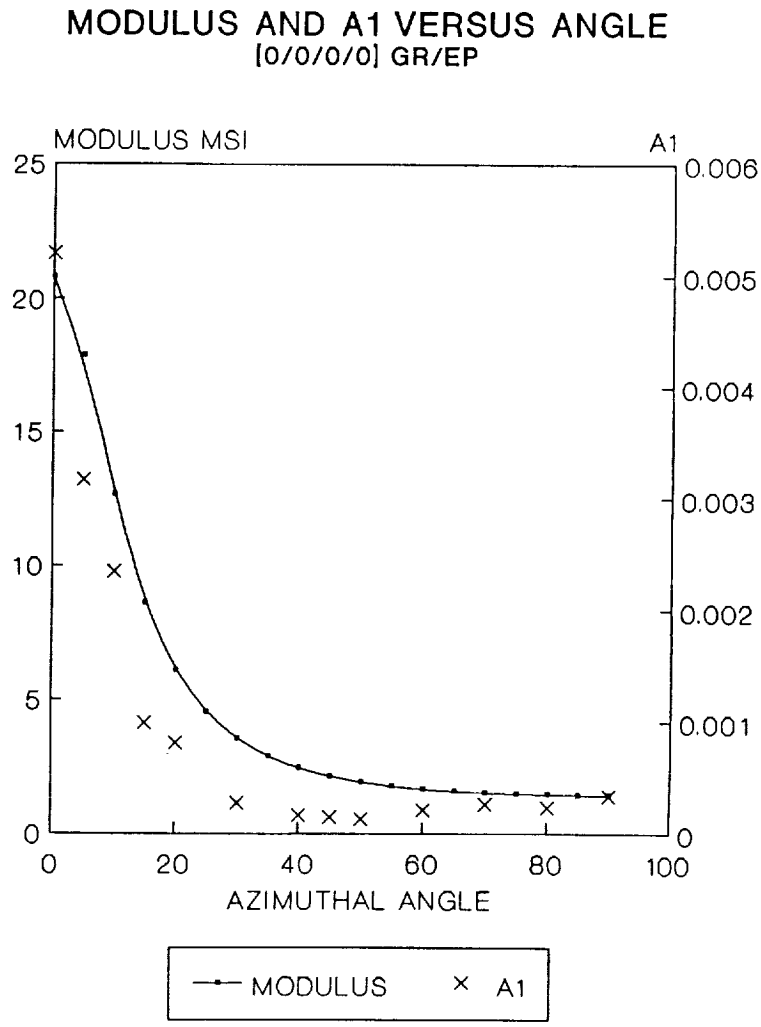

Figure 15. A1, modulus versus azimuthal angle for [0,0,0,0] laminate

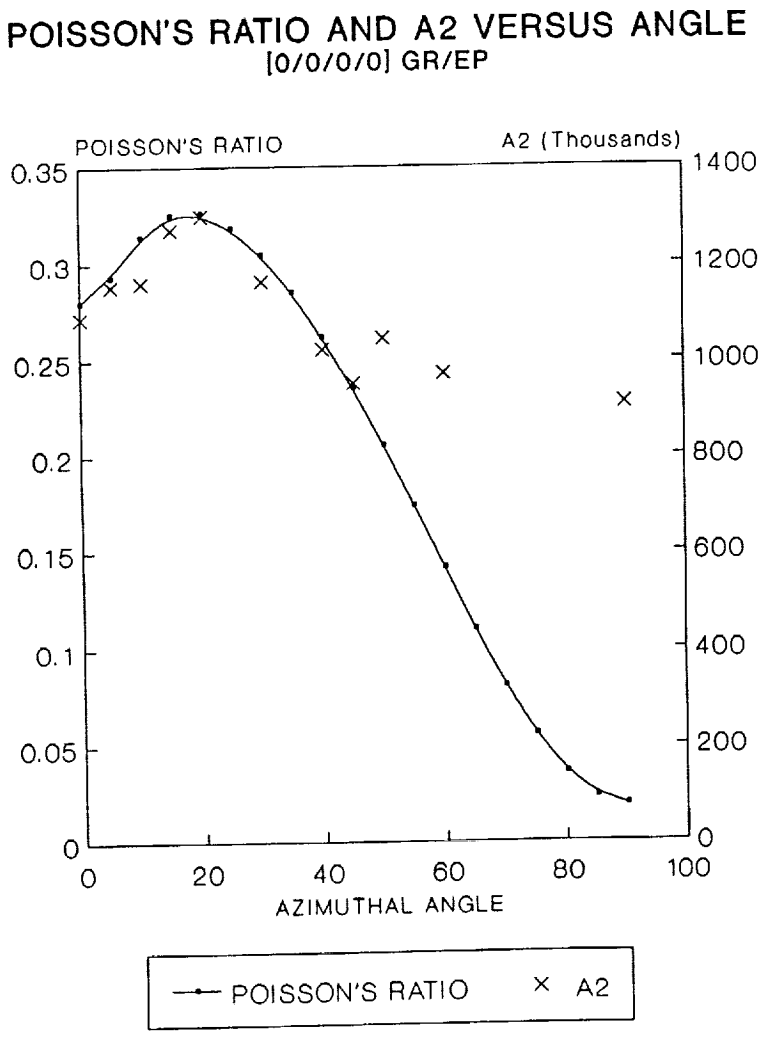

Figure 16. A2, Poisson's ratio versus azimuthal angle for [0,0,0,0] laminate

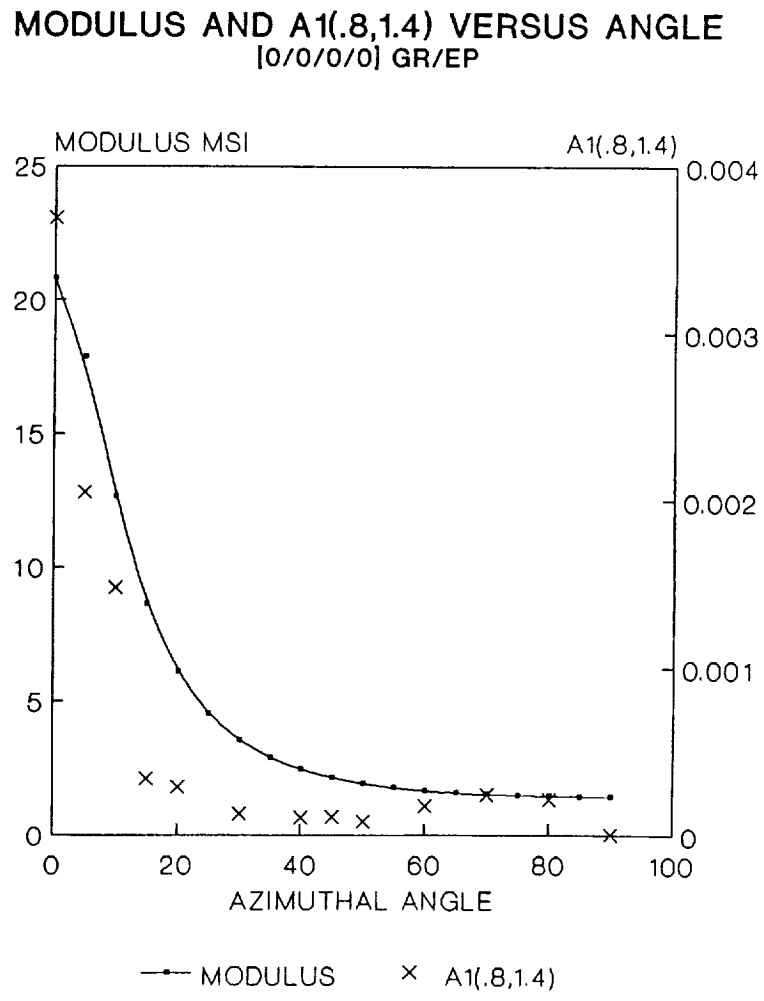

Figure 17. A1(.8,1.2), modulus versus azimuthal angle for [0,0,0,0] laminate

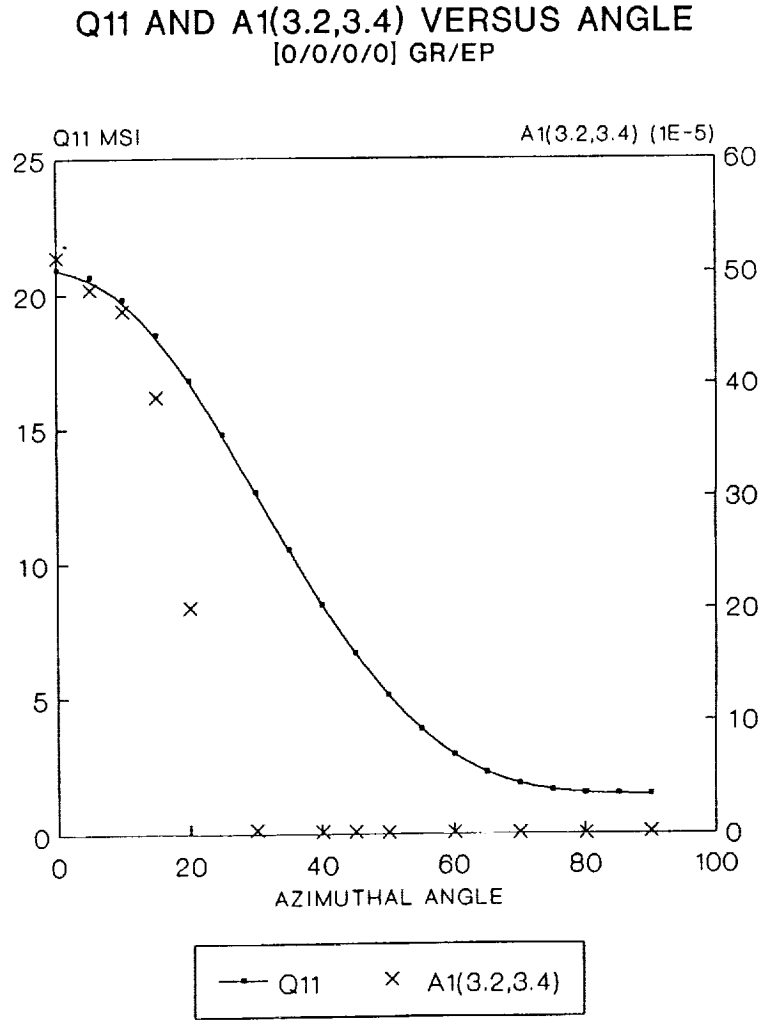

Figure 18. A1(3.2,3.6), modulus versus azimuthal angle for [0,0,0,0] laminate

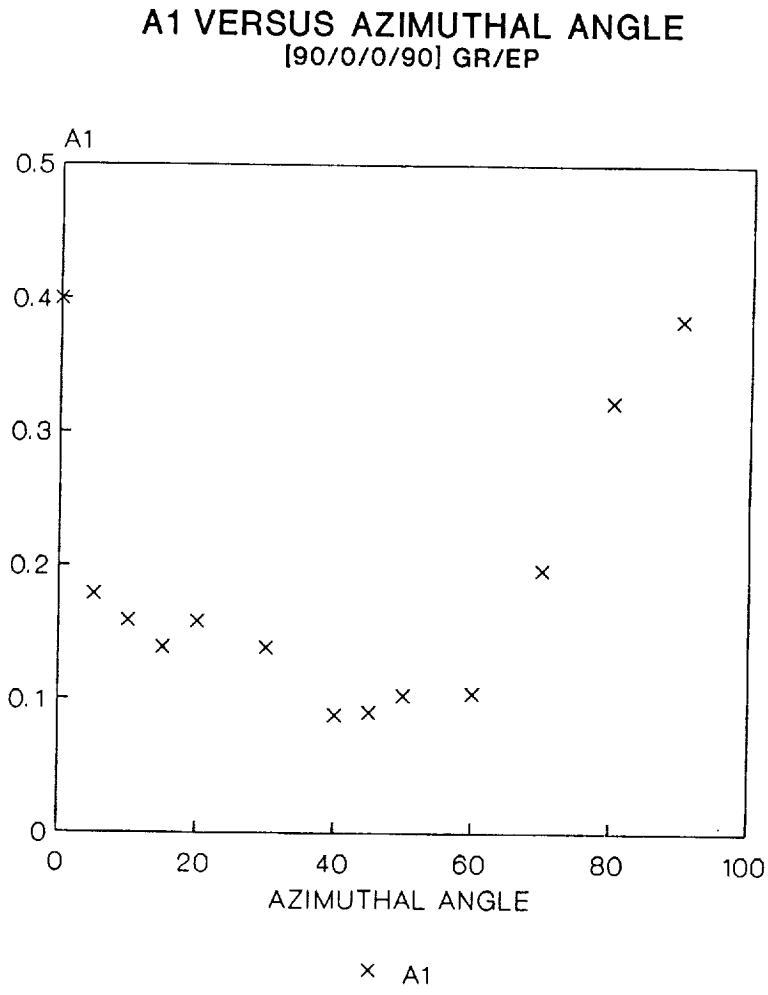

Figure 19. A1 versus azimuthal angle for [90,0,0,90] laminate

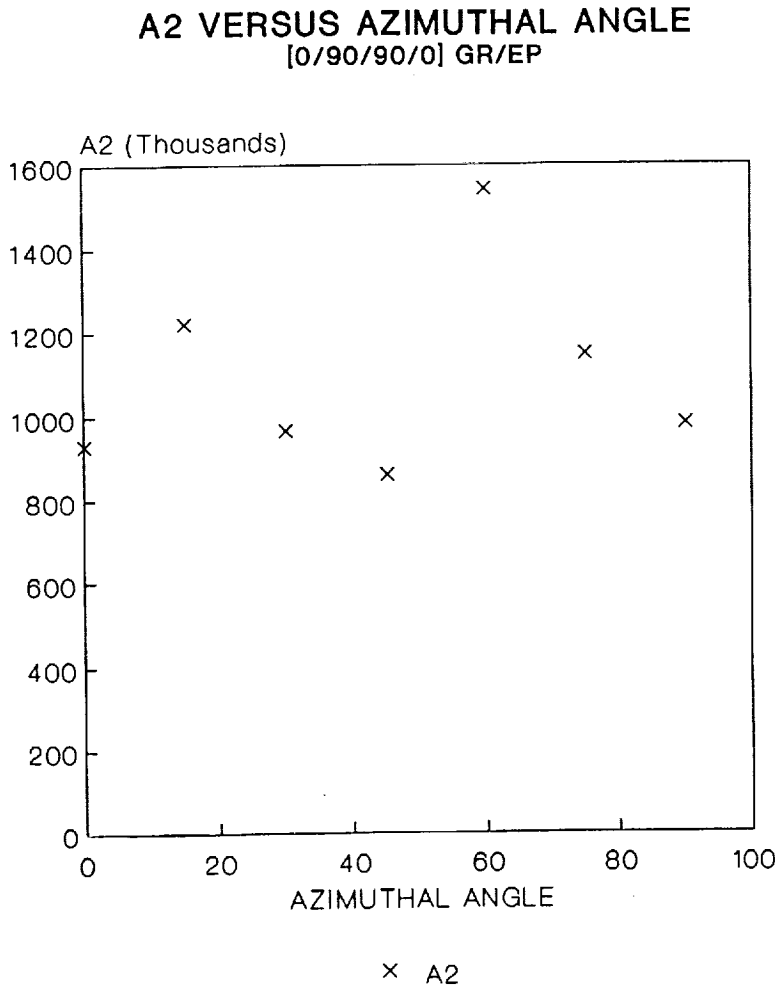

Figure 20. A2 versus azimuthal angle for [90,0,0,90] laminate

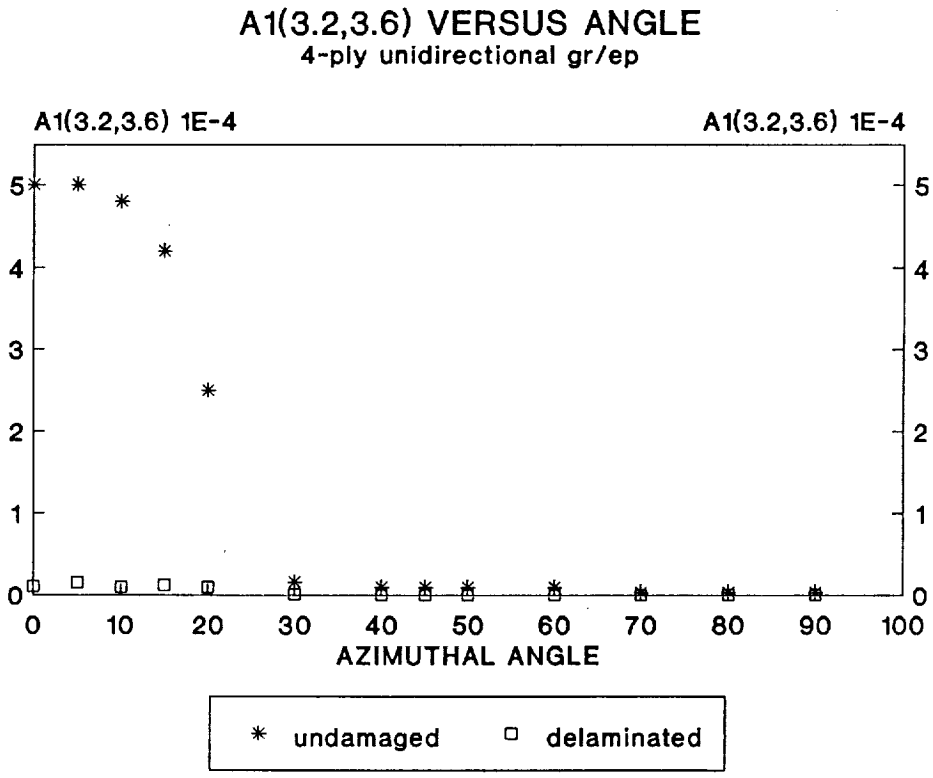

Figure 21. **A1(3.2, 3.6) versus azimuthal angle for unidirectional panels:** comparison between plate with delamination and undamaged plate

Although numerous applications of the AU technique have been found, there is still a general lack of understanding concerning the physics of the method for the application to composite plates. Several authors have noted that Lamb waves seem to be present in signals (ref. 9 and 95). However, there seems to be no specific mention of the modes which are present and how they are excited. Kautz (ref. 97) has suggested using the ray tracing technique as a model, but has yet to fully apply the approach to composite materials. This approach involves modelling the high frequency portion of the signal as a guided wave in the fiber. Other authors have suggested using diffuse wave theory (ref. 148) to describe the AU technique. However, a working model has yet to result from this work. In general, although the AU method has been applied to a variety of applications for composite materials, no real model exists for the method. Moreover, the basic physical understanding of the wave motion occurring in the AU method is still not well understood. In order to gain full advantage of the method and obtain quantitative information on the state of a material, a basic model must be developed which relates the mechanical state of the material to AU results. Thus, it is the goal of this proposal to understand the basic physics of the AU method for composite materials and to propose an elementary model of material response associated with the AU method.

Experimental Procedure

A very important facet of modeling and understanding any NDE method starts with a thorough consideration of experimental equipment, procedure, and analysis. As mentioned earlier, developing transducers, computer software, and AU systems is a subject of current research. Although results have been obtained using a number of transducers and experimental arrangements, this section describes very specific experimental arrangement and computer analysis which were used to obtain the bulk of the results utilized for this work. However, comments are offered on some results obtained with other experimental arrangements and the effect of changing various aspects of the set-up on results. Also, comments are offered on how various aspects of the experimental set-up and procedure relate to the physics of the problem.

The experimental equipment consists of a pulsing/receiving unit, a preamplifier, 2 piezoelectric transducers, and an IBM-XT equipped with a data acquisition system. Each of these items can be seen in the system set-up diagram, figure 22. It is very important to note, that for the experiments discussed in this work, the transducers are positioned normal to the face of the plate which is under examination. However, some additional experiments were performed with the transducers at a ten degree incline. Material thickness, mechanical properties, and geometry are other very important factors for interpreting and modeling AU results.

The major concern with an experimental set-up, beyond instrumentation and proper electrical connections, is the proper positioning of the transducers. This involves where on the plate each of the transducers is placed, the uniform application of couplant, and placing proper pressure on each transducer. The AU method characterizes the material between the sending and the receiving transducer, where the sending transducer is pulsed to generate the excitation and the receiving transducer senses the disturbance at another position on the material surface. Hence, this method is concerned with characterizing a general region. First, the general size of this region is defined by the distance between the two transducers and the size of the active elements of the transducers. The distance between the transducers is defined by the variable d. Varying the value of d may be utilized to gain information on the characteristics of wave propagation. Secondly, the directional orientation of the transducers on the plate is an important parameter, especially when working with anisotropic materials. This is characterized by the azimuthal angle (θ), defined in chapter 2 (figure 3). Finally, the exact coordinates for the position or general area being characterized should be determined. For instance, the coordinates of the point directly between the transducers could be utilized. Hence, a coordinate can be defined to designate a general region and then the variables d and θ may be varied to obtain AU signals to characterize the given region. Most of the results presented in this work are meant to show representative results for an undamaged composite plate. Thus, the experiments were performed at the center of the plates, in order to minimize the effect of edges. Therefore, the results given in this work will not state coordinates for the position on the plate where the AU method was performed. However, in this work major emphasis is given to how varying d and θ affects AU results, leading to physical interpretation of the character of the wave propagation generated and measured with the AU method. Also, results are included that indicate how the transducer diameter a affects the AU signal. Additionally, consideration is given to how the resonant frequency of the transducers affects AU results.

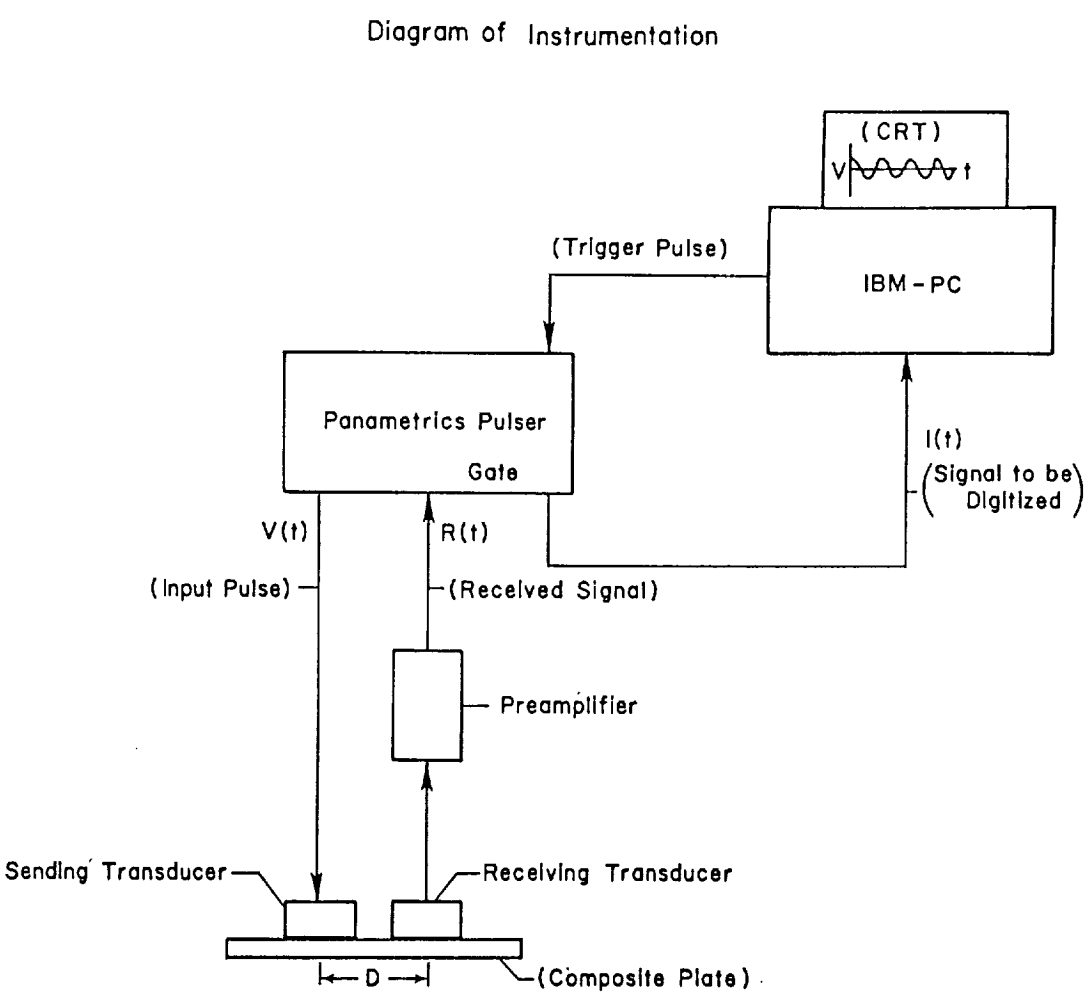

Figure 22. Experimental configuration

Experimental Set-up

The experimental procedure begins with the data acquisition board on the computer sending a trigger pulse to the pulsing unit. Upon receiving the trigger pulse, the pulser produces a high frequency electronic pulse, that passes to the sending transducer. The sending transducer converts the electronic energy of the pulse to a mechanical excitation on the face of the plate. This excitation induces wave propagation motion in the plate, that travels in the plane of the plate. The motion induced by this wave propagation is sensed by the receiving transducer, which converts the motion from the wave propagation to an electrical signal. This electrical signal is the source of signal analysis for the acoustic-ultrasonic method. First, the signal from the receiving transducer is amplified by a preamplifier. Then, the signal from the preamplifier is sent to the pulsing/receiver unit. The pulsing/receiving unit allows for high pass filtering of the signal, gating of the signal, attenuating of the signal, and further amplifying of the signal. The conditioned signal is then connected to an analog to digital (A to D) converter board in the PC by means of a BNC connector. The A to D board is triggered to start taking data by the same trigger pulse which is sent to the pulsing unit initiating the excitation pulse. Hence, the time of a disturbance in the signal relates to the time after excitation. The digital signal is displayed on the CRT screen in nearly real time, much as with an oscilloscope. This can be used to make immediate observations on time domain information. System software allows the signal to be frozen on screen and for spectral information to be obtained through an FFT on up to 512 points. A screen displayed gate, whose length and position in the time domain is keyboard controlled, is used for selecting the points to be used in the FFT. Finally, the signal can be stored for further analysis using keyboard control. Further analysis is performed using moment calculation software, such as was described in the second chapter.

Description of System Components

Pulser/Receiving Unit

A Panametrics model 5052 pulsing/receiving unit was used to provide the excitation pulse. The energy and damping settings allow some control of the pulse width and voltage. The exact relationship between these settings can be found in the reference manual (ref. 158). Four energy settings exist which allow the input amplitude to be varied between 100 and 300 volts (TYP), depending on the damping setting. The damping can be varied from 25 to 500 ohms. The pulse width varies between 10 to 600 nanoseconds, depending on the energy setting and damping. Increasing the energy setting or the damping causes the pulse width to increase. A high setting for both causes a drastic increase in pulse width which may decrease the signal input of high frequency energy and hence decrease the relative amount of high frequency content in the output signal. The receiving part of the unit offers the capability of amplifying the signal either 20 or 40 dB and attenuating the signal from 0 to 68 dB (with 2 dB increments). Also, the signal may be high pass filtered above 1 kHz, 30 kHz, 100 kHz, 300 kHz and 1 MHz. The upper cutoff frequencies are well out of the range of the other electronic components.

Preamplifier

A Panametrics ultrasonic preamplifier with 40 or 60 dB gain settings was used. The bandwidth for the preamplifier is .02 to 10 MHz. The purpose of the preamplifier is to amplify the signal from the receiving transducer, so that it is of proper amplitude for the receiving unit electronics. For the work reported in this dissertation, the preamplifier seemed to have little effect on results, besides amplifying the signal. However, if a battery operated preamplifier is used, care should be taken not

to let the batteries run low. In early experiments with battery operated preamplifiers, it was noted that amplitudes of AU signals decreased due to batteries losing power. The major concern with preamps powered from electrical outlets is making sure the power line is clean or isolated from noise in the working frequency range. The other major concern is that the signal is well inside the bandwidth of the preamp, again this had little effect on the results reported in this dissertation.

Transducers

Transducers are probably the most difficult part of the system to characterize and model. Research in this area is discussed in the literature search. In addition to the inherent difficulty of characterizing the response of the transducer, is the problem of understanding how the couplant transmits the pulse of the transducer to the material surface. This includes concerns with keeping the transducer properly oriented. For the tests performed, SONOTRACE 30[1] ultrasonic couplant was used. The couplant proved to be fairly viscous, so care had to be taken in applying the couplant evenly. Finally, the viscous nature of the couplant made it somewhat slow in flowing into the ridges left by the scrimcloth. Hence, care was taken to allow ample time, or atleast consistent time, for couplant flow before performing AU measurements.

Although a number of transducers were utilized in the experimental work conducted, the experimental results presented in this dissertation were obtained using two pairs of Panametrics piezoelectric transducers. Both pairs are 2.25 MHz center frequency broadband, heavily damped, transducers. Figure 24 shows the frequency response of the half inch transducer, obtained by a pulse echo test on a large aluminum block. Even though the transducer is broadband, there is a very definite frequency dependent response associated with the transducer. Efforts to try to account for the frequency dependent response of transducers are covered in reference 10. Figure 23 compares the AU frequency responses obtained on the same specimen using a 5 MHz and a 2.25 MHz

1 Trade Mark of Echo Ultrasound, Inc.

resonant transducer, respectively. Notice, that the 5 MHz transducer actually caused more energy to be present in the second specimen resonance (3.4 MHz) than the first (1.7 MHz). In comparison, the 2.25 MHz transducer had most of its high frequency energy in the first specimen resonance (1.7 MHz). Thus, AU results are extremely sensitive to the transducer's frequency response.

The major transducer used to produce the subsequent experimental results was a 2.25 MHz (V105) broadband transducer with a half inch diameter active element. However, a couple of measurements were made with similar (V166) transducers, containing a quarter inch diameter active element. The half inch diameter transducers were used to measure energy and attenuation, and the quarter inch transducers were used to measure certain phase velocities and to determine the effect of source size.

Couplant was applied both to the specimen and the transducer before placing them in contact. Then the transducer and specimen were pressed together with uniformily distributed pressure and then weights were applied. Two pound weights were used to apply pressure to the transducers. For some experiments, such as phase velocity measurements, the transducers were not weighted and the transducers were simply pressed by hand and moved slowly over the material surface. A Proctor transducer (ref. 155) was used simply to gain an increased understanding on the effect of source size.

Data Acquisition

Signal observation and storage was performed using PC-DAS, a data acquisition system marketed by General Research Corporation to be used with the IBM-PC. PC-DAS utilizes a PCTR-160 A/D board and control software to provide flexible, easy, and high data rate signal capture. The PCTR-160 allows sampling rates from 156 KHz up to 20 MHz in transient mode and sampling rates of 40, 80, and 160 MHz in the time equivalent sampling mode which can easily be utilized

a)

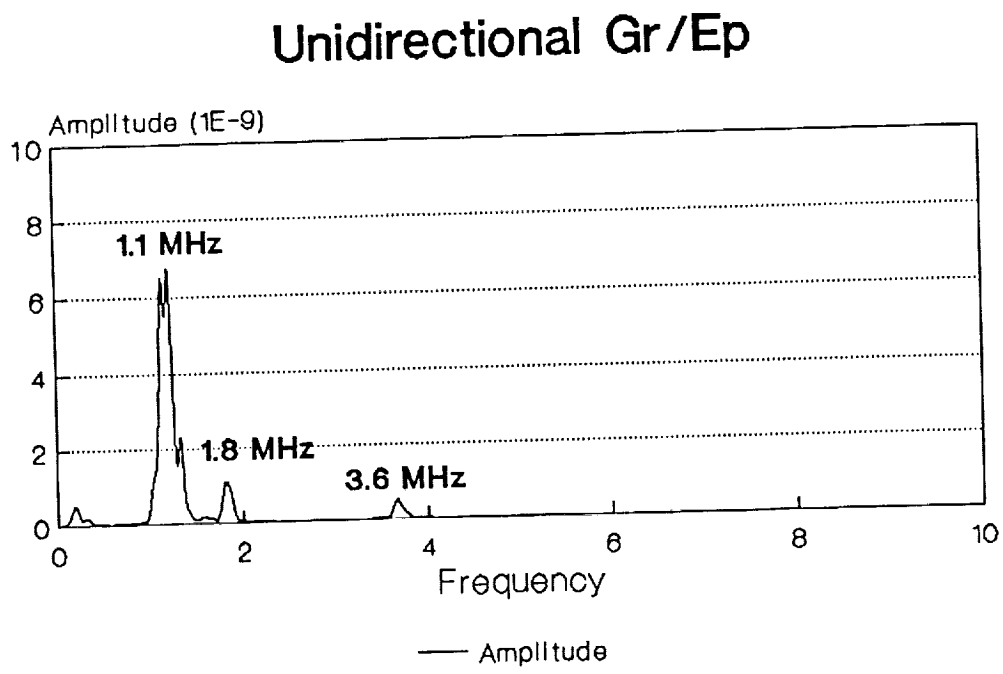

2.25 MHz transducers

b)

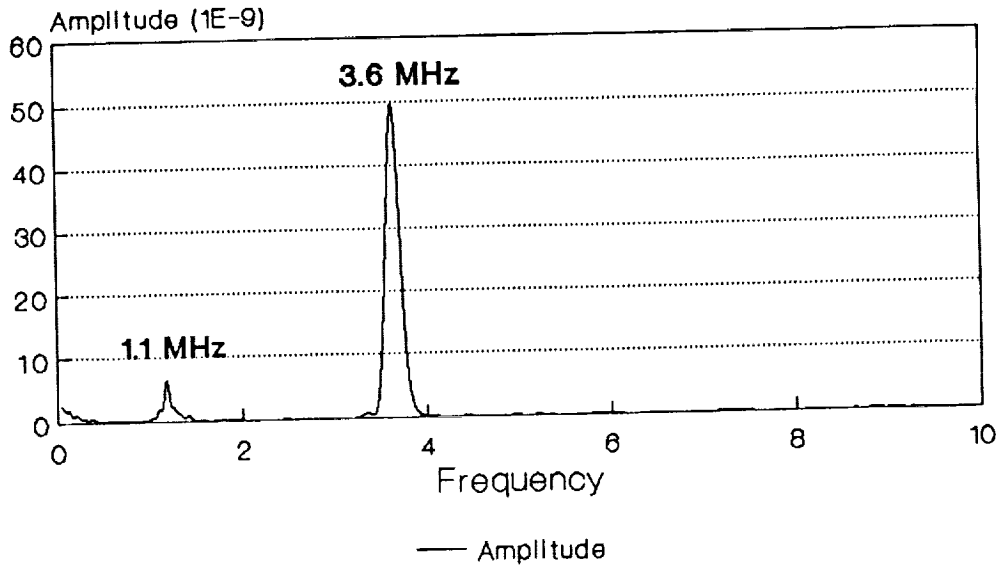

5.0 MHz transducers

Figure 23. Comparison of AU signal from a)2.25 and b)5.0, MIIz transducers

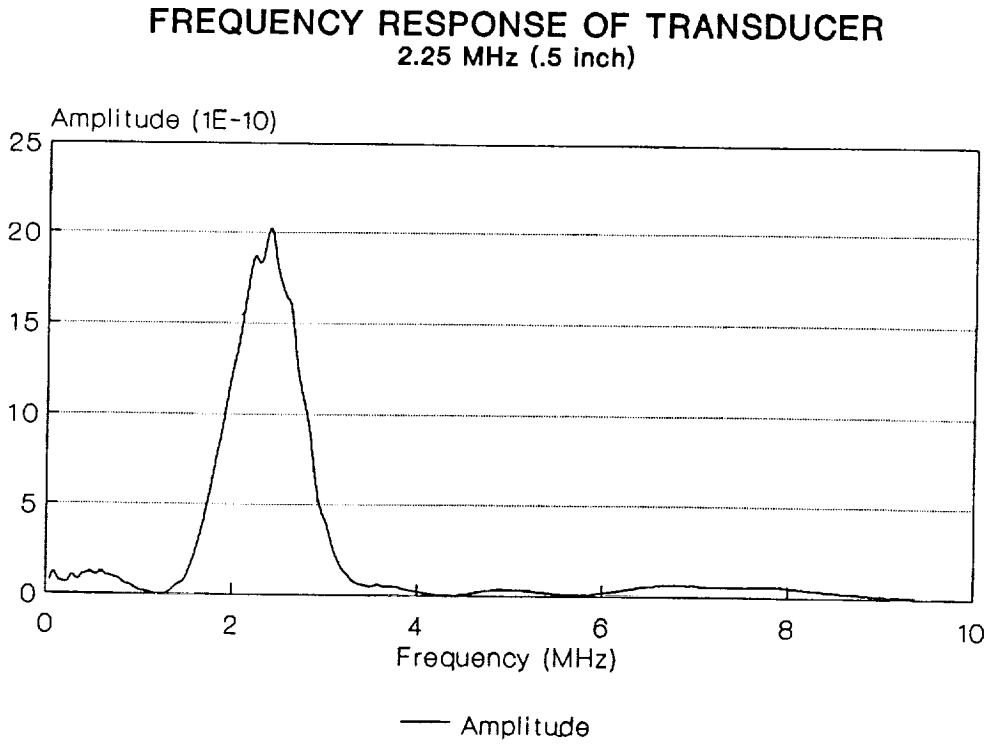

Figure 24. Frequency response of 1/2 inch (2.25 MHz) transducer

with the AU arrangement. However for the frequency ranges generated with the AU system and specimens, the 20 MHz sampling rate proved to be adequate.

The signal can be displayed so that the whole signal (4096 points) appears on screen or in expanded form so that a detailed view of 1/12th of the signal is displayed. The signal can then be frozen and a gate which is movable in the display can be used to make exact time measurements, since the numerical value corresponding to the position of the gate in the time domain is displayed on screen to the resolution of the digital data. This feature of the data analysis software was used to measure phase velocities by tracing the exact placement in the time domain of a phase point when the transducers are moved (ie. d is changed). The value Δt was determined by tracing a phase point on the CRT and Δd by measuring the displacement of the transducer on the specimen, then the phase velocity was calculated

$$v_{ph} = (\Delta d)/(\Delta t)$$

As mentioned, this gate can also be used to select up to 512 points for spectral analysis which is displayed on screen, thus giving immediate information on the frequency content in a specific portion of a signal. Again a keyboard controlled marker may be used on screen with screen displayed numerical values to gain exact information on frequency content. Thus, as experiments are performed quantitative information on both the time domain and frequency domain may be ascertained. Software then allows the digital data and sampling parameters to be stored in a data file for further analysis.

Software Analysis of AU Signal

In order to obtain more physically significant signal description parameters, signal analysis software has been developed. The program used to generate results for this work is a third generation Lahey

Fortran version (ref. 131) of the program described in chapter 2. This program utilizes the same theory and equations stated in that discussion. This version of the program allows for the calculation of the same parameters, utilizing the Hartley transform for faster calculation of amplitudes of frequency components.

Figure 25 shows a block diagram of data transfer to get various results and the use of batch files to create data files in order to show how AU values vary with another parameter (eg. azimuthal angle).

First, data files must be converted to ASCII format, so that data can be read to plotting and moment analysis software. For purposes of example, let (file) stand for any group of data files created using PCDAS and (###) stand for the incremented number representing one data file in the set. If a number of files with the same data name (ie. file###.dat), but incremented numbers, need to be converted, then a batch file can be created to convert files. This batch file can be created using the Basic software program (conbat.bat). This automatically gives the file name of the batch file the same name as the prefix for the data files and the file type (con). Thus, when the program (convert.exe) asks for the batch file: type-(file.con). Next, batch files can be created for Fortran files by using the Basic program (forbat.bas). This yields a batch file named (file.fat). Then another Fortran program (mitt.exe) can be used to obtain voltage/time data and amplitude/frequency data, and another Fortran program (mike2.exe) to obtain AU parameters for all data files and then store them in a single file, which can be named by the user. The data files for the voltage/time and amplitude/frequency data is ready for use with standard plotting packages. The output file from (mike2.exe) can be manipulated by another Fortran program to generate data sets for graphic packages. For instance, the program (aupa.bas) reads each value for A1, A2, and two filtered A1 parameters, pairs them with the corresponding values of θ and d to produce a number of data sets. However, this program can only be used if data is taken in the proper order for the proper angles (θ) and distances (d). The following data sets are produced:

A1 versus azimuthal angle (at $d = 1$ and $d = 2$ inches)

Attenuation of A1 versus azimuthal angle between 1 and 2 inches

A2 versus azimuthal angle (at $d = 1$ and $d = 2$ inches)

A1(f1,f2) versus azimuthal angle (at $d = 1$ and $d = 2$ inches)

Attenuation of A1(f1,f2) versus azimuthal angle between 1 and 2 inches

A1(f3,f4) versus azimuthal angle (at $d = 1$ and $d = 2$ inches)

Attenuation of A1(f3,f4) versus azimuthal angle between 1 and 2 inches

The f1 and f2 are simply the low and high frequencies for the first filter, while f3 and f4 are the low and high frequencies, respectively, for the second filter. These data sets may then be graphed using plotting routines.

Graphs of these results for a number of plates are included in chapter 4. These results along with the phase velocity measurements offer a great deal of physical insight on the nature of wave propagation taking place during the AU method. Additionally, advances in analytical ultrasonics (instrumentation and calculation schemes) may allow angular variations of pertinent AU parameters, such as these, to be obtained quickly, in order to determine increased information on the condition of composite materials being used in service conditions.

Experiments

Although a myriad of experiments have been performed in pursuit of a better understanding of the AU method, discussion will be limited to a simple set of experiments performed to understand and elucidate the basic mechanics associated with the AU method. The experiments involve using

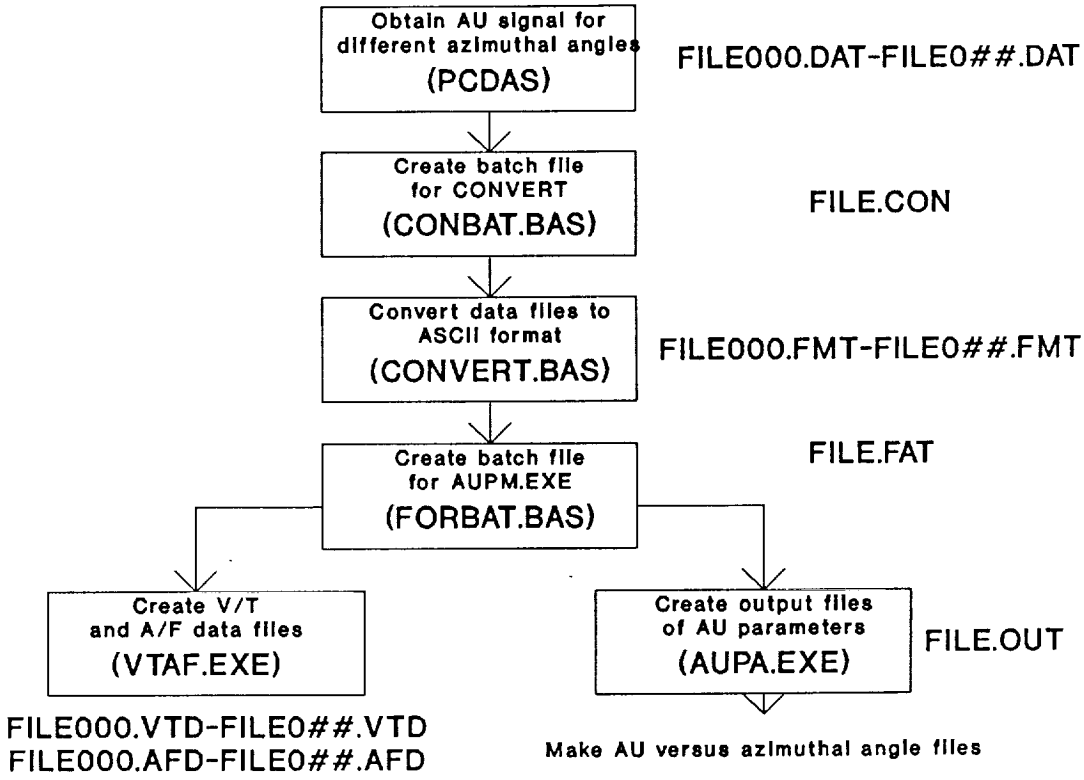

Figure 25. Diagram of AU data flow to obtain various output

aluminum plates and a number of Gr/Ep plates. This experimental work endeavored to systematically examine the general character of wave propagation occurring when the AU method is performed. These experiments were performed using the experimental arrangement described previously. The following specimens were utilized:

.0625 inch thick aluminum plate (6061-T6)

.125 inch thick aluminum plate (6061-T6)

An aluminum plate tapered from .0625 section to .125 section (see figure 26) (6061-T6)

24-ply unidirectional Gr/Ep plate (AS-4 Gr/Pr 288)

12-ply unidirectional Gr/Ep plate (AS-4 Gr/Pr 288)

Experiments were performed to produce both qualitative and quantitative information on the AU method. Some experiments involved performing very mechanized steps to obtain specific measurements, while others involved less rigorous steps. In general, a different set of experiments were performed for each specimen, however a number of experiments were performed on more than one specimen. Thus, a description of general experimental procedures is given first and then each specimen is considered separately, with more detailed descriptions of experiments performed only on that specimen.

General Procedures

The basic quantities measured in this set of experiments are A1, A1(filtered), A2, attenuation, and estimated phase and group velocities.

The measurement of AU parameters and attenuation is quite simple and is the basis of the AU method. The standard AU configuration described above was utilized, with transducers oriented normal to the plate. In order to obtain the attenuation measurements, the AU method was performed at both $d = 1$ and $d = 2$ inches. It should be kept in mind that the attenuation measurement was done only for material intervals between 1 and 2 inches from the sending transducer in this set of experiments and is likely to be quite different for another choice of d's, even though their difference may still be 1 inch. For the composite plates, these measurements were made at azimuthal angles of 0, 15, 30, 45, 60, 75, and 90 degrees. Phase velocity is measured for a single frequency content to determine the phase velocity for that particular mode. This procedure involved simply tracing the displacement of a phase point (usually a peak in harmonic function of single frequency), for a given displacement of transducers on the plate. The measurement of phase velocities was more difficult than measuring AU parameters and required a more artful experimental technique (trial and error, inorder to fully separate different harmonic modes). In certain cases, the signal content did not facilitate the measurement of a phase velocity for a particular mode. Specifically, in the composite plates , certain frequencies were of such a small amplitude for certain azimuthal angles that phase velocity measurements were impossible. The measurement of phase velocities were again made for different frequency contents at various azimuthal angles, however, in certain cases, the phase velocities varied from measurement to measurement. Even more difficult was the measurement of group velocity for a particular mode or frequency content. Often, these values turned out to be impossible to measure exactly, however, estimates were made to provide qualitative results about AU wave propagation. Estimates of the group velocity entailed defining a modulating hump for a certain frequency content and noting how far it translated in the time domain for a change in d. Thus, the measurement of group velocity, simply involves the motion of the wave modulating term.

The AU parameters and the attenuation measurements were made with the conventional AU configuration. For all plates, besides the tapered aluminum plate, the sending transducer was placed at the center of the plate. AU measurements for any direction were made for $d = 1$ and $d = 2$

inches. For the aluminum plates, the AU measurement were only performed in one direction. For the composite plates, fudiciary lines were drawn for azimuthal angles of 0, 15, 30, 45, 60, 75, and 90. These were drawn from the center of the plate, where the sending transducer was positioned. The receiving transducer was initially placed at $\theta = 0$ degrees and $d = 1$ inches. Then, the receiving transducer was moved to $d = 2$ inches. Next, the receiving transducer was moved to $\theta = 15$ degrees and $d = 1$ inch. The sending transducer was kept at the same spot (center of the plate), however it was rotated 15 degrees, as was the receiving transducer. This was done to eliminate any effect of unsymmetric or misaligned transducer elements. Next, the receiving transducer was moved to $d = 2$ inches. The same procedure was continued, ending with $\theta = 90$ and $d = 2$ inches. All measurements were made with the weights on the transducers.

Specific Experiments

This section will simply catalogue the particular experiments performed on each specimen. The experimental procedures described above will only be referenced and will not be described in detail again.

Aluminum Plate (.0625 inches thick)

Aluminum plates were utilized to obtain basic information on the nature of wave propagation occurring in plates when the AU method is performed. As a first step, the aluminum plates offered a more simple situation than the composite material because of the readily available material properties and their nomially isotropic behavior.

First, a basic AU measurement at one inch was performed to determine the components present in the signal. Then the procedure to obtain the AU parameters and the attenuation factors was performed. Phase velocity and group velocity measurements were made for each frequency

conponent in the signal that was of sufficient amplitude. A simple pulse echo test was also performed using the .25 inch diameter sending transducer.

Several additional experiments were performed to determine the effect of changing certain variables. First, the AU method was performed with the two .25 inch diameter transducers to determine the effect of transducer size, and, one test was performed with a 5 MHz set of transducers to determine the effect of transducer resonance frequency. Also, a simple test was performed using the Proctor transducer. Finally, a test was performed to determine the effect of tilting the sending transducer slightly. Basically, this was done by applying an extra thick portion of couplant under the sending transducer and then tilting the transducer to approximately 10 degrees to determine the effect on the frequency content of the signal. The tilt was oriented away from the receiving transducer (see figure 26).

Aluminum Plate (.125 inches thick)

Experiments similar to those performed on the .0625 inch thick plate were performed on a thicker (.125 inch thick) plate. These experiments were done in order to determine the effect of specimen thickness on AU results.

Composite Plate (24-ply unidirectional Gr/Ep)

A number of measurement were made on a 24-ply unidirectional Gr/Ep plate. The composite plate allowed for the investigation of the effect material variation with azimuthal angle has on AU results.

First, basic AU measurements were made to determine what frequencies were present in the signal. Next, the procedure for determining AU parameters and attenuation factors was carried out for each azimuthal angle. Then, the phase velocities of various frequency components were measured for

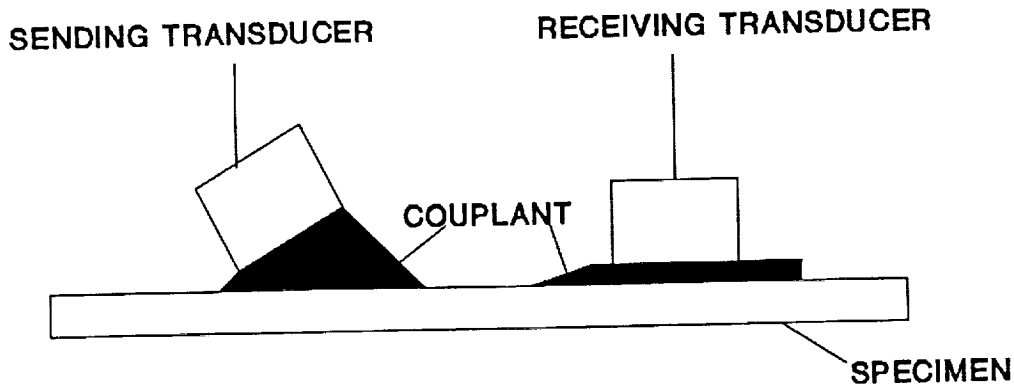

Figure 26. Experiment to determine the effect of transducer tilt

each azimuthal angle possible; also, group velocities were measured when possible. A basic pulse echo experiment was also performed. Finally, basic tests were performed to determine the effects of using .5 inch diameter transducers and 5 MHz transducers.

Composite Plate (12-ply unidirectional Gr/Ep)

In order to determine the effect of plate thickness with composite plates, a 12-ply unidirectional plate of the same material used to make the 24-ply plate was investigated. The same tests were performed on both the 12-ply plate and the 24-ply plate.

Tapered Aluminum Plate

A tapered aluminum plate (fig.27) was investigated to gain more insight into the physics of how waves detected with AU measurements are created. This type of experimental work may also be useful in developing a basic understanding of the AU method applied to complex structures.

First, AU signals were generated in each of the flat portions of the plate, well away from the tapered region. This was done to determine what frequencies were being generated in each region. Next, the sending transducer was placed in the .0625 inch thick section, an inch from the taper, and the receiving transducer was placed in the .125 inch thick section, 6 inches from the sending transducer. An AU signal was then captured in this configuration. Next, the same procedure was performed with the sending transducer in the .125 thick section and the receiving transducer in the .0625 inch thick section.

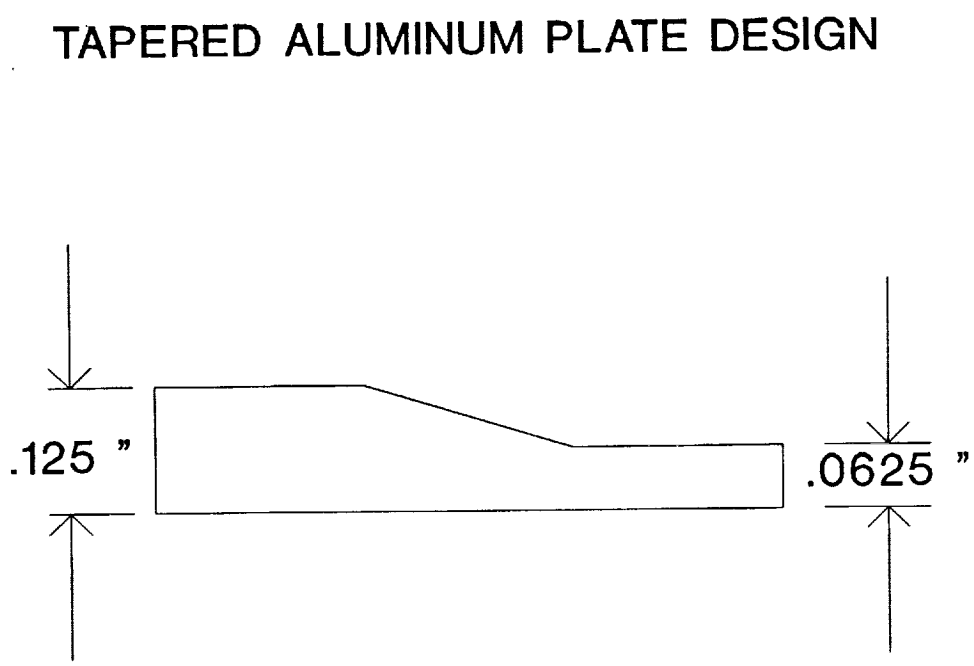

Figure 27. Design of tapered aluminum plate

Experimental Results

The experimental procedure described in the previous chapter revealed definite trends and a number of results useful for understanding the AU method. This chapter will present these results.

General Comments

AU signals generated in this set of experiments showed wavetrains with components at very definite frequencies for a given plate. Observing the amplitude/frequency curves generated by these experiments illustrates this with sharp peaks at definite frequencies (e.g. see figure 38). Furthermore, these components are separable in the wavetrain by separating the transducers further apart, as a result of dispersion. This results in harmonic components which show very definite peaks and troughs (harmonic behavior) and which translate across the time domain if the receiving transducer is translated relative the sending transducer. However, in some instances the amplitude of a given phase point will change quickly due to a small change in distance, this is thought to be an effect of a slow group velocity modulation. Figure 28 shows an AU signal obtained with the transducers on a composite plate and $d = 1.0$ inches.. Notice that there seems to be a periodic modulation of

the signal. Figure 29 shows a signal obtained from the same plate with $d = 2.0$ inches. This shows how the modulation and phase points shift. This can make the measurement of phase velocity more tricky. Additionally, notice that the shape of the modulation changes.
Basically, results indicate that frequency components are present in the signal, that they separate in the time domain when the transducers are separated, and that phase points can in some instances be picked out to make phase velocity measurements. It is observed that some phase velocity (motion in the time domain for motion in the spatial domain) is associated with these motions and that, as mentioned, for certain modes, a group velocity is modulating the harmonic components.

For the composite plates, it is evident that the same frequencies are present at all azimuthal angles, but that the proportions of each frequency content changes drastically with azimuthal angle. In fact, for some azimuthal angles, certain frequency components were of such small magnitude that velocity measurements were not possible. Furthermore, it is quite obvious that the energy content in the signal is heavily influenced by changes in azimuthal angle, as is the position of certain components of the wave train in the time domain. In order to quantify the change of wave motion with azimuthal angle on composite plates, the behavior of AU parameters and wave velocities of a certain harmonic component of the signal were monitored as a function of azimuthal angle.

Aluminum Plate (.0625 inches thick)

The signals and corresponding spectrums generated by performing the AU method on the .0625 inch thick aluminum plate at $d = 1$ and $d = 2$ inches are shown in figs. 30 and 31. Figure 32 shows an expanded view of the early portion of the signal obtained by performing the AU with $d = 1$ inch. From this plot it is evident that certain phase points may be identified for a given harmonic component in the signal.

Notice that the major components in the signal were at .7, 1.0, and 2.0 MHz. The very early part of the signal consisted of a small amplitude .7 MHz signal content. This part of the signal was of

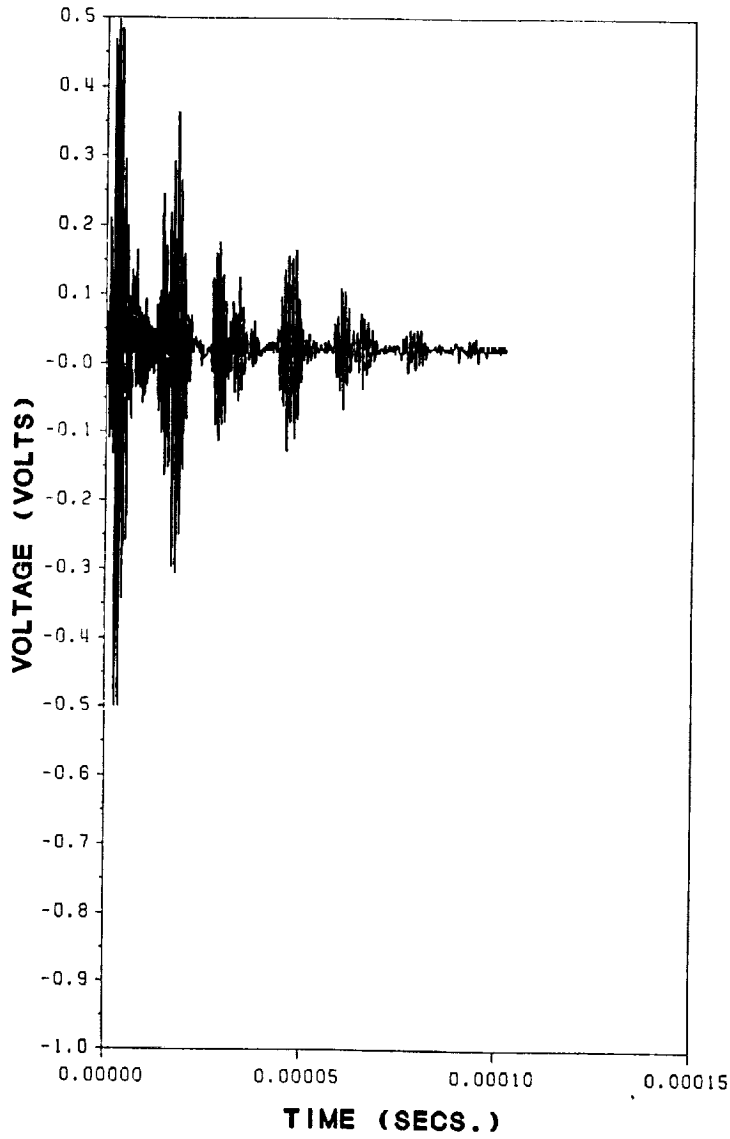

Figure 28. AU signal obtained from Gr/Ep specimen (d = 1 inch)

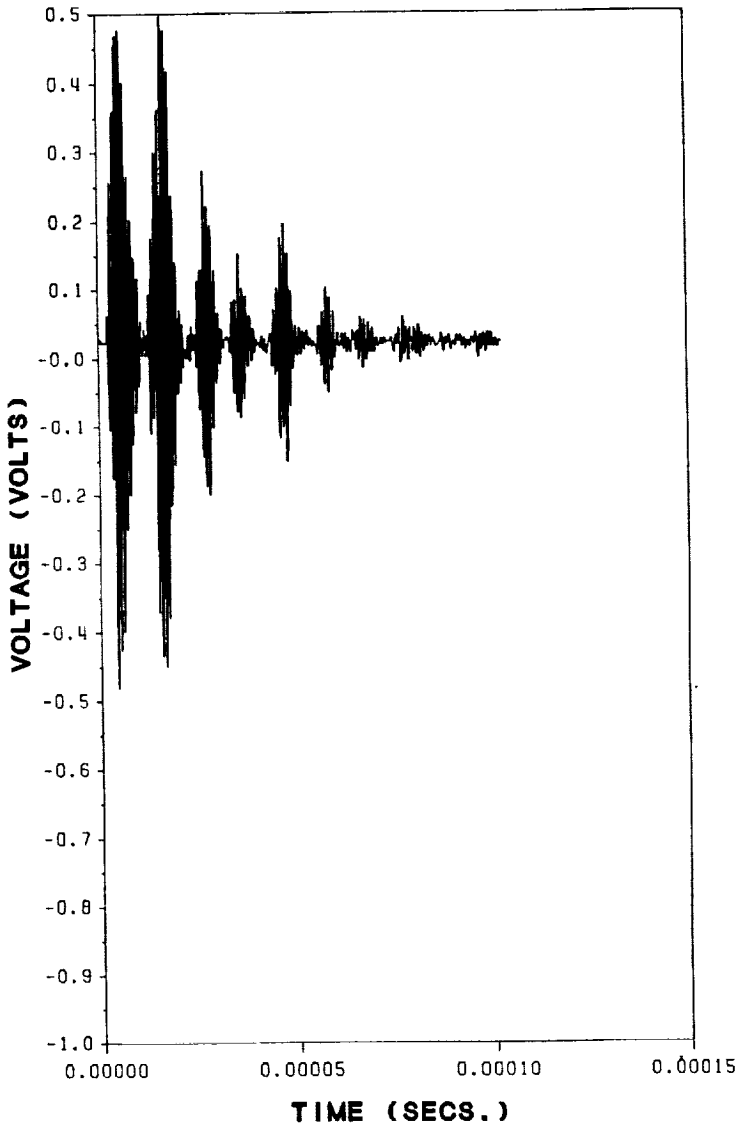

Figure 29. AU signal obtained from Gr/Ep specimen (d = 2 inch)

a)

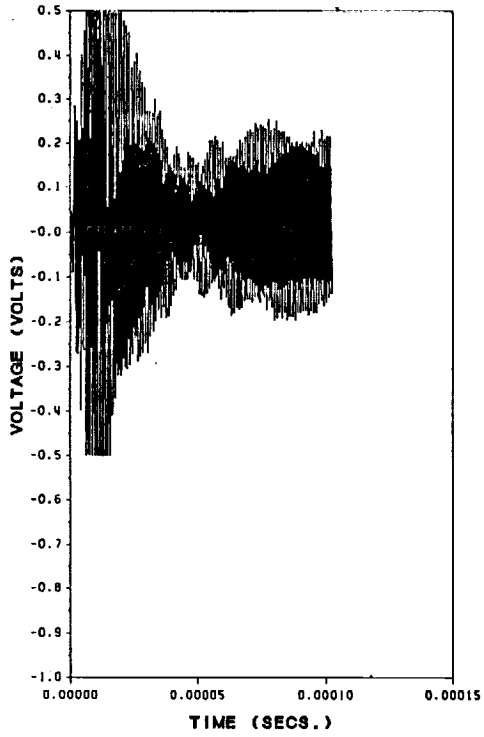

b)

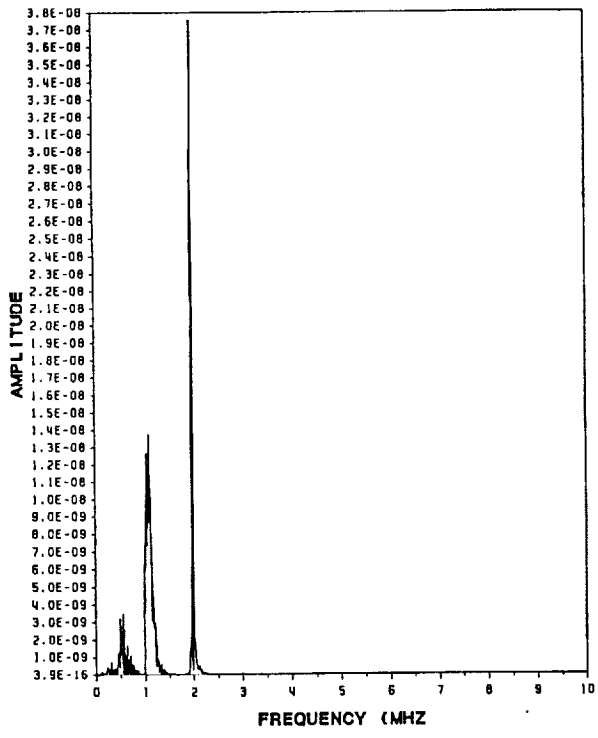

Figure 30. a)V/T and b)A/F, plots for aluminum plate (d = 1") (.0625" thick)

a)

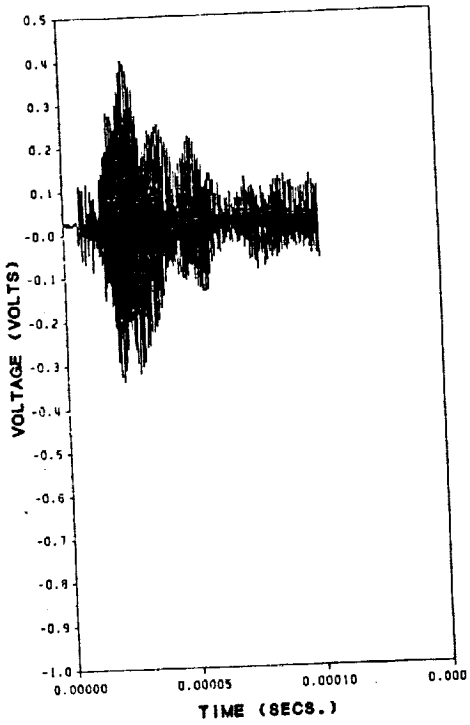

b)

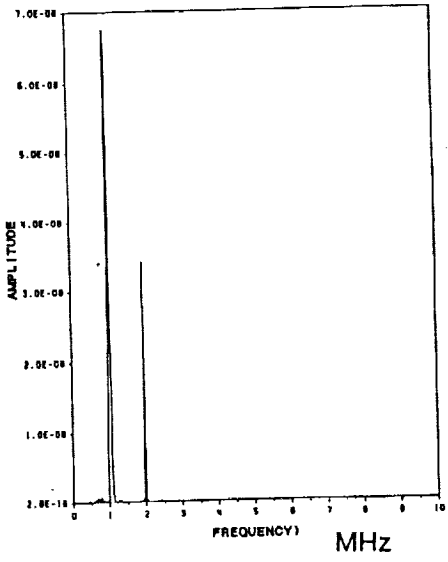

Figure 31. a)V/T and b)A/F, plots for aluminum plate (d = 2″) (.0625″ thick)

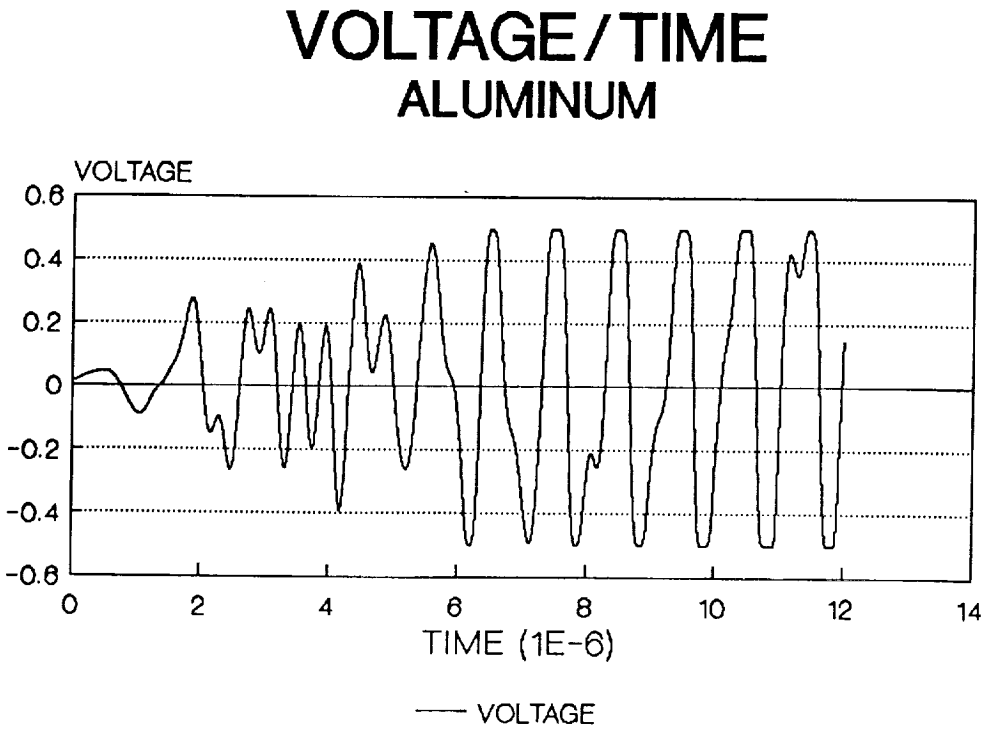

Figure 32. Expanded view of portion of voltage/time plot

very short duration (5 μsecs.), which is on the order of the pulse duration. Additionally, the .7 MHz portion of the signal was of relatively low amplitude. The following parts of the signal consists of the 1 and 2 MHz components. These portions of the signal were of considerably higher amplitude and persisted much longer in the wave train. In figures 30 and 31, the large contribution of the 1 and 2 MHz components is evidenced by the large amplitude peaks. Thus, the frequency spectrum shows larger peaks at 1 and 2 MHz and the resulting energy content or filtered AU parameters are larger. In comparing the .7 MHz component to the 1 and 2 MHz components, see (fig. 30 and fig. 31 (chp. 4)), it should be noted that the 2 MHz showed a large sharp modulation hump that travelled at a much slower velocity than phase points, compared to the 1 MHz which did not show as definite of a modulation hump and the .7 MHz which showed no dispersive effects. Another point to be noted is that the 2 MHz signal content dominated the end portion of the wave train, indicating a slow group velocity. Note, also that the 1 MHz peak in the amplitude/frequency is of a wider frequency band and is skewed to the right. A modest indication in the spectrum also appears at 2.3 MHz. Figure 33 shows the relative energy content in each of the frequency ranges for the signal at $d = 1$ and $d = 2$ inches. This figure also shows the attenuation of each mode between 1 and 2 inches. The 2 and the 1 MHz components of the signal were of fairly comparable amplitude at 1 inch, but the 2 MHz component was significantly more attenuated than the 1 MHz content. One problem with these measurements is that the long wavetrain associated with the signal was longer than the data recording capabilities of the system and the end part of the wavetrain interacted with edge reflections. The .7 MHz portion of the signal separated from the rest of the wave train (due to higher group velocity) and appeared less attenuated.

Finally, figure 37 displays a chart of the phase velocity for each frequency component of wave motion. Phase velocity measurements were not possible for the 2.3 MHz signal content because these components never really separated from the other frequency components which were of higher amplitude. Notice that the 2 and 1 MHz components had substantially higher phase velocities than the .7 MHz component. It should be noted that the phase velocity for the 1 MHz component was found to be slightly greater at the end of the signal than at the beginning. In gen-

AU PARAMETERS

.0625 inch thick aluminum plate

VARIABLE	1 INCH	2 INCH	2 INCH / 1 INCH
A1	.16E-1	.49E-2	.31
A2	.78	.59	.76
A1(.5,.8)	.13E-3	.68E-4	.52
A1(.8,1.2)	.72E-2	.40E-2	.56
A1(1.8,2.2)	.85E-2	.83E-3	.10

Figure 33. AU parameters for .0625 inch thick aluminum plate

eral, phase velocities showed variation as a function of position in the wavetrain. Measurements were made on the earliest part of the wavetrain, where the mode on which the phase velocity was being made, was separated from other modes enough, so that definite phase points for that mode could be traced.

Group velocity measurements were difficult to make for the aluminum plate. However, it was noted that the .7 MHz signal content moved at a group velocity similar to its phase velocity. In contrast, it was estimated that the 1 MHz signal content had a group velocity of roughly 60,000 inches per sec. and that the 2 MHz signal content was roughly 65,000 inches per sec., however the end portion of the signal was dominated by a 2 MHz signal content of a slow group velocity. It should be noted that these measurements were made for components of the signal early in the wavetrain. Moreover, another point of interest is the rather large value of the measured phase velocity compared to the rather small value of estimated group velocity for the 1 and 2 MHz components. In general, the 2 MHz signal content showed a greater phase velocity than the 1 MHz, but contained a slow group velocity portion at the end of the wavetrain.

Tilting the sending transducer, so that its face was not parallel to the face of the plate, resulted in an increase in the value of the frequencies for the peaks in the spectrum. Additionally, changing the transducer size from .5 to .25 inches in diameter had little effect on the 1, 2, and 2.3 MHz components, but caused the .7 MHz (early arriving part of the wavetrain) to change to .5 MHz. Lastly, the Proctor transducer also caused peaks in the spectrum from the signal to occur at 1,2, and 2.3 MHz. Thus these frequencies are excited by a number of different transducers.

Aluminum (.125 inches thick)

Figure 35 shows the voltage/time and amplitude/frequency plots for the .125 inch thick plate. The signal content consisted of .35, .5, 1.0 and 1.15 MHz components.

PHASE VELOCITY MEASUREMENTS

.0625 inch thick aluminum plate

FREQUENCY	PHASE VELOCITY
.7 MHz	210,000
1.0 MHz	620,000
2.0 MHz	1,000,000 +

Phase velocity measurements are in (inches per second)

Figure 34. Phase velocity measurements for .0625 inch thick aluminum plate

a)

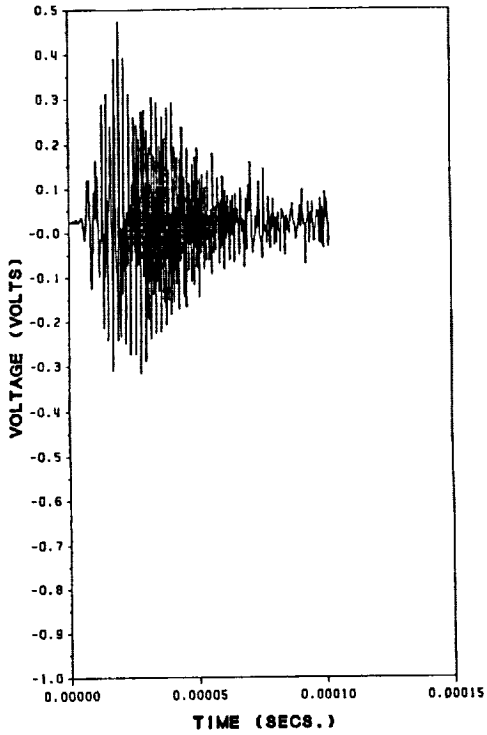

b)

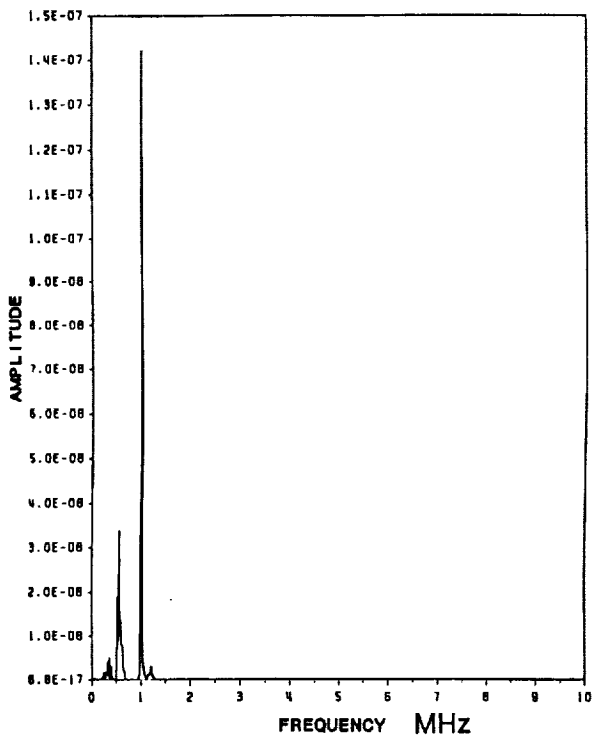

Figure 35. a)V/T and b)A/F, plots for .125″ thick aluminum plate

In general, the signal consisted of a spectrum with major peaks at frequency values half that of the .0625 inch thick plate. In fact, the signal was very similar to that of the signal obtained on the .0625 inch thick plate, except that the frequency of each mode identified in the signature was half. The comparison of the AU values for these components can be seen in figure 36. Notice that the 1 MHz component is the highest energy content part of the signal for $d = 1$ inch and is the most heavily attenuated part of the signal. In fact, the 1 MHz signal content is roughly twice as attenuated as the .5 MHz signal content.

Figure 37 displays the values of the phase velocities for the .125 inch thick plate. The phase velocity for the 1 MHz mode on .125 inch thick plate is the same as the 2 MHz mode on the .0625 inch thick plate, and so forth for the other modes. Thus, it appears that phase velocities were similar on the .125 inch plate and the .0625 inch plate.

Group velocity measurements were much less than the phase velocity measurements for the .5 and 1.0 MHz components, a result that is similar to that obtained for the .0625 inch thick plate.

24 Ply Gr/Ep Plate (Unidirectional)

Although a number of frequency components existed in the 24-ply plate, the dominant frequency components present at each azimuthal angle where at .23, .66, and 1.1 MHz. Each of these components varied in a unique manner with azimuthal angle. Figure 38 shows a representative signal and amplitude/frequency plot obtained with $d = 1$ inches and an azimuthal angle of 0 degrees. This signal is very representative of the signal in the zero degree direction for Gr/Ep plates. The signal shows a definite high amplitude part of the signal at an early arrival time (predominately .66 MHz), followed by a small portion of predominately 1.1 MHz signal content, and a late part of the signal dominated by .23 MHz signal content. Each of these frequency peaks is labeled in the amplitude/frequency plot (also in figure 38). The amplitude/frequency plot shows that higher fre-

AU PARAMETERS

.125 inch thick aluminum plate

VARIABLE	1 INCH	2 INCH	2 INCH / 1 INCH
A1	.12E-1	.55E-2	.45
A2	.50	.41	.82
A1(.3,.4)	.19E-3	.18E-3	.95
A1(.4,.6)	.16E-2	.14E-2	.88
A1(.8,1.2)	.81E-2	.32E-2	.40

Figure 36. AU parameters for .125 inch thick aluminum plate

PHASE VELOCITY MEASUREMENTS

.125 inch thick aluminum plate

FREQUENCY	PHASE VELOCITY
.35 MHz	215,000
.50 MHz	620,000
1.0 MHz	1,500,000 +

Phase velocity measurements are in (inches per second)

Figure 37. Phase velocities for .125 inch thick aluminum plate

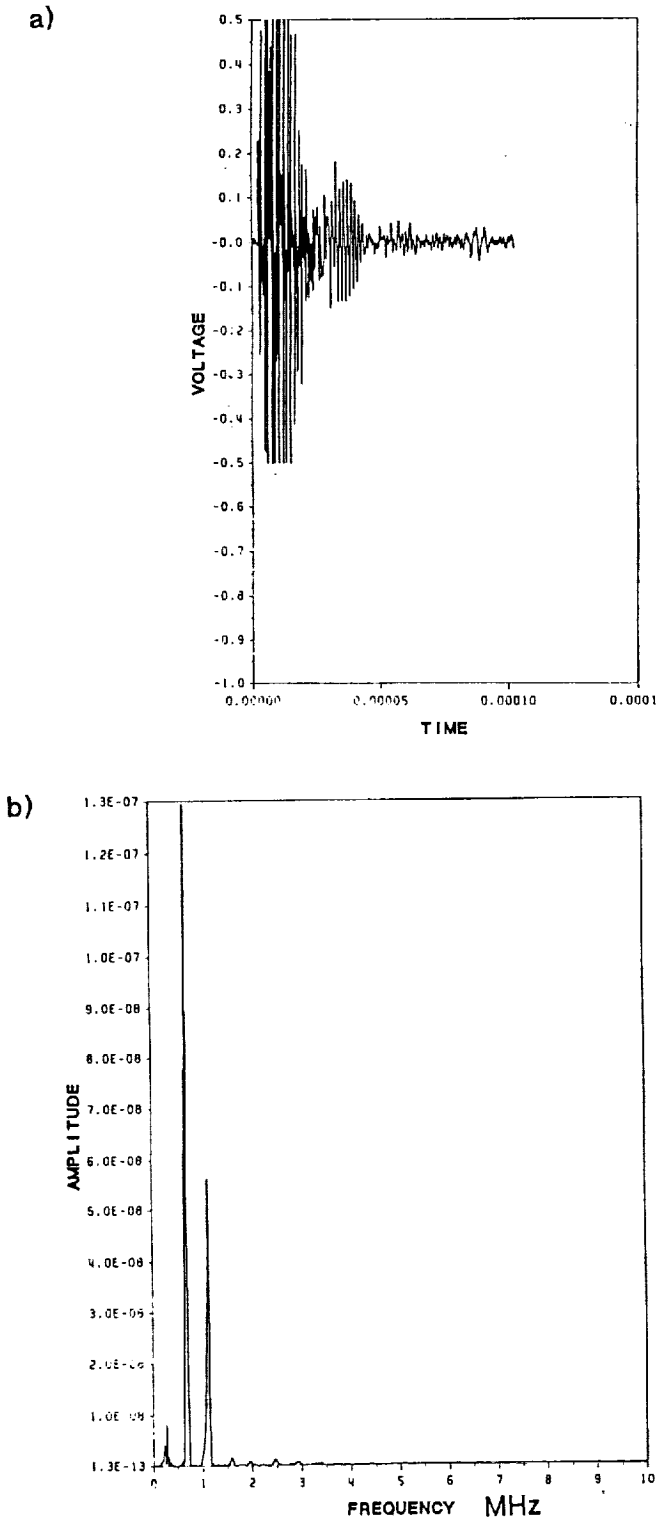

Figure 38. a)V/T and b)A/F, plots for Gr/Ep plate (24-ply, unidirirectional)

quency peaks were in the signal for the 0 degree direction and $d = 1$ inch, but most other measurements do not show these frequency peaks.

The signal obtained at $d = 2$ inches showed the same signal content, but the early portion of the signal was greatly distorted. At 15 degrees the 1.1 MHz signal content was of higher relative magnitude compared to the other components than at other azimuthal angles. This type of behavior has been seen in previous results (refs. 9 and 99). Moving the transducer to $d = 2$ inches at 15 degrees resulted in a great deal of attenuation in the AU signal. As the azimuthal angle was increased, the .23 MHz signal content began to dominate the signal. In fact, at higher angles the other components became very hard and in some cases impossible to pick out of the signal. The effect of d and azimuthal angle on AU results can be seen in figures 39-45.

The plots of A1 and the attenuation of A1 versus azimuthal angle (figure 39) shows how the energy content and attenuation were affected by changes in azimuthal angle. Notice the AU signal was of high energy for 0 degrees and dropped off to a fairly constant value. This behavior is very similar to that shown for the Gr/Ep unidirectional shown in chapter 2 (fig. 13). Additionally, the highest attenuation of the AU signal was at 15 and 90 degrees.

The plot of A2 versus azimuthal angle (figure 40) shows that the high frequency content of the signal drops off at roughly 45 degrees to a value almost half that seen at early angles. This is due to the .23 MHz signal content becoming more dominant than the higher frequency content for higher angles.

For the .23 MHz signal content, A1(.15,.32) and A1(.15,.32)-ATTEN. were plotted versus azimuthal angle (figure 41). For $d = 1$ inches the A1(.15,.32) is slightly high in the 0 degree direction and very high for 90 degrees. In fact, the AU signal in the 90 degree direction showed an almost perfect sine wave pattern at .23 MHz throughout the wave train, with very little modulation (see figure 42). Heavy attenuation of the .23 MHz signal content occurred at 90 degrees and as a

a)

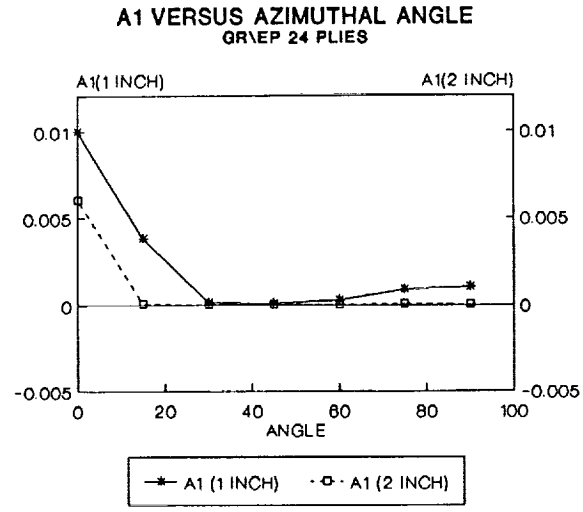

b)

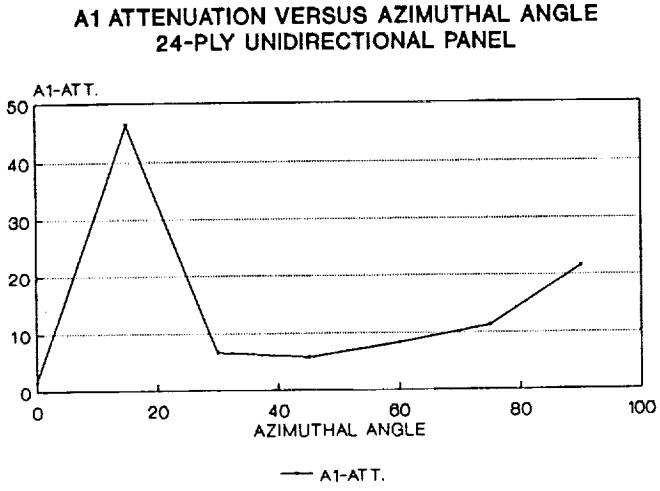

Figure 39. a)A1 and b)A1-ATTEN. versus azimuthal angle for Gr/Ep plate

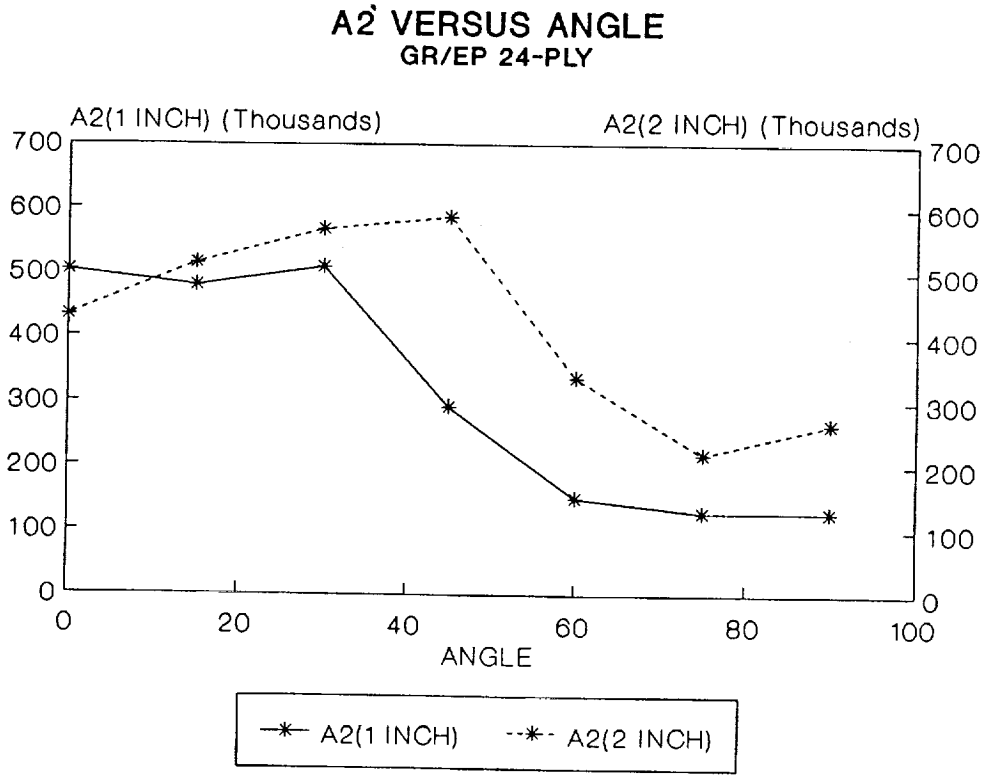

Figure 40. A2 versus azimuthal angle for Gr/Ep plate

result the A1(.15,.32) for $d = 2$ inches is rather flat and does not curve back up as does the curve for $d = 1$ inches.

Figure 43 shows how A1(.55,.75) for $d = 1$ and $d = 2$ inches and A1(.55,.75)-ATTEN. vary with azimuthal angle. At low angles A1(.55,.75) varies much like A1, since the .66 MHz content dominated the signal. However, at high angles the .66 MHz signal content was not very strong and hence A1(.55,.75) fell to practically zero. The attenuation for A1(.55,.75) was relatively low for 0 degrees, peaked at 15 degrees, and reached an intermediate value at higher angles.

A1(.9,1.3) for $d = 1$ and $d = 2$ inches, along with the calculated attenuation parameter versus azimuthal angle are shown in figure 44. The A1(.9,1.3) for $d = 1$ inch shows a high value at 0 degrees and drops off less slowly at 15 degrees compared to A1(.55,.75), but then falls off at 30 degrees. The 1.1 MHz signal content or A1(.9,1.3) was attenuated very little in the 0 degree direction, but showed high attenuation between 15 and 30 degrees.

Plots demonstrating how phase velocities varied with azimuthal angle are displayed in figure 45. The first plot (a) shows the variation of phase velocity for the .23 MHz signal content with azimuthal angle. The .23 MHz signal content had a phase velocity which varied fairly smoothly from a value of 277,000 inches per second at 0 degrees to 156,000 inches per second at 90 degrees. The .66 MHz signal content showed a value of 450,000 inches per second for the phase velocity at 0 degrees and dropped to 113,000 at 90 degrees, showing a quick drop off between 15 and 30 degrees. The 1.1 MHz signal content had a phase velocity of 800,000 inches per second at 0 degrees and a phase velocity of 700,000 inches per second at 15 degrees, but was of such low amplitude at higher angles that phase velocity measurements were not possible. Notice that the phase velocities for the 1.1 MHz signal content is roughly twice that of the phase velocity for the .66 MHz (half the frequency value) signal content. This same type of behavior was observed for the aluminum plates.

In general, the 24-ply composite plate produced signals with frequency content at .27, .66, and 1.1 MHz. However, the AU signal did possess signal content in other frequency ranges. In fact, the

a)

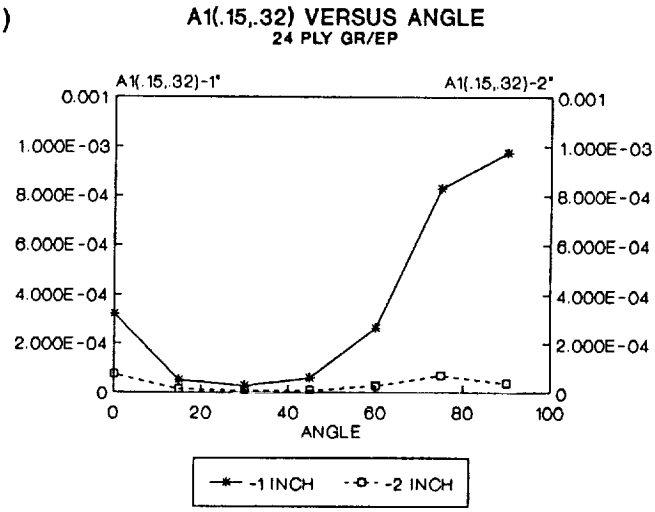

b)

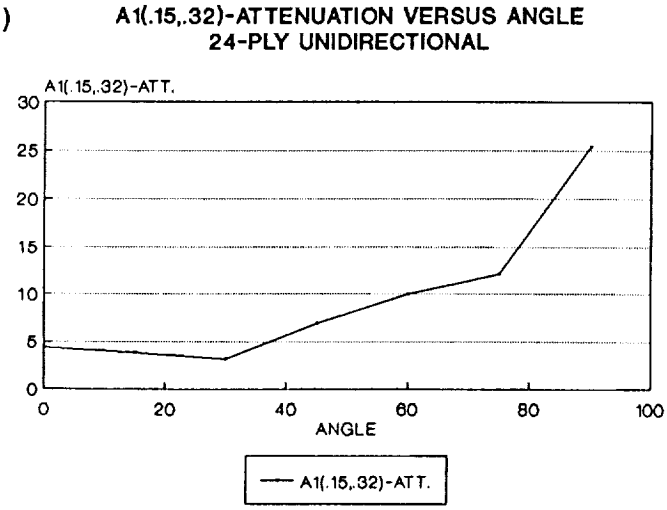

Figure 41. A1(.15,.32) versus azimuthal angle for Gr/Ep plate

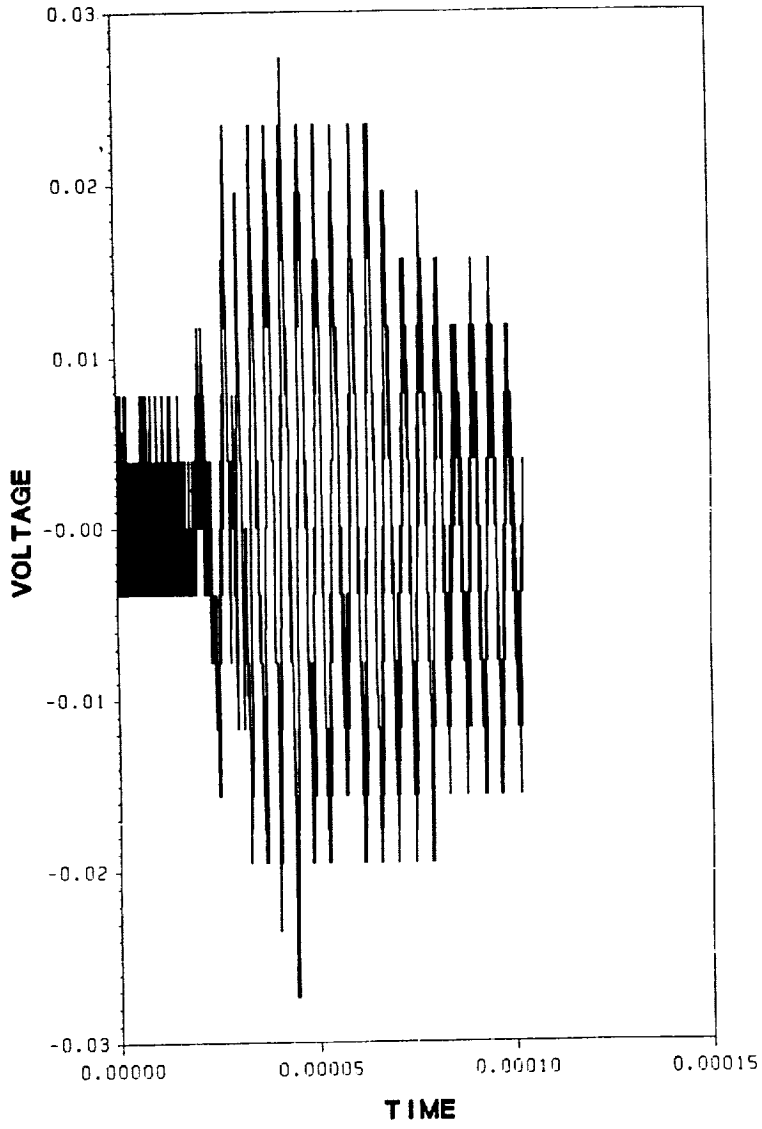

Figure 42. V/T plot for Gr/Ep plate in 90 degree direction

a)

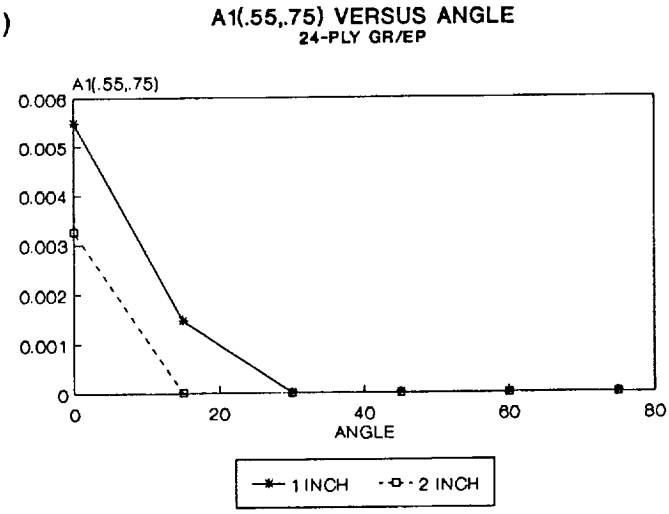

b)

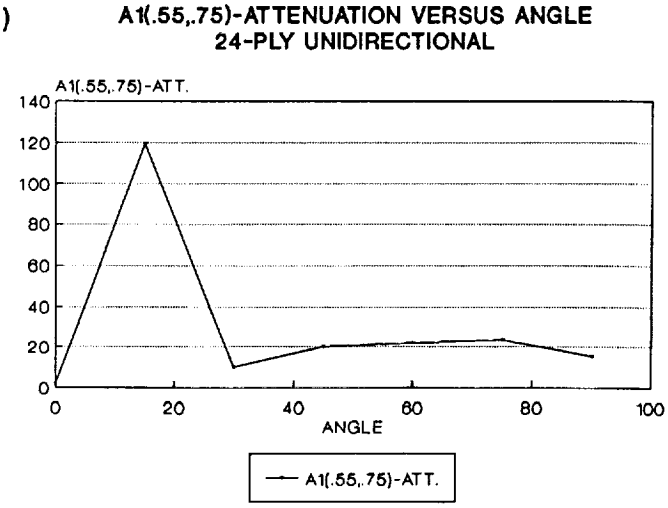

Figure 43. A1(.55,.75) versus azimuthal angle for Gr/Ep plate

a)

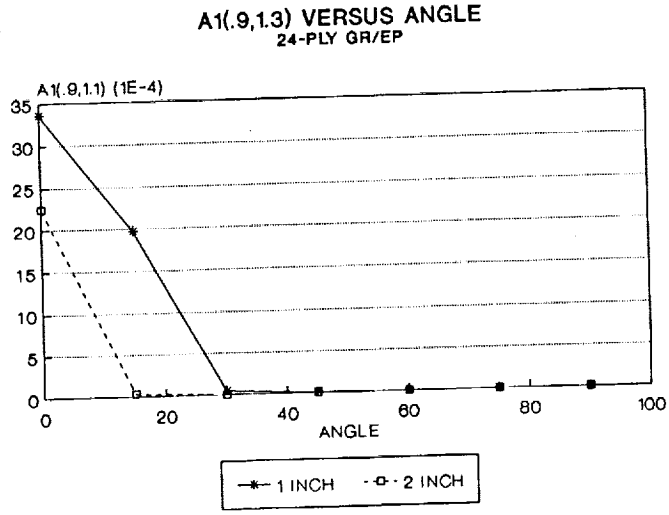

b)

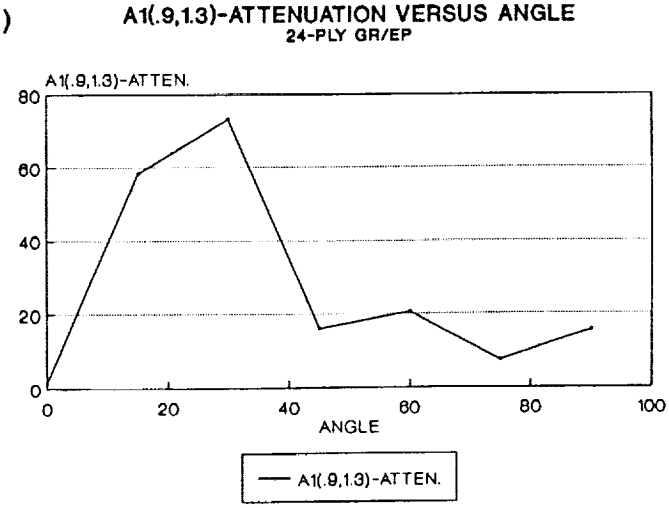

Figure 44. A1(.9,1.3) versus azimuthal angle for Gr/Ep plate

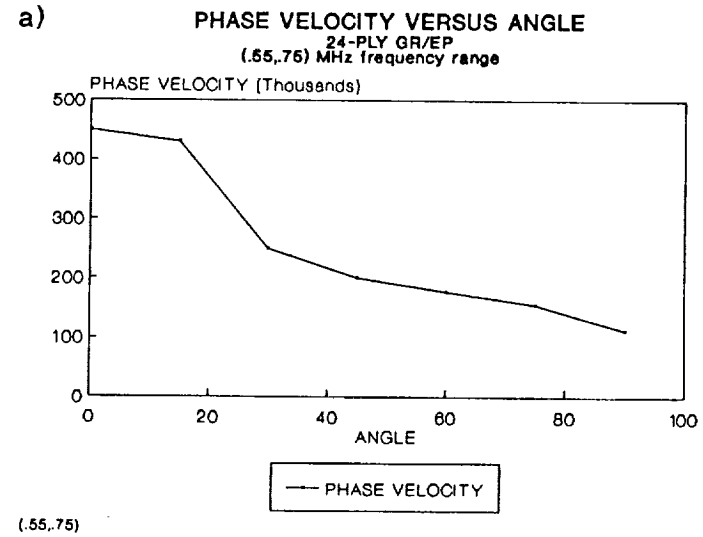

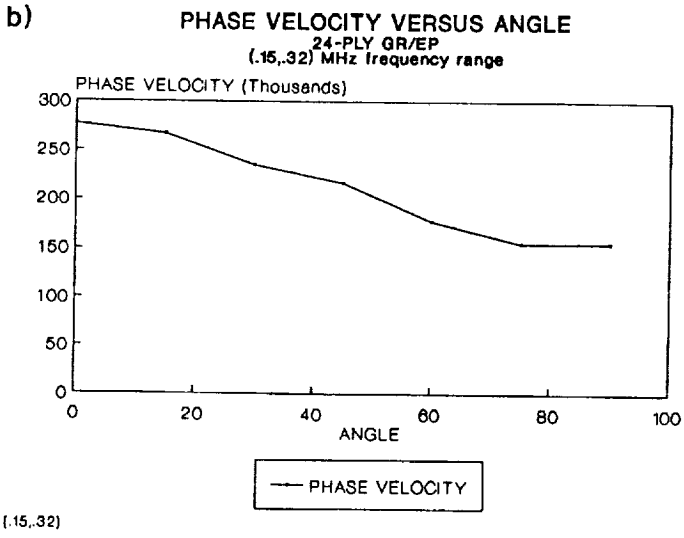

Figure 45. Phase velocity versus azimuthal angle, a).66 b).27 MHz content

AU signals from the composite plate resulted in more peaks and wider band widths for those peaks, compared to the aluminum plate. The AU signals from the composite plate, except for the 0 degree direction, did not show the strong modulated pulse shape that was observed for the AU signals obtained from the aluminum plates.

12 Ply Gr/Ep Plate (Unidirectional)

The 12-ply unidirectional specimen produced AU results with the predominant frequency content at .46, 1.2, and 2.2 MHz. Note these values are twice that seen on the 24-ply specimen. Hence, the composite plates showed the same inverse dependence of frequency on thickness as the aluminum plate, as would be expected with plate modes of wave propagation. Each of the frequency components for the 12-ply plate showed similar behavior to the corresponding frequency component on the 24-ply plate, with some slight exceptions. In order to glean more exact information on how the AU signal varied with azimuthal angle, figures 46-51 show how AU parameters varied with azimuthal angle on the 12-ply plate.

The plot of A1 versus azimuthal angle for the 12-ply laminate is shown in figure 46. Again the AU signal showed the greatest energy content in the 0 degree direction with the signal dropping off quicker for $d = 2$ inches than for $d = 1$ inch. Also, the A1 value jumped to a rather a high value for $d = 1$ inch at 90 degrees. This jump in A1 at 90 degrees was even more rapid than what was seen in the 24-ply plate. There are probably a number of factors contributing to the jump in the energy of this mode at 90 degrees. It should also be noted that the attenuation was greatest at between 15 and 30 degrees and at 90 degrees.

Figure 47 displays the plots of A2 versus azimuthal angle. For $d = 1$ inch, the plot showed a peak at 15 degrees. This type of behavior is similar to that seen in the thin plates discussed in chapter 2 (figure 16).

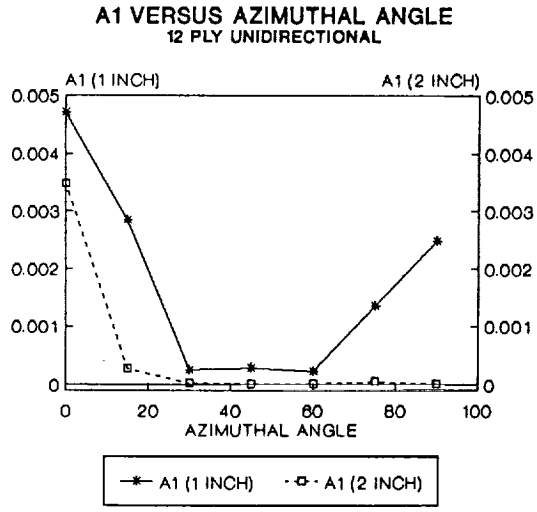

Figure 46. A1 versus azimuthal angle for 12-ply Gr/Ep plate

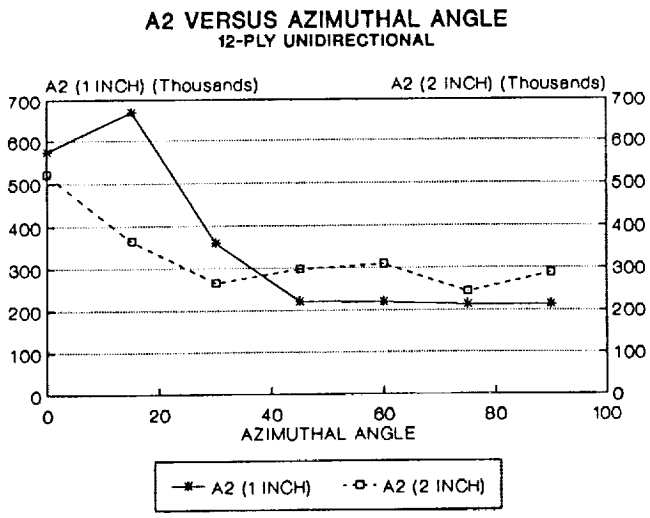

Figure 47. A2 versus azimuthal angle for Gr/Ep plate

The plots of A1(.25,.7) and A1(.25,.7)-Atten. (figure 48) show how the energy of the .46 MHz signal content varied with azimuthal angle for $d = 1$ inch and $d = 2$ inches. For $d = 1$ inch, the A1(.25,.7) parameter showed a definite high value at 90 degrees. Fairly high values of A1(.25,.7) also existed at 0 degrees for both $d = 1$ inch and $d = 2$ inches. The attenuation of the .46 MHz signal content was very low for low azimuthal angles.

The variation of the 1.2 MHz signal content with azimuthal angle and distance can be seen in figure 49. This signal content showed a high energy content at low azimuthal angles and reached a very low value after 45 degrees. The maximum attenuation was between 15 and 30 degrees. This shows that most of the energy for the 1.2 MHz signal content is sent in the fiber direction and very little is sent in the cross fiber direction.

Figure 50 displays plots which show how the 2.1 MHz signal content is affected by changes in azimuthal angle and d. The major point is that the 2.1 MHz signal content is heavily directed into the low angle directions and seems to attenuate rather quickly even in the low angle directions.

Figure 51 displays the variation of phase velocity for the two dominant modes in the AU signal. The plot of phase velocity versus azimuthal angle for the .47 MHz signal content descended smoothly from a value of 385,000 inches per second to a value of 156,000 inches per second. The plot for the 1.3 MHz signal content dropped from a very high value of 2,000,0000 inches per second to a value of 120,000 inches per second inside of 45 degrees. Phase velocity measurements for the 1.3 MHz signal content were hard to make past 45 degrees because the signal was of such low amplitude at these angles. The 2.1 MHz signal content showed an extremely high phase velocity in the 0 degree direction and measurements were not possible at higher angles.

a)

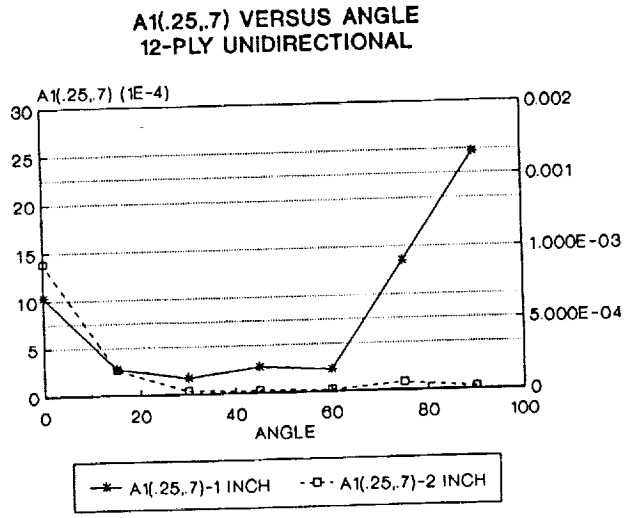

b)

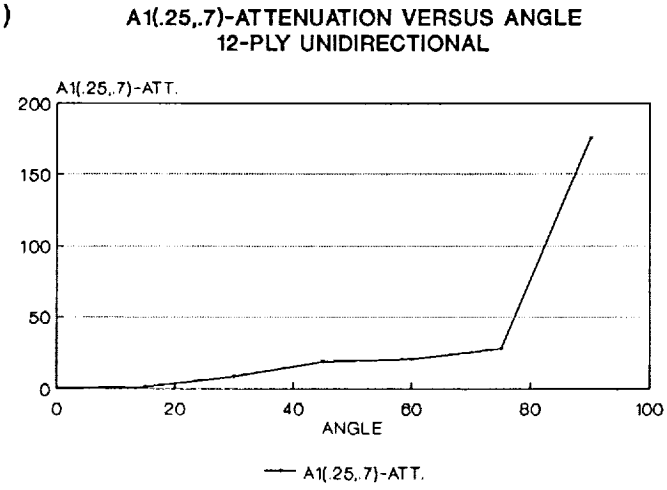

Figure 48. A1(.25,.7) versus azimuthal angle for Gr/Ep plate

a)

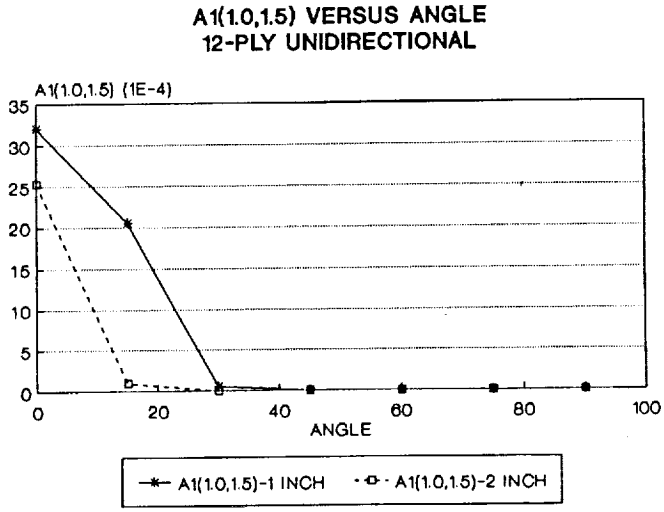

b)

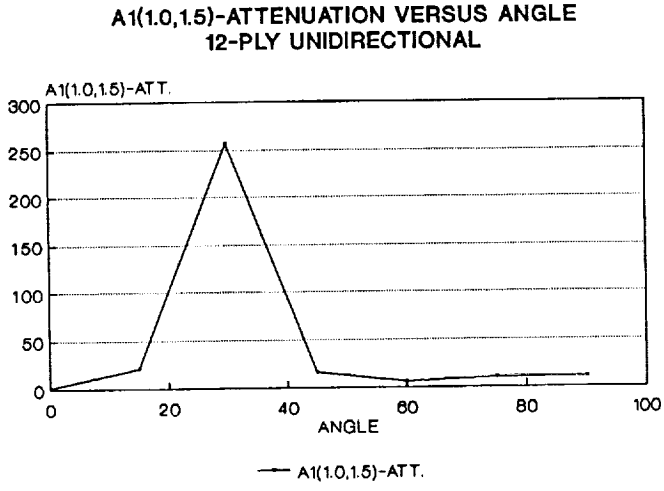

Figure 49. A1(1.0,1.5) versus azimuthal angle for Gr/Ep plate

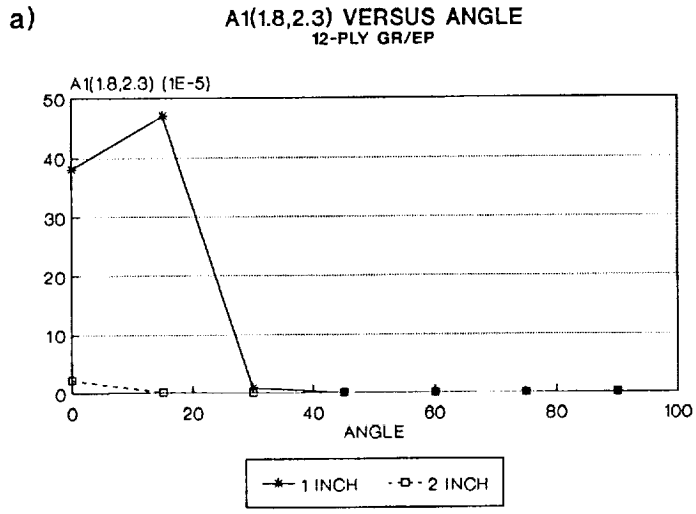

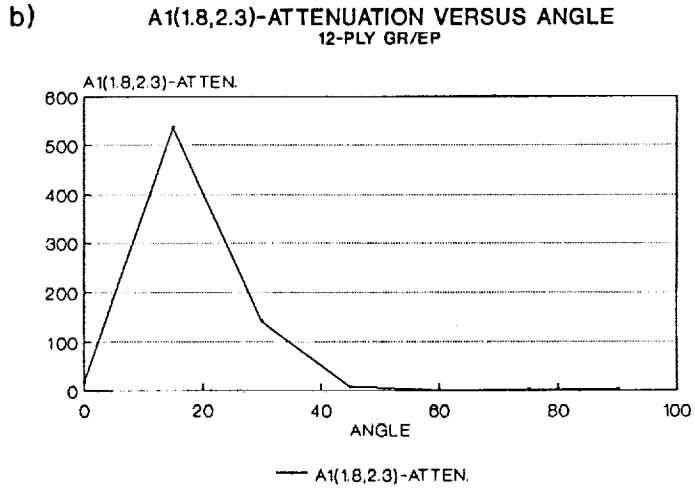

Figure 50. A1(1.8,2.3) versus azimuthal angle for Gr/Ep plate

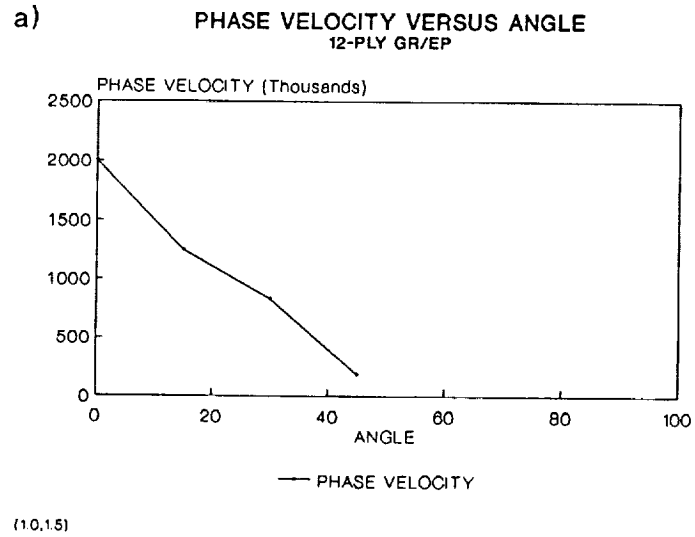

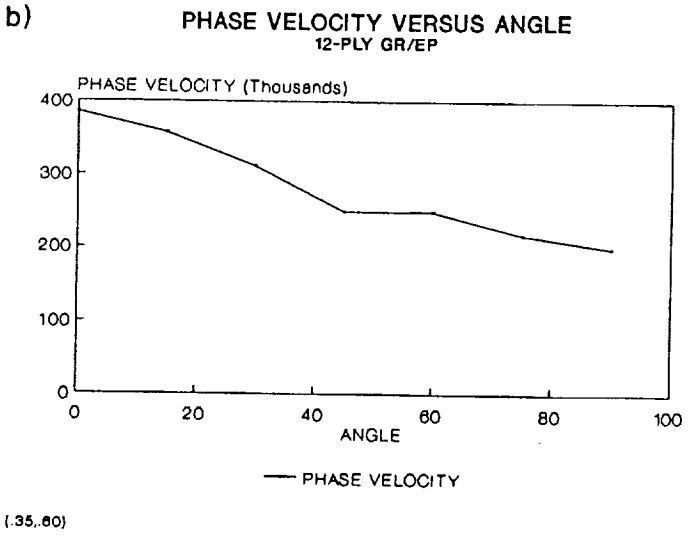

Figure 51. Phase velocity versus azimuthal angle, a)1.3 b).47 MHz content

Tapered Aluminum Plate

AU measurements performed on the tapered aluminum plate revealed some interesting results. Figures 52-55 display amplitude/frequency plots obtained from the various measurements on the tapered plate. Again these measurements where made with a large transducer separation distance ($d = 6$ inches) and hence show results somewhat different than seen in earlier results ($d = 1$ and $d = 2$ inches).

Performing the AU technique on the thick (.125 inch thick) section with $d = 6$ inches revealed the amplitude/frequency plot shown in figure 52. Note that the primary peak is at .5 MHz with another major peak at 1.0 MHz. These are the same major frequency components seen in the .125 inch thick aluminum plate discussed previously. However, this spectrum does not possess as sharp or as well defined peaks and additionally contains other small peaks at other frequencies. These effects are attributed to the extra distance between the sending and receiving transducers.

Figure 53 pictures the amplitude/frequency plot obtained by placing the sending transducer on the .125 inch section and the receiving transducer 6 inches away on the .0625 inch thick section. The major result here is that the .5 MHz signal content is replaced by the 1.0 MHz signal content as the dominant frequency content and the appearance of the 2 MHz signal content at a magnitude higher than what existed when the AU measurement was performed in just the .125 inch thick section.

Performing the AU method in the .0625 inch section revealed the amplitude/frequency plot in figure 54. This measurement resulted in a sharp peak at 1 MHz and very little other signal content in other frequency ranges.

Finally, the AU measurement made with the sending transducer in the .0625 inch thick section and the receiving transducer 6 inches away in the .125 inch thick section produced the amplitude/frequency plot shown in figure 55. This plot reveals a strong 1 MHz peak and higher proportional values for .3, .5, and 2 MHz peaks, especially, the .3 MHz peak, which was also of a

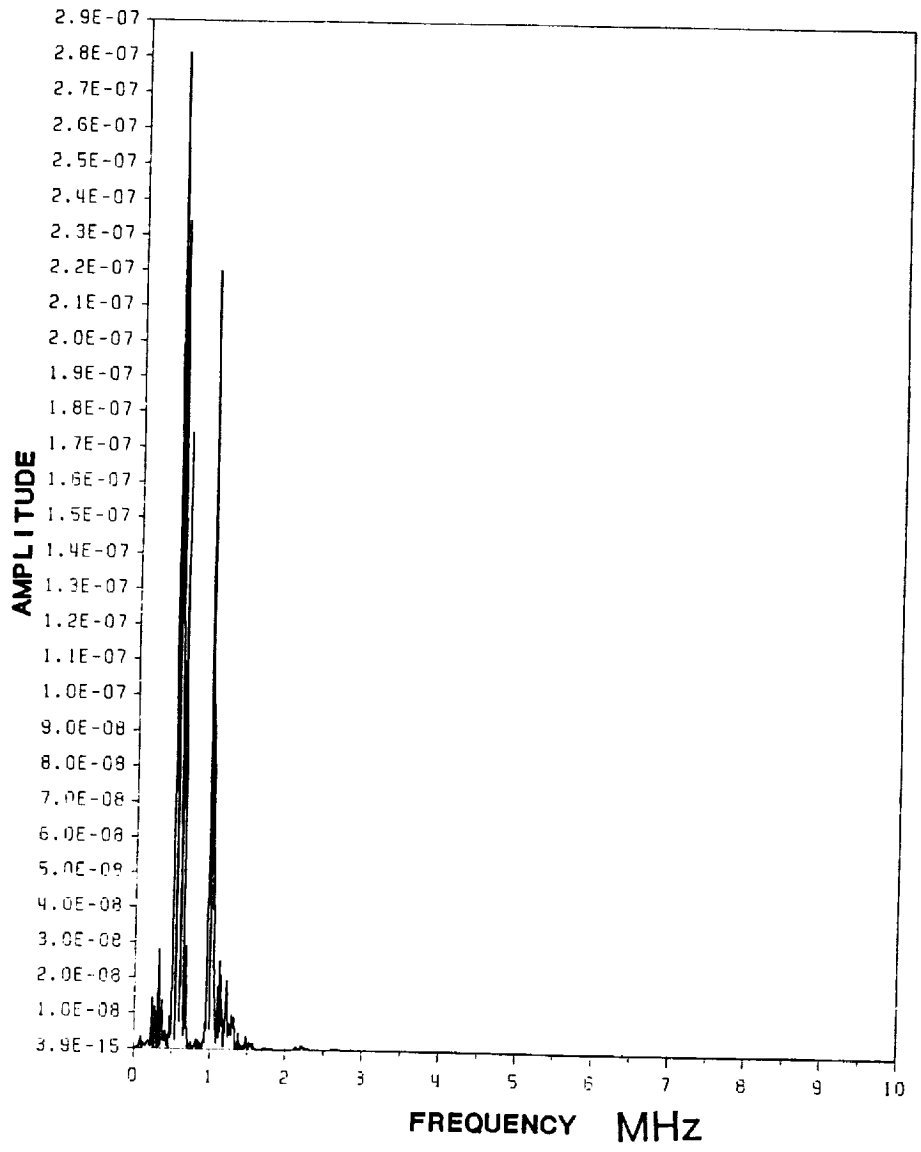

Figure 52. Amplitude/frequency (tapered aluminum plate) (.125 " section)

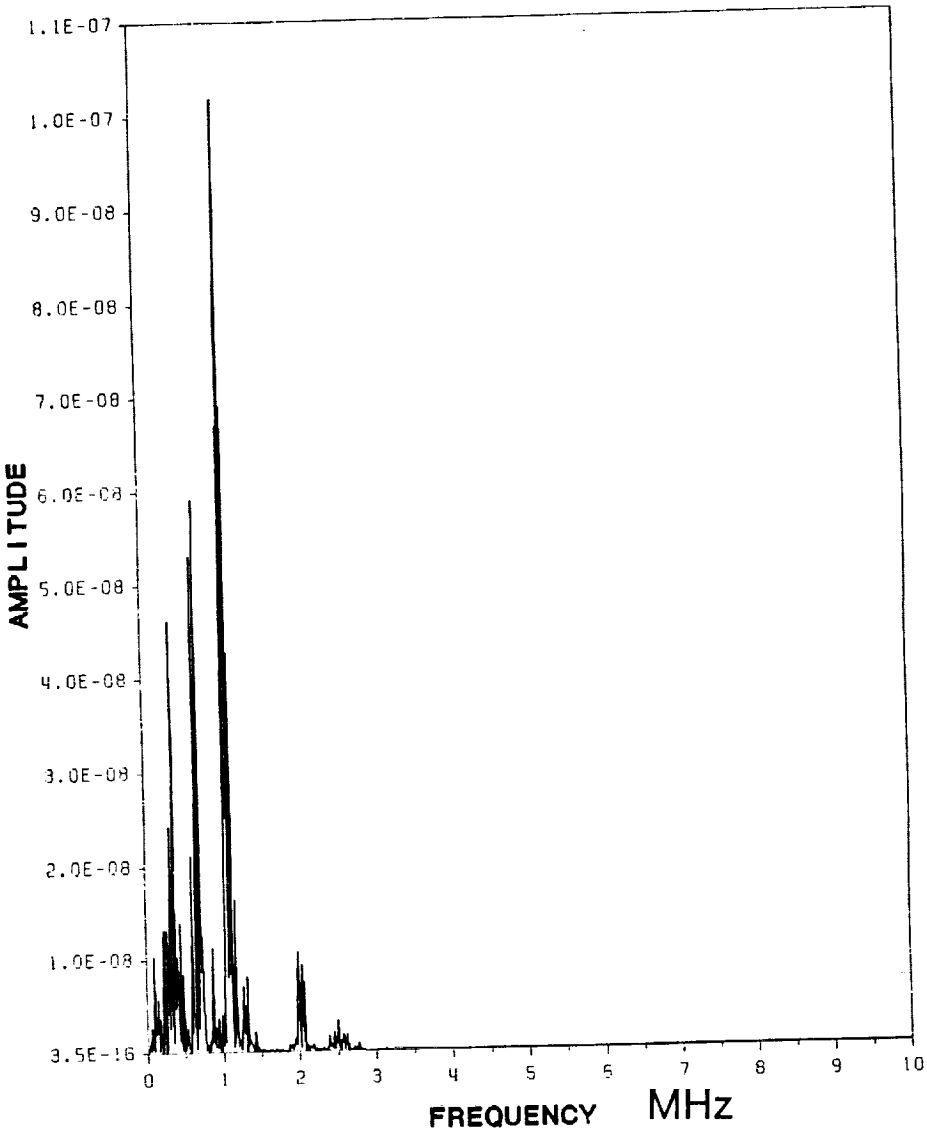

Figure 53. Amplitude/frequency (tapered plate) (.125 "-.0625 " section)

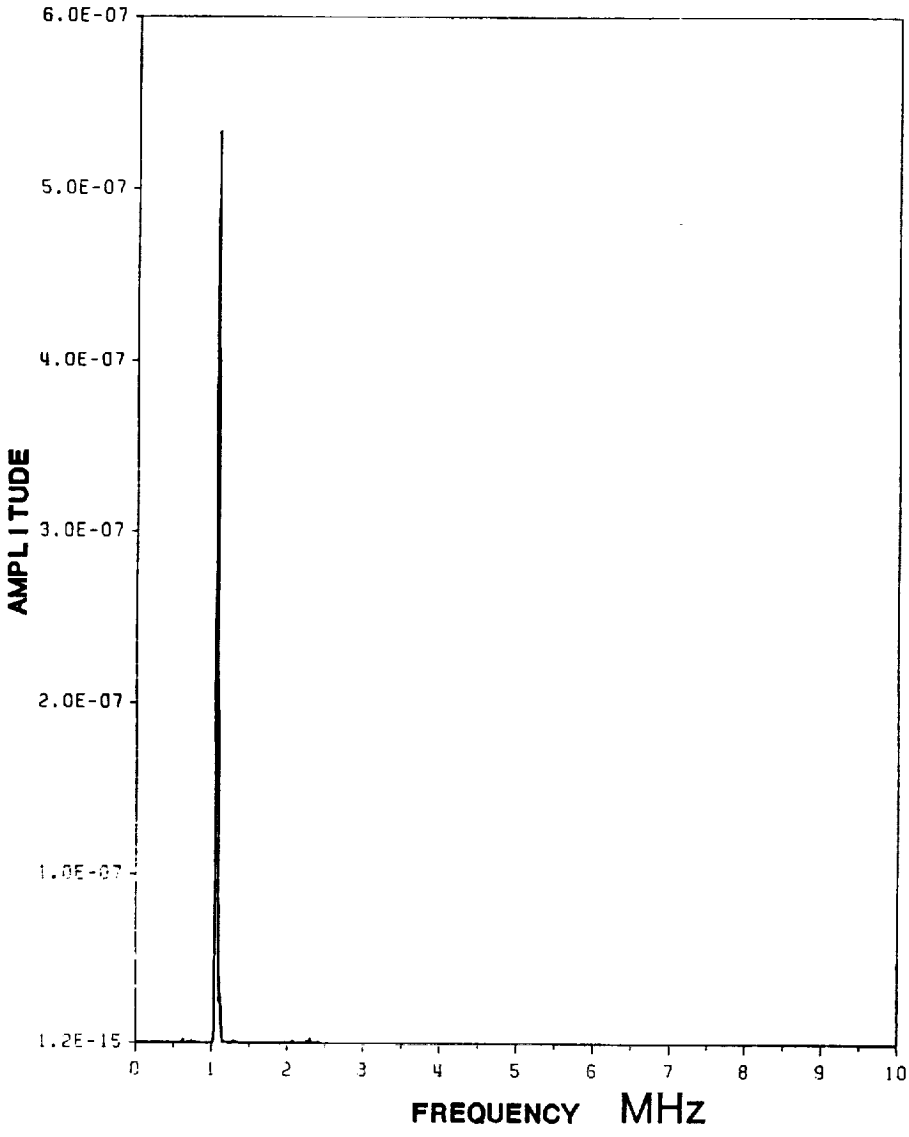

Figure 54. Amplitude/frequency (tapered aluminum plate) (.0625 " section)

relatively high value for the case where the sender and receiver are in reverse locations (figure 26). A major point is the .5 MHz signal content not present in the AU measurement for the thin section.

Overview of Experimental Data

The preceding results exemplify many of the basic features associated with the physics of the AU technique. In particular, information has been presented on disturbance frequency content and on wave velocities and energy content for various frequency components. Moreover, the issue of how these variables are affected by changes in azimuthal angle has been displayed. Additionally, the attenuation of the various frequency components for various measurements have been calculated to help understand the basic mechanics of AU wave propagation.

In the next chapter, the results from this chapter are compared to basic theoretical ideas that form an elementary model of the AU method. This will include comparing frequency peaks seen in the amplitude/frequency plots to frequencies for through-thickness-transverse resonance modes. Additionally, this includes looking at plate wave dispersion curves and predicted plate wave phase velocities. Plots of how variables change with azimuthal angle will also be compared with theoretical predictions of how certain measurements should change with azimuthal angle. Comparisons are both quantitative (based on numerical results) and qualitative (based on examining equations and general trends).

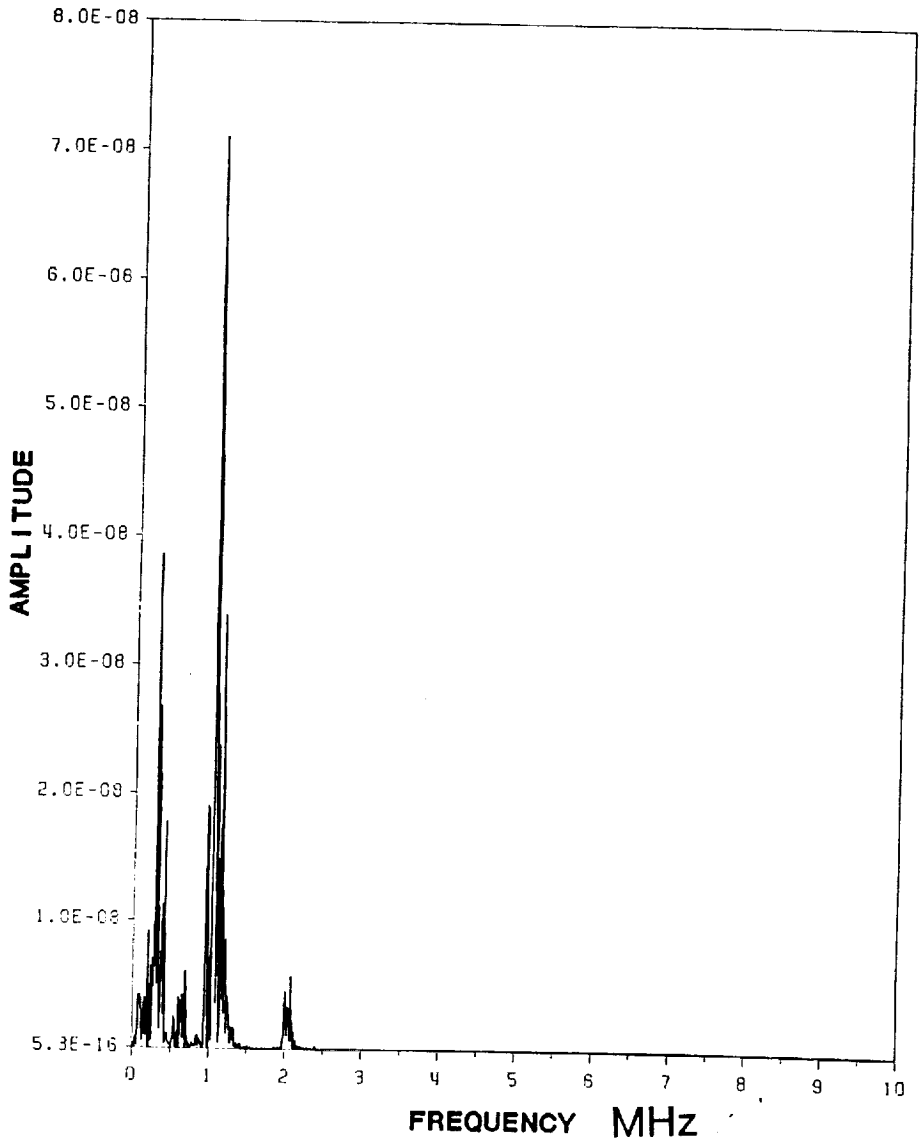

Figure 55. Amplitude/frequency (tapered plate) (.0625 ″-.125 ″ section)

Physical Understanding

In this chapter a physical understanding of the AU method, based on comparing experimental data with theory, is presented. Most of the experimental data utilized is contained in the previous chapter, however some comments relate to the literature review.

Theory of elasticity, Lamb wave theory, and TTTR provide the basis for the physical understanding of the AU technique. Additionally, the contribution of energy flux deviation to AU results is noted. Lamb wave theory and TTTR were both reviewed in chapter two, therefore comments in these subject areas concentrate on utilization of the theory for computer applications, as well as comparisons to AU experiments. Specifically, dispersion curves and TTTR calculations are used to suggest which modes may be present at frequencies seen in the AU results, while phase velocity calculations are used to identify which of the possible modes is actually showing up in AU results. The elasticity solution is used simply to give an indication of what disturbances the piezoelectric source might create. Thus, coverage of the elasticity solution consists of general equations, computer results, and ramifications of how the elasticity solution may relate to AU results.

First, a very basic description of the physical problem is presented. This reiterates how a number of concepts forwarded in chapter 2 are related to the AU method. The discussion emphasizes how elasticity, Lamb wave theory, and TTTR may be used to provide a basic understanding of AU re-

sults. Next, each of the three basic concepts (elasticity, TTTR, and Lamb wave theory) used to understand the AU method are covered separately. For each subject, this entails the following four steps:

Statement of the basic physical concepts and equations

Discussion of computer codes or solution technique

Presentation of the numerical results for material systems utilized in experimental results

Comparison of numerical results with experimental results

Finally, a general overview of the physical understanding of the AU method is forwarded. This will include statements on other experimental results and qualitative comments on theory.

Physical Problem

A number of mechanical and electrical components affect the final AU signal used to characterize a section of material. Understanding each of these components creates separate engineering problems, which may be solved using analysis of varying degrees of complexity. These problems arise from such concerns as:

Characteristics of the pulse sent from the pulser

Transducer response to pulse (mechanical and electrical coupling)

Variation of response over transducer face

Interaction of transducer disturbance with couplant and material surface

Basic mechanical excitation seen by material (Boundary Value Problem)

Local wave disturbances resulting from mechanical excitation

How plate wave motion develops and propagates to other transducer (how to model material)

How motion caused by plate wave propagation interacts with other transducer

How interaction of plate wave motion with the receiving transducer causes the received signal

How signal from receiving transducer is electrically altered by receiving instrumentation

Although these questions are all, in their own right, complicated and to some degree worthy of separate research, some primary understanding of these issues helps provide insight to basic results and helps determine possible assumptions for modelling purposes. More importantly, these concerns determine where future research should be directed to develop yet more refined AU techniques. Specifically, understanding the full complexity of the situation, facilitates future improvements of present simplified models and shows where difficulties exist in understanding experimental equipment, so that new equipment may be designed. For these reasons, some of the issues above, although not totally accounted for, will be discussed briefly. Obviously, many assumptions must be used to get a working model for this complex line of problems.

The first issue is how the pulse produced by the pulsing unit produces stress waves in the material. The pulse sent to the sending transducer is not a perfect pulse, but a finite width pulse of sinusoidal shape. However if the proper settings are utilized, the pulse can be reduced to a fairly sharp pulse width. In any case, an imperfect pulse is sent to the sending transducer, so that the input from the onset has a nonuniform spectral density, even before pulsing the sending transducer. Obviously, this affects the spectral density of the output. The character of this pulse may be ascertained by

consulting the user's manual of the pulsing unit or experimentally analyzing the pulse using data acquisition equipment. It is necessary to ascertain the general frequency content of the input pulse to make sure it is in the range of the transducer's resonance frequency and in the range of frequencies for AU results of interest. A further complication involves the manner in which the electrical characteristics of this pulse affect the piezoelectric element and the circuitry of the sending transducers (ref. 133). A crucial concern is the frequency content and the duration of the resulting transducer vibration. This issue was partially addressed in chapter 3 by considering the pulse echo spectrum of a large aluminum block (fig. 24). Note that although the sending transducer is a heavily damped, wide band transducer, the spectral density of the excitation is very nonuniform for the range of frequencies seen in AU results. In other words, certain frequencies seen in AU results have higher energies of input than others by sizeable margins. An additional complication involves how the actual transducer vibration as a result of the signal may not be uniform as a function of position. For instance, the crystal may not be perfectly aligned or uniform. Ultimately, a very careful and exact characterization of a transducer should give the displacement field of the transducer face as a function space and time for electrical input pulses. This most likely will involve experimental characterization by methods such as optical interferometry. Certainly, the signal generated by the receiving transducer is not a result of a perfectly uniform field, but an integrated effect of a displacement field varying in time and space (ref. 152). To make matters even worse, the displacement and stress of the piezoelectric element is transferred by couplant to the material surface. This is a source of great problem for modeling purposes and presents practical problems in regard to reproducibility of results.

Eventually, the material surface experiences a force varying with time and position. Furthermore, this force disturbance most likely involves both shearing and normal forces, even in cases where the sending transducer is a longitudinal mode transducer. However, most models for normal mode transducers involve treating the transducer disturbance as a time varying distributed normal load (ref. 99).

Hence, although realizing the situation is definitely more complex, elasticity results for the stresses caused by a point force on a half space are utilized to determine what type of disturbances might be caused in a plate due to a transducer placed on the top surface. This approach neglects a number of effects, but does allow some indication of how the energy for input stress waves may vary as a function of angle off the normal and as a function of azimuthal angle. A few of the effects which this neglects are:

Effect of bottom surface

Effect of pulse shape or frequency content of input

Effect of load being distributed nonuniformly over a finite area

Effect of shearing forces which may be generated

However, using a point normal force load, still allows a comparison of what effects the variation of material properties with azimuthal angle might have on how certain wave motions vary with azimuthal angle. Moreover, the normal mode of input is the dominant mode of input for this experimental arrangement. This provides a good qualitative picture of the situation and provides a crude tool for quantitative modeling efforts. Also, for the case of an isotropic plate the problem of distributed loading is considered, in a qualitative manner, to yield an indication of how transducer size may affect results.

Next, consideration is shifted to how local disturbances created by the transducer may travel and interact. More specifically, the focus is on characteristics of waves traveling normal to the plate surface and to which wave motions would satisfy boundary conditions on the top and bottom surfaces by through the thickness transverse resonance. The following are reasons for considering the TTTR case:

The greatest input is through the thickness or just off at small angles (θ's), so characteristics of these waves are indicative of waves causing AU results

For higher order modes (that are TTTR modes for $\theta = 0$), even for a range of low angles of θ, the frequency is still near that of TTTR - this is central to understanding AU results

Results indicate that frequencies measured in AU results correlate to frequencies for TTTR

The main output for TTTR analysis are:

Displacements associated with wave travel for bulk waves through the thickness of the plate (specifically the variation of displacement for a shear wave motion with azimuthal angle for a composite plate)

Frequencies for TTTR modes

Waves propagating slightly off the normal will have many characteristics that are just slightly different than the TTTR modes. The reasons for this are elucidated when consideration is moved to the Lamb wave equations. Hence, one purpose of looking at TTTR is to get an indication of what characteristics might be present for modes that are included in Lamb wave analysis and to understand these modes better.

The boundary value problem for waves traveling in a plate are described by Lamb wave equations. The derivation and basic approach to solving these equations were discussed in chapter 2. Obviously, since the AU method has been performed on a plate, equations describing wave motion for a plate are relevant to the physical problem of AU propagation in aluminum and composite plates. Moreover, many experimentalists have noted that characteristics of disturbances seen in AU results resemble that of Lamb waves (ref. 9, 13, and 95).

Since the Lamb wave equations are physically representative of the AU problem, their solutions have been programmed. Appendices C, D, and E contain 3 programs which calculate Lamb wave results for the three separate cases of an isotropic plate, a unidirectional composite plate (0 and 90 degree directions), and a unidirectional composite plate (any general direction). Two additional appendices provide information on how the programs may be improved to yield a more general code. Appendix G lists a program which solves the Christoffel equation for a general direction; this is essential to using the method of uncoupled solutions. Next, a description is given of how the method of uncoupled solutions may be combined with present codes to arrive at a more general, easy to use solution code for Lamb wave analysis.

The strategy of the computer program involved solving the dispersion equation and using other equations relating the physical parameters of the plate wave problem to each other. An endless combination of plots showing the relationship between various variables are possible. However, computer plots are given only for the following results:

Dispersion curves

Velocities versus frequency

Displacements versus frequency

The purpose of these results is to identify what modes of wave propagation are present in AU results. Also, plots are provided to compare Lamb wave behavior at different azimuthal angles.

Signal Reception

Another important issue is the manner in which the receiving transducer integrates the disturbance over its face to produce an output signal. To obtain an understanding of this situation consideration must be given to what type of transducer is utilized. For instance, if a longitudinal mode

transducer is utilized, concern should be given to u_3. Since longitudinal transducers were used in AU experiments, the calculation of u_3 is of interest in deriving theoretical comparisons.

Finally, the signal from the receiving transducer is operated on by the transfer function associated with the amplifier, attenuator, and filter. The effects of this are important in developing a standardized method where the amplitude has an absolute value independent of instrumentation. Unfortunately, the modeling of other components is such that this is not yet attainable. In any case, it is important to make sure that the transfer function for this section of electronics does not filter out frequencies of interest or does not preferentially amplify certain frequency components.

Elasticity Solutions

This section chronicles solutions to the the elasticity problem for normal loads placed on an infinite half space to approximate what stresses a similar load would cause on a plate of thickness $2b$. This shows how stresses vary relative to the angle of inclination from the source, hence paving the way for determining how the input disturbance may cause more energy to be channeled into certain Lamb wave modes relative to others, and moreover how drastically material anisotropy may affect these results.

These solutions are for a single sagittal plane and the loading is assumed to be uniform as a function of the direction perpendicular to the sagittal plane. For the anisotropic case, this leads to a difficulty in interpreting results, because the load is distributed infinitely in the perpendicular direction, causing the calculated stress in the direction perpendicular to the free surface to be different depending on which azimuthal direction is considered. Hence, in these results the magnitudes of the stresses are normalized to the value for the through thickness direction. The purpose of these results is to provide some indication of how the energy for Lamb waves varies due to the angle θ

associated with the P-wave input. Thus, the point here is to use this solution to approximate the magnitude of the stress waves impinging on the bottom surface of the plate, for various angles θ and relating the angle θ and the magnitude ot the stress to the angle θ_3 for the P-wave, and hence to the magnitude for the Lamb wave related to that θ_3.

Point Load on an Isotropic Plate

The basic notation and geometry for the problem of a point load on a semi-infinite half space is shown in figure 56. The dotted line corresponds to the surface where stresses are calculated to approximate the magnitude of stress waves impinging on the bottom surface of a plate. Once this relative value is found the solution technique is be shifted to Lamb wave equations. This portion of the solution serves to provide an exact value for the undetermined coefficient which multiplies the displacement values found using the classical Lamb wave solution.

A simple solution exists for the stress field caused by this point load. In polar coordinates, this solution is given by the following formula:

$$\sigma_r = 2\frac{P}{\pi}\frac{\cos(\theta)}{r}$$

Now, if we consider what stress this causes at positions corresponding to a plate thickness b, this leads to the following formula:

$$\sigma_r = 2\frac{P}{\pi}\frac{\cos^2(\theta)}{2b}$$

Figure 57 shows how σ_r varies with θ. The angle θ relates to the input angle θ_3, the input angle for a P-wave. This may then be related to the frequency for a given mode by using the basic dispersion relations:

$$\omega = f(\xi)$$

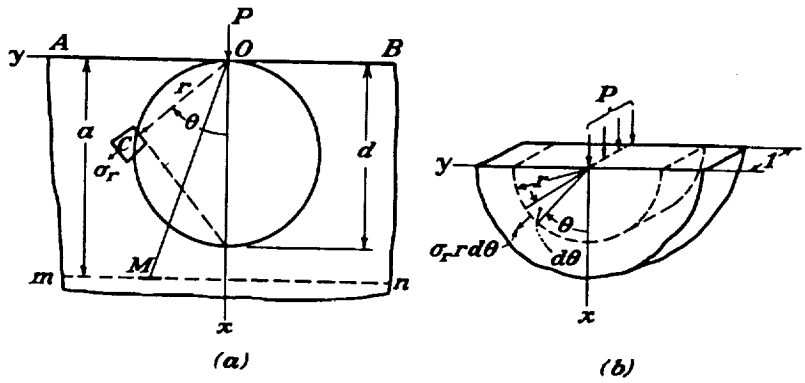

[ref. 154]

Figure 56. Definition of coordinate system and geometry for point load

and the following equations:

$$\alpha^2 + \xi^2 = (\omega^2/(v_p)^2)$$

$$\theta_3 = \tan^{-1}(\frac{\xi}{\alpha})$$

Hence, relations can be made between the input and the resulting character of Lamb waves which may be excited. This connection will be discussed later in the next chapter with regard to modeling.

Isotropic Plate- Distributed Load

Figure 58 displays the geometry and notation utilized in the solution of a isotropic half space with a distributed load placed on the top surface (reference 154). This causes a uniform compressive load:

$$p = -2A\alpha$$

where

$$A = \frac{1}{(2\pi)} q$$

Obviously, this causes the stress to be less for a greater distance correlating to the distance for plate thickness 2*b*. Also, this value is lower for greater angles of inclination to the area covered by the distributed loading.

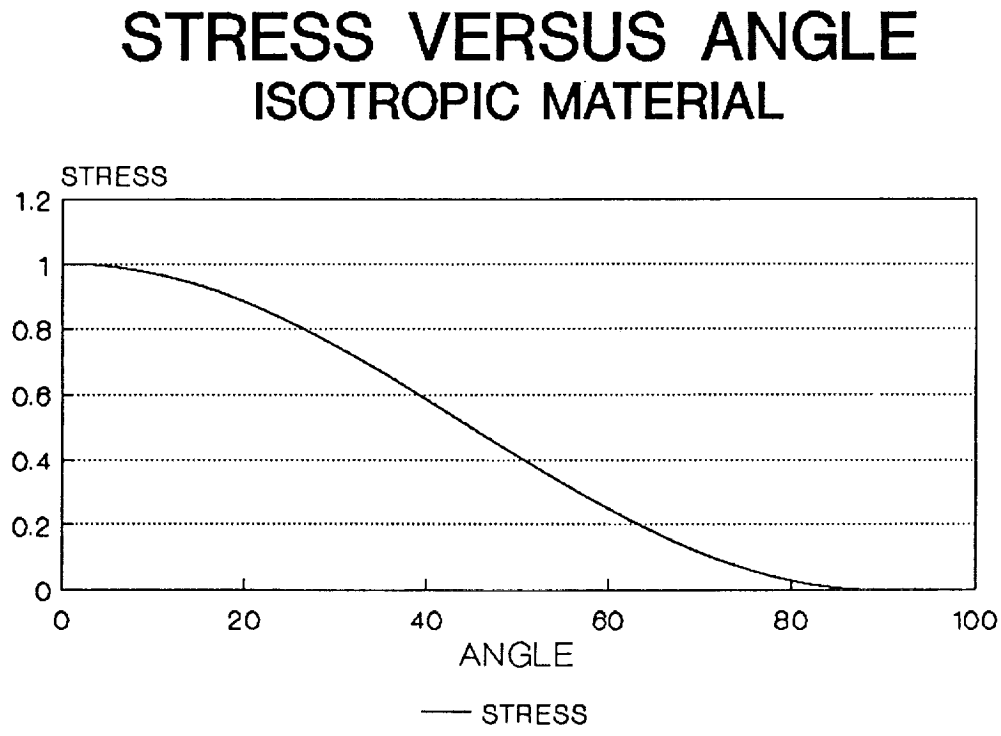

Figure 57. Variation of stress with input angle for point load

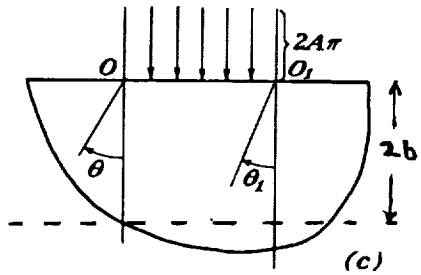

[ref. 154]

Figure 58. Definition of coordinate system for distributed load

Point Loading on an Anisotropic Plate

The equations describing the stresses resulting from a point load on an anisotropic half space are much more complex than those describing stresses caused by a point load on an isotropic half space. Results of these equations indicate a large variance in how stresses vary for different orientations on the top surface plane (or different azimuthal angles for for the plate constructed from collapsing the half space to a plate). Thus, a normal input results in vastly different amounts of stress and hence energy being transferred in different directions, due to variation of material properties. Specifically, this section will forward Lekhnitskii's solution for point loading on an anisotropic half space. The strong dependence azimuthal angle has on how stress varies with angle from the normal to top plane should be noted. In general, stresses tend to be much greater at angles off the normal for azimuthal angles relating to high material moduli. This would contribute to the higher energy content for waves travelling in these directions.

A large system of equations must be solved to arrive at an answer to the stresses caused by point loading on an anisotropic half space. Hence, this section will present the solution to this problem utilizing Lekhnitskii's notation (ref. 151) and state only the most relelevant equations. A more detailed review of the theory used to arrive at these equations may be found in the above reference by Lekhnitskii.

The first relevant equation involved in the solution to this problem is the general 6th degree algebraic characteristic equation for solving anisotropic elasticity problems:

$$l_4(\mu)l_2(\mu) - l_3^2(\mu) = 0$$

where

$$l_4 = S_{11}\mu^4 - 2S_{16}\mu^3 + (2S_{12} + S_{66})\mu^2 - 2S_{26}\mu + S_{22}$$

$$l_3 = S_{15}\mu^3 - (S_{14} + S_{56})\mu^2 + (S_{25}\mu + S_{46})\mu - S_{24}$$

$$l_2 = S_{55}\mu^3 - 2_{45}\mu + S_{66}$$

Using this the additional parameters may be defined:

$$\lambda_1 = -\frac{l_3(\mu_1)}{l_2(\mu_1)}$$

$$\lambda_2 = -\frac{l_3(\mu_2)}{l_2(\mu_2)}$$

$$\lambda_3 = -\frac{l_3(\mu_3)}{l_4(\mu_3)}$$

In polar coordinates, the solution to this problem is:

$$\sigma_r = -\frac{p}{\pi r} Re(i/\Delta(AD_1(\theta) + BD_2(\theta) + \lambda_3 CD_3(\theta)))$$

$$\tau_{rz} = -\frac{p}{\pi r} Re(i/\Delta(\lambda_1 AE_1(\theta) + \lambda_2 BE_2(\theta) + CE_3(\theta)))$$

where

$$\Delta = \mu_2 - \mu_1 + \lambda_2\lambda_3(\mu_1 - \mu_3) + \lambda_1\lambda_3(\mu_3 - \mu_2)$$

$$A = (\mu_3\lambda_2\lambda_3 - \mu_2)$$

$$B = (\mu_1 - \mu_3\lambda_1\lambda_3)$$

$$C = \lambda_3(\mu_2\lambda_1 - \mu_1\lambda_2)$$

$$D_1(\theta) = (\cos(\theta) + \mu_1 \sin(\theta))^2/(\sin(\theta) - \mu_1 \cos(\theta))$$

$$D_2(\theta) = (\cos(\theta) + \mu_2 \sin(\theta))^2/(\sin(\theta) - \mu_2 \cos(\theta))$$

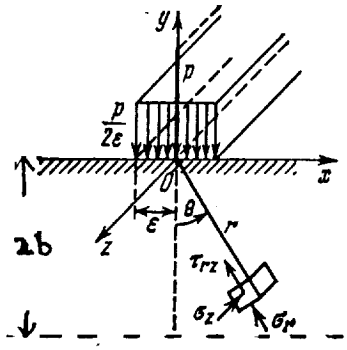

[ref. 151]

Figure 59. Definition of coordinate system for anisotropic case

$$D_3(\theta) = (\cos(\theta) + \mu_3 \sin(\theta))^2/(\sin(\theta) - \mu_3 \cos(\theta))$$

$$E_1(\theta) = (\cos(\theta) + \mu_1 \sin(\theta))/(\sin(\theta) - \mu_1 \cos(\theta))$$

$$E_2(\theta) = (\cos(\theta) + \mu_2 \sin(\theta))/(\sin(\theta) - \mu_2 \cos(\theta))$$

$$E_3(\theta) = (\cos(\theta) + \mu_3 \sin(\theta))/(\sin(\theta) - \mu_3 \cos(\theta))$$

If the case of orthotropy is considered the equations are greatly simplified and can be expressed as:

$$\sigma_r = -\frac{p}{\pi}(u_1 + u_2)(S_{11}S_{22})^{.5} \cos\theta/(rL(\theta))$$

where

$$L(\theta) = S_{11}\sin^4\theta + (2S_{12} + S_{66})\sin^2\theta\cos^2\theta + S_{22}\cos^4\theta$$

and u_1 and u_2 are the roots of the equation

$$S_{11}u^4 - (2S_{12} + S_{66})u^2 + S_{22} = 0$$

Note that in this notation S_{ij} are the compliance values and the 1-direction corresponds to the direction along the length of the plate. Thus, the values used in the expression depend on azimuthal angle and hence the stress state varies as a function of azimuthal angle.

Two programs were written to calculate how the stresses vary as a function of θ for different material directions. The first, (ORIN.FOR), calculates how σ_r varies as a function of θ in both the fiber direction and the cross fiber direction (see figure 60 for results). The second, (GEIN.FOR), will provide the same results from above for any direction. In these results, the values for the stresses have all been normalized to the value in the through-the-thickness direction ($\theta = 0$). The

code for ORIN.FOR is in appendix A and the code for GEIN.FOR is in appendix B. The calculations for these programs follow straight from the equations stated above.

In example, the dependence of σ_r on θ, for the cases where the fiber direction and perpendicular to the fiber direction define the planes to be considered, are shown in figure 60. The major difference in the two curves is the rather quick drop in σ_r when the wave is sent in the cross fiber direction compared to the much slower descent of σ_r with angle in the fiber direction. Basically for directions with high stiffness, the value of σ_r stays relatively high for increased angle off the normal θ. This amounts to the basic effect of a stiff material seeing a greater stress for a given displacement set up locally and hence relaying more of the energy than less stiff material directions. The difference in magnitude becomes apparent at angles greater than 45 degrees. Hence, the fiber direction seems to draw a higher magnitude disturbance at high angles, corresponding to the fiber direction.

In regard to the AU method, the variation of the radial disturbance with angle relates to what angles stress waves may be directed. In relation to Lamb wave propagation, a higher angle θ relates to a higher wave number in the direction of propagation. Depending on the mode of Lamb wave propagation this would have different effects on the nature of the Lamb waves. For many of the higher order modes, the higher input angle would cause higher group velocities, causing the wavetrain to arrive earlier in the time domain. Also in context to wave tracing approaches, a wave launched at a higher angle travels through less material, hence arriving earlier and experiencing less material attenuation. This may relate to the high magnitude of energy early in the AU signal for the fiber direction, since the higher angle would travel less distance to get to the receiver it should show up earlier in the signal. Another way of looking at this involves noting the higher group velocity for the higher order Lamb waves associtated with higher angles (this will be discussed later in the section on Lamb waves).

The major point here is that for a vertical type loading to a free surface the variation of the radial disturbance with angle can be calculated. Moreover, in general these calculations show the greatest radial disturbance to be in the normal direction. In the case of anisotropic materials, these results

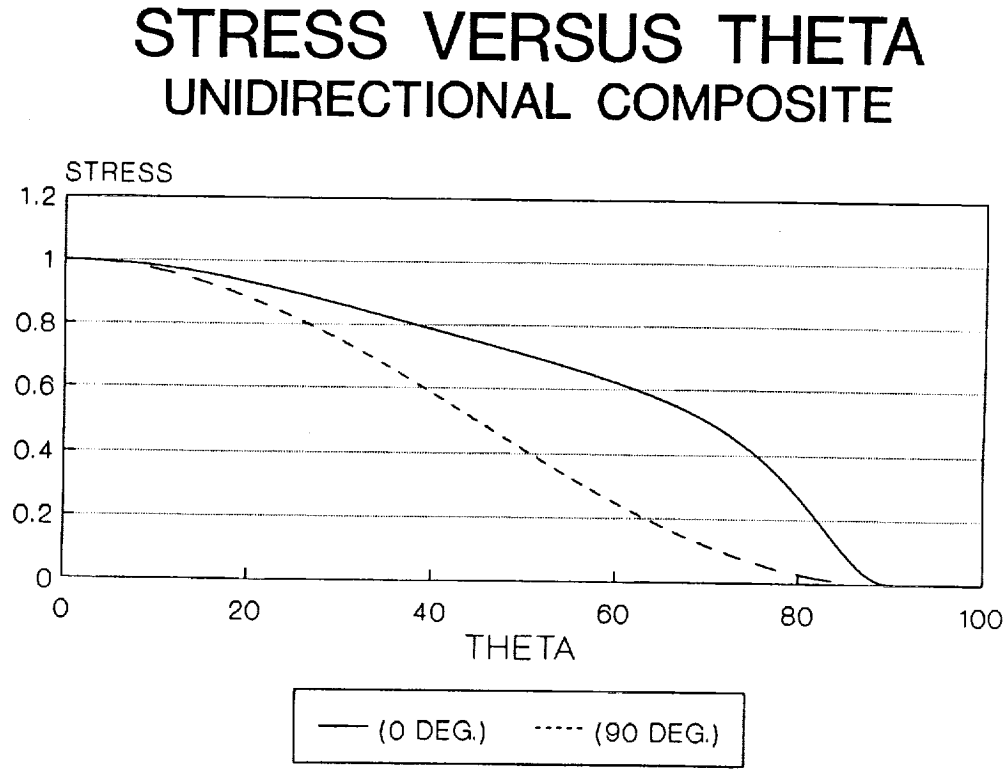

Figure 60. Variation of stress with input angle for unidirectional composite

show that the disturbance may result in more energy being relayed in the stiffest directions and for directions where the material is stiffest, the radial disturbance stays large at higher angles θ. Hence, for the composite plate we would expect a greater disturbance in the fiber direction and for more of the disturbance to take place at higher angles (resulting in a greater disturbance earlier in the signal). In terms of the AU method, this would correspond to greater energy content for the AU signal in the fiber direction. Additionally, this would cause the wave characteristics for the fiber direction to be associated with waves that have higher wave numbers in the fiber direction. This is in agreement with the high energy content at the beginning of the signal for the AU in the fiber direction. For higher order modes, this is because of the higher group velocities for the higher wave numbers associated with the higher input angles θ_3.

It should be kept in mind that Fraunhofer and Fresnel fields may also contribute to input effects, hence, peaks in the loading function may occur at directions other than through-the-thickness, which may result in a mode having more than one peak, where the peaks are closely spaced. Furthermore, certain cases of anisotropy may cause peaks to occur at other directions than 0 degrees, naturally.

Through the Thickness Transverse Resonance

The basic idea behind the TTTR concept is understanding how waves propagate perpendicular to the plane of the plate and how they must be of proper frequency and phase to meet boundary conditions. This section will concentrate on obtaining characteristics of TTTR modes for the plates examined in the experiments in chapter 4, for the purpose of comparison. Basically, this will involve finding the displacement vector for the direction of propagation of TTTR modes and then the frequencies for TTTR modes.

Aluminum Plates

For the aluminum plates, the equations describing wave propagation are simple and wave motion is independent of the direction of propagation. For bulk plane waves, the motion of possible disturbances is one of three waves:

P-wave

SV-wave

SH-wave

For propagation in the thickness direction, this leads to an infinite number of possible directions for perpendicular SV-wave and SH-wave motion, with both these motions perpendicular to the P-wave (thickness direction) motion. Thus, the plane associated with any azimuthal angle would possess the same properties for wave propagation characteristics. Therefore, it would be expected that a symmetric input disturbance would result in an even amount of energy existing for a given Lamb wave for all azimuthal angles (ie. symmetry prevails). Hence, this may provide a means for checking the symmetry of a transducer.

Calculating the resonance (TTTR) frequencies resulting from this is rather simple and was covered in chapter 2. The frequencies for various TTTR modes are displayed in figure 61 for the .0625 inch thick plate and figure 62 for the .125 inch thick plate.

First, notice that the major frequencies seen experimentally for each plate correspond to frequencies associated with TTTR modes, except the .7 MHz and .35 MHz low energy components seen at the beginning of the signal and the very low energy 2.3 MHz component. Also, note that TTTR predicts frequencies for the .0625 plate to be double those seen in the .125 plate as was noted experimentally. Finally, the particular material parameters associated with aluminum cause certain

CUTOFF FREQUENCIES FOR ALUMINUM PLATE

6061-T6 (.0625 INCHES THICK)

MODE NUMBER	SYMMETRIC FREQUENCY (MHz)	ANTISYMMETRIC FREQUENCY (MHz)
0	0.0	0.0
1	1.95	.97
2	1.95	3.9
3	5.9	2.9
4	3.9	7.8
5	9.8	4.8

Figure 61. TTTR frequencies (MHz) for .0625 inch thick aluminum plate

CUTOFF FREQUENCIES FOR ALUMINUM PLATE

6061-T6 ALUMINUM (.125" THICK)

MODE NUMBER	SYMMETRIC FREQUENCY (MHz)	ANTISYMMETRIC FREQUENCY (MHz)
0	0.0	0.0
1	.95	.5
2	1.0	1.9
3	2.9	1.5
4	2.0	3.8
5	4.8	2.5

Figure 62. TTTR frequencies (MHz) for .125 inch thick aluminum plate

modes to possess nearly the same frequencies. For instance, for the .0625 thick plate both the first order symmetric and the second order symmetric TTTR mode are at nearly 2 MHz. However, in this instance the first order symmetric mode possesses a negative group velocity for this frequency range and may be contributing less to the signal.

Composite Plates

The problem associated with TTTR for composite plates is much more complicated than for the aluminum plates. First, for the plane associated with any given azimuthal angle the motion of a wave propagating in the thickness direction is not the same. Specifically, a wave propagating through the thickness of a composite plate has only one solution (3 waves), compared with infinite solutions (for infinite planes) for a wave traveling through the thickness of an aluminum plate. This means the motion of the SV-wave and SH-wave (for the case of x_3 propagation) are constrained to take place in certain directions. Therefore, the first problem involves solving the bulk wave propagation problem for the thickness direction and noting the displacement vectors associated with each mode. Next, the frequencies for TTTR modes are calculated using equations stated earlier.

Bulk Wave Propagation Problem for Composite Plates

Solving the bulk wave problem for wave propagation in the thickness direction of a composite material involves solving Christoffel's equation for the x_3 direction. Hence, the Christoffel equation indicates a P-wave with only u_3 displacement. The one shear wave shows displacement in only the fiber direction and the other only in the cross fiber direction. However, the displacements for a given wave will have components in each of the coordinate directions when the wave is sent in a more general direction. However, for small angles the values vary smoothly from the TTTR, so that values are still predominately in the directions found for the TTTR case with smaller values

for the other directions, hence these waves become pseudo waves. A more exact analysis of this problem may be carried out by using the program (CHRIS.FOR - listing in Appendix G).

The complication of trying to propagate waves at angles slightly off of the x_3 direction may be extremely pertinent to understanding AU results. In the Christoffel equation both v_2 and or v_1 are not zero and the resulting version of the Christoffel equation is much more complicated. The solution to these equations results in shear waves with α_1, α_2, and α_3 terms. However, the general nature of the wave should smoothly vary from that for the x_3 direction solution. Hence, one might still expect the resonance due to the each type of shear wave to perhaps be greatest in that respective direction. This is suspected to be the cause for the high values in the following data:

A1(.23,.35) for the 12-ply specimen in the 90 degree direction (this corresponds to the 1st order antisymmetric wave in figure 64)

A1(.53,.75) for the 24-ply specimen in the 90 degree direction (this corresponds to the 1st order antisymmetric wave in figure 63)

Also, the resonance for the fiber direction oriented SV-wave may contribute to the relatively high values of these variables in the 0 degree direction, since the TTTR frequency for this resonance is so close to that for the SV-wave in the cross fiber direction. This points out a general problem of trying to identify closely spaced and overlapping peaks. Thus, this TTTR frequency is thought to be associated with the resonance of a shear wave with motion in the cross fiber direction, causing greatest motion in the direction where the SV motion is greatest for the plane bulk wave.

Hence, the physical understanding of the AU method and modeling should account for the general nature of bulk wave propagation in the thickness direction and at angles slightly off of the thickness direction. Specifically, it should be understood that the amplitude of the pseudo SV-wave is of much greater value for the fiber and cross fiber direction for the particular SV-wave associated with each direction.

TTTR Frequencies for Composite Plates

Calculating the frequencies for the TTTR modes of an anisotropic material involves using formulas stated in chapter 2. Notice that extra modes exist due to separate resonances for each shear wave polarization. Figure 63 shows a table with values for the first few TTTR modes of the 24-ply Gr/Ep plate, where material properties were estimated using bulk wave velocity measurements. Figure 64 shows similar results for the 12-ply specimen. The extra antisymmetric mode makes picking out particular modes somewhat more complicated for the composite material. However, again notice that frequency peaks seen in the AU experiments correspond to TTTR frequency values predicted by theory, using measured bulk wave velocity values. The frequency for TTTR modes are inversely dependent on plate thickness and agrees with experiment. In general, TTTR seems to adequately predict frequencies found to be present in the AU data.

Lamb Waves

Solving the Lamb wave equations is by no means a trivial exercise and involves a great deal of care and computer time. The equations are transcendental for even the simple case of an isotropic material. In effort, to gain understanding and to decrease computation time, three computer programs where written for cases of increasing difficulty. Specifically, the following three programs were utilized:

DISA- Determines the dispersion relations, phase velocities, and displacements for a Lamb wave in an isotropic material

TTTR FREQUENCIES
24-PLY GR/EP

MODE	SYMMETRIC	ANTISYMMETRIC
1	.36	.23 .31
2	.46 .62	.71
3	1.1	.69 .93
4	.92 1.2	1.4
5	1.8	1.2 1.6

Figure 63. TTTR frequencies (MIIz) for 24-ply Gr/Ep plate

TTTR FREQUENCIES
12-PLY GR/EP PLATE

MODE	SYMMETRIC	ANTISYMMETRIC
1	.70	.46 .61
2	.82 1.24	1.42
3	2.2	1.24 1.8
4	1.8 1.2	2.8
5	3.5	2.3 3.1

Figure 64. TTTR frequencies (MHz) for 12-ply Gr/Ep plate

ORTII- Determines the dispersion relations, finds phase velocities, and displacements for a Lamb wave in an orthotropic material where the the wave is sent in a principal direction (for a composite material this means in either the fiber or cross fiber direction)

GENE- Determines the dispersion relations and finds phase velocities for a Lamb wave in an orthotropic material where the the wave is sent in any direction (for a composite material this means the wave may be sent in any direction relative to the fiber direction)

Basically, each of these programs involves solving the motion equation and meeting the stress free boundary conditions using an assumed linear type of motion. Each case involves careful attention to where the solution takes place on the dispersion curve (ie. whether the wave numbers are real or imaginary). For the isotropic case, this has been formalized and the equations are fairly straight forward. The major concern here is noting when the wave numbers are real or imaginary to understand how the solution may have local maxima and minima which may or may not be confused as solutions. For the anisotropic solutions (ORTH and GENE), whether the wave numbers are real or imaginary effects how the eigenvectors (wave number ratios l) are determined from the motion equation. This situation is especially confusing for the general case (GENE), where the solution is the superposition of many quasi-waves, waves with both normal and shear components.

In fact, finding solutions for the anisotropic cases involved using knowledge gained from the isotropic case and utilizing the method of uncoupled solutions (ref. 127) to guide where solutions are sought for the Lamb wave case. The method of uncoupled solutions is covered in reference 127 and in appendix H, it involves setting boundary conditions that decouple shear and longitudinal waves at plate surfaces. These can then be used as bounds for the Lamb wave solution. The programs were written to allow this information to be utilized. However, this requires that the user modify the program code. In the future, these programs should be made more modular and robust, so that computing can become more automated. Undoubtedly, this will entail some ingenious programming. Appendix H discusses how the method of uncoupled solutions may be combined with the existing codes to yield an improved program.

The following sections and subsections discuss the programs utilized (program listings are in appendices C, D and E), basic results and the relationship they have to AU results. Major emphasis is given to identifying the modes of Lamb wave propagation which are present in the AU signal. This involves examining at the dispersion curve and comparing the values of phase velocities stated in chapter 4 to the values calculated by the programs for the Lamb waves.

Aluminum Plates

The solution to the Lamb wave problem for aluminum plates involves rather straight forward application of the equations stated in chapter 2 for an isotropic plate. For the aluminum plate, there is no effect due to azimuthal angle, so the Lamb wave problem only needs to be solved for one plane. The solution can be obtained for symmetric and antisymmetric modes for any order mode (fundamental, 1st, 2nd...). The same program calculates all these modes, however the user must input whether the solution is for a symmetric or antisymmetric mode. Data sets from this program were used for the plots in figures 65-69.

Computer Solution Technique

The equations utilized for obtaining the solution to the Lamb wave propagation in isotropic materials were covered in chapter 2, the same notation is utilized in the discussion below. The solution involves picking values of the wave number in the plate direction ξ, starting with low values and increasing to higher values, making sure they are in the range of interest. The equations stated for $F(\alpha, \beta, \xi) = 0$ are utilized, along with the other two equations relating the wave numbers to the wave frequency and bulk wave velocities, to find the value of ω that along with ξ satisfy the conditions for the desired mode of Lamb wave motion. Basically, this involves looking for where the function F either gets very close to zero or crosses from a positive value to a negative value. The

computer program is named DISA.FOR and is listed in appendix C. The program variables include:

Velocity of longitudinal wave

Mode of Lamb wave

Velocity of shear wave

Plate thickness

From this, the program calculates and stores in an output file:

Wave number in the plate direction, ξ, and circular frequency, ω (in pairs)

Values for relative amplitudes A, B, C, and D for each pair

UTTT.FOR (Appendix F), reads the output file and then calculates, and sends to separate files each of the following data sets:

Dispersion curve (ω versus ξ)

Phase velocity versus frequency

Displacement, u_3, versus frequency (other parameters could be calculated from given information, such as stress)

The plots shown and discussed below were produced from these data sets.

Computer Results for .0625″ Thick Aluminum Plate

The results of the computer program are comparable for the two aluminum plates with the frequency values of the .125″ thick plate are only half those of the .0625″ thick plate. Only the results for the .0625″ thick plate are given.

The plots of the dispersion curve and of the phase velocity versus frequency for the fundamental symmetric mode of the .0625″ thick aluminum plate are displayed in figure 65. Notice the dispersion curve for the fundamental symmetric mode is linear for low frequency/low wave number values. This means that the phase velocity and group velocity should be roughly the same value. Then notice the decrease in slope over a short period and then the constant lower slope afterwards. In the plot of phase velocity versus frequency, the phase velocity is shown to start at a value of roughly 210,000 inches per second and asymptotically approaches a phase velocity of roughly 110,000 inches per second. It should be noticed that the main change in the phase velocity occurs at roughly 1 MHz, which is the frequency corresponding to the first TTTR mode.

Figure 66 shows comparable plots for the fundamental antisymmetric mode. Unlike the symmetric mode, the antisymmetric mode starts out very nonlinear at a very low slope and approaches a fairly constant slope for higher wave number values. The plot of phase velocity versus frequency shows that for low frequencies that the phase velocity for the antisymmetric fundamental mode is very low and increases to approximately 110,000 inches per second, the same value the symmetric mode approaches. In fact, this is due to the fact that both modes degenerate to Rayleigh type waves for high wave numbers (ξ) and hence have the same phase velocity as a Rayleigh wave.

Similar plots for the first order antisymmetric mode are displayed in figure 67. Notice that the dispersion curve does not start at the origin as does the two fundamental modes, but starts at the first TTTR frequency (1 MHz). This leads to nearly infinite phase velocities, shown in the phase velocity versus frequency plots. Also, the small slope for small values of ξ corresponds to a low

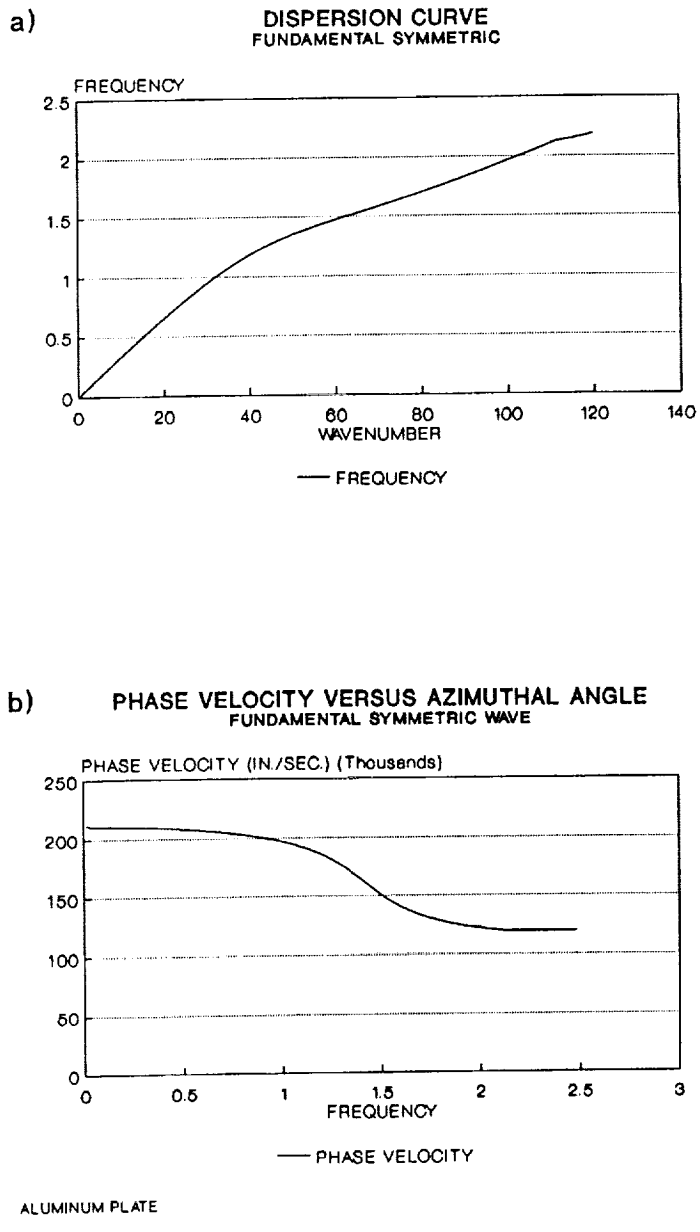

Figure 65. a)Disp. curve and b)V(phase)/freq., plots for fund. symm. mode

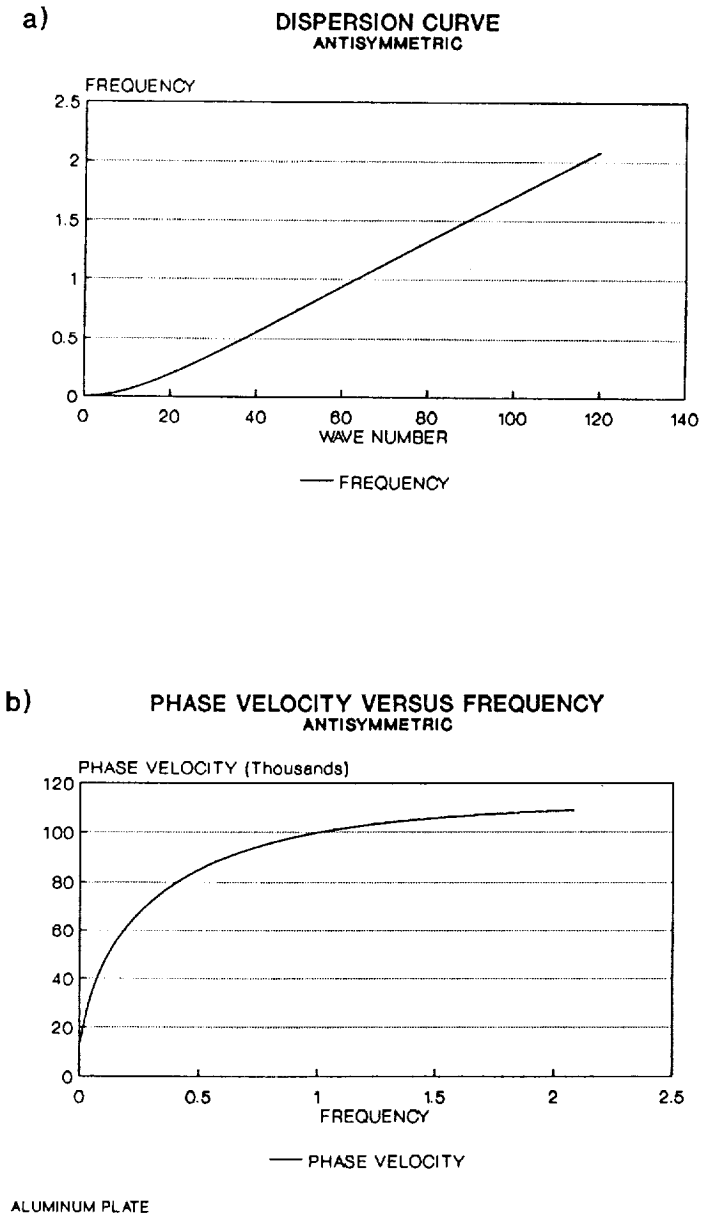

Figure 66. a)Disp. curve and b)V(phase)/freq., plots for fund. anti. mode

group velocity and also means that for a range of values of ξ, relating to a number of input angles θ, the frequency is practically the same value. For low angles of input or small values of ξ, this mode would have high values of phase velocity and would have very low group velocities. An important point here is that a relatively large amount of the energy for this mode may show up at a frequency range close to the TTTR frequency, displaying a variety of phase velocities (of fairly high value) and a variety of group velocities. Analysis shows that even for an input angle of almost 90 degrees, the frequency for the first order antisymmetric mode is still at roughly 1.3 MHz (see figure 67). The variety of group velocities could relate to the fact that the AU signal (for a given frequency) is spread out in the time domain. Also, note that the values of the phase velocity vary quickly with very small changes in frequency and over a fairly small frequency range, while the phase velocity approaches the Rayleigh wave phase velocity.

The first order symmetric wave shows an even stranger type of behavior. The dispersion curve starts out with a negative curvature. This means that the group velocity is negative. The meaning of this is not really clear. It may be that at low wave numbers this mode actually propagates energy backwards for modes with positive phase velocities. Also, this means that for certain specific frequency values, this mode of Lamb wave propagation may have two different phase velocities, group velocities, and wave numbers. Additionally, this means there is a value of ξ where the slope of the dispersion curve is zero, and hence the group velocity is zero. As with the first order antisymmetric mode, this mode shows high phase velocities for low value wave numbers. Finally, notice that this mode starts at just below 2.0 MHz and dips to 1.7 MHz and then climbs back up.

The second order symmetric mode shows behavior much like the first order antisymmetric mode, but of course for $\xi = 0$ shows a frequency value of 2.0 MHz.

The higher order modes show similar behavior, but of course show higher frequency values for the TTTR situation $\xi = 0$. The only other mode to show a negative slope is the second order antisymmetric mode. Also, the higher order modes show dispersion curves with increasingly flat behavior for low values of ξ.

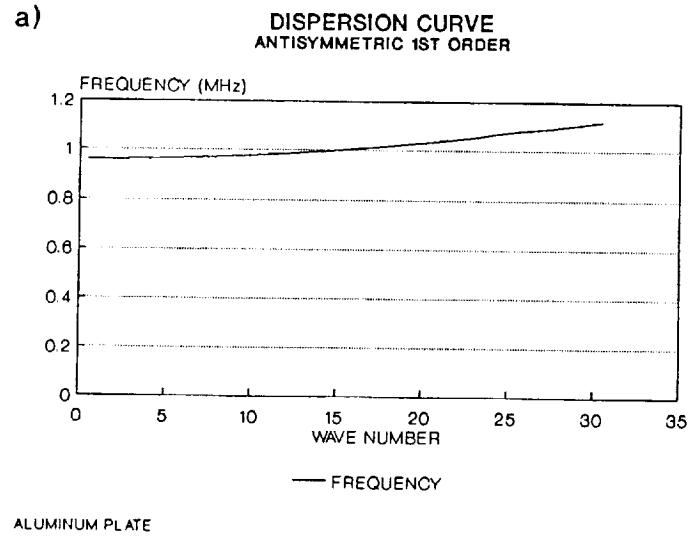

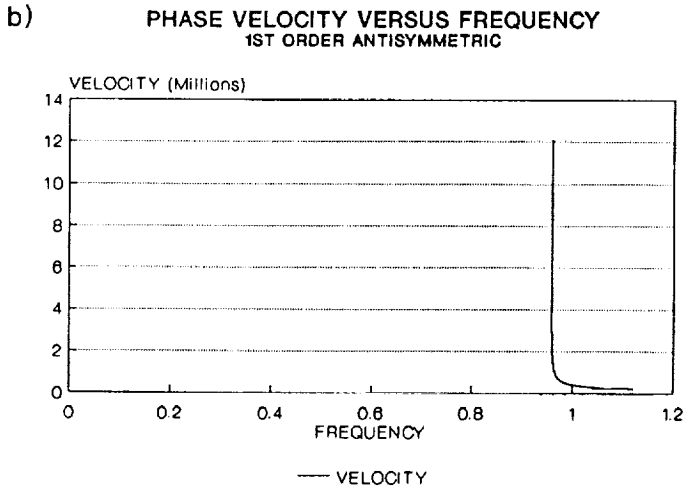

Figure 67. a)Disp. curve and b)V(phase)/freq., plots for 1st anti. mode

Comparison of Computer Results to Experimental Results

For the aluminum plates, the TTTR frequencies seem to be inversely related to the plate thickness for both the experimental and numerical results. Specifically, the frequency for the higher order modes shows a linear inverse relation to plate thickness. Since the experiments and theory agree in this matter and the experimental data shows little other major differences, the rest of the discussion is specified to the .0625″ thick plate.

For the .0625″ thick aluminum plate, only 3 modes are possible for the 1 MHz signal content- the fundamental symmetric, fundamental antisymmetric, and the first order antisymmetric modes. However, the large value for the experimentally measured phase velocity (chapter 2, fig. 34), immediately disqualifies the two fundamental modes as the possible means of wave propagation. Hence, further investigation should be centered on the first order antisymmetric mode as a possible mode of wave propagation for the 1 MHz signal content seen in the AU signal. Further evidence for this conclusion will be presented in the section on modeling. It should be noted that the 1 MHz area of the first order antisymmetric mode is in the low wave number ξ area, relating to a low input angle, agreeing with the predominately normal input associated with the AU method. Additionally, the group velocity for the 1 MHz component of the signal was measured to be much lower than the phase velocity, the exact situation that would be expected for the higher order Lamb wave modes at low wave numbers. In figure 30 and 31, the peak at 1 MHz in the spectrum seems to trail off slowly, indicating that a number of wave numbers are contributing to the energy content in this frequency range. In otherwords, the the wider band width indicates that disturbances sent out at a number of angles may be contributing to the signal in this frequency range (see fig. 74). In general, the 1 MHz signal content possessed characteristics that agree with the first order antisymmetric Lamb wave for low wave numbers.

The 2 MHz signal content showed behavior that indicates that it is either the second or first order symmetric Lamb wave. Although the frequency (2 MHz) of the first order symmetric mode agrees

with the data, the negative group velocity associated with this mode does not agree with experimental measurements. Hence, the 2 MHz signal content seems to be the second order symmetric mode at low wave numbers. Notice in figures 30 and 31 that the peak in the spectrum for this frequency content is much sharper, this may indicate that only the very lowest wave numbers are contributing. This is also supported by the extremely high phase velocities measured for the 2 MHz signal content. Thus, the 2 MHz shows a sharper peak and a higher phase velocity than the 1 MHz signal content, indicating that the 2 MHz (possibly the second order symmetric Lamb wave) signal content may be due to radial disturbances more closely aligned with the vertical than the disturbances associated with the 1 MHz (first order symmetric Lamb wave). Additionally, certain features of the 2 MHz peak (lack of skewness), indicate that the first order symmetric mode may also be contributing to the energy in the signal at this frequency range.

The .7 MHz content at the beginning of the signal showed characteristics of a fundamental symmetric wave. This is supported by the measured phase velocity measurement and the fact that the group velocity was the same as the phase velocity. This wave could be a bulk P-wave, however the wave velocity is lower and agrees more with that of the symmetric fundamental mode. However, more work needs to be conducted to understand why the wave is centered at .7 MHz. This may be a combined effect of transducer size and pulsing frequency. An understanding of this could most likely be obtained by comparing Green's function results (ref. 14) to Lamb wave theory.

Finally, it is noted that a small 2.3 MHz signal content was noted and that this frequency is that of the Goodier-Bishop mode (ref. 142). It was not possible to measure the velocity of this mode because of its low energy content.

Effects of Lamb Waves on AU Signal

For the aluminum plate, the AU signal consists of an early portion of the signal (.7 MHz for the .0625" thick plate) which separates from the rest of the wave train due to a much faster group ve-

locity. This early portion of the signal seems to be a fundamental symmetric Lamb wave and is present in the wave train for a time on the order of the pulse width.

The bulk of the wavetrain consists of a higher amplitude, very fast phase velocity (yet varied), slow group velocity, signal content which continues on in the wavetrain for a much longer time than the early part of the signal. It is believed that this portion of the wave train is made up of the higher order modes at low wave numbers, corresponding to low input angles θ_3. The order of the modes which are excited depends on the frequency of the transducers and the thickness of the plate. As indicated, the long wave train associated with the AU method agrees with what would be expected from higher order Lamb waves. As a result of the higher amplitude and the wavetrain length associated with these modes, it appears that the energy content of the signal is dominated by these higher order modes. This situation may not necessarily be true for all experimental arrangements, however most reported data, including the early work by Vary that related AU to strength, utilizes this type of experimental arrangement. Basically, the standard AU configuration directs most of the energy in the through-the-thickness direction at a frequency range associated with TTTR values, thus exciting higher order Lamb wave modes.

Experimentally, the effect of the wave velocities can be clearly seen by separating the sending and receiving transducers and noting the effect on the wavetrain. For the .0625 plate, the .7 MHz content separates into the early portion of the wave train, due to the fast group velocity and moves rather undistorted, since the group velocity is comparable to the phase velocity. The other parts of the wave train (1 and 2 MHz portions) show phase points that move slightly in the time scale, in other words display very fast phase velocities, but whose amplitude values change rapidly due to a modulating term which moves great distances in the wave train due to a very slow group velocity.

In general, utilizing a conventional AU arrangement on an aluminum plate resulted in a signal which seemed to be dominated, in terms of energy content, by waves showing characteristics of higher order Lamb waves. Specifically, this resulted in a long wave train dominated by frequencies close to TTTR values.

Composite Plates

The Lamb wave problem for composite plates is much more complicated than for isotropic materials, solving this problem involved using the method of partial waves. An additional problem is that the solution to the Lamb wave problem is different for every azimuthal angle. Additionally, the computation involved for every azimuthal angle is much more complicated. Also, the anisotropy of the material allows for additional modes of Lamb wave propagation.

Another major difference is that the Lamb waves for anisotropic materials tend to have kinks in their dispersion curves, due to the crossing of the uncoupled modes (ref. 127). In other words, the curves are not nearly as smooth, but tend to follow one asymptote and then follow another, resulting in a change in direction. This is caused by the different material properties associated with the different directions (θ_3) associated with the different wavenumbers.

As with the elasticity solution, the Lamb wave problem for composite materials is easier to solve in the fiber and cross fiber directions. One program (ORTH.FOR) was written to solve the Lamb wave problem for the simplified cases, fiber and cross fiber directions, and another (GENE.FOR) was written to solve the problem for the more general case, where waves can propagate in any direction.

It is believed that increased understanding and modeling of the AU method is possible through rigorous application and amplification of the ORTH.FOR and GENE.FOR codes. The purpose of this dissertation is to set the foundation for this approach, utilizing these two codes. Since these codes are central to both present and future efforts, this text includes a discussion on the two programs, as well as the listings in the appendices (appendices D and E). Moreover, comments concerning how these codes may be utilized and perhaps amplified are offered. In fact, discussion on modeling in the next chapter involves utilizing these codes.

Computer Solution Technique

As mentioned, the method of partial waves is utilized in both the ORTH.FOR and GENE.FOR codes. The basic solution technique involves the following steps:

1. Define wave number value, k

2. Find a good initial guess for ω

3. Solve Christoffel matrix equation to obtain the values for wave number ratio l_z

4. Find eigenvectors or displacement vectors α_i (choosing the right eigenvector is not a simple matter and can drastically effect results if the wrong one is picked)

5. Calculate K_{ij} from stress free boundary conditions

6. Calculate F by taking the determinant of K_{ij}

7. Determine if F is sufficiently close to zero (If $F$is not zero, then go back to step 3 and try a new value of ω and if F is close enough to zero then continue)

8. If the correct values for a k and ω pair have been found, then use boundary conditions to find values for C_n's and also calculate the phase velocity

9. Store data

10. If k is equal to the counter value stop, if k is lower than the counter then return to step one

Solving this problem provides the dispersion information (ω and k pairs). In addition, velocity and displacement information can be ascertained in a simple fashion. In addition, other variables such as group velocity may be estimated by additional calculations.

In general, the solution strategy is fairly straight forward, however there are a couple of issues which can cause difficulties when generating results. These include both problems with interpreting results from calculations and with choosing proper eigenvectors.

First, the function F may appear to be close to zero and yet not actually be going to zero. This is due to the complex nature of the function and the many local maxima and minima associated with the F function. Alleviating this difficulty is possible by judiciously selecting ω values that are close to the correct ω for the given k. This can be done by utilizing general knowledge on how dispersion curves of Lamb waves behave and by utilizing the uncoupled mode theory to provide values for initial guesses.

The other problem which may be encountered in blindly appplying the partial wave equations is that of not choosing the proper eigenvectors or displacement vector upon solving the Christroffel equation for the partial waves. Attention must be given to choosing eigenvectors which represent the proper motion for the partial waves to make Lamb waves (see ref. 127).

The input for each code involves the following parameters:

Stiffness matrix

Material density

Plate thickness

Azimuthal angle

Information on guesses, this defines what mode the solution is finding (eventually this should be included in program logic- see appendix H)

ORTH.FOR

As mentioned, the solution for the case where the wave is sent in the direction of the fibers or the cross fiber direction is much simpler due to the decoupling of P-wave and SV-wave modes from SH-wave modes. This is observed when one looks at the eigenvalue problem derived from the partial wave Christoffel equation:

$$\begin{bmatrix} (D_{11} + l^2 C_{55}) & 0 & (l(C_{13} + C_{55})) \\ 0 & (D_{66} + l^2 C_{44}) & 0 \\ (l(C_{13} + C_{55})) & 0 & (D_{55} + l^2 C_{33}) \end{bmatrix} \begin{bmatrix} \alpha_1 \\ \alpha_2 \\ \alpha_3 \end{bmatrix} = 0$$

where $D_{ij} = C_{ij} - \frac{\rho\omega^2}{k^2}$, l is the wave number ratio, and α_i are the displacement vector values. Obviously, the middle term can be decoupled and solved for the SH-wave modes. However, the solution to this problem for the general case of waves propagating in a general direction (ie. not the fiber or cross fiber direction) leaves this matrix problem fully populated.

It should also be noted that the equation for the wave number ratio for the (P-wave and SV-wave coupled) case yields four values of l that relate each of the four partial waves that make up the symmetric and antisymmetric Lamb waves. This equation is derived upon setting the determinant of the matrix to zero, factoring out the quadratic equation for the SH-mode and solving the 4-th order polynomial. Since the equation only involves squared terms, the solution follows easily from the quadratic equation. Then the values of the α_i's corresponding to each of the l's can be determined up to a constant through back substitution. It is important to properly choose the α values. This involves choosing partial waves where the displacement vectors are properly oriented. These functions are performed in sections 4 and 5 of the code.

Next, the partial waves are superposed to obtain the displacement equation:

$$u_j = \sum_{n=1}^{6} C_n \alpha_j^{(n)} \exp(ik(x + l_z^{(n)} z))$$

These values were then differentiated to produce strains associated with the stress wave propagation. The strains were then combined with the constitutive relations to yield stresses. It should be noted that the values of C_n determine the nature of the displacement field for any mode of propagation. The stress free boundary conditions determine these up to a constant, but it is the domain of modeling efforts to determine this constant. This is discussed in the next chapter.

Next, the stress equations were used with the boundary conditions

$$\tau_3(x_3 = \pm b) = 0$$

and

$$\tau_5(x_3 = \pm b) = 0$$

to yield the next eigenvalue problem. Note these boundary conditions are only for the P-wave and SV-wave modes. In this problem, the values of C_n are the eigenvector values.

The matrix K_{ij} is obtained by taking the coefficient of each C_n for each of the four boundary conditions. Hence, the rows (i-value) of the K_{ij} matrix are determined by which boundary condition is used and the columns (j-value) by which C_n is used. The terms of the matrix are defined in section 6 of the program ORTII.FOR.

Finding the determinant of K_{ij} is used to determine if the dispersion condition is met. This involves taking the magnitude of the determinant and checking if it is close enough to zero, mathematically this is expressed by $F(\omega, \xi, l_n, \alpha_n) = 0$. This determinant of the matrix and the value F is found in section 7 of the program. The equation for F is utilized to see if the ω -k pair is appropriate (ie.

if the determinant $K_{ij} = 0$). Section 8 checks to see if the dispersion condition is met. If the determinant is zero then the equations from the stress conditions can be used to solve for the values of C_n up to the constant, which may be approximated by the elasticity solution. The values for C_n and the phase velocity are determined in section 9. Section 10 writes the results to output files.

GENE.FOR

The procedure for solving the Lamb wave equations in the general case are the same except that the preliminary step of defining an azimuthal angle is necessary and each basic step is much more complicated.

Steps 1-3 set up the value used for k and ω, in the same manner they were in ORTH.FOR. The only extra complication is that choosing guess values for the general case is orders of magnitude more difficult.

Solving the Christoffel equation for the partial waves involves solving a 6-th order polynomial since the SH-mode is coupled with the other solutions. However, the equation can be treated as a cubic equation of squared values. This was solved using a standard approach (ref. 37). Section 4 contains the solution to the Christoffel equation for the partial waves.

The equation for u_j is similar, except all six partial waves must be included in the summed equation. Application of strain and constitutive equations are similar, except that the extra shear stresses in the x_2 direction (τ_{23}) must be considered. Thus, the matrix K_{ij} is a 6 by 6 matrix, instead of a 4 by 4. This makes the calculation of the determinant, and hence the calculation of F much more difficult. Sections 6-7 make these calculations

In general, the rest of the solution is similar and can be followed by comparing the listing for GENE.FOR to ORTH.FOR. It should be noted that extra modes exist for the general case, hence

extra special care must be taken to look for the solution of a particular mode in the right area. In fact some of the higher modes, start at the same value of frequency ω for $\xi = 0$, but quickly turn into different curves where different ω's exist for the same ξ (ref. 127). Determining these curves, for just one azimuthal angle is a very arduous and time consumming endeavor.

Computer Results

This section will show some sample results found using the above codes for the purpose of showing the utility of the codes and for the purpose of identifying modes of wave propagation associated with the AU method.

The plots for the fundamental antisymmetric modes for waves sent in the fiber direction and cross fiber direction are shown in figures 68 and 69, respectively. Notice the effect of the material properties on the shapes of the dispersion curves.

Figure 70 displays the dispersion curve and phase velocity versus frequency for the fundamental symmetric Lamb wave sent in the 0 degree direction. Figure 71 displays a similar plot for the fundamental Lamb wave sent in the 90 degree direction. Similar plots for the third order symmetric Lamb wave are shown in figure 72 for the 0 degree direction and figure 73 for the 90 degree direction.

Comparison of Computer Results to Experimental Results

Information from these plots is useful for identifying the modes of propagation in the composite plates and for helping to understand the general behavior seen in the experimental results. This includes using both wave velocity calculations and dispersion curve results. Much of this discussion is of a qualitative nature.

a)

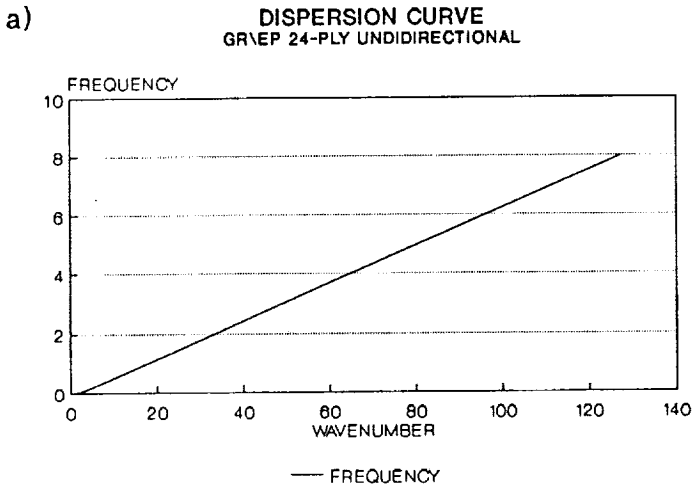

b)

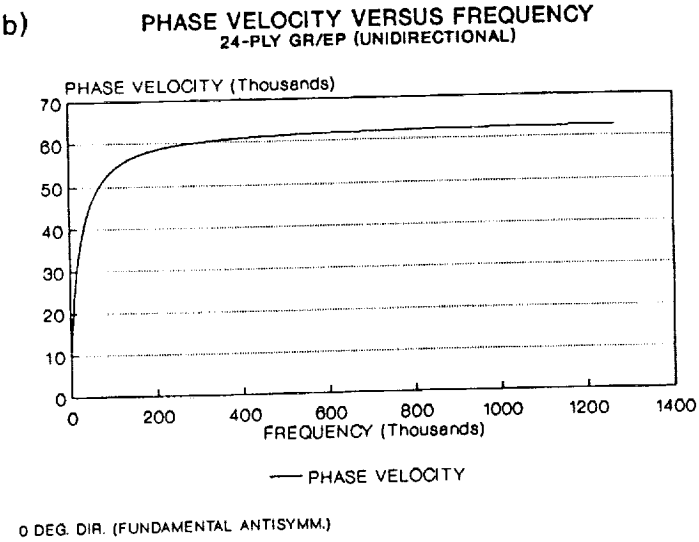

Figure 68. a)Disp. curve and b)V(phase)/freq. plots, fun. ant. 0-deg. dir.

a)

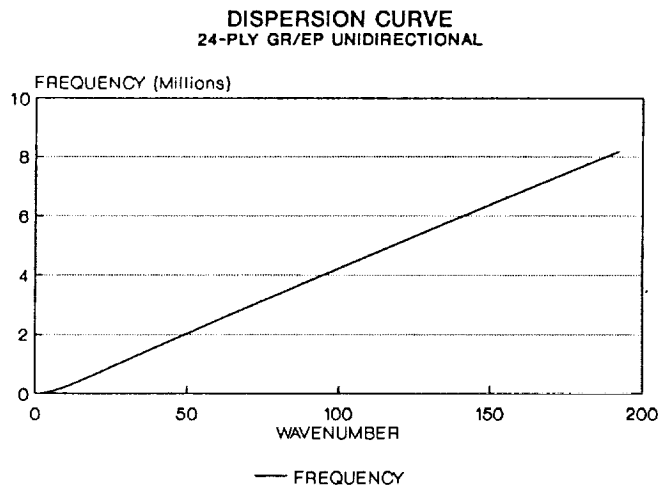

90 deg. fund. antl.

b)

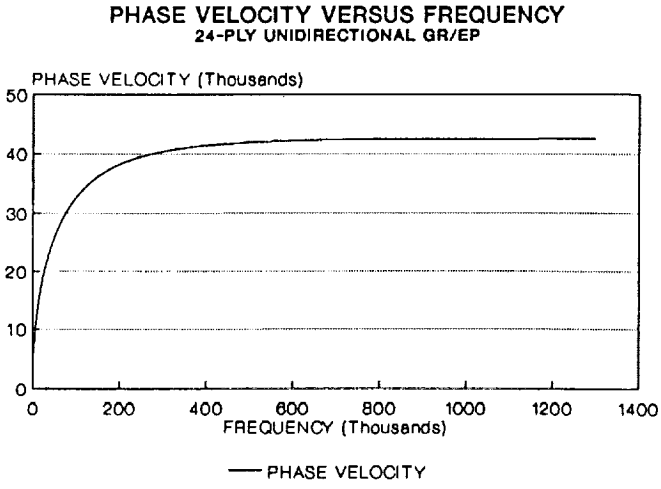

90 deg. fund. symm.

Figure 69. a)Disp. curve and b)V(phase)/freq. plots, fun. ant. 90-deg. dir.

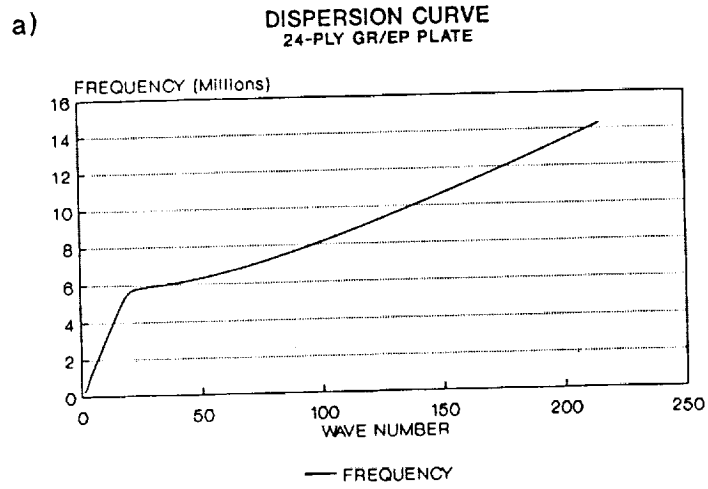

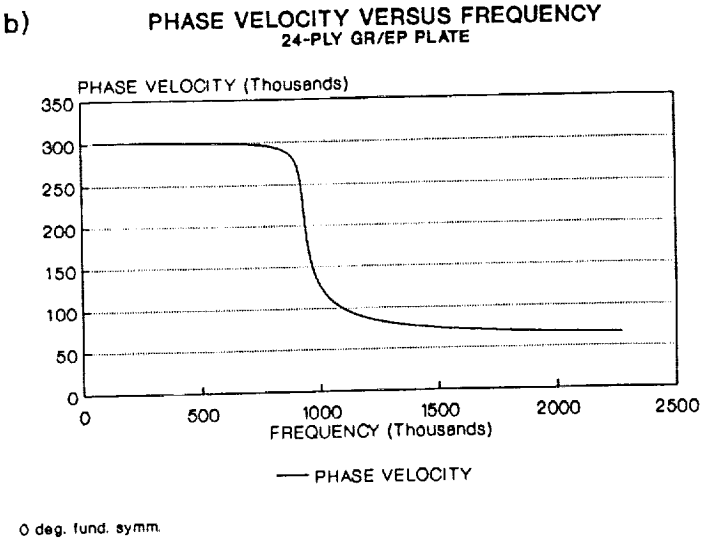

Figure 70. a)Disp. curve and b)V(phase)/freq. plots, fun. symm. 0-deg. dir.

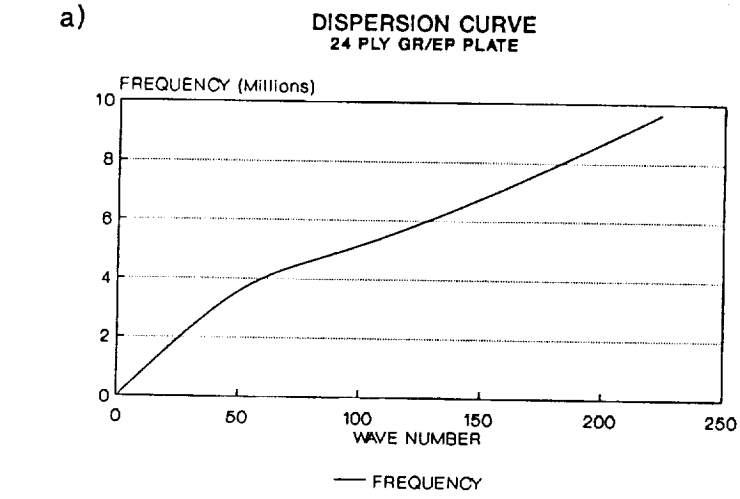

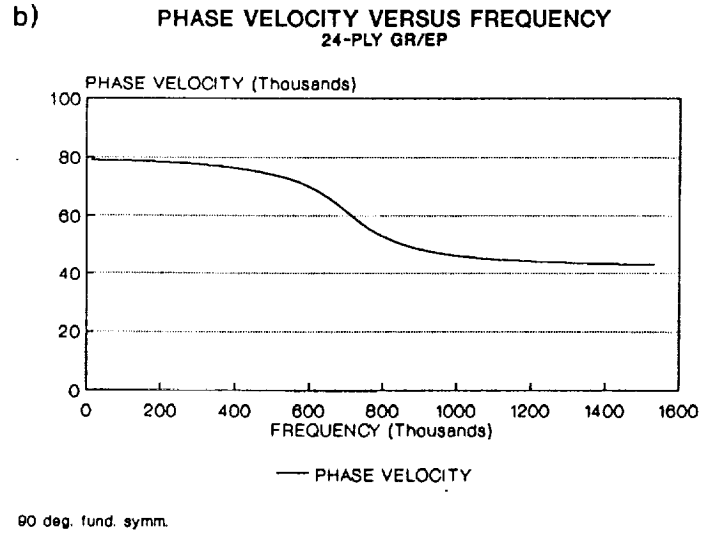

Figure 71. a)Disp. curve and b)V(phase)/freq. plots, fun. symm. 90-deg.

a)

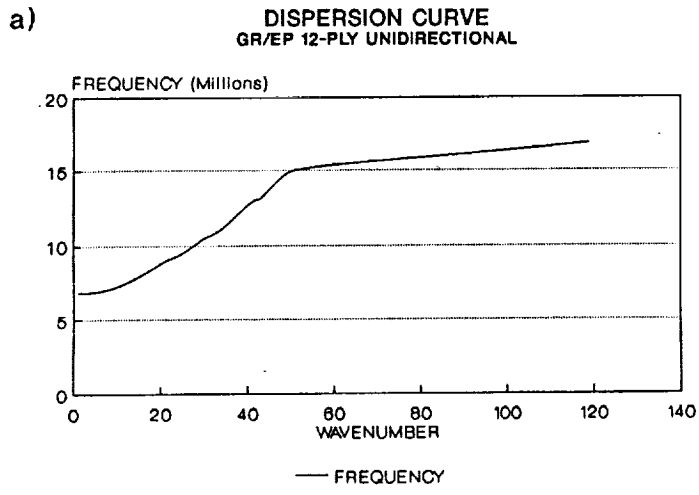

b)

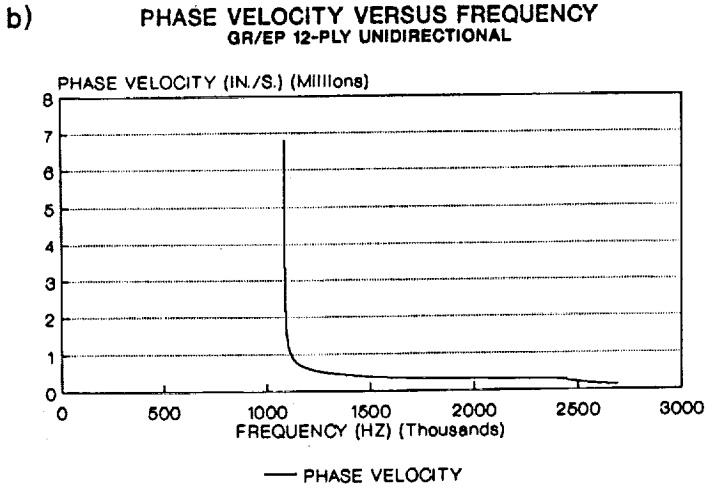

Figure 72. a)Disp. curve and b)V(phase)/freq. plots, 3rd. symm. 0-deg. dir.

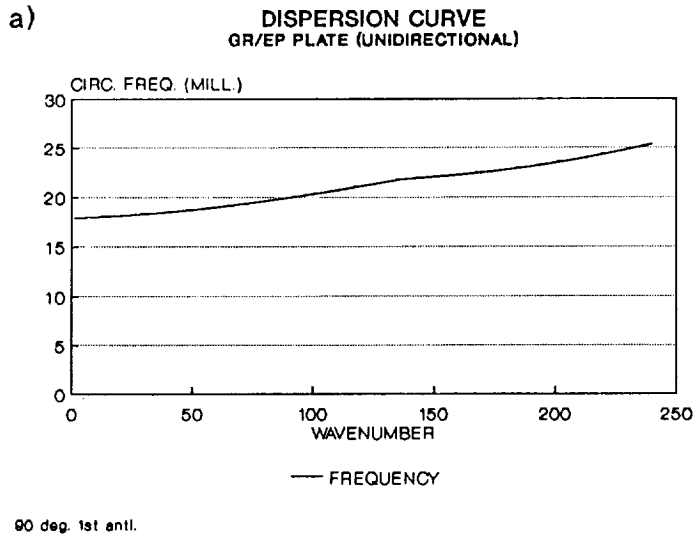

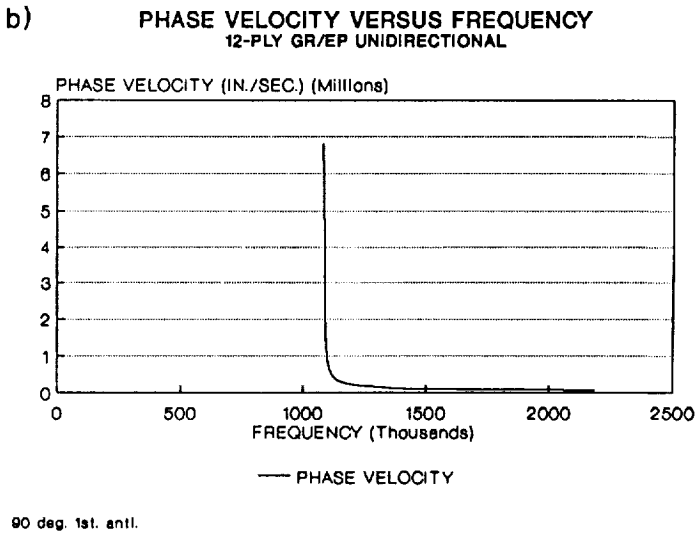

Figure 73. a)Disp. curve and b)V(phase)/freq. plots, 3rd. symm. 90-deg.

The main issue here in terms of comparison to experimental results is that the phase velocities for the fundamental modes are below those measured with the AU method. However, the AU results for the composite plate do not show nearly so drastic a difference in the phase velocities measured in AU results compared to those predicted for fundamental Lamb waves.

Also, it is interesting to note the effect of the azimuthal angle (variation of material properties) on how the higher order mode, 3rd order symmetric mode, behaves for small values of ξ. This shows how the dispersion curve for the fiber direction turns upward (higher slope - higher group velocity), much earlier than the 90 degree direction (see figs. 72 and 73). Also, note the abrupt change from the quick rise to a slow move across, this is due to the 5th order uncoupled shear wave crossing the uncoupled P-wave (see appendix H). The early steep rise corroborates experimental results, which show more energy for this mode to be present earlier in the wavetrain for the fiber direction.

A more intensive study of how higher order mode velocity versus frequency plots vary with azimuthal angle may help to explain the measured phase velocities given in chapter 4. In general, the very nonlinear behavior of the curves for the higher order modes has a drastic effect on results and the variation of material properties with azimuthal angle has an effect on the nonlinear behavior of the curves for higher order Lamb wave modes.

Lamb Wave Propagation and AU for Composite Plates

Results indicate that, as with the aluminum plate, composite plates propagate the bulk of the energy in the AU signal via higher order Lamb wave modes at relatively low wave numbers, corresponding to small angles θ_3. This is not quite as obvious for the composite plates (especially the 24-ply plate), since the measured phase velocities are not nearly as large for the composite plates as they are for the aluminum plates. This may be due to a variety of reasons. For example, the general anisotropy of the plates may cause the energy to be less centered at low angles, corresponding to the higher phase velocities. Also, the higher material attenuation may cause the low angle (low wave number)

(high phase velocity) waves to be more attenuated due to the increased distance of plane wave travel. This idea is supported by the fact that the 12-ply plate showed much faster phase velocities than the 24-ply plate (thicker plate with more material for reflected waves to travel through). The wider bandwidth for frequency peaks in the composite plates experimentally supports the notion that increased spread of energy exists in the composite plate, compared to the aluminum.

In addition, due to the variation of material properties with azimuthal angles, a number of interesting phenomena affect the dispersion and displacement behavior of these modes with azimuthal angle.

First, the displacement vector associated with shear waves sent in directions just off the normal direction, x_3, may have an effect on the disturbance caused by certain modes. This relates to the discussion on the TTTR mode where it was noted that the two possible shear waves which may propagate in the thickness direction are:

Shear wave where displacement is in the fiber direction

Shear wave where displacement is in the cross fiber direction

Thus, one would expect that for shear waves sent just off the normal, in for example the cross fiber direction, the shear wave with displacement in the cross fiber direction would behave as a mostly SV-wave and contribute to exciting out of plane displacement. The other shear wave would relate to the SH-mode with just in-plane displacement for the cross fiber direction. Hence, one would expect the high order mode that crosses the frequency curve at the value associated with the TTTR for that shear wave to have a higher out of plane displacement in the cross fiber direction, where the motion is predominately SV-wave type and hence contributes more to out of plane Lamb wave motion, as opposed to SH-Lamb wave motion. This is an explanation for the high value of the .234 MHz signal content for the 24-ply plate in the 90 degree direction. A full utilization of modeling efforts can be used to confirm or reject this heuristic argument.

For certain modes the displacement out of plane is large, while for others the in-plane displacement is large. For the higher order modes at low wave numbers, the resonances associated with the P-wave resonance (1st order symmetric, 2nd order antisymmetric, 3rd order symmetric, 4th order antisymmetric) would be expected to have greater out of plane displacements. In fact, the 2nd order antisymmetric seems to be one of the modes of propagation, while the 3rd order symmetric is most definitely a mode seen for the 12-ply and 24-ply panels. Additionally, the 24-ply panel showed a peak for the 4th order antisymmetric mode at low azimuthal angles. Thus, the P-wave resonance modes, which would cause a large disturbance at low wave number values, seem to contribute largely to the AU results for the composite plate signal in the low azimuthal angle (high stiffness) directions, this is confirmed by the high values of A1(.9,1.1), 3rd order symmetric wave (P-wave resonance), seen in the 24-ply panel and the similar results for A1(1.9,2.1) obtained on the 12-ply laminate.

Another interesting phenomenon is the quicker drop in energy content of the 2nd order antisymmetric mode at low azimuthal angles compared to the 3rd order symmetric. For the 24-ply panel this can be seen in the azimuthal plots of A1(.62,.68)-2nd order antisymmetric and A1(.9,1.1)-3rd order symmetric. The 12-ply panels showed the same type of variation, in fact the results for the 12-ply panel showed an even more drastic effect of a high energy content at 15 degrees for the 3rd order symmetric mode. This behavior has also been noted in numerous other panels (ref. 9,99). A search for an explanation leads to a couple of places:

Does the energy flux for the antisymmetric motion draw energy over to the fiber direction more than for the symmetric (Modeling efforts should provide this comparison)

How does the displacement behavior of the 3rd order symmetric wave compare with C_{11} (plane strain) variation with azimuthal angle, the displacement field associated with the 2nd order antisymmetric wave, and E_x (plane stress), variation with azimuthal angle

It should be noted that the measurement of energy content of the 3rd order symmetric mode at 15 degrees is relatively low for the 2 inch measurement, compared to the 1 inch measurement. This tends to indicate that the 1 inch results are simply due to a lesser energy flux deviation angle for 3rd order symmetric mode, compared to the 2nd order antisymmetric mode, in the 15 degree direction. Hence, it may be simply a matter of energy flux and geometry. An understanding of this effect may eventually become possible by utilizing modeling ideas forwarded in the next chapter. Eventually, energy flux behavior may be more directly related to engineering properties discussed in the literature search (coefficient of mutual influence etc.) and these results may provide a good experimental means of determining how local values of these parameters which measure material anisotropy change with damage.

Another aspect associated with the higher order modes is the fact that for low wave numbers the frequency is practically the same for a sizeable range of wave numbers. This means that the energy seen for a certain higher order mode at a certain azimuthal angle is actually the integrated effect of the energy associated with a range of low wave numbers. Thus, this is where the issue of how material properties affect the nature of these curves and where they curve up (show a higher group velocity) becomes an issue. Figures 72 and 73 show how the stiffer material in the 0 degree direction affects the shape of the dispersion curve for the higher order mode, and hence signal energy content, frequency content, and time placement.

In general, a number of effects control how the energy originally introduced to the top surface of the composite plate is channeled through the plate in the various azimuthal directions. These include the following:

How surface input disturbance causes different radial disturbances (elasticity solution)

Dispersion curve behavior

Displacement associated with each mode and how it is affected by direction (this effect is especially noted in the high energy for the 1st order antisymmetric wave related to the SV-wave for the cross fiber resonance condition)

Energy flux behavior

Variation of damping effects with azimuthal angle

Directional effects of damage on different modes

The identification of the higher order modes which make up the AU signal will allow the understanding and computation of these effects to be accomplished.

General Physical Understanding of AU Results

A series of carefully performed experiments on the AU technique have identified the major modes of wave propagation present in the AU signal as higher order Lamb waves with low wave numbers k that correlate to low input angles. A number of factors contribute to this conclusion:

Results indicate disturbances are the same on the top and bottom surface (ref. 8)

Phase velocity measurements

Group velocity measurements

Frequency content

These modes agree with modes that would have maximum displacement out of plane

These modes would be expected based on theory and characterization of input

Furthermore, an understanding of why these waves dominate the AU signal can be ascertained by looking at several factors:

Elasticity solution for point load on a half space (idealization of transducer input) shows that the major radial disturbance takes place at low angles, corresponding to low wave numbers, agreeing with general observed behavior and other theory

The frequency response of the transducer used in this work (representative of transducers used in general AU configurations) causes disturbances that are of a frequency range (TTTR frequencies) for the higher order modes at low angles instead of the lower frequency range that the fundamental Lamb waves would have for low angles of θ_3

The higher order modes show disturbances at a range of low input angles that are of a relatively constant value of frequency, hence the peak in the frequency domain corresponds to a number of points where the dispersion curve is flat and of a fairly constant value

Some of the higher order modes seen have a large u_3 (however, other modes seen would not be expected to have as large of a u_3?)

In simple terms this means, that if you apply a predominately normal force sufficiently fast to the face of a plate, then radial disturbances will emanate outward at various angles, with by far the greatest energy content in the thickness direction or at small angles off of the thickness direction. Disturbances that contain frequencies relating to wavelengths that are half multiples of the plate thickness and of proper phase will meet the stress free boundary conditions and hence propagate through the material by reflecting back and forth between surfaces. Results indicate that by using higher frequency transducers, it is possible to excite higher order Lamb waves. The Lamb wave equations describe the plate modes caused by the plane waves resonating between the top and bottom surface of the plate. Hence, a physical understanding of this behavior may be obtained by

attempting to trace this reflection problem or by simply using the Lamb wave equations. Obviously, wave motion impinges upon the stress free surfaces and results in sizeable surface displacements, to be measured by the receiving transducers.

Another interesting fact is that in all cases the phase velocity measured for the higher frequency was higher than the lower frequency. This may be explained by noting that for a given k value, the higher frequency value will obviously have a higher phase velocity ($v_{phase} = \frac{\omega}{k}$). Hence, for the range of k's associated with the AU method, higher frequencies should cause a higher phase velocity, for higher order Lamb waves. In this regard, experimental results again agree with a physical understanding based on higher order Lamb waves.

Also, the wavetrain for the .0625" thick aluminum plate showed the 2 MHz signal to dominate the end of the wavetrain, which agrees with the expected behavior of the 2nd order symmetric Lamb wave, relating to the long smooth slope of the dispersion curve. The small bandwidth on the 2 MHz peak also agrees with the slower rising behavior of the 2nd order symmetric mode.

The experiment on tilting the sending transducer showed that by causing more of the disturbance to be sent at higher angles of inclination to the normal causes a slight increase in the values of the frequency peaks. This shows that the higher angle θ_3, causes a higher wave number k, causing a higher frequency value. In terms of resonance this generally relates to a longer wavelength. Another major point here is that this tends to indicate that the mode of propagation related to the negative group velocity portion of the 1st order symmetric mode is not contributing to the signal, validating claims in a couple of incidences where this mode was discounted as a mode of propagation, in place of another mode with a closely placed frequency value.

Experiments performed on the tapered plate provide further information on the general nature of the wave propagation associated with the AU method. One major interest in performing these tests was to see if the frequency content of the signal obtained across the taper was more indicative of the frequency content of the side where the sender was placed or where the receiver was placed.

Results showed that the signal across the taper showed frequency peaks associated with both the sending side and the receiving side. One notable result is that a .5 MHz peak was produced by placing the sending transducer on the thin side (where the lowest TTTR frequency is 1.0 MHz) and the receiving transducer on the thicker side. The major point is that the disturbance is not produced solely by way of the sending transducer creating resonances directly through the thickness, but is the result of plate waves being produced by plane type waves sent off at various angles. Hence, this set of experiments substantiated the physical understanding obtained from experiments on the flat plates.

AU Modeling

As stated in the introduction, engineering requires basic models for use in relating measurable parameters to parameters which predict ensuing material behavior. The purpose of modeling the AU technique is to relate AU parameters to parameters which describe composite material behavior. To start with, AU results can be related to the moduli of composite materials. This is possible utilizing concepts from our physical understanding of the AU method. Thus, the first section of this chapter will forward a basic approach for modeling the AU method using the physical understanding of the AU technique forwarded last chapter. This will include a partial example for an aluminum plate. Comments are offered on the procedure for modeling the AU of a composite plate and the difficulty in computing all the results. Next, comments are offered on other factors which contribute to AU results and how to possibly account for them. This section consists of a good deal of conjecture and is presented to foster further developments in AU modeling.

The final section of this chapter contributes statements on relations between AU modeling and fatigue modeling. This is the fusing step which should help transform the AU method from a nondestructive testing technique to a nondestructive evaluation technique.

Simple AU Model

Utilizing concepts from the last chapter, a procedure for modeling the AU technique may be developed. Obviously, this will involve using the theory forwarded in the last chapter along with information obtained by comparing this theory with experimental results. Specifically, certain assumptions are made based on experimental results. The outline for this procedure follows these basic steps:

1. Determine spectral density of input force from transducer

2. Determine dependence of the magnitude of the radial disturbance on angle (θ) [elasticity, finite element method etc]

3. Solve TTTR problem with particular attention to displacement vectors for transverse resonance modes (this gives information on frequencies of interest and on displacement for transverse modes)

4. Solve Lamb wave problem for higher order modes and obtain basic dispersion information

5. Solve for u_i coefficient values, at low wave numbers, by using stress free boundary conditions and setting the value of the coefficient for partial wave (composite solution) or P-wave potential (isotropic plate solution) equal to relative magnitude based on radial value of σ_r from elasticity solution or other method like finite element method

6. If solving for a general direction on the composite material, solve for the value of $\tau_{r\theta}$ and set the magnitude of the corresponding shear wave equal to the same value and then solve for u_i again

7. Add the values of u_i together from both the P-wave and the SV-wave

8. For composite plate do steps 1-7 for different azimuthal angles

9. Compute energy fluxes for various azimuthal angles on plots

10. Compute the energy flux by some sort of integration scheme for a given region of area related to region of arc associated with how many azimuthal angles are utilized (this is discussed later)

11. For each mode of propagation over a range of frequencies calculate the magnitude of disturbance for that mode (ie. u_3, magnitude of E_i vector, etc.)

12. Compare variation of magnitude indicator with frequency to spectrum output and compare values of relative peaks

This gives us basic information on the relative values to expect for various peaks in the frequency spectrum for an undamaged specimen and an indication of what AU values should be relative to each other. Moreover, for a composite material this provides a means for predicting how various AU parameters may vary with azimuthal angle. At the very least, it provides a means for predicting what frequency content should be present for various applications, contributing a tool which may be used for developing optimal AU systems to get the most informative AU signal. Also, with improvements in the model and the method in general, this may provide a means for keeping track of the materials energy dissipating mechanisms. An understanding of how the energy in the various modes, with their various displacement and stress fields (given by theory), is transmitted or dissipated may provide important information on the mechanical effects of different damage states. Conversely, this provides a means for identifying the damage state and perhaps the magnitude of its mechanical effect. This type of understanding is possible now that a physical understanding of the AU method for composite materials exists.

Information on stiffness may be determined by measurements made in the time domain which indicate phase velocities and group velocities. If a phase velocity and a group velocity can be experimentally measured for a given frequency range over the length of the signal, it may be possible to

obtain a fairly accurate dispersion curve. Using theory, the same dispersion curve may be constructed a number of times using various values for material properties. By comparing dispersion curves, it may be possible to infer (eg.regression techniques) the variation in material properties with angle for that direction. In fact, a system could be designed that has one sending transducer and two or more transducers at various azmimuthal angles to determine material properties in a number of directions. The system may also be improved by filtering the signal to certain frequency ranges to keep out the effects of other modes and to hence make velocity measurements easier. Modeling efforts may make it possible to make quick stiffness measurements in all directions via the AU technique. However, this will involve using more advanced signal processing techniques, such as the analytic signal (refs. 16 and 147). Also, it will entail using an altered experimental set-up with multiple transducers and various other experimental additions. Again, interpreting results from this type of arrangement are possible now that a physical understanding of the AU method exists. In general, the long wavetrain associated with the AU method is packed with information from the numerous modes and ranges of wavenumbers on the dispersion curve, which contribute to the signal. Now that these modes have been identified, experimental set-up and signal analysis can be used to obtain as much information as possible on material state. Undoubtedly, this will take years of further work, but now that a basic physical model is formulated, this work has a direction to follow.

Aluminum Plate Application

In order to understand the application of the modeling approach, a short example is provided to exemplify how the frequency spectrum for a Lamb wave mode may be calculated for AU on a .0625″ thick aluminum plate using 2.25 MHz transducers. Also, this application of the model acts to exemplify certain aspects of the physical understanding which were tacitly stated in the last chapter. The effects of other facets of the problem, such as frequency dependent attenuation, are

not accounted for in these predictions. Because of this and the simplification of other facets of the problem, the purpose here is not to reproduce the exact spectrum, but to show the general trend.

The AU method was performed on the .0625″ thick aluminum plate, using 2.25 MHz transducers. The characterization of the sender was shown in figure 24 in chapter 3. The effect of the transducer frequency response and the effect of the way the radial response varies with the angle from the normal are included in calculations. First, the functional dependence of the magnitude of the input was shown to be $\cos^2(\theta_3)$. This value was just substituted into the value for the P-wave magnitude in the displacement equations. Displacement values for a set frequency were then multiplied by the magnitude of the transducer response for that frequency to account for the frequency dependence of the input.

A plot of u_3 (displacement) magnitude is offered for the 1st order antisymmetric mode on the .0625″ thick plate, along with a comparison spectrum for the same plate, in figure 74. This plot shows that the frequency dependent behavior of the displacement values are similar to the behavior of the 1 MHz peak in the AU spectrum. Note that both the model and the signal spectrum show a curve which rises rapidly to a peak at 1 MHz and trail off to zero at about 1.3 MHz. Another point of interest is the symmetrical nature of the 2.0 MHz peak and the minima value at around 2.0 MHz in the signal spectrum. This may be due to the combined effects of the 1st and 2nd order symmetric Lamb waves, where the 1st order is contributing to the rising part of the left part of the peak (e.g. for lower frequency values after the minima of this function).

An additional, concern here is the idealization of the $\cos^2(\theta_3)$ as the input variation. In reality, Fresnel and Fraunhofer diffraction effects are most likely taking place. Future models should attempt to include these type of effects on the input and, hence AU results.

Ultimately, a less simplified model should sum the effects of every Lamb mode that is within the frequency range of the system. This would provide a means for noticing abnormalities in results and perhaps at some point modeling these effects.

a)

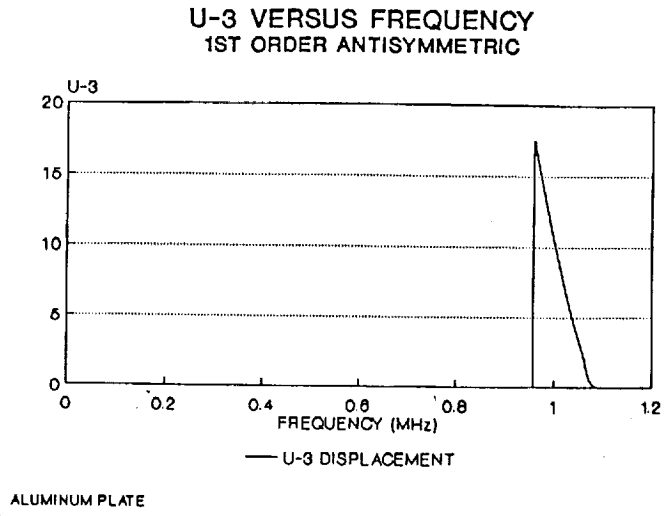

b)

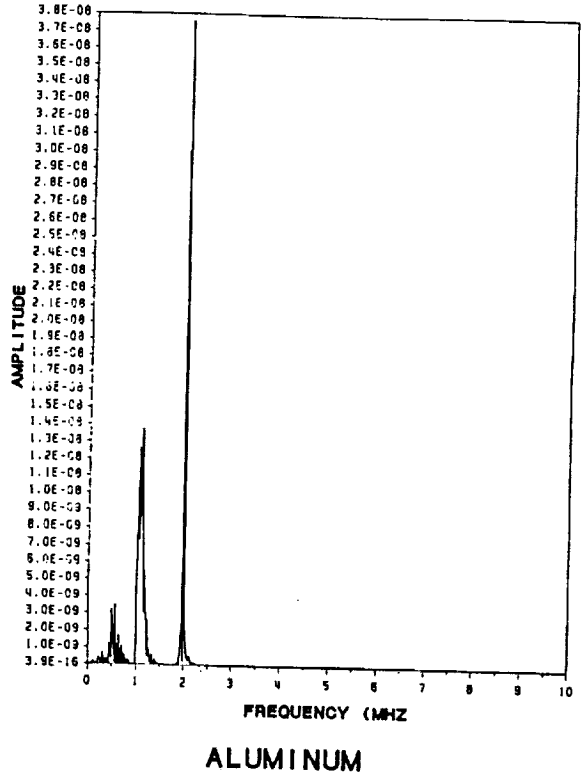

Figure 74. comparison of a)modeled AU response (1st. anti.) b)exper. spect.

A couple of the more pertinent issues concerning this approach include:

How the effect of the input disturbance is included in the Lamb wave equations

What to use to model the magnitude of the output for AU signal (eg. u_3 etc.)

Here the input stress (calculated from the elasticity solution) was simply used to control the magnitude of the P-wave potential. However, there may be a more appropriate means of accounting for the input.

For normal mode transducers, it would be expected that the u_3 value at the top surface would correlate most closely to the output signal, but for other measurement techniques, the values of other displacement terms or stresses may be of use.

Discussion of Applying Model to Composites

The problem of modeling the AU method for composite materials is significantly more complicated than for isotropic materials. Anisotropic properties not only cause the variation of the AU response with azimuthal angles, but make the calculation of Lamb wave dispersion curves much more complicated due to the variation of properties with the angle off the normal and the coupled behavior of the quasi P-wave, quasi SV-wave, and quasi SH-wave. Major problems, beyond concept, exist with the computing problem and the huge effort that it takes to even obtain the basic dispersion information in a general direction using the uncoupled mode method.

First, the elasticity problem provides stresses to indicate the magnitude of the disturbance at each input angle θ_1 or θ_3. This involves a good deal of computation, just to get the stresses. Then, the shear and normal stress are each used in separate calculations with the Lamb waves. However,

there may be a more appropriate means for including both these stresses in one Lamb wave displacement equation solution.

Next, the general solution for a Lamb wave is the summation of a six term displacement equation. The 6 term displacement equation is then differentiated for strains and utilized in the constitutive relations to get stresses. This then creates very long terms which describe the stress field. These equations are then used in the stress free boundary conditions to create a 6 by 6 system of equations which need to be checked for the dispersion condition and then can be used with the elasticity results to calculate the coefficients of each of the 6 partial waves. Just to find a point on the curve involves stepping through this procedure 100's of times. Then to obtain the whole curve involves going through the whole procedure including the search for the right solution hundreds of times. This must be done for a number of modes and then a number of azimuthal angles.

Finally, consideration must be given to energy flux. Calculating the energy flux deviation for a Lamb wave, where the displacement equation is represented by 6 terms, creates another huge computational chore. Accounting for the effect of the energy flux deviation causes one of the major conceptial difficulties associated with modeling AU of composites. The following is a simple approach for including the effect of energy flux in AU results:

Solve the Lamb wave problem for certain discrete azimuthal angles

Calculate energy flux direction for each Lamb wave mode

Solve the geometric problem in order to find, for a particular transducer size and transducer separation distance, where on the arc subtended by the receiving transducer the effect of displacement is present

Integrate displacement for each azimuthal angle to find a distribution of displacement along the arc

Then the value for each experimental reading can be compared to that of the integrated value for the distance over the arc associated with the receiving transducer diameter

This may mean that attenuation, with d, is caused by the decreased range of azimuthal angles the receiving transducer covers for increased separation distance between transducers. Additionally, this may explain why the 3rd order symmetric mode declines slower at low azimuthal angles than the 2nd order antisymmetric mode for $d = 1$ inch. Since the flux deviation for plane waves can be on the order of 40 degrees for a composite material (ref. 128), this effect can not be overlooked for AU, especially for situations utilizing small transducers separated by larger distances.

Ideas for More Advanced AU Modeling Efforts

Obviously, the modeling mentioned above assumes the absolute ideal situation of a material with a linearly elastic constitutive relation and no damage or inhomogeneities. Work on including the effects of nonideal situations is still being developed for plane wave propagation, as was mentioned in the second chapter. Since we understand basic modes of propagation, future work could include introducing these considerations to the present understanding of AU results. It may be especially important to include more complex effects to help model how damage may alter AU results. Since little information in general exists concerning Lamb waves in anisotropic materials, models including more advanced material behavior would most likely involve even further theoretical work. Additionally, the already prohibitive calculations could very easily become totally impractical. However, theoretical work could still be utilized to provide qualitative information and to develop reasonable methods of approximation.

Source Modeling

Also, possible improvements could be made by using finite element or finite difference to determine radial variation of input disturbances for the composite plate for different azimuthal angles. This could allow for inclusion of the plate geometry, the transducer size, and the spatial variation of the transducer disturbance.

Geometric Effects

Another issue to be considered is that of geometry associated with the source and receiver. In this regard, a host of drastic idealizations are involved with the present modeling of the AU method.

First, the sending transducer does not produce a perfect plane wave. In fact, it would probably be more appropriate to model the source using cylindrical coordinates, such as was done for an isotropic plate (ref. 140). Note, this analysis yielded a Bessel function solution which degenerated to a plate wave type solution at distances far from the source. Although this analysis is not suited for anisotropic materials, it may be advisable to at least note the 1/r dependence of displacement with distance from source.

Also, it should be noted that the receiving transducer is actually picking up disturbances associated with a range of angles. This effect is especially large when the distance between transducers is small. This practical difficulty along with angular variation of energy flux is consistent with the fact that AU results show that the 1st order symmetric mode decreases much slower at small angles than the 2nd order antisymmetric mode.

Time Domain Information

The prediction of the voltage/time signal for an aluminum plate has been accomplished utilizing a variety of theoretical approaches. However, no such results exist for a composite material. Solving this problem would provide an extremely useful tool for understanding more of the physics associated with the AU results and make time domain calulations of wave velocities and calculation of material properties more feasible.

The approach utilized by Vusedeven and Mal (ref.129) provided results for the response for a source on the face of an aluminum plate that resembled AU results. Their approach utilized the analysis of Lamb wave equations to develop a fairly efficient computational scheme. However, this approach has not been extended to anisotropic materials. Application of the exact approach is not theoretically possible for an anisotropic material, however a variation of the approach may provide an eventual means for developing a method to predict the voltage/time signal for a composite material. Work of this type would most likely require a concentrated effort from researchers in a number of areas working together. A more practical approach may be to use a multi-transducer configuration with AU to measure phase velocities and group velocities and use this and spectral information to reproduce dispersion curves for use in NDE (refs. 12 and 13). Hence, a single measurement could be used to reproduce a whole section of a dispersion curve. However, this approach would involve a great deal of instrumentation and other developments that would require years of work.

Relating AU to Damage Modeling (NDE)

A number of approaches could be used to relate AU results, AU modeling and damage modeling. These ideas run from making very simple empirical relations to making very idealized, yet complex energy arguments. A good middle ground for starting is to try to utilize how changes in mechanical properties arise in both models. The real strength of the AU technique may be its interaction with various material components on a high frequency scale and the attendant mechanisms for energy loss or redistribution due to damage, imperfections, inhomogeneities, or general nonideal material behavior.

First, the AU measurement may be utilized directly with the simple modeling procedure forwarded by Poursartip and Beaumont (ref. 108). Application of the AU method with this model simply involves making empirical relations between AU measurements as a function of fatigue cycles and failure. The AU value has been shown to be more sensitive than the stiffness measurement as a means of tracking damage (ref. 88). This is due to the large effects of damage on the high frequency waves associated with the AU method. But, the mechanical understanding of the effects of damage on the wave propagation are not nearly as developed as the understanding between damage and stiffness change. Therefore, at present the use of the AU value in the model would be totally ad hoc. However, future developments with models such as the one being developed here may change this. In fact, the model presented posesses the possibility of obtaining stiffness information and may be further developed to include the effects of damage on AU values through changes in stiffness, damping, reflections, scattering, etc..

Stress redistribution and concentration is one area where the AU method shows promise of relating to the critical element model, especially with an understanding of the stress states associated with Lamb waves. Eventually, the variation of AU with azimuthal angle may be utilized to give local values for $F^L(n)$. Thus, it may be possible to obtain information on impending failure modes and

stress concentrations by noting how the local stress state or displacement field for Lamb waves is modified by damage in a material. In other words, the AU method may possess the ability to map the way a given type of displacement (eg. longitudinal and shear) are distributed in a local region of material. The exact relations between how the redistribution of stress for a high frequency Lamb wave and fatigue loading is not directly clear. However, starting with this model of wave propagation for the AU method, work can be geared toward deriving the elasticity problem that would produce the results given for stress state changes of the AU waves. At the very least, the AU results may be utilized to understand how damage is controlling mechanical behavior at various azimuthal angles.

In this vein, research has already been conducted by Duke and Kiernan (refs. 70 and 100) to utilize the variation of AU with azimuthal angle to predict the direction of damage growth in composite materials that are impacted with a steel ball. This work has shown that damage shows some tendency to grow in directions of high AU.

Effects of damage on AU results for some directions has been noted (refs. 102 and 130). How certain types of damage states interact with material motion may yield a means of identifying certain damage modes and additionally assessing their mechanical effects. However, caution should be used in relating the mechanical behavior of a high frequency stress wave to other forms of loading.

Also, it has been noted that localized impact damage has even caused AU measurements to increase in some directions (perhaps due to redirection of reflected energy) this could perhaps help to calculate stress concentration factors.

In general, the present physical understanding of how material properties affect AU results provides understanding of certain AU results and paves the way for utilizing the AU technique to determine material properties, thus providing information for use with damage models. Information may also be obtained on other energy dissipating and redistribution mechanisms for use in damage models.

It may involve a good deal of future work to reach this level of understanding, but the present groundwork at least provides a starting point for research efforts.

Although the present modeling efforts are rudimentary, they provide a building block for utilizing the physical understanding, obtained through experiment, to develop advanced models for NDE applications. The first major problem in this effort is the computing difficulties associated with the composite material AU modeling. Unfortunately, the inclusion of more advanced models would only compound this problem. Perhaps improved computer technology will lessen this problem. In any case, by relating AU models to material properties, it is hoped that further relations may be made to prediction models of material failure, due to things such as fatigue.

Conclusions and Overview

The AU method has proved to be a viable NDT technique in a wide variety of laboratory studies (refs, 4,6, and 103). Presently, the need exists to usher the method into practical real world applications. For this to take place, research on the AU method has to extend beyond feasibility studies. As mentioned, a primary need has been a more sound physical basis for AU results. In fact, prior to this dissertation, no general physical explanation for AU results in composite materials had been offered. The theoretical methods most often used for understanding results in aluminum plates are impractical and in most cases impossible to apply to composite plates. Hence, it is the purpose of this dissertation to provide a basic paradigm by which to understand the mechanics of the AU method for composite materials. This stands to contribute to the application of the AU method in the following ways:

Acceptance is based on physical understanding

Physical models allow forethought to be given to applications, so that proper instrumentation is utilized and results can most appropriately be interpreted

Physical models may make it possible to understand how certain forms of damage may effect AU results

Physical models can be used to interpret AU results in terms of the mechanical state of the material, and hence lead to NDE applications - the ultimate goal of an NDT technique

Thus, this dissertation is viewed as a building block in the maturation of the AU method into an NDE technique.

Experimental Work

A basic ingredient of this work is the use of experimental results to guide physical understanding and to validate theoretical predictions. In fact, a large part of the contribution of this work is the painstaking measurements made to obtain the experimental results presented in chapter 4. Moreover, it is hoped that the experimental results presented here will provide the basis for more advanced models and increased basic physical experimentation.

Physical Understanding

The basis of the physical understanding of the AU method was the identification of higher order Lamb waves as the dominant mode of wave propagation. This involved comparing velocity measurements and frequency content of AU measurements to Lamb wave theory predictions. Additionally, the variation of the input disturbance was shown to affect AU results. An elasticity solution was utilized to account for the angular dependence of the radial disturbance for a point force input. The radial variation of stress was then input to the Lamb wave solution. The frequency content of the input was also shown to affect AU results and was accounted for by multiplying the output spectrum by a frequency dependent weighting function.

Current physical understanding of the AU method provides a means for explaining experimentally observed behavior of AU signals for composite materials, including the way certain components of the signal vary with azimuthal angle.

One major contribution here is the identification of what type of motion each frequency component belongs to and what waves or partial waves cause that motion. This helps understand phenomena such as why the .234 MHz signal content is of a high energy value in the 90 degree direction for the 24 ply panel. This explains the slight increase seen in the overall energy content of the AU signal at 90 degrees from lower values at 80 degrees (refs. 99 and 130).

Also, the high radial disturbance for high angles in the fiber direction explains the large signal content in the beginning of the signal for the zero degree direction, due to the higher group velocity. Specifically, the fact that the fiber direction causes more energy to be directed at higher angles, results in more energy being present at higher wavenumbers where the group velocity is of higher value. The shape of the dispersion curve and energy flux also contribute, along with the higher input energy, to the large A1 in the fiber direction. Also, this provides a means for relating how the high modulus of the fiber pulls energy from the 15 degree direction, and hence causes such high attenuation between the 1 and 2 inch distance for the 3rd order symmetric mode.

Additionally, the fact that the phase velocity is given by circular frequency over wave number explains why the higher frequency waves have higher phase velocity values than the lower frequency waves. Thus, if one assumes the wave numbers are comparable, then the phase velocities should be roughly the same ratio as the frequencies. This agrees with the experimental data for all the wave components that are identified as higher order Lamb waves.

This physical description also provides a means for understanding certain aspects of the problem with reproducibility. Specifically, the fact that the major mode of propagation seems to be waves that are excited by stress waves sent off at just slightly off the normal means that a slight cantor of the transducer (just a matter of a couple of degrees) could drastically effect how much energy is sent

in a given direction. This could explain the noted observation that the larger transducers cause much more repeatable results than the smaller transducers- due to the more stable state of a large diameter transducer. Moreover, this obviates the fact that repeatibility is most difficult in the fiber direction- due to the fact that even more of the energy content is drawn in from the large angles.

Finally, the Lamb wave analysis provides a means of analyzing how damage and certain material states may interact with wave motion. For instance, the stress state of a given Lamb wave mode can be compared to known effects of damage on stress. Thus, a delamination could be treated as a stress free boundary and then a wave could be excited that possessed a nonzero stress for that position. Next, a Lamb wave could be excited that possessed the proper boundary condition or most nearly (ie. the major stress field for that mode satisfy the boundary condition). Unfortunately, existing data for the delamination signal contained two modes where the major stress met the stress free boundary of the delamination. However, these waves were still severely attenuated. Finally, it is interesting to note that the initial application of the AU method involved determining shear strength by using measurements in the 90 degree direction of unidirctional panels (ref. 4). The results of this work, combined with the physical explanation would predict that the dominant mode in this case would be the 1st order antisymmetric mode. For the low wave number results seen in experiments, this would show a wave that produced mainly shear stress in the direction the wave was sent. Hence, the high resin areas that weaken the shear strength would also cause damping of the shear stresses caused by the antisymmetric wave. Thus, the physical explanation forwarded may be utilized in the future to identify the proper AU parameter to analyze, for a given type of damage assessment and strength evaluation.

The importance of the damage position relative to the source must also be stressed. If the damage is so close to the source that the Lamb wave is not yet excited, then attention should be centered on how the stress waves emanating directly from the source may interact with the damage and how that may affect the resulting Lamb wave. This again relates to the "grey area" of the geometry problem associated with the region needed for the input plane waves to reflect and interact suffi-

ciently to cause Lamb waves. In general, the physical interpretation of the AU method must acknowlege the importance of the source and the area close to source in AU results.

Implementation of AU

The implementation of the AU technique requires that reproducible, quick, inexpensive, and informative measurements can be made on materials that are in structures. In order to achieve these objectives, a number of advancements need to be made in separate areas.

Practical Difficulties

A number of practical difficulties need to be solved before the AU method can be fully utilized. These involve simple type of concerns that need to be accounted for in transforming the lab experiments into a working field method. Hopefully, some of the problems which may arise in this transformation may be alleviated by the physical understanding forwarded in this dissertation.

First, the digital calculations used in these experiments are too slow for many real applications. However, an RMS voltmeter and a specified filter may be utilized to obtain the energy of a specified mode that would give the proper information. Obtaining the right experimental hook-up could be expedited by using calculations from the physical understanding forwarded in this dissertation.

One practical difficulty of the AU method is the reproducibility of results. The major reason is that a slight reorientation in the direction of the transducer face drastically changes the energy input for the dominate angles seen in the AU signal. Another problem in this regard is the couplant. The solution to this problem involves utilizing new experimental techniques and transducers, perhaps

laser excitation. However, laser input is not very easy to characterize. In any case, a great deal of attention needs to be given to viable sources and sensors. Also, complementary efforts should be directed toward characterizing these sources and their mechanical interaction with materials.

In order for the AU method to receive mass utilization, the results need to be standardized and must lead to easy interpretation. Although, early application of the method on thin specimens indicated that a low AU energy value correlated to a low strength, the application of this idea to more complex geometries of higher dimension with different material properties in different directions causes this type of interpretation to become difficult. For instance, the effect of impact damage has caused the AU energy to be redirected in certain directions, so that the AU energy was even higher in these directions after damage than before, however, it may not be correct to interpret the material as being stronger. Generally, damage may either attenuate or reflect energy- physically understanding wave motion helps to interpret results of these mechanisms for help in standardization of the AU method.

One solution to the standardization and interpretation problem is to continue trying to relate the mechanics of the AU technique to the mechanics of damage models. For instance, arrayed transducers may be able to note a very localized alteration in directional material properties by measuring Lamb wave velocities. This may then be compared to predicted changes by damage models or conversely the material properties could be fed into damage models. Also, more effort can be directed at relating actual energy attenuation in the AU signal to damage and then this information to damage model. Ultimately, only with increased modeling and computations can the AU method be united with damage models to yield usable NDE methods for general application.

Instrumentation

A number of the problems which exist with the AU method may be solved by modifying instrumentation for specific applications. Hence, a good deal of research needs to be directed at developing new AU systems. The following serve as a list of instrumentation that needs to be developed:

Develop a system with RMS meter and capabilities for gating and filtering signal

Develop system for more repeatible characterized input that does not require a laborious operator procedure

Develop a system that has a number of arrayed and multiplexed transducers that yields time domain , frequency domain, and amplitude results

Develop real time computer analysis capabilities

Obviously, this is only a partial list of possible ideas for developing the experimental means to use the AU for real world applications. Hopefully, further ideas and work in this area will spawn from the physical understanding of the AU method developed above.

Advanced Applications

Smart skins is one of many advance technologies that may benefit from progress being made in the AU field. The basic goal of smart skin technology is to be able to simulate, for aircraft wings, the activities of the central nervous system in human beings. Work in this area is focusing on the use of optical fibers embedded in materials to sense the vibration of the material and to show damage

when the fiber is broken. Also, a good deal of concentration is centered on the great computational effort associated with all the information.

AU may provide a way for checking the integrity of the material where there are not fibers, since it would be highly impractical to have the optical fibers everywhere. In particular, a source, such as KYNAR film, could be embedded at one location and the optical fiber at another location could act as the receiver. Thus, the components could act to perform an in-situ AU test that could serve the smart skin function of sensing pain from an abnormality in the material. Depending on the sophistication of the software utilized, the severity of the damage, the location, and other variables could be accounted for in order to make certain decisions and to give as much information as possible. In general, the AU method may find a niche in the smart skin technolgy.

Future Work

The basic physical model based on the elasticity solution, TTTR, and Lamb wave analysis opens many doors for directions to complement this work and to further develop the AU method. A partial list of future areas for possible research work includes:

Study of interdependence of parameters used in physical model

Develop self contained and efficient codes of computer model

Develop more complex models including effects of damage on wave dispersion and energy dissipation

Use FE or FD to model the disturbance input by the transducer

Try to apply Vusedevan and Mal's approach, used on isotropic Lamb wave equations, to anisotropic materials

Try to make predictions on which modes and which directions might be more affected by various types of damage and to perform experimental validation

Use the model to develop better experimental set-ups

Do the full calculation of how AU varies with azimuthal angle including the effect of energy flux (this will require using a lot of computer time on a super computer)

Alter model for use with other and more general experimental arrangements

Develop application of AU to smart skin technology

More work should be devoted to understanding the behavior of unidirectional panels at 15 degrees, this may help find and evaluate fiber breaks

Expand analysis to more general laminates

Do fatigue test work and really try to correlate AU results and critical element model

All of these issues are topics that could be explored in great detail and would undoubtedly contribute to the AU method and associated technology. In general, a great number of areas exist for further research on the AU method, due to the newness of the method and its importance to new technologies. Furthermore, now that the AU NDT method for composite materials has shown experimental merits and a physical understanding of results exists, wise choices for further research areas and proper approaches can be made.

Closing Remarks

A wealth of information is present in the AU signal. This information may be especially helpful, when consideration is given to the variation of the AU signal with azimuthal angle for composite materials and the great variation in local composite material state. Past research efforts have relied on hit or miss experiments and complex signal analysis schemes to obtain as much information as possible from AU analysis of composite materials. The physical understanding and modeling efforts of this disertation are meant to add order to the search to obtain as much information as possible from AU results.

The physics and wave propagation associated with this work are interesting in their own right. It is interesting to note the great deal of information which can be ascertained from Lamb wave analysis. Furthermore, it is fascinating to experimentally observe behavior qualitatively and quantitatively predicted by analyzing dispersion curve information. This dissertation confirms the usefulness of conventional theoretical tools for understanding experimentally observed wave motion. Also, this work points out the physics associated with the AU results in composite materials. The physics shows the complex situations associated with trying to understand the basic mechanical behavior of composite materials. Hopefully, this understanding may be of use in other areas of research associated with composites.

This work highlights how source characteristics (frequency, orientation, etc.) and experimental arrangement control waveguide effects, since all of these influence acoustic emission results, the same complexities involved in AU analysis should be considered in understanding acoustic emission results. For instance, researchers in acoustic emission should be aware of the effects the orientation of the AE source may have on what waves are set-up. Additionally, it points out the importance of the receiver orientation (azimuthal angle) relative to the emission source on what results are de-

tected by the receiver. Also, it suggests that damage in the material between the acoustic emission and the receiver may affect results.

In closing, the AU method shows promise as a means of assessing the quality of composite materials. With increased understanding of the physics associated with AU results, such as given here, the application of the AU method for composite materials may further contribute to efforts to nondestructively evaluate these materials in real applications. Thus, the purpose of this dissertation is to contribute, through experimental data and wave motion analysis, a physical understanding/model of the AU method for the purpose of developing a refined AU method for use with advance composite material systems.

References

1. D. E. Newland, *An Introduction to Random Vibrations and Spectral Analysis,* Longman Inc., New York, (1983).

2. A. V. Oppenheim and R. W. Schafer, "Digital Signal Processing," Prentice-Hall, Inc., Englewood Cliffs, New Jersey, 1975.

3. J. D. Achenbach, "Wave Propagation in Elastic Solids," American Elsevier, New York, NY., 1973.

4. A. Vary and K. J. Bowles, "Ultrasonic Evaluation of the Strength of Unidirectional Graphite/Polyimide Composites," NASA TM X-73646, 1977.

5. A. Vary and R. F. Lark, "Correlation of Fiber Composite Tensile Strength with the Ultrasonic Stress Wave Factor," NASA TM-78846, 1978.

6. A. K. Govada, J. C. Duke, Jr., E. G. Henneke II, "A Study of the Stress Wave Factor Technique for the Characterization of Composite Materials," NASA CR 17480, (1985).

7. R. Talreja, A. Govada and E. G. Henneke, II, "Quantitative Assessment of Damage Growth in Graphite/Epoxy Laminates by Acousto-Ultrasonic Measurements," *Review of Progress in Quantitative Nondestructive Evaluation, Vol.3B,*eds. D. O. Thompson and D. E. Chementi, Plenum Press, New York, (1984), pp. 1099-1106.

8. M. T. Kiernan, "An Acousto-Ultrasonic System for the Evaluation of Composite Materials" Masters Thesis, College of Engineering, Virginia Polytechnique Institute and State University, Blacksburg, Va., Oct. (1986).

9. M. T. Kiernan and J. C. Duke,"Acousto-Ultrasonics as a Monitor of Material Anisotropy" *Materials Evaluation,* Vol. 46, No. 8, July 1988, p1105.

10. M. T. Kiernan and J. C. Duke,"PC Analysis of an Acousto-Ultrasonic Signal" *Materials Evaluation,* Vol. 46, No. 10, Sept. 1988, p1344.

11. Y. Pao and R. K. Kaul, "Waves and Vibrations in Isotropic and Anisotropic Plates," *R. D. Mindlin and Applied Mechanics,* Pergamon Press Inc., New York, (1974), pp. 149-196.

12. R. C. Stiffler and E. G. Henneke, II, "Low Frequency Plate Wave Modes"in *Ultrasonic Stress Wave Characterization of Composite Materials* NASA Contractor Report 3976 under Grant NAG3-323, edited by J. C. Duke, Jr., E. G. Henneke II, and W. W. Stinchcomb, May (1986).

13. R. C. Stiffler, "Wave Propagation in Composite Plates" Phd. Dissertation, College of Engineering, Virginia Polytechnical Institute and State University, Blacksburg, Va., Nov. (1986).

14. L. J. Johnson, "Green's Function for Lamb's Problem," *Geophysics,* V. 37, 1974, pp. 99-131.

15. S. O. Rice, "Matematical Analysis of Random Noise" *Bell System Technical Journal,* Vol. 23, 1944, pp. 282-332, and Vol.24, 1945, pp. 46-156. reprinted in *Selected Papers on Noise and Stochastic Processes,* ed. N. Wax, Dover, New York, 1954.

16. P. M. Gammell, "Improved Ultrasonic Detection Using the Analytic Signal Magnitude" *Ultrasonics,* March 1981, p. 73.

17. R. A. Kline and Z. T. Chen, "Ultrasonic Technique for Global Anisotropic Property Measurement in Composite Materials" *Materials Evaluation* 46, March 1988, p. 986-992.

18. B. Hosten and Tittmann, "Elastic Anisotropy of Carbon-Carbon Composites During the Fabrication Process," *IEEE Transactions of Ultrasonics, Ferroelectrics, and Frequency Control,* Vol. vffc-34, no. 3, May 1987.

19. M. J. P. Musgrave, "Crystal Acoustics," Holden-Day, Inc., San Francisco, Ca., 1970.

20. F. I. Fedorov, "Theory of Elastic Waves in Crystals," Plenum Press, San Francisco, Ca., 1970.

21. R. Halmshaw, "Non-destructive Testing," Edward Arnold Publishers, London, 1987.

22. E. G. Henneke, "Reflection and Refraction of a Stress Wave at a Plane Boundary Between Anisotropic Media" *Journal of the Acoustical Society of America,* Vol. 51, 1972, pp. 210-217.

23. E. G. Henneke, "Critical Angles for Reflection at a Liquid-Solid Interface in Single Crystals" *Journal of the Acoustical Society of America,* Vol. 59, 1976, pp. 204-205.

24. H. Kolsky, "Stress Waves in Solids," Dover Publications, New York, New York, 1963.

25. A. Vary, "Concepts and Techniques for Ultrasonic Evaluation of Material Mechanic Properties"in *Mechanics of Nondestructive Testing* , Ed. W. W. Stinchcomb, Plenum Press, 1980, pp. 123-141.

26. R. S. Sharpe, "Innovation and Opportunity in NDT" *British Journal of Non-Destructive Testing* 18, 4, 98, 1976.

27. L. E. Pitts, J. P. Thomas, and W. G. Mayer, "Theoretical Similarities of Rayleigh and Lamb Modes of Vibration,"in *JASA* , Vol. 60, pp374-377.

28. J. H. Hemann and G. Y. Baaklini, "Effect of Stress on Ultrasonic Pulses in Fiber Reinforced Composites" *Materials Analysis by Ultrasonics of Metals, Ceramics and Composites* , Ed. A. Vary, Noyes Data Corporation, 1987, pp. 176-181.

29. L. S. Fu, "Dynamic Moduli and Localized Damage in Composites" *Materials Analysis by Ultrasonics of Metals, Ceramics and Composites* , Ed. A. Vary, Noyes Data Corporation, 1987, pp. 225-248.

30. J. H. Williams, Jr., H. Nageb-Hashemi, and S. S. Lee, "Ultrasonic Attenuation and Velocity in AS/3501-G Graphite/Epoxy Fiber Composite," NASA CR-3180, Dec 1979.

31. J. H. Williams and B. Doll, "Ultrasonic Attenuation as an Indicator of Fatigue Life of Gr/Ep Composites," NASA CR-3179, 1979.

32. G. Maze, J. L. Izibicki, J. Ripoche, A. Nagl, H. Uberall, and K. B. Yoo, "Transient Acoustic Scattering from Layers and Plates ," *JASA,* Vol. 80, pp 295-301, 1986.

33. A. Vary and K. J. Bowles, "Use of an Ultrasonic-Acoustic Technique for Nondestructive Evaluation of Fiber Composite Strength," NASA TM-73813, Feb. 1978.

34. A. Sarrafzdeh-Khoee, M. T. Kiernan, J. C. Duke, Jr., E. G. Henneke, II, "A Study of the Stress Wave Factor Technique for Nondestructive Evaluation of Composite Materials," NASA CR-4002, 1986.

35. A. Vary, "Correlations Among Ultrasonic Propagation Factors and Fracture Toughness Properties of Metallic Materi-

als" *Materials Evaluation* 36, No. 7, June 1978, p. 55-64.

36. A. Vary, "Quantitative Ultrasonic Evaluation of Mechanical Properties of Engineering Materials," NASA TM-78905, June 1978.

37. W. H. Beyer, ed., *CRC Standard Mathematical Tables,* 26th edition, CRC Press, Boca Raton, Fl., 1982.

38. D. M. Egle, "Using the Acoustoelastic Effect to Measure Stress in Plates," UCRL-52914, Lawrence Livermore Laboratory, 1980.

39. S. C. Cowin, V. Buskirk, and R. Carter, "A Theory of Acoustic Measurement of the Elastic Constants of a Anisotropic Solid," in Proceedings of 1986 SEM Spring Conference, New Orleans, LA, 1986, pp 737-745.

40. R. A. Kline, "Wave Propagation in Fiber Reinforced Composites for Oblique Incidence" *Journal of Composite Materials,* Vol. 22, March 1988, pp. 287-303.

41. S. T. Rokhlin, T. Bolland, and L. Adler, "Reflection and Refraction of Elastic Waves on a Plane Interface Between Two Generally Anisotropic Media," *Journal of Acoustic Society of America,* 79, 1986, pp. 906-919.

42. J. E. Zimmer, and J. R. Cost, "Determination of the Elastic Constants of Unidirectional Fiber Composites Using Ultrasonic Velocity Measurements," *Journal of Acoustic Society of America,* 41, 1970, pp. 795-799.

43. K. L. Reifsnider and W. W. Stinchcomb, "A Critical-Element Model of the Residual Strength and Life of Fatigue-Loaded Composite Coupons," in *Composite Materials : Fatigue and Fracture* ASTM STP 907, H. T. Hahn Ed., ASTM, Philadelphia, 1986, pp. 298-313.

44. L. J. Broutman and S. Sahu, "Composite Coupons," in *Materials : Testing and Design* Second Conference, ASTM STP 497, ASTM, Philadelphia, 1972, pp. 170-188.

45. J. C. Halpin, T. A. Johnson, and M. R. Waddoups, "Between Two Generally Anisotropic Media," *International Journal of Fracture Mechanics,* Vol. 8, 1972, pp. 465-472.

46. H. T. Hahn, and R. Y. Kim, *Journal of Composite Materials,* Vol. 9, 1975, pp. 297-311.

47. H. T. Hahn, and R. Y. Kim, *Journal of Composite Materials,* Vol. 10, 1976, pp. 156-179.

48. Z. Hashin and A. Rotem, *Materials Science and Engineering,* Vol. 34, 1978, pp. 147-179.

49. J. H Williams, Jr., Karaguelle, and S. S. Lee, "Ultrasonic Input-Output for Transmitting and Receiving Longitudinal Transducers Coupled to the Same Face of an Isotropic Elastic Plate," *Materials Evaluation* Vol. 40, No. 6, May 1982, pp. 655-662.

50. R. E. Green, Jr., "Ultrasonic Investigation of Mechanical Properties"inVol. 3 of *Treatise of Materials Science and Technology* , Academic Press, New York, 1973.

51. J. C. Peck and G. A. Gurtman, "Dispersive Pulse Propagation Parrallel to the Interfaces of a Laminated Composite," *J. of Applied Mech.*, 36, 479, 1969.

52. R. D. Mindlin, "Waves and Vibrations in Isotropic, Elastic Plates" *Structural Mechanics*, New York, 1960, pp. 199-232.

53. F. R. Breckenridge, C. E. Tschiegg, and M. Greenspan, "Some Applications of Lamb's Problem" *JASA*,57, (3), pp626-631, March 1975.

54. H. Karaguelle, J. H. Williams, Jr., and S. S. Lee, "Stress Waves in Isotropic Elastic Plate Excited by Circular Transducers," *Materials Evaluation*, 44, March 1986, pp. 455-462.

55. G. F. Miller and H. Pursey, "The Field and Radiation Impedance of Mechanical Radiators on the Free Surface of a Semi-infinite Isotropic Solid," *Proceedings of the Royal Society of London,* Series A, Vol. 223, May 1954, pp 521-541.

56. J. H. Williams, Jr. and N. R. Lampert, "Ultrasonic Evaluation of Impact-Damaged Graphite Fiber Composite," *Mtls. Eval.*, Vol. 38, No. 12, Dec. 1980, pp 68-72.

57. Y. H. Pao and R. R. Gajewski, "The Generalized Ray Theory and Transient Responses of Layered Elastic Solids," *Physical Acoustics,* eds. W. P. Mason and R. N. Thurston, Academic Press, NY. NY., Vol. 13, 1977, pp. 183-265.

58. H. Lamb, "On Waves in an Elastic Plate," *Proceedings of the Royal Society of London,* March 1917.

59. D. C. Worlton, "Lamb Waves at Ultrasonic Frequencies," HW-60662, June 1959.

60. C. L. Frederick and D. C. Worlton, "Ultrasonic Thickness Measurements with Lamb Waves" *Nondestructive Testing* Jan.-Feb. 1962, pp51-55.

61. T. N. Grisby and E. J. Tajchman, "Properties of Lamb Waves Relevent to the Ultrasonic Inspection of Thin Plates," *IRE Trans. of Ultrasonics Eng.,* March 1961, Vol. VE-8, No. 1, pp 26-33.

62. R. A. DiNovi, "Lamb Waves and Their Use in Nondestructive Testing," ANL-6630, March 1963.

63. H Karaguelle, J. H. Williams, and S. S. Lee, "Application of Homomorphic Signal Processing to Stress Wave Factor Analysis" *Mtls. Eval.* Vol. 43, Oct. 1985, pp 1446-1454.

64. R. E. Green, Jr., "Ultrasonic Nondestructive Materials Characterization" *Analytical Ultrasonics in Materials Research and Testing,* ed. A. Vary,NASA Conference Publication 2383, 1986.

65. J. S. Heyman and M. Namkung, "Residual Stress Measurements in Carbon Steel" *Analytical Ultrasonics in Materials Research and Testing,* ed. A. Vary,NASA Conference Publication 2383, 1986.

66. O. Buck, R. B. Thompson, and D. K. Rehbein, "On the Interaction of Ultrasound With Cracks: Applications to Fatigue Growth" *Analytical Ultrasonics in Materials Research and Testing,* ed. A. Vary,NASA Conference Publication 2383, 1986.

67. E. G. Henneke, II and J. C. Duke, Jr. , "Analytical Ultrasonics for Evaluation of Composite Materials Response: Pt. I Physical Interpretation" *Analytical Ultrasonics in Materials Research and Testing,* ed. A. Vary,NASA Conference Publication 2383, 1986.

68. J. C. Duke, Jr. and E. G. Henneke, II, "Analytical Ultrasonics for Evaluation of Composite Materials Response: Pt. II Generation and Detection" *Analytical Ultrasonics in Materials Research and Testing,* ed. A. Vary,NASA Conference Publication 2383, 1986.

69. J. A. G. Temple, "Modelling the Propagation and Scattering of Elastic Waves in Inhomogeneous Anisotropic Media," To be submitted to the J. Phys.

70. J. C. Duke, Jr. and M. T. Kiernan, "Impact Damage Development in Damaged Composite Materials," *Proceedings of the 4th US-Japan Conference on Composite Materials,* American Society of Composites, Dayton, 1988.

71. R. B. Thompson, J. F. Smith and S. S. Lee, "Inference of Stress and Texture From Angular Dependence of Ultrasonic Plate Mode Velocities" *Analytical Ultrasonics in Materials Research and Testing,* ed. A. Vary,NASA Conference Publication 2383, 1986.

72. A. Wieczorek and G. Schmitz, "Development of Nondestructive Testing Methods For The Evaluation of Thin and Ultrathin Sheet Materials" *AFML-TR-65-320,* Dec., 1965.

73. I. Tolstoy and E. Usdin, "Wave Propagation in Elastic Plates: Low and High Mode Dispersion" *JASA,* 29, pp. 37-42, 1957.

74. A. Vary and H. E. Kautz, "Transfer Function Concept for Ultrasonic Characterization of Material Microstructures" *Analytical Ultrasonics in Materials Research and Testing,* ed. A. Vary,NASA Conference Publication 2383, 1986.

75. Y. H. Pao, W. Sachse and H. Fukuoka, "Acoustoelasticity and Ultrasonic Measurements of Residual Stresses" In Vol. XVII *Physical Acoustics*, W. P. Mason and R. N. Thurston (eds.), Academic Press, Orlando, Fla., (1984) pp61-143.

76. M. Rosen, "Analytical Ultrasonics for Characterization of Metallurgical Microstructures and Transformations" *Analytical Ultrasonics in Materials Research and Testing,* ed. A. Vary,NASA Conference Publication 2383, 1986.

77. S. J. Klima and G. Y. Baaklini, "Ultrasonic Characterization of Structural Ceramics" *Analytical Ultrasonics in Materials Research and Testing,* ed. A. Vary,NASA Conference Publication 2383, 1986.

78. D. R. Allen, H. B. Cooper, C. M. Sayers and M. G. Silk, "The Use of Ultrasonics to Measure Residual Stresses," in *Research Techniques in Nondestructive Testing,* Vol. VI, ed. R. S. Sharpe, Academic Press, NY., 1982

79. S. O. Harold, "Ultrasonic Focusing Techniques," in *Research Techniques in Nondestructive Testing,* Vol. VI, ed. R. S. Sharpe, Academic Press, NY., 1982

80. L. W. Schmerr, Jr., "Ultrasonic Scattering in Composites Using Spatial Fourier Transform Techniques," *Review of Progress in Quantitative Nondestructive Evaluation, Vol.4A,*eds. D. O. Thompson and D. E. Chementi, Plenum Press, New York, (1985), pp. 53-60

81. D. K. Rehbein, R. B. Thompson and O. Buck, "Interaction of Ultrasonic Waves with Simulated and Real Fatigue Cracks," *Review of Progress in Quantitative Nondestructive Evaluation, Vol.4A,*eds. D. O. Thompson and D. E. Chementi, Plenum Press, New York, (1985), pp. 61-82

82. Y. C. Angel and J. D. Achenbach, "Reflection of Ultrasonic Waves by an Array of Microcracks ," *Review of Progress in Quantitative Nondestructive Evaluation, Vol.4A,*eds. D. O. Thompson and D. E. Chementi, Plenum Press, New York, (1985)

83. E. R. Generazio, "The Role of the Reflection Coefficient in Precision Measurement of Ultrasonic Attenuation," *Review of Progress in Quantitative Nondestructive Evaluation, Vol.4B,*eds. D. O. Thompson and D. E. Chementi, Plenum Press, New York, (1985)

84. B. W. Reed, "A High Precision Ultrasonic Velocity and Attenuation Measurement of Lamb Waves in Anisotropic Plates," *Review of Progress in Quantitative Nondestructive Evaluation, Vol.4B,*eds. D. O. Thompson and D. E. Chementi, Plenum Press, New York, (1985)

85. E. G. Henneke, II, J. C. Duke, Jr., W. W. Stinchcomb, A. Govada, and A. Lemascon, "A Study of the Stress Wave Factor Technique for the Characterization of Composite Materials," NASA CR-3670, 1983.

86. C. J. Rebello and J. C. Duke, Jr. "Factors Influencing the Ultrasonic Stress Wave Factor Evaluation of Material Structures," *J. of Comp. Tech. and Research* 8, 18, 1986.

87. A. Vary, "The Acousto-ultrasonic Approach ," *Acousto-Ultrasonics : Theory and Application* eds. J. C. Duke, Plenum Press, New York, (1988), pp. 1-22.

88. A. Govada, E. G. Henneke, II, and R. Talreja, "Acousto-ultrasonic Measurements to Monitor Damage During Fatigue of Composites," in *1984 Advances in Aerospace Sciences and Engineering,* eds. V. Yuceoglu and R. Hesser, ASME, NY, 1984.

89. B. Tang, E. G. Henneke, II, and R. C. Stiffler, "Low Frequency Flexural Wave Propagation in Laminated Composite Plates," *Acousto-Ultrasonics : Theory and Application* eds. J. C. Duke, Plenum Press, New York, (1988), pp. 45-66.

90. W. A. Green, "Bending Waves in Strongly Anisotropic Elastic Plates" *Quarterly J. of Mech. and Appl. Math.* 35, 485, 1982.

91. A. Vary, "Acousto-ultrasonic Characteriztion of Fiber Reinforced Composites," *Mtls. Eval.,* 40, 650, 1982.

92. M. Schoenburg, "Elastic Waves Behavior Across Linear Slip Interface," *J. of Acoustic Soc. Am.,* 68, 1516, 1980.

93. S. K. Datta, "A Self-Consistent Approach to Multiple Scattering of Elastic Waves," *J. Appl. Mech.,* 44, p657, 1986.

94. M. Billy, L. Adler, and G. Quentin, "Measurements of Backscattered Leaky Lamb Waves in Plates," *J. Acoust. Soc. Amer.,* 75, 998, 1984.

95. S. M. Moon, K. L. Jerina, and H. T. Hahn, "Acousto-Ultrasonic Wave Propagation in Composite Laminates ," *Acousto-Ultrasonics : Theory and Application* eds. J. C. Duke, Plenum Press, New York, (1988), pp. 111-126.

96. R. L. Weaver, "Diffuse Waves in Finite Plates," *J. Sound and Vib.,* 94, p 319, 1984.

97. H. E. Kautz, "Ray Propagation Path Analysis of Acousto-Ultrasonic Signals in Composites," *Acousto-Ultrasonics : Theory and Application* eds. J. C. Duke, Plenum Press, New York, (1988), pp.

98. R. Roberts, J. Qu and J. D. Achenbach, "Experimental and Theoretical Analysis of Backscattering Mechanisms in Fiber-Reinforced Composites," *Acousto-Ultrasonics : Theory and Application* eds. J. C. Duke, Plenum Press, New York, (1988), pp. 151-164

99. R. Talreja, "Application of Acousto-Ultrasonics to Quality Control and Damage Assessment of Composites," *Acousto-Ultrasonics : Theory and Application* eds. J. C. Duke, Plenum Press, New York, (1988), pp. 177-190.

100. J. C. Duke and M. T. Kiernan, "Predicting Damage Development in Composite Materials Based on Acousto-Ultrasonic Evaluation," *Acousto-Ultrasonics : Theory and Application* eds. J. C. Duke, Plenum Press, New York, (1988), pp. 191-200.

101. J. D. Leaird and M. C. Kingdon, "Considerations for Developing Calibration Standards for Acousto-Ultrasonic Inspection," *Acousto-Ultrasonics : Theory and Application* eds. J. C. Duke, Plenum Press, New York, (1988), pp. 247-258.

102. J. H. Hemann, P. Cavano, H. Kautz and K. Bowles, "Trans-Ply Crack Density Detection By Acousto-Ultrasonics," *Acousto-Ultrasonics : Theory and Application* eds. J. C. Duke, Plenum Press, New York, (1988), pp. 319-326.

103. K. K. Phani and N. R. Rose, "Application of Acousto-Ulatrasonics for Predicting Hygrothermal Degradation," *Acousto-Ultrasonics : Theory and Application* eds. J. C. Duke, Plenum Press, New York, (1988), pp. 327-336.

104. P. J. Torvik, "Shock Propagation in a Composite Material," *J. Comp. Mtls.,* Vol. 4, 1970, p296.

105. D. Frederick, "Continuum Mechanics," Cambridge Pub., Cambridge Mass., 1963.

106. C. D. Lundergan and D. S. Drumhelker, "Propagation of Stress Waves in a Laminated Plate Composite" *J. Appl. Phys.,* Vol. 42, No. 2, Feb. 1971.

107. H. J. Sutherland and R. Lingle, "Geometric Dispersion of Acoustic Waves by a Fibrous Composite" *J. of Composite Mtls.,* Vol. 6, Oct. 1972, p. 490.

108. A. Poursartip and P. W. R. Beaumont, "A Damage Approach to the Fatigue of Composites" *Nonlinear Behavior of Composite Mtls.* ASME, AMD-Vol. 13, pp. 93-103, 1975.

109. K. L. Reifsnider, E. G. Henneke, II, W. W. Stinchcomb, and J. C. Duke, "Damage Mechanics and NDE of Composite Laminates," *Mechanics of Composite Materials: Recent Advances* ed. Z. Hashin and C. T. Herokovich, Pergamon Press, 1982, pp. 399-420.

110. E. P. Papadakis, "Ultrasonic Transducer Evaluation in Five Domains: Time, Space, Frequency, Surface Motion, and Theory" 1977 Ultrasonics Symposium Proceedings IEEE Cat. 77CH1264-150.

111. R. J. Nuismer and S. C. Tan, "The Role of Matrix Cracking in the Continuum Constitutive Behavior of a Damaged Composite Ply," *Mechanics of Comp. Mtls.* P437-448.

112. J. H. Williams, Jr., E. B. Kahn, and S. S. Lee, "Effects of Specimen Resonances on Acousto-ultrasonics" *Mtls. Eval.,* 41, p 1502, 1983.

113. H. Ekstein, "High Frequency Vibrations of Thin Crystal Plates," in *Phys. Rev.*, 68, 1945, pp. 11-23.

114. T. K. O'Brien, "Characterization of Delamination Onset and Growth in a Composite Laminate,"in *Damage in Composite Materials* ASTM STP775, 1982.

115. B. A. Auld and M. Tan, "Symmetrical Lamb Wave Scattering at a Symmetrical Pair of Thin Slots," 1977 Ultrasonics Symposium Proceedings, IEEE Cat. #77CH1264-150, pp 61-66.

116. C. A. Ross, L. E. Ross, L. E. Malvern, R. L. Sierakowsli, and N. Takeda, "Finite-Element Analysis of Interlaminar Shear Stress Due to Local Impact," in *Recent Advances in Composites in the United States and Japan,* ASTM STP864, J. R. Vinson and M. Taya eds., ASTM, Phil. 1985, pp. 355-367.

117. S. P. Joshi and C. T. Sun, "Impact-Induced Fracture in a Quasi-Isotropic Laminate," *J. of Comp. Tech. and Res.*,Vol. 9, No. 2, Sum. 1987, pp. 40-46.

118. F. C. Moon, "Wave Surfaces Due to Impact on Anisotropic Plates," *J. of Comp. Mtls.*, Vol. 6, Jan. 1972, pp 62-79.

119. C. T. Herakovich, "On the Relationship Between Engineering Properties and Delamination of Composite Materials" *J. of Comp. Mtls.*, Vol. 15, July 1981, pp 336-348.

120. A. Vary, "Ultrasonic Measurement of Material Properties" in *Research Techniques in Nondestructive Testing IV* ed. R. S. Sharpe, Acad. Press, NY., 1980, pp. 159-204.

121. A. N. Ceranoglu and Y. H. Pao, "Propagation of Elastic Pulses and Acoustic Emission in a Plate," ASME *J. of Appl. Mech.*, 48, 1981, pp. 125-147.

122. Y. H. Pao, R. R. Gajewski, and A. N. Ceranoglu, "Acoustic Emission and Transient Waves in an Elastic Plate," *J. Acoust. Soc. of Am.*, 65(1), 1979, pp. 96-105.

123. R. M. Jones, *Mechanics of Composite Mtls.* McGraw-Hill, New York, 1975.

124. J. M. Whitney *Structural Analysis of Laminated Anisotropic Plates,* Technomic Pub., Lancaster, Pa., 1987.

125. R. Plunkett, "Damping Mechanisms in Fiber Reinforced Laminates" *Mechanics of Composite Materials: Recent Advances.* ASME, AMD-Vol. 13, pp. 93-103, 1975.

126. R. M. Christensen,. *Theory of Viscoelasticity* Academic Press, NY, 1982.

127. L. P. Solie and B. A. Auld, "Elastic Waves in Free Anisotropic Plates" *The Jour. of Acoust. Soc. of Am.,* Vol. 54, No. 1, 1973.

128. R. D. Kriz and W. W. Stinchcomb, "Elastic Moduli of Transversely Isotropic Graphite Fibers and Their Composites" *Experimental Mechanics,* Vol. 19, No. 2, Feb. 1979, pp 41-49.

129. N. Vasudevan and A. K. Mal, "Response of an Elastic Plate to Surface Loads and Buried Dislocation and Sources," *Review of Progress in Quantitative Nondestructive Evaluation, Vol.4A,*eds. D. O. Thompson and D. E. Chementi, Plenum Press, New York, (1985), pp. 53-60

130. J. C. Duke, Jr., E. G. Henneke, II, M. T. Kiernan, and P. P. Grosskopf, "A Study of the Stress Wave Factor Technique for Evaluation of Composite Materials (Interim Report-IV)," CR-4178.

131. S. T. Bartlett, "Nondestructive Evaluation of Complex Geometry Advanced Material Material Components" Masters Thesis, College of Engineering, Virginia Polytechnique Institute and State University, Blacksburg, Va., April (1989).

132. I. A. Viktrov, "Rayleigh and Lamb Waves," New York, 1967.

133. N. N. Hsu and F. R. Breckenridge, "Characterization and Calibration of Acoustic Emission Sensors" *Mtls. Eval.,* Vol. 39, No. 1, pp. 60-68.

134. P. M. Egle and A. E. Brown, "Considerations for the Detection of Acoustic Emission Waves in Thin Plates," *JASA,* 12 (1), pp. 140-146, 1975.

135. J. Krautkramer and H. Krautkramer, *Ultrasonic Testing of Materials, 2nd Edition,* Springer Verlag, New York, 1969.

136. S. I. Rokhlin, "Adhesive Joint Evaluation by Ultrasonic Interface and Lamb Waves" *Analytical Ultrasonics in Materials Research and Testing,* ed. A. Vary,NASA Conference Publication 2383, 1986.

137. A. Vary, "Acousto-ultrasonics: An Update" *Proceeding of Journal of Acoustic Emission,* Vol. 8, No. 1-2, pp. 175-178, 1989.

138. H. J. Pain, *The Physics of Vibrations and Waves,* John Wiley and Sons, New York, 1983.

139. C. A. Coulson and A. Jeffrey, "Waves: A Mathematical Approach to the Common Types of Wave Motion," Longman Inc., New York, 1977.

140. Mme S. Claes, "La Forme des Signaux d' Emission Acoustique et Leur Role dans les Essais de Localisation" *Journees d'Etudes sur l'Emission Acoustique,* pp. 215-301, March 15, 1975.

141. H. J. Filmore, *The Physics of Wave Motion,* John Wiley and Sons, New York, 1983.

142. J. N. Goodier and R. E. D. Bishop, "A Note on Critical Reflection of Elastic Waves at Free Surfaces" *J. of Applied Physics,* 23, 1952, pp 124-126.

143. M. A. Majeed and C. R. L. Murthy, "An Efficient Unsupervised Pattern Recognition Procedure for Acoustic Emission Signal Analysis" *Proceeding of Journal of Acoustic Emission,* Vol. 8, No. 1-2, pp. 16-19, 1989.

144. H. L. M.dos Reis, "Acousto-Ultrasonics: Applications to Wire Rope, Wood Fiber Hardwood, and Adhesion," *Acousto-Ultrasonics : Theory and Application* eds. J. C. Duke, Plenum Press, New York, (1988), pp. 283-300.

145. A. Mittelman, I. Roman, A. Bivas, I. Leichter, J. Y. Margulies, and A. Weinreb, "Acousto-Ultrasonics Characterization of Physical Properties of Human Bones," *Acousto-Ultrasonics : Theory and Application* eds. J. C. Duke, Plenum Press, New York, (1988), pp. 305-310.

146. A. Madhav and J. A. Nachlas, "Statistical Evaluation of Quality in Composites Using the Stress Wave Factor Technique," *Acousto-Ultrasonics : Theory and Application* eds. J. C. Duke, Plenum Press, New York, (1988), pp. 165-176.

147. G. S. Kino, *Acoustic Waves: Devices, Imaging, and Analog Signal Processing* Prentice-Hall, Inc., Englewood Cliffs, New Jersey, 1988.

148. R. L. Weaver, "Diffuse Waves for Materials NDE ," *Acousto-Ultrasonics : Theory and Application* eds. J. C. Duke, Plenum Press, New York, (1988), pp. 35-44.

149. W. W. Stinchcomb, K. L. Reifsnider, L. A. Marcus, and R. S. Williams, "Effects of Frequency on the Mechanical Response of Two Composite Materials to Fatigue Loads," *Fatigue of Composite Materials,* ASTM STP 569, 1975, pp 115-129.

150. L. R. Testardi, S. J. Norton, and T. Hsieh, "Determination of Inhomogeneities of Elastic Modulus for One Dimensional Structures Using Acoustic Dimensional Resonances" Preprint

151. S. G. Lekhnitskii, *Theory of Elasticity of an Anisotropic Body,* Mir Publishers, Moscow, 1981.

152. J. S. Heyman, "Phase Insensitive Acoustic-electric Transducer," *JASA,* V. 64, 1978, pp 243-249.

153. W. J. Pardee, "Acoustic Emission and the Plate Green's Function," *J. Mathematical Physics* V. 18, 1977, pp. 676-686.

154. S. P. Timoshenko and J. N. Goodier, *Theory of Elasticity,* McGraw-Hill, NY, 1934.

155. T. M. Proctor, Jr., "An Improved Piezoelectric Acoustic Emission Transducer," *JASA,* 71, 1982, pp. 1163-1168.

156. G. C. Sih and E. P. Chen, "Sudden Stretching of a Four-Layered Composite Plate," *Engineering Fracture Mechanics,* No. 1-2, 1981, pp. 243-252.

157. *PC-DAS User,s Manual* General Research Corporation, McLean, Va., 1985.

158. *Instruction Manual for Ultrasonic Analyzer Model 5052 UA,* Panametrics, Waltham, Mass.

159. A. Sarrafzadeh-Khoee and J. C. Duke, "Small In-Plane/Out of Plane displacement Measurement Using Laser-Speckle Interferometry," *Experimental Techniques,* 18: 18, 1986.

160. A. Sarrafzadeh-Khoee and J. C. Duke, "Noncontacting Detection in Ultrasonic Nondestructive Evaluation of Materials: Simple Optical Sensor and Fiber Optic Interferometric Application," *Review of Scientific Instrumentation,* 57: 2321, 1986.

161. A. Sarrafzadeh-Khoee, R. J. Churchill, M. G. Niimura, "Laser Generated Ultrasound," *Acousto-Ultrasonics : Theory and Application* eds. J. C. Duke, Plenum Press, New York, (1988), pp. 201-207.

162. W. W. Duley, *Laser Processing and Analysis of Materials,* Plenum Press, NY, 1983.

163. J. H. Williams and P. Liao, "Preliminary Evaluation of Non-Contact Acousto-Ulrasonic Displacement Fields in Polymeric Matrix Composite," *Acousto-Ultrasonics : Theory and Application* eds. J. C. Duke, Plenum Press, New York, (1988), pp. 67-78.

164. A. Pilarski, J. L. Rose, K. Balasubramaniam, and J. Da-Le, "Utilization of Oblique Incidence in Acousto-Ulrasonics," *Acousto-Ultrasonics : Theory and Application* eds. J. C. Duke, Plenum Press, New York, (1988), pp. 67-78.

165. *KYNAR Piezoelectric Film Technical Manual,* Pennwalt Corp., 1983.

166. J. A. Bunk, C. J. Valenza, and M. C. Bhardwaj, "Applications and Advantages of Dry Coupling Ulrasonic Transducers for Materials Characterization and Inspection," *Acousto-Ultrasonics : Theory and Application* eds. J. C. Duke, Plenum Press, New York, (1988), pp. 221-238.

167. M. Patton-Mallory and K. D. Anderson, "An Acousto-Ultrasonic Method for Evaluating Wood Products," *Acousto-Ultrasonics : Theory and Application* eds. J. C. Duke, Plenum Press, New York, (1988), pp. 301-304.

Appendix A. (ORIN.FOR)- fortran program

```
*****Program to compute variation of disturbance ********
*****with angle theta as a result of force on a composite*******
*****half space in fiber and cross fiber direction        *******
      CHARACTER*12 DIFF
      COMPLEX A(2),B(2),C(2),D(2),U(2),V(2),SGP(2)
      DIMENSION S(6,6),RL(2),SG(2),AMP(2)
      WRITE(*,*) " FILENAME FOR OUTPUT"
      READ(*,*) DIFF
      OPEN (UNIT=9,FILE=DIFF)
      PI=3.1456
      E1=21.E6
      E2=1.4E6
      V12=.3
      G12=.85E6
      G23=.5E6
      V23=.5*E2/G23-1
      V21=E2/E1*V12
      V13=V12
      E3=E2
      S(1,1)=1/E1
      S(1,2)=-V12/E1
      S(1,3)=-V13/E1
      S(2,2)=1/E2
      S(2,3)=-V23/E2
      S(3,3)=1/E3
      S(4,4)=1/G23
      S(5,5)=1/G12
      S(6,6)=1/G12
      DO 30 IF=1,6
      DO 25 IJ=1,6
      WRITE(*,*) S(IF,IJ)
   25 CONTINUE
   30 CONTINUE
      A(1)=CMPLX(S(1,1),0.)
      B(1)=CMPLX(-(2.*S(1,3)+S(5,5)),0.)
      C(1)=CMPLX(S(3,3),0.)
      A(2)=CMPLX(S(2,2),0.)
      B(2)=CMPLX(-(2.*S(2,3)+S(4,4)),0.)
      C(2)=CMPLX(S(3,3),0.)
      D(1)=CSQRT(B(1)*B(1)-CMPLX(4.,0.)*A(1)*C(1))
      D(2)=CSQRT(B(2)*B(2)-CMPLX(4.,0.)*A(2)*C(2))
      U(1)=CSQRT((-B(1)+D(1))/(CMPLX(2.,0.)*A(1)))
      U(2)=CSQRT((-B(2)+D(2))/(CMPLX(2.,0.)*A(2)))
      V(1)=CSQRT((-B(1)-D(1))/(CMPLX(2.,0.)*A(1)))
      V(2)=CSQRT((-B(2)-D(2))/(CMPLX(2.,0.)*A(2)))
      DO 100 I=1,91
      K=I-1
      RK=FLOAT(K)
      REK=RK*PI/180.
      CS=COS(REK)
      SN=SIN(REK)
      WRITE(*,*) CS,SN
      RL(1)=S(1,1)*SN**4+(2.*S(1,3)+S(5,5))*SN**2*CS**2
     ++S(3,3)*CS**4
      RL(2)=S(2,2)*SN**4+(2.*S(2,3)+S(4,4))*SN**2*CS**2
     ++S(3,3)*CS**4
      WRITE(*,*) RL(1),RL(2)
      SGP(1)=U(1)+V(1)
      SGP(2)=U(2)+V(2)
```

Appendix A. (ORIN.FOR)- fortran program

```
      SG(1)=SGP(1)
      SG(2)=SGP(2)
      SG(1)=SG(1)*(S(1,1)*S(3,3))**.5*CS*CS/RL(1)
      SG(2)=SG(2)*(S(2,2)*S(3,3))**.5*CS*CS/RL(2)
      IF(I.EQ.1) AMP(1)=SG(1)
      IF(I.EQ.1) AMP(2)=SG(2)
      SG(1)=SG(1)/AMP(1)
      SG(2)=SG(2)/AMP(2)
      WRITE(9,90) RK, SG(1), SG(2)
   90 FORMAT(3E18.5)
  100 CONTINUE
  990 STOP
  995 END
```

Appendix A. (ORIN.FOR)- fortran program

Appendix B. (GEIN.FOR)- fortran program

```
      CHARACTER*12 DIFF
      COMPLEX A(2),B(2),C(2),D(2),U(2),V(2),SGP(2)
      DIMENSION S(6,6),SS(6,6),GL(3),TL(4,3),EM(3),
      WRITE(*,*) " FILENAME FOR OUTPUT"
      READ(*,*) DIFF
      OPEN (UNIT=9,FILE=DIFF)
      PI=3.1456
      E1=21.E6
      E2=1.4E6
      V12=.3
      G12=.85E6
      G23=.5E6
      V23=.5*E2/G23-1
      V21=E2/E1*V12
      V13=V12
      E3=E2
      SS(1,1)=1/E1
      SS(1,2)=-V12/E1
      SS(1,3)=-V13/E1
      SS(2,2)=1/E2
      SS(2,3)=-V23/E2
      SS(3,3)=1/E3
      SS(4,4)=1/G23
      SS(5,5)=1/G12
      SS(6,6)=1/G12
      WRITE(*,*) 'INPUT AZIMUTHAL ANGLE'
      READ(*,*) AZ
      DO 200 ITH=1,90
      TH=FLOAT(ITH)
      DATA AR(6,6)/36*0./
      SN=SIN(AZ)
      CS=COS(AZ)
      AR(1,1)=CS**2
      AR(1,2)=SN**2
      AR(1,6)=CS*SN
      AR(2,1)=SN**2
      AR(2,2)=CS**2
      AR(2,6)=-SN*CS
      AR(3,3)=1.
      AR(4,4)=CS
      AR(4,5)=-SN
      AR(5,4)=SN
      AR(5,5)=CS
      AR(6,1)=-2.*SN*CS
      AR(6,2)=2.*SN*CS
      AR(6,6)=CS**2-SN**2
      DO 10 I=1,6
      DO 10 J=1,6
      DO 10 M=1,6
      DO 10 N=1,6
      S(I,J)=SS(M,N)*AR(I,M)*AR(J,N)
   10 CONTINUE
      SA=S(1,1)
      SB=-2.*S(1,6)
      SC=2.*S(1,6)+S(6,6)
      SD=-2.*S(2,6)
```

Appendix B. (GEIN.FOR)- fortran program

```
      SE=S(2,2)
      SF=S(5,5)
      SG=-2.*S(4,5)
      SH=S(4,4)
      SI=S(1,5)
      SJ=-(S(1,4)+S(5,6))
      SK=S(2,5)+S(4,6)
      SL=-S(2,4)
      TA=SA*SF-SI*SI
      TB=SB*SF+SA*SG-2.*SI*SJ
      TC=SC*SF+SB*SG+SA*SH-SJ*SJ-2.*SI*SK
      TD=SD*SF+SC*SG+SB*SH-2.*SK*SJ-2.*SL*SI
      TE=SE*SF+SD*SG+SC*SH-2.*SJ*SL-SK*SK
      TF=SE*SG+SD*SH-2.*SK*SL
      TG=SE*SH-SL*SL
      A=TB/TA
      B=TC/TA
      C=TD/TA
      D=TE/TA
      E=TF/TA
      F=TG/TA
%%%%%%%%%%%%%%%%%%%%%%CALL SUBROUTINE OR INPUT USING SEPARATE SOUR
      WRITE(*,*) A,B,C,D,E,F
      DO 20 I=1,3
      WRITE(*,*) "PUT IN MU VALUES"
      WRITE(*,*) I
      READ(*,*) EM(I)
   20 CONTINUE
      DO 30 I=1,3
      TL(2,I)=SF*EM(I)**2+SG*EM(I)+SH
      TL(3,I)=SI*EM(I)**3+SJ*EM(I)**2+SK*EM(I)+SL
      TL(4,I)=SA*EM(I)**4+SB*EM(I)**3+SC*EM(I)**2+SD*EM(I)+SE
   30 CONTINUE
      GL(1)=-TL(3,1)/TL(2,1)
      GL(2)=-TL(3,2)/TL(2,2)
      GL(3)=-TL(3,3)/TL(4,3)
      CA=EM(3)*GL(2)*GL(3)-EM(2)
      CB=EM(1)-EM(3)*GL(1)*GL(3)
      CC=EM(2)*GL(1)-EM(1)*GL(2)
      AT=COS(TH)+EM(1)*SIN(TH)
      AB=SIN(TH)-EM(1)*COS(TH)
      BT=COS(TH)+EM(2)*SIN(TH)
      BB=SIN(TH)-EM(2)*COS(TH)
      CT=COS(TH)+EM(3)*SIN(TH)
      CB=SIN(TH)-EM(3)*COS(TH)
      SRA=CA*AT**2/AB+CB*BT**2/BB+GL(3)*CC*CT**2/CB
      SRB=GL(1)*CA*AT/AB+GL(2)*CB*BT/BB+CC*CT/CB
      SR=-COS(TH)*REAL(CMPLX(0.,1.)*SRA)
      TR=-COS(TH)*REAL(CMPLX(0.,1.)*SRB)
      WRITE(*,*) TH,SR,TR
  200 CONTINUE
      STOP
      END
```

Appendix B. (GEIN.FOR)- fortran program

Appendix C. (DISA.FOR)- fortran program

```
c*****Program to compute dispersion curves, displacements ********
c*****for an isotropic material                             ********
C     DIMENSION AM(300),BM(300),ZTM(300),CCM(300)
C     DIMENSION BBM(300),OMM(300),RVM(300)
      CHARACTER *12 DISC, DISS, DIFF
      WRITE(*,*) " FILENAME FOR OUTPUT"
      READ(*,*) DIFF
      OPEN (UNIT=9,FILE=DIFF)
      WRITE(*,*) " INPUT I=1 FOR SYMM. I=-1 FOR ANTI. "
      READ(*,*) K
      REK=FLOAT(K)
      IFF=1
      VP=250000.
      D=.0625/2.
      VS=120000.
      IF(K.EQ.1) VR=.7*VS
      IF(K.EQ.-1) VR=.95*VS
C####LOOP TO VARY OMEGA (FREQUENCY VALUE)                  ########
      NOZ=1
      NOT=100
      DO 200 NZT=NOZ,240
      ZT=NZT/2.0
      IOV=0
      IF(K.EQ.-1) NOT=IFIX(VR*ZT*.001)-3
      IF(K.EQ.-1) GO TO 25
      IF(IFF.EQ.1) NOT=IFIX(VS*ZT*.001)+1
      IF(IFF.EQ.0) NOT=IFIX(VR*ZT*.001)-3
   25 CONTINUE
      DO 80 NOMG=NOT,1000000
C     IV=0
C     IOV=0
C     OMG=NOMG/0.0001
      IF(K.EQ.-1) OMG=(NOT-(NOMG-NOT))/.001
      IF(K.EQ.-1) GO TO 28
      OMG=NOMG/.001
   28 CONTINUE
C     OMG=NOMG/.000001
C $$$$ LOOP TO FIND VALUE FOR ZETA IN DISPERSION EQNS. $$$$$$
C     ZT=NZT/10000.0
C     ZT=NZT/100.0
C     ZT=NZT
      ZTT=ZT**2
      DVP=(OMG/VP)**2
      DVS=(OMG/VS)**2
      RV=OMG/ZT
      WRITE(*,*) RV
      IF (DVP.GT.ZTT) GOTO 35
      IF (DVS.LT.ZTT) GOTO 33
C     IFG=1
      WRITE(*,*) "VP<RV>VS"
      A=(ZTT-DVP)**.5
      B=(DVS-ZTT)**.5
      BD=B*D
      AD=A*D
      EAP=EXP(AD)
      EAN=EXP(-AD)
      EBP=EXP(BD)
      EBN=EXP(-BD)
      WRITE(*,*) EAP,EAN
      IF (EAP.EQ.EAN) GO TO 40
```

```
      F=(EXP(-AD)+EXP(AD))/(EXP(-AD)-EXP(AD))*TAN(BD)
     ++REK*((4.*A*B*ZTT)/(ZTT-B**2)**2)**K
      GO TO 40
   33 WRITE(*,*) "RV<VS"
C     IFG=2
      A=(ZTT-DVP)**.5
      B=(ZTT-DVS)**.5
      AD=A*D
      BD=B*D
      EAP=EXP(AD)
      EAN=EXP(-AD)
      EBP=EXP(BD)
      EBN=EXP(-BD)
      F=((EAN+EAP)/(EAN-EAP))*((EBN-EBP)/(EBN+EBP))
     +-((4.*A*B*ZTT)/(ZTT+B**2)**2)**K
      GO TO 40
   35 WRITE(*,*) "RV>VP"
C     IFG=3
      A=(DVP-ZTT)**.5
      B=(DVS-ZTT)**.5
      AD=A*D
      BD=B*D
      F=TAN(BD)/TAN(AD)
     ++((4.*A*B*ZTT)/(ZTT-B**2)**2)**K
C***SECTION TO DECIDE IF DISPERSION COND. IS MET
   40 CONTINUE
      WRITE(*,*) NOMG, NZT, F
C     IF (IFG.EQ.IOFG) GO TO 45
C     IF (NOT.EQ.NOMG) GO TO 45
C     IOV=0
C     GO TO 75
C  45 CONTINUE
      IF (F.LT.0.00005.AND.F.GT.-.00005) GO TO 85
      IF (F.GT.0.0) IV=1
      IF (F.LT.0.0) IV=-1
   50 IIV=IV+IOV
      WRITE(*,*) IV, IOV, IIV
      IF(IIV.EQ.0) GO TO 85
      IOV=IV
C  75 IOFG=IFG
   80 CONTINUE
   85 IF (NOMG-NOT.LT.3) IFF=0
      IF (K.EQ.-1) GO TO 100
C $$$$$$$$$$$$$$$$$$$$$$$$$$$$$$$$$$$$$$$$$$$$$$$$$$$$$$$$$$$$$$$$$$$$$$$
      IF(DVS.LT.ZTT) GO TO 95
      IF(DVP.LT.ZTT) GO TO 90
      BB=-2.*ZT*B*COS(BD)
      CC=(ZTT-B**2)*COS(AD)
      GO TO 150
   90 BB=-2.*ZT*B*COS(BD)
      CC=(ZTT-B**2)*(EXP(-AD)+EXP(AD))/2
      GO TO 150
   95 BB=-ZT*B*(EXP(-BD)+EXP(BD))
      CC=(ZTT+B**2)*(EXP(-AD)+EXP(AD))/2.
      GO TO 150
C****AREA FOR ANTI.        ******
  100 CONTINUE
      IF (DVS.LT.ZTT) GO TO 110
      IF (DVP.LT.ZTT) GO TO 115
      AA=2.*ZT*B*SIN(BD)
```

Appendix C. (DISA.FOR)- fortran program

```
      DD=(ZTT-B**2)*SIN(AD)
      GO TO 150
  110 AA=2.*ZT*B*SIN(BD)
      DD=(ZTT-B**2)*(EXP(-AD)-EXP(AD))/2.
      GO TO 150
  115 AA=ZT*B*(EXP(-BD)-EXP(BD))
      DD=(ZTT+B**2)*(EXP(-AD)-EXP(AD))/2.
C****AREA FOR ANTI.        ******.
  150 CONTINUE
C     AM(NOMG)=A
C     BM(NOMG)=B
C     CCM(NOMG)=CC
C     BBM(NOMG)=BB
C     ZTM(NOMG)=ZT
C     OMM(NOMG)=OMG
C     RVM(NOMG)=RV
C     FREQ=OMG/(2.*PI)
      WRITE (9,160) ZT,OMG
      WRITE (9,160) A,B
      IF (K.EQ.-1) GO TO 155
      WRITE (9,160) BB,CC
      GO TO 200
  155 WRITE (9,160) AA,DD
  160 FORMAT ( 2E18.6)
  200 CONTINUE
C#########################################################
C****THIS SECTION WRITES DISPERSION INFORMATION INTO
C** AN OUTPUT FILE
C*
C     WRITE(*,*) " FILENAME FOR DISP OUTPUT? "
C     READ(*,*) DISC
C 250 OPEN (UNIT=7,FILE=DISC)
C     DO 290 I=1,300
C     ZT=ZTM(I)
C     OMG=OMM(I)
C     WRITE(7,260) ZT, OMG
C 260 FORMAT( 2E15.7)
C 290 CONTINUE
C****THIS SECTION CALCULATES AND STORES DISPLACEMENTS
C**** AS A FUNCTION OF ZETA OR THE WAVE NUMBER
C**** IN THE DIRECTION OF PROPAGATION
C     WRITE(*,*) " FILE NAME FOR U2 OUTPUT? "
C     READ(*,*) DISS
C     WRITE(*,*) " WHERE DO YOU WANT U2 CALCULATED? "
C     READ(*,*) XT
C 300 OPEN (UNIT=8,FILE=DISS)
C     DO 380 J=1,300
C     A=AM(J)
C     B=BM(J)
C     BB=BBM(J)
C     CC=CCM(J)
C     BCM=(BB**2+CC**2)**.5
C     ZT=ZTM(J)
C     OMG=OMM(J)
C     RV=RVM(J)
C     AX=A*XT
C     BX=B*XT
C     IF (RV.LT.VS) GO TO 340
C     IF (RV.LT.VP) GO TO 330
C     UTT=(-BB*A*SIN(AX)+CC*ZT*SIN(BX))/BCM
```

```
C      GO TO 350
C 330 UTT=(-BB*A*(EXP(-AX)-EXP(AX))/2+CC*ZT*SIN(BX))
C     +/BCM
C      GO TO 350
C 340 UTT=(-BB*A*(EXP(-AX)-EXP(AX))/2+CC*ZT
C     +*(EXP(-BX)-EXP(BX))/2)/BCM
C 350 CONTINUE
C      WRITE(8,360) OMG, UTT
C 360 FORMAT ( 2E18.7)
C 380 CONTINUE
  990 STOP
  995 END
```

Appendix C. (DISA.FOR)- fortran program

Appendix D. (UTTT.FOR)- fortran program

```
C******CALCULATES DISPLACEMENT VERSUS FREQUENCY
C******CALCULATES PHASE VELOCITY VERSUS FREQUENCY
C******FOR AN ISOTROPIC MATERIAL FROM  (DISA.FOR) PROGRAM
C***WRITES DATA TO OUTPUT FILES FOR USE IN PLOTTING
C
C
C     DIMENSION AM(300), BM(300), CCM(300), ZTM(300)
C     DIMENSION OMM(300),MVM(300)
      CHARACTER *12 DISC, DDSC, DPHV, DISS, DISP
      WRITE(*,*) "READ FILENAME? "
      READ(*,*) DISC
      WRITE(*,*) "FILENAME FOR DISPLACEMENTS? "
      READ(*,*) DDSC
      WRITE(*,*) "FILENAME FOR PHASE VELOCITIES? "
      READ(*,*) DPHV
      OPEN (UNIT=5,FILE=DISC)
      WRITE(*,*) "FILENAME DISPERSION CURVE? "
      READ(*,*) DISP
      OPEN (UNIT=7,FILE=DISP)
      WRITE(*,*) "IS THIS FOR 1)SYM 2)ANTI.? "
      READ(*,*) ISY
      WRITE(*,*) " WHERE DO YOU WANT U2 CALCULATED? "
      READ(*,*) XT
C
C****SYMM.  U2 CALC.
C
C
      OPEN (UNIT=9,FILE=DPHV)
      OPEN (UNIT=8,FILE=DDSC)
      PI=3.1456
      DO 200 I=1,300
      READ(5,30) ZT,OMG
      FRE=.000001*OMG/(2.*PI)
      WRITE(7,60) ZT,FRE
      READ(5,30) A,B
      IF (ISY.EQ.2) GO TO 25
      READ(5,30) BB,CC
      GO TO 27
   25 READ(5,30) AA,DD
C     READ(5,30) VS,VP
   27 CONTINUE
      VP=260000
      VS=110000
   30 FORMAT ( 2E18.6)
      BCM=(BB**2+CC**2)**.5
      PHV=OMG/ZT
      AX=A*XT
      BX=B*XT
      ZTT=ZT**2
      DVP=(OMG/VP)**2
      DVS=(OMG/VS)**2
      IF (ISY.EQ.2) GO TO 100
      IF (DVS.LT.ZTT) GO TO 40
      IF (DVP.LT.ZTT) GO TO 35
      UTT=(-BB*A*SIN(AX)+CC*ZT*SIN(BX))/BCM
      GO TO 50
   35 UTT=(-BB*A*(EXP(-AX)-EXP(AX))/2+CC*ZT*SIN(BX))
     +/BCM
      GO TO 50
   40 UTT=(-BB*A*(EXP(-AX)-EXP(AX))/2+CC*ZT
```

Appendix D. (UTTT.FOR)- fortran program

```
     +*(EXP(-BX)-EXP(BX))/2)/BCM
   50 CONTINUE
      UTT=(UTT**2)**.5
      WRITE(8,60) FRE, UTT
   60 FORMAT ( 2E18.6)
C***U2 VELOCITY CALCULATION
      WRITE(9,65) FRE,PHV
   65 FORMAT ( 2E18.6)
   80 GO TO 200
C-&&&&ANTISYMM.                          &&&&&&&&&&&&&&&&&&&&&&&&&&&&
  100 CONTINUE
      EAP=EXP(A*XT)
      EAN=EXP(-A*XT)
      EBP=EXP(B*XT)
      EBN=EXP(-B*XT)
      IF (DVP.GT.ZTT) GO TO 120
      IF (DVS.LT.ZTT) GO TO 130
      CVA=(EAN+EAP)/2.
      CVB=COS(B*XT)
      GO TO 140
  120 CVA=COS(A*XT)
      CVB=COS(B*XT)
      GO TO 140
  130 CVA=(EAN+EAP)/2.
      CVB=(EBN+EBP)/2.
  140 CONTINUE
      UTT=AA*A*CVA+DD*ZT*CVB
      UTT=(UTT**2)**.5
      OMG=.000001*OMG/(2.*PI)
      WRITE(8,60) OMG, UTT
C***U2 VELOCITY CALCULATION
      WRITE(9,65) OMG,PHV
  200 CONTINUE
      STOP
      END
```

Appendix D. (UTTT.FOR)- fortran program

Appendix E. (ORTH.FOR)- fortran program

```
C*****THIS PROGRAM DETERMINES THE DISPERSION RELATIONS FOR
C***** AN ORTHOTROPIC MATERIAL WHERE THE WAVE IS SENT IN
C*****THE DIRECTION OF MATERIAL SYMMETRY
      DIMENSION C(6,6), D(6,6)
      CHARACTER *12 DISC,DIVE
      COMPLEX L(6),ALO(6),FF,DV,KK(4,4),ALT(6)
      COMPLEX CI(6,6),DI(6,6),KA,KB,KC,KD,RKB,RNB
      COMPLEX CMPLX,CEXP,CAC(3),DAD(3),CZ(4),CSQRT
      IV=0
      B=.024
      KO=1
      PI=3.145
      RHO=.000151
      C(1,1)=23.4E6
      C(1,2)=.943E6
      C(1,3)=C(1,2)
      C(2,2)=2.1E6
      C(2,3)=1.05E6
      C(3,3)=2.1E6
      C(4,4)=.527E6
      C(5,5)=1.03E6
      C(6,6)=1.03E6
      WRITE(*,*) "WHAT IS THE NAME FOR OUT-FILE? "
      READ(*,*) DISC
      OPEN (UNIT=7,FILE=DISC)
      WRITE(*,*) "WHAT IS THE NAME FOR VEL.-OUT? "
      READ(*,*) DIVE
      OPEN (UNIT=8,FILE=DIVE)
      DO 300 NOMG=1,300
      IOV=0
      ROMG=FLOAT(NOMG)
C     OMG=ROMG/.00002
C     OMG=ROMG/.00004
      OMG=ROMG/.00005
      DO 200 K=KO,3000000
      RK=FLOAT(K)
      WRITE(*,*) "OMG=,RK="
      WRITE(*,*) OMG,RK
C     RK=RK/100.
      RK=RK/1000.
      RL=RHO*OMG**2/RK**2
      WRITE(*,*) "RL="
      WRITE(*,*) RL
      D(1,1)=C(1,1)-RL
      D(6,6)=C(6,6)-RL
      D(5,5)=C(5,5)-RL
C###### WAVE NUMBERS FOR SH-MODES
      L(5)=CSQRT(CMPLX(-D(6,6)/C(4,4),0.))
      L(6)=-L(5)
C#########################
      AA=C(5,5)*C(3,3)/1.E5
      DOB=D(1,1)/1.E5
      DFB=D(5,5)/1.E5
      COFS=(C(1,3)+C(5,5))**2/1.E5
      BB=-COFS+DOB*C(3,3)+DFB*C(5,5)
      CC=D(1,1)*DFB
      DV=CSQRT(CMPLX(BB**2-4.*AA*CC,0.))
C#####WAVE NUMBERS FOR SV,P-MODES
      L(1)=CSQRT((CMPLX(-BB,0.)+DV)/CMPLX(2.*AA,0.))
      L(3)=CSQRT((CMPLX(-BB,0.)-DV)/CMPLX(2.*AA,0.))
```

Appendix E. (ORTH.FOR)- fortran program

```
      L(2)=-L(1)
      L(4)=-L(3)
 ##################
      DO 50 I=1,4
      RRLV=REAL(L(I))
      RILV=AIMAG(L(I))
      WRITE(*,*) I,RRLV,RILV
   50 CONTINUE
      DO 120 IJ=1,6
      DO 110 JI=1,6
      CI(IJ,JI)=CMPLX(C(IJ,JI),0.)
      DI(IJ,JI)=CMPLX(D(IJ,JI),0.)
  110 CONTINUE
  120 CONTINUE
      DO 150 J=1,4
      ALO(J)=L(J)*(CI(1,3)+CI(5,5))
      ALT(J)=-(DI(1,1)+L(J)*L(J)*CI(5,5))
      WRITE(*,*) ALO(J),ALT(J)
      ALO(J)=ALO(J)/1.E13
      ALT(J)=ALT(J)/1.E13
  150 CONTINUE
      RKB=CMPLX(0.,RK*B)
      RNB=CMPLX(0.,-RK*B)
      DO 170 J=1,4
      KK(1,J)=(CI(1,3)*ALO(J)+CI(3,3)*ALT(J)*L(J))
     +*CEXP(RKB*L(J))
      WRITE(*,*) KK(1,J)
  170 CONTINUE
      DO 180 J=1,4
      KK(2,J)=(CI(1,3)*ALO(J)+CI(3,3)*ALT(J)*L(J))
     +*CEXP(RNB*L(J))
      WRITE(*,*) KK(2,J)
  180 CONTINUE
      DO 185 J=1,4
      KK(3,J)=CI(5,5)/CMPLX(2.,0.)*(L(J)*ALO(J)+ALT(J))
     +*CEXP(RKB*L(J))
      KK(3,J)=CI(5,5)*(L(J)*ALO(J)+ALT(J))
     +*CEXP(RKB*L(J))
      WRITE(*,*) KK(3,J)
  185 CONTINUE
      DO 190 J=1,4
      KK(4,J)=CI(5,5)/CMPLX(2.,0.)*(L(J)*ALO(J)+ALT(J))
     +*CEXP(RNB*L(J))
      KK(4,J)=CI(5,5)*(L(J)*ALO(J)+ALT(J))
     +*CEXP(RNB*L(J))
      WRITE(*,*) KK(4,J)
  190 CONTINUE
      KA=KK(2,2)*(KK(3,3)*KK(4,4)-KK(3,4)*KK(4,3))
     +-KK(2,3)*(KK(3,2)*KK(4,4)-KK(3,4)*KK(4,2))
     ++KK(2,4)*(KK(3,2)*KK(4,3)-KK(3,3)*KK(4,2))
      WRITE(*,*) "KA="
      WRITE(*,*) KA
      KB=KK(2,1)*(KK(3,3)*KK(4,4)-KK(3,4)*KK(4,3))
     +-KK(2,3)*(KK(3,1)*KK(4,4)-KK(3,4)*KK(4,1))
     ++KK(2,4)*(KK(3,1)*KK(4,3)-KK(3,3)*KK(4,1))
      WRITE(*,*) "KB="
      WRITE(*,*) KB
      KC=KK(2,1)*(KK(3,2)*KK(4,4)-KK(3,4)*KK(4,2))
     +-KK(2,2)*(KK(3,1)*KK(4,4)-KK(3,4)*KK(4,1))
     ++KK(2,4)*(KK(3,1)*KK(4,2)-KK(3,2)*KK(4,1))
```

Appendix E. (ORTH.FOR)- fortran program

```
      WRITE(*,*) "KC="
      WRITE(*,*) KC
      KD=KK(2,1)*(KK(3,2)*KK(4,3)-KK(3,3)*KK(4,2))
     +-KK(2,2)*(KK(3,1)*KK(4,3)-KK(3,3)*KK(4,1))
     ++KK(2,3)*(KK(3,1)*KK(4,2)-KK(3,2)*KK(4,1))
      WRITE(*,*) "KD="
      WRITE(*,*) KD
      FF=KK(1,1)*KA-KK(1,2)*KB+KK(1,3)*KC-KK(1,4)*KD
      CKV=CABS(FF)
      WRITE(*,*) "CKV="
      WRITE(*,*) CKV
C     IF (CKV.LT.0.0001) GO TO 220
      IF (CKV.LT.0.0010) GO TO 220
C     IF (K.EQ.1) GO TO 195
C     IF (CKV.GT.OKV) IV=1
C     IF (CKV.LT.OKV) IV=-1
C     IIV=IV+IOV
C     IF (IIV.EQ.0) GO TO 220
C195  IOV=IV
C     OKV=CKV
  200 CONTINUE
  220 CONTINUE
C#####       CALCULATE CZ CONSTANTS      ##########
      DO 240 J=1,3
      JP=J+1
      CAC(J)=(KK(2,1)*KK(3,JP))/KK(3,1)+KK(2,JP)
      DAD(J)=(KK(1,1)*KK(3,JP))/KK(3,1)+KK(1,JP)
  240 CONTINUE
      CZ(4)=1.
      CZ(3)=((DAD(1)*CAC(3))/CAC(1)-DAD(3))
     +/(DAD(2)-DAD(1)*DAD(2)/CAC(1))
      CZ(2)=-(CAC(3)+CAC(2)*CZ(3))/CAC(1)
      CZ(1)=(KK(3,2)*CZ(2)+KK(3,3)*CZ(3)+KK(3,4))/KK(3,1)
      KO=K
      WRITE(7,250) FR,OMG
      VPH=OMG/RK
      FR=OMG/(2.*PI)
      WRITE(8,250) FR,VPH
C     DO 245 J=1,4
C     WRITE(9,255) ALO(J),ALT(J),L(J)
C245  CONTINUE
C     WRITE(9,250) CZ(1),CZ(2)
C     WRITE(9,250) CZ(3),CZ(4)
  250 FORMAT( 2E18.6)
C255  FORMAT( 3E18.6)
  300 CONTINUE
      STOP
      END
```

Appendix E. (ORTII.FOR)- fortran program

Appendix F. (GENE.FOR)- fortran program

```
C*****THIS PROGRAM DETERMINES THE DISPERSION RELATIONS FOR
C***** AN ORTHOTROPIC MATERIAL WHERE THE WAVE IS SENT IN
C*****ANY DIRECTION DEFINED BY THE INPUT DIRECTION
      DIMENSION C(6,6), D(6,6), CO(6,6)
      CHARACTER *12 DISC
      COMPLEX FF
      COMPLEX RKB,RNB,CMD,CKD
      COMPLEX CMPLX,CEXP,X(3)
      COMPLEX Y(3),TL(6),CM(3,3),AL(6,3),RKB,RNB
      COMPLEX CEP,CEN,KK(6,6),CSQRT
      IV=0
C%%%%%%%B-HALF PLATE THICKNESS
C%%%%%%%RHO-MATERIAL DENSITY
C%%%%%%%CO(I,J)-STIFFNESS MATRIX FOR ORTHOTROPIC DIRECTION
      IDIOT=0
      IV=0
      B=.063
      KO=1
      RHO=.000151
      CO(1,1)=23.4E6
      CO(1,2)=.943E6
      CO(1,3)=C(1,2)
      CO(2,2)=2.1E6
      CO(2,3)=1.05E6
      CO(3,3)=2.1E6
      CO(4,4)=.527E6
      CO(5,5)=1.03E6
      CO(6,6)=1.03E6
      PI=3.1456
C********  ROTATE STIFFNESS MATRIX    ********************************
C
C*******INPUT ROTATION ANGLE (IE. DEFINE AZIMUTHAL ANGLE)
      WRITE(*,*) "WHAT ANGLE DO YOU WANT FOR ROTATION"
      READ(*,*) ANG
      ANG=PI*ANG/180.
      SN=SIN(ANG)
      CSM=COS(ANG)
      CF=CSM**4
      CS=CSM**2
      SF=SN**4
      SS=SN**2
      DO 25 I=1,6
      DO 25 J=1,6
      C(I,J)=0.0
   25 CONTINUE
      C(1,1)=CO(1,1)*CF+2.*CS*SS*(CO(1,2)+CO(6,6))
     ++CO(2,2)*SF
      WRITE(*,*) C(1,1)
      C(1,2)=CS*SS*(CO(1,1)+CO(2,2)-4.*CO(6,6))
     ++CO(1,2)*(CF+SF)
      WRITE(*,*) C(1,2)
      C(1,3)=CO(1,3)*CS+CO(2,3)*SS
      WRITE(*,*) C(1,3)
      C(1,6)=SN*CSM*(CO(1,1)*CS-CO(2,2)*SS
     +-(CO(1,2)+2.*CO(6,6))*(CS-SS))
      WRITE(*,*) C(1,6)
      C(2,2)=CO(1,1)*SF+2.*CS*SS*(CO(1,2)+2.*CO(6,6))
     ++CO(2,2)*CF
      WRITE(*,*) C(2,2)
      C(2,3)=CO(1,3)*SS+CO(2,3)*CS
```

```
      WRITE(*,*) C(2,3)
      C(2,6)=CSM*SN*(CO(1,1)*SS-CO(2,2)*CS
     ++(CO(1,2)+2.*CO(6,6))*(CS-SS))
      WRITE(*,*) C(2,6)
      C(3,3)=CO(3,3)
      WRITE(*,*) C(3,3)
      C(3,6)=(CO(2,3)-CO(1,3))*SN*CSM
      WRITE(*,*) C(3,6)
      C(4,4)=CO(4,4)*CS+CO(5,5)*SS
      WRITE(*,*) C(4,4)
      C(4,5)=(CO(4,4)-CO(5,5))*SN*CSM
      WRITE(*,*) C(4,5)
      C(5,5)=CO(4,4)*SS+CO(5,5)*CS
      WRITE(*,*) C(5,5)
      C(6,6)=(CO(1,1)+CO(2,2)-2.*CO(1,2))*CS*SS
     ++CO(6,6)*(CS-SS)**2
      WRITE(*,*) C(6,6)
C%%%%%%%%%%%%%%%C(I,J)-ROTATED STIFFNESS MATRIX%%%%%%%%%%%%%%%%%%%%%%%
C
C***NAME OUTPUT FILE*********************************
      WRITE(*,*) "WHAT IS THE NAME FOR OUT-FILE? "
      READ(*,*) DISC
      OPEN (UNIT=7,FILE=DISC)
      NOMG=1
C########SECTION 1######SECTION 1########SECTION 1##########
C@@@@@DEFINE K-WAVENUMBER FOR VARIOUS POINTS ON DISPERSION CURVE
      DO 500 K=1,240
      RK=FLOAT(K)
C###END SECTION 1############END SECTION 1#############
C#######SECTION 2############SECTION 2#######SECTION 2##########
C%%%DEFINE THE VALUE FOR NOO%%%%%%%%%%%%%%%%%%%%
C@@@@DEFINES WHERE THE PROGRAM STARTS LOOKING FOR THE SOLUTION
C@@@@WHICH MEETS DISPERSION CONDITION
C
      NOO=NOMG
      IF (K.EQ.1) NOO=1
C
      IOV=0
C
C########SECTION 3########SECTION 3#########SECTION 3#########
C@@@@@DEFINES THE OMG VALUE
C%%%%OMG-CIRCULAR FREQUENCY FOR WAVE
C
      DO 400 NOMG=NOO,99999999
      ROMG=FLOAT(NOMG)
C     OMG=ROMG/.00002
      OMG=ROMG/.002
c     OMG=ROMG/.001
C     OMG=ROMG/.05
C
C#######END SECTION 3###################################
C
      WRITE(*,*) "OMG=,RK="
      WRITE(*,*) OMG,RK
C     RK=RK/100.
C     RK=RK/1000.
      RL=RHO*OMG**2/RK**2
C     WRITE(*,*) "RL="
C     WRITE(*,*) RL
C####SECTION 4#####SECTION 4######SECTION 4###########
```

Appendix F. (GENE.FOR)- fortran program

```
C@@@@@SOLVE THE CHRISTOFFEL EQUATION FOR THE PARTIAL WAVES
C@@@@FIND THE WAVE NUMBERS
C%%%%%%%%TL(6)-WAVENUMBER RATIOS OF X-3 WAVENUMBER TO X-1 WAVENUMBER
C%%%FOR EACH SLOUTION
C
      D(1,1)=C(1,1)-RL
      D(6,6)=C(6,6)-RL
      D(5,5)=C(5,5)-RL
      XT=C(3,3)*D(6,6)+C(4,4)*D(5,5)-(C(3,6)+C(4,5))**2
      YT=D(5,5)*C(4,5)+C(1,6)*C(3,3)-(C(4,5)+C(3,6))
     +*(C(1,3)+C(5,5))
      Z=C(1,6)*(C(3,6)+C(4,5))-D(6,6)*(C(1,3)+C(5,5))
      W=C(4,5)*(C(3,6)+C(4,5))-C(4,4)*(C(1,3)+C(5,5))
      AE=C(3,3)*(C(4,4)*C(5,5)-C(4,5)**2)
      BE=XT*C(5,5)+D(1,1)*C(4,4)*C(3,3)-C(1,6)*C(4,5)*C(3,3)
     +-C(4,5)*YT+W*(C(1,3)+C(5,5))
      CE=C(5,5)*D(6,6)*D(5,5)+D(1,1)*XT-C(4,5)*D(5,5)*C(1,6)
     +-C(1,6)*YT+Z*(C(1,3)+C(5,5))
      DE=D(1,1)*D(6,6)*D(5,5)-C(1,6)**2*D(5,5)
      P=BE/AE
      Q=CE/AE
      R=DE/AE
      WRITE(*,*) "P    Q   R"
      WRITE(*,*) P,Q,R
      AS=(3.*Q-P*P)/3.
      BS=(2.*P*P*P-9.*P*Q+27.*R)/27.
      ZI=BS*BS/4.+AS*AS*AS/27.
      WRITE(*,*) "ZI=", ZI
      IF(ZI.EQ.0.) GO TO 50
      IF(ZI.GT.0.) GO TO 55
      ZL=-(BS/2.)
      WRITE(*,*) "ZL=", ZL
      ZB=(-ZI)**.5
      WRITE(*,*) "ZB=", ZB
      THT=ATAN(ZB/ZL)
      ZM=(ZB**2+ZL**2)**.5
      AT=THT/3.
      BPA=ZM**.333333*2.*COS(AT)
      BMA=ZM**.333333*2.*SIN(AT)
      X(1)=BPA
      X(2)=-BPA/2.-BMA/2.*(3.)**.5
      X(3)=-BPA/2.+BMA/2.*(3.)**.5
      GO TO 65
   50 CONTINUE
      X(1)=-2.*(BS/2.)**.333333
      X(2)=-X(1)/2.
      X(3)=-X(1)/2.
      GO TO 65
   55 CONTINUE
      ZL=BS/2.
      ZB=SQRT(ZI)
      BML=-ZL+ZB
      BPL=ZL+ZB
      QML=1.
      QPL=1.
      IF(BML.LT.0.) QML=-1.
      IF(BPL.LT.0.) QPL=-1.
      BML=BML*QML
      BPL=BPL*QPL
C     WRITE(*,*) "BEFORE"
```

```
      AB=QML*(BML)**.333333
      BA=QPL*(-(BPL)**.333333)
C     WRITE(*,*) "AFTER"
      TRE=SQRT(3.)
C
C
      X(1)=AB+BA
      X(2)=-X(1)/2.+CMPLX((AB-BA)/2.*TRE,0.)*CMPLX(0.,1.)
      X(3)=-X(1)/2.-CMPLX((AB-BA)/2.*TRE,0.)*CMPLX(0.,1.)
   65 CONTINUE
      DO 75 I=1,3
      Y(I)=X(I)-P/3.
      WRITE(*,*) "I,Y(I)",I,Y(I)
C
   75 CONTINUE
C
C****CALCULATE WAVE NUMBER RATIOS FOUND
C%%%%TL(I)-WAVENUMBER RATIO
C
      DO 95 I=1,3
      TL(I)=CSQRT(Y(I))
      TL(I+3)=-TL(I)
      WRITE(*,*) "I,TL(I)",I,TL(I)
   95 CONTINUE
C     WRITE(*,*) "END OF SECTION 4"
C
C####END SECTION 4#####################
C
C####SECTION 5#######SECTION 5###########SECTION 5########
C@@@@@THIS SECTION FINDS THE DISPLACEMENT VECTOR TERMS
C
C%%%%AL(I,J)-DISPLACEMENT VECTORS (I)=WHICH SOLUTION OR PARTIAL WAVE
C(J)=THE INDICE THAT INDICATES THE DIRECTION OF THE VECTOR
C
      CMD=CMPLX(1.E8,0.)
C
      DO 100 I=1,6
      CM(1,1)=D(1,1)+TL(I)**2*C(5,5)
      CM(1,2)=C(1,6)+TL(I)**2*C(4,5)
      CM(1,3)=TL(I)*(C(1,3)+C(5,5))
      CM(2,2)=D(6,6)+TL(I)**2*C(4,4)
      CM(2,3)=TL(I)*(C(4,5)+C(3,6))
      CM(3,3)=TL(I)**2*C(3,3)+D(5,5)
      WRITE(*,*) "I=",I
      AL(I,2)=1./CMD
      WRITE(*,*) "AL",I,"2",AL(I,2)
      AL(I,1)=-(CM(1,3)*CM(2,2)-CM(1,2)*CM(2,3))/
     +(CM(1,1)*CM(2,3)-CM(1,2)*CM(1,3))
      AL(I,1)=AL(I,1)/CMD
      WRITE(*,*) "AL",I,"1",AL(I,1)
      AL(I,3)=(CM(1,2)+AL(I,1)*CM(1,2))/CM(2,3)
      AL(I,3)=AL(I,3)/CMD
      WRITE(*,*) "AL",I,"3",AL(I,3)
  100 CONTINUE
C     WRITE(*,*) "END OF SECTION 5"
C
C
C######END SECTION 5#################################
C
C####SECTION 6####SECTION 6#######SECTION 6############
```

Appendix F. (GENE.FOR)- fortran program

```
C@@@@@THIS SECTION DEFINES THE KK(I,J) MATRIX FROM STRESS FREE BC'S
C%%%%KK(I,J)-MATRIX SET-UP BY IMPOSING THE STRESS FREE BC'S
C@@@THIS MATRIX MULTIPLIED BY DISPLACEMENT VECTORS AND MUST EQUAL
C@@@MUST EQUAL THE IDENTITY VECTOR
C
      DO 110 I=1,6
      RKB=CMPLX(0.,RK*B)*TL(I)
      RNB=CMPLX(0.,-RK*B)*TL(I)*2.
      WRITE(*,*) "RKB, RNB", RKB, RNB

      CEP=CEXP(RKB)
      CEN=CEXP(RNB)
      KK(1,I)=CEP*(C(1,3)*AL(I,1)+C(3,3)*AL(I,3)*TL(I)
     ++C(3,6)*AL(I,2))
      KK(2,I)=CEN*KK(1,I)
      KK(3,I)=CEP*(C(4,4)*AL(I,2)*TL(I)
     ++C(4,5)*(AL(I,1)*TL(I)+AL(I,3)))
      KK(4,I)=CEN*KK(3,I)
      KK(5,I)=CEP*(C(4,5)*AL(I,2)*TL(I)
     ++C(5,5)*(AL(I,1)*TL(I)+AL(I,3)))
      KK(6,I)=CEN*KK(5,I)
  110 CONTINUE
C     WRITE(*,*) "END OF SECTION 6"
C     CKD=CMPLX(1.E-27,0.)
      DO 125 I=1,6
      DO 125 J=1,6
C     KK(I,J)=KK(I,J)/CKD
C     WRITE(*,*) "KK(",I,",",J,")",KK(I,J)
  125 CONTINUE
C
C###END SECTION 6####################
C
C###SECTION 7#####SECTION 7#####SECTION 7###########
C@@@@@THIS SECTION CALCULATES THE DETERMINANT OF KK(I,J)
C%%%FF-IS THE VALUE FOR THE DETERMINANT OF KK(I,J)
C
      FF=0.
      DO 340 J=1,6
      AN=(-1.)**(1+J)
      DO 330 LP=1,6
      IF(LP.EQ.J)GO TO 330
      BN=(-1.)**(2+LP)
      IF(LP.LT.J) BN=-BN
      DO 320 N=1,6
      IF(N.EQ.J.OR.N.EQ.LP) GO TO 320
      CN=(-1.)**(3+N)
      IF(N.LT.J.AND.N.GT.LP) CN=-CN
      IF(N.LT.LP.AND.N.GT.J) CN=-CN
      DO 310 I=1,6
      IF(I.EQ.J.OR.I.EQ.LP.OR.I.EQ.N) GO TO 310
      DN=(-1.)**(4+I)
      IF(I.LT.J.AND.I.LT.LP.AND.I.LT.N) DN=-DN
      IF(I.GT.J.AND.I.GT.LP.AND.I.LT.N) DN=-DN
      IF(I.GT.N.AND.I.GT.J.AND.I.LT.LP) DN=-DN
      IF(I.GT.LP.AND.I.GT.N.AND.I.LT.J) DN=-DN
      DO 300 M=1,6
      IF(M.EQ.J.OR.M.EQ.LP.OR.M.EQ.N.OR.M.EQ.I)GO TO 300
      EN=(-1.)**(5+M)
      IF(M.GT.J.AND.M.LT.LP.AND.M.LT.N.AND.M.LT.I)EN=-EN
      IF(M.GT.LP.AND.M.LT.J.AND.M.LT.N.AND.M.LT.I)EN=-EN
```

```
      IF(M.GT.N.AND.M.LT.J.AND.M.LT.LP.AND.M.LT.I)EN=-EN
      IF(M.GT.I.AND.M.LT.J.AND.M.LT.LP.AND.M.LT.N)EN=-EN
      IF(M.LT.J.AND.M.GT.LP.AND.M.GT.N.AND.M.GT.I)EN=-EN
      IF(M.LT.LP.AND.M.GT.J.AND.M.GT.N.AND.M.GT.I)EN=-EN
      IF(M.LT.N.AND.M.GT.J.AND.M.GT.LP.AND.M.GT.I)EN=-EN
      IF(M.LT.I.AND.M.GT.J.AND.M.GT.LP.AND.M.GT.N)EN=-EN
C     IF(M.GT.J.AND.M.GT.LP.AND.M.LT.N.AND.M.LT.I)EN=-EN
C     IF(M.GT.J.AND.M.GT.N.AND.M.LT.LP.AND.M.LT.I)EN=-EN
C     IF(M.GT.J.AND.M.GT.I.AND.M.LT.LP.AND.M.LT.N)EN=-EN
C     IF(M.GT.LP.AND.M.GT.N.AND.M.LT.J.AND.M.LT.I)EN=-EN
C     IF(M.GT.LP.AND.M.GT.I.AND.M.LT.J.AND.M.LT.N)EN=-EN
C     IF(M.GT.N.AND.M.GT.I.AND.M.LT.J.AND.M.LT.LP)EN=-EN
      DO 290 IT=1,6
      IF(IT.EQ.J.OR.IT.EQ.LP.OR.IT.EQ.N.OR.IT.EQ.I.OR.IT.EQ.M) GO TO 290
C     WRITE(*,*) "CALCULATE FF"
      FF=FF+KK(1,J)*KK(2,LP)*KK(3,N)*KK(4,I)*KK(5,M)
     +*KK(6,IT)*AN*BN*CN*DN*EN
C     WRITE(*,*) "FF=",FF
  290 CONTINUE
  300 CONTINUE
  310 CONTINUE
  320 CONTINUE
  330 CONTINUE
  340 CONTINUE
C     WRITE(*,*) "END OF SECTION 7"
C
C#####END OF SECTION 7####END OF SECTION 7##########
C
C####SECTION 8######SECTION 8####SECTION 8##########
C@@@@THIS SECTION CHECKS TO SEE IF FF IS CLOSE TO ZERO
C@@@OR IN OTHER WORDS, IF THE DISPERSION CONDITION IS MET
C
      CKV=CABS(FF)
      WRITE(*,*) "CKV="
      WRITE(*,*) CKV
      IF (CKV.LT.1.E-10) GO TO 420
      IF (NOMG.EQ.NOO) GO TO 195
      IF (CKV.GT.OKV) IV=1
      IF (CKV.LT.OKV) IV=-1
      IIV=IV+IOV
      WRITE(*,*) IV,IOV,IIV
      IF (IIV.EQ.0.AND.CKV.GT.OKV) GO TO 420
  195 IOV=IV
      OKV=CKV
C#######END SECTION 8##################
C
  400 CONTINUE
  420 CONTINUE
      NOO=NOMG
      WRITE(7,450) RK,OMG
C     WRITE(7,450) CZ(1),CZ(2)
C     WRITE(7,450) CZ(3),CZ(4)
  450 FORMAT( 2E18.6)
  500 CONTINUE
      STOP
      END
```

Appendix G. (CHRIS.FOR)- fortran program

```
C*****THIS PROGRAM CALCULATES VELOCITIES AND DISPLACEMENT VECTORS
C*****FOR STRESS WAVES PROPAGING IN ANY DIRECTION IN A COMPOSITE
C*****PLATE, BY SOLVING THE CHRISTOFFEL EQUATION.
C*****THE DIRECTION OF WAVE PROPAGATION IS DEFINED BY
C*****THE AZIMUTHAL ANGLE ON THE PLATE AND THEN AN INCLINATION ANGLE
C*****IN THE PLANE FOR THAT AZIMUTHAL ANGLE
      DIMENSION CA(6,6), VA(3), VB(3), V(3), DV(3,3)
      DIMENSION C(3,3,3,3), CL(3,3), VL(3), VP(3), CN(3,3)
      CHARACTER *12 DISC
      DATA C/81*0./
      PI=3.1450
C*****INPUT AZIMUTHAL ANGLE ROTATION FOR DEFINING DIRECTION OF WAVE
C******WAVE PROPAGATION
      WRITE(*,*) "INPUT AZIMUTHAL ANGLE? "
      READ(*,*) AZ
C******INPUT ROTATION ANGLE FOR ROTATION IN THE PLANE DEFINED
C******BY THE AZIMUTHAL ANGLE (THIS DEFINES ULTIMATE WAVE PROPAGATION
C******DIRECTION)
      WRITE(*,*) "INPUT INCLINATION ANGLE? "
      READ(*,*) TH
      AZ=AZ*PI/180.
      TH=TH*PI/180.
C*****VA(I) DEFINES THE ORIGNAL DIRECTION OF WAVE PROPAGATION
C***** IN THE X-DIRECTION OR FIBER DIRECTION
      VA(1)=1.
      VA(2)=0.
      VA(3)=0.
C*****THIS SECTION CALCULATES THE ROTATION MATRIX TO ROTATE
C*****VA(I) AT ANY ORIENTATION DESIRED RELATIVE TO THE FIBER
C*****DIRECTION
      CA(1,1)=COS(AZ)
      CA(1,2)=COS(PI/2.-AZ)
      CA(1,3)=0.
      CA(2,1)=-SIN(AZ)
      CA(2,2)=COS(AZ)
      CA(2,3)=0.
      CA(3,1)=0.
      CA(3,2)=0.
      CA(3,3)=1.
C****THIS SECTION ROTATES THE VA(I) MATRIX TO NEW AZIMUTHAL ANGLE
C****AND RENAMES MATRIX VB(I) THE DIRECTION OF PROPAGATION
      DO 25 I=1,3
      DO 25 J=1,3
      VB(I)=VA(J)*CA(I,J)
   25 CONTINUE
C*****THIS SECTION CALCULATES THE ROTATION MATRIX FOR INCLINING
C*****THE WAVE VECTOR VB(I) IN THE PLANE DEFINED AFTER THE
C*****ROTATION INTO THE AZIMUTHAL ANGLE
      CA(1,1)=COS(TH)
      CA(1,2)=0.
      CA(1,3)=-SIN(TH)
      CA(2,1)=0.
      CA(2,2)=1.
      CA(2,3)=0.
      CA(3,1)=COS(PI/2.-TH)
      CA(3,2)=0.
      CA(3,3)=COS(TH)
C****THIS SECTION ROTATES THE VB(I) MATRIX TO NEW INCLINATION ANGLE
C****AND RENAMES MATRIX V(I) THE DIRECTION OF PROPAGATION
C****THIS IS THE ULTIMATE WAVE VECTOR FOR THE WAVE PROPAGATION
```

Appendix G. (CHRIS.FOR)- fortran program

```
      DO 50 I=1,3
      DO 50 J=1,3
      V(I)=VB(J)*CA(I,J)
   25 CONTINUE
C*****C(I,J,K,L) IS THE STIFFNESS TENSOR FOR GR/EP AND RHO IS THE
C*****DENSITY FOR GR/EP
      RHO=.000151
      C(1,1,1,1)=23.4E6
      C(1,1,2,2)=.943E6
      C(2,2,1,1)=.943E6
      C(1,1,3,3)=C(1,1,2,2)
      C(3,3,1,1)=C(1,1,2,2)
      C(2,2,2,2)=2.1E6
      C(2,2,3,3)=1.05E6
      C(3,3,2,2)=1.05E6
      C(3,3,3,3)=2.1E6
      C(2,3,2,3)=.527E6/2.
      C(2,3,3,2)=.527E6/2.
      C(3,2,2,3)=.527E6/2.
      C(3,2,3,2)=.527E6/2.
      C(3,1,3,1)=1.03E6/2.
      C(3,1,1,3)=1.03E6/2.
      C(1,3,3,1)=1.03E6/2.
      C(1,3,1,3)=1.03E6/2.
      C(1,2,1,2)=1.03E6/2.
      C(1,2,2,1)=1.03E6/2.
      C(2,1,1,2)=1.03E6/2.
      C(2,1,2,1)=1.03E6/2.
C****THIS SECTION CARRIES OUT THE MULTIPLICATIONS FOR THE CHRISTOFFEL
C****EQUATION'S RIGHT SIDE OR THE STIFFNESS TERMS
      DO 75 I=1,3
      DO 75 K=1,3
      DO 75 J=1,3
      DO 75 L=1,3
      CL(I,K)=C(I,J,K,L)*V(J)*V(L)
   75 CONTINUE
      B=0.
C****THIS SECTION CALCULATES THE COEFFICIENTS FOR THE CUBIC EQUATION
C***THAT RESULTS FROM SUBTRACTING THE UNKNOWN VELOCITY IN THE
C***INERTIAL TERM FROM THE STIFFNESS TERMS
C***SOLVING THIS EQUATION GIVES THE VELOCITIES OF POSSIBLE
C***STRESS WAVES
      DO 100 I=1,3
C****P IS THE COEFFICIENT OF THE QUADRATIC TERM
      P=CL(I,I)+B
  100 CONTINUE
C****Q IS THE COEFFICIENT OF THE LINEAR TERM
      Q=CL(2,2)*CL(3,3)-CL(2,3)*CL(2,3)
     ++CL(3,3)*CL(1,1)-CL(3,1)*CL(3,1)
     ++CL(1,1)*CL(2,2)-CL(1,2)*CL(1,2)
C****R IS THE CONSTANT TERM
      R=CL(1,1)*(CL(2,2)*CL(3,3)-CL(2,3)*CL(3,2))
     +-CL(1,2)*(CL(3,3)*CL(1,1)-CL(3,1)*CL(3,1))
     ++CL(1,3)*(CL(1,1)*CL(2,2)-CL(1,2)*CL(1,2))
C****THIS SECTION SOLVES THE CUBIC EQUATION TO FIND THE PHASE
C****VELOCITIES BY USING A STANDARD SOLUTION FROM THE CRC
C****HANDBOOK PAGE
      A=3.*Q-P*P
      B=(2.*P**3-9.*P*Q+27.*R)/27.
      BT=-B/2.
```

Appendix G. (CHRIS.FOR)- fortran program

```
      AT=-(B*B/4.+A**3/27.)
      IF (AT.LT.0.) AT=-AT
      AT=AT**.5
      KT=(BT*BT+AT*AT)**.5
      TT=ATAN(BT/AT)
      TA=TT/3.
      KT=KT**.333333
      APB=2.*KT*COS(TA)
      AMB=2.*KT*SIN(TA)
C$$$$$$$$$$$$$$$$$$$$$$$$$$$$$$$$$$$$$$$$$$$$$$$$$$$$$$$$$$$$$$$$$$$$$$$$$$$
C*****CALCULATE PHASE VELOCITIES FOR WAVES
      VL(1)=APB-P/3.
      VL(2)=-APB-AMB*3.**.5-P/3.
      VL(3)=-APB+AMB*3.**.5-P/3.
      DO 125 I=1,3
      VP(I)=(VL(I)/RHO)**.5
  125 CONTINUE
C$$$$$$$$$$$$$$$$$$$$$$$$$$$$$$$$$$$$$$$$$$$$$$$$$$$$$$$$$$$$$$$$$$$$$$$$$$$
C*****CALCULATE DISPLACEMENT VECTORS
      DO 175 K=1,3
      DO 150 I=1,3
      DO 150 J=1,3
      CN(I,J)=CL(I,J)
      CN(J,J)=CL(J,J)-VL(K)
  150 CONTINUE
      DV(K,3)=1.
      DVN=CN(2,2)*CN(1,1)
      DV(K,1)=DV(K,3)*(CN(1,2)*CN(2,3)/DVN-CN(1,3)/CN(1,1))
     +/(1-CN(1,2)*CN(2,1)/DVN)
      DV(K.2)=-(CN(2,1)*DV(K,1)+DV(K,3)*CN(2,3))/CN(2,2)
  175 CONTINUE
C****WRITE PHASE VELOCITIES TO FILE
      DO 225 I=1,3
      WRITE(6,200) AZ, TH, VP(I)
  200 FORMAT (3E18.6)
C****STOP AREA
  500 STOP
      END
```

Appendix G. (CHRIS.FOR)- fortran program

Appendix H. Improved approaches for programming

As mentioned, the present programs need to be upgraded before full advantage can be taken of the physical understanding of the AU technique which has been reached. Particularly, the programs need to be optimized, so that all modes are automatically found, without the user manipulating code, as is presently done. The following is a partial list of ideas for improving the programming efforts:

Up load to mainframe

Apply numerical methods, such as Newton's method to the function F

Use method of uncoupled modes to improve solution search (see discussion below)

Key solution only to areas of interest

The method of uncoupled modes (ref. 127) involves solving the boundary value problem for mixed boundary conditions, which uncouples the P-wave and SV-wave. Then the dispersion curve for the resonating uncoupled modes can be obtained. The following equations describe these modes

$$(M\pi)^2 = (\omega h/V_m)^2 - (kh)^2$$

$$\frac{k}{\omega} = \sin(\theta)\frac{1}{V_m}$$

where M is an integer, V_m is the phase velocity for the mode of propagation (P-wave or S-wave), in the direction associated with the angle, θ, while h is half the plate thickness, and k is the wavenumber in the plate direction for the partial wave solution. In this scheme, the value of V_m is found by solving the plane wave Christoffel problem (appendix G). These two equations can then be used to obtain asymptotes for the coupled wave solution, the ω and k values are simply plotted. It should be noted that these are not simple hyperbolas for anisotropic materials, because the value of V_m varies with angle θ.

Basically, the coupled modes follow these curves, intersecting their crossings for certain conditions and then following other curves, drastically changing directions in some cases (see figs. 70 and 72). Perhaps advanced work geared toward understanding how modes are guided in between these curves and their crossings could greatly improve the ability to find points on the dispersion curve.

*U.S. GOVERNMENT PRINTING OFFICE: 1990-548-086/20305

NASA
National Aeronautics and Space Administration

Report Documentation Page

1. Report No.	2. Government Accession No.	3. Recipient's Catalog No.
NASA CR-185294		

4. Title and Subtitle	5. Report Date
A Physical Model for the Acousto-Ultrasonic Method	October 1990
	6. Performing Organization Code

7. Author(s)	8. Performing Organization Report No.
Michael T. Kiernan and John C. Duke, Jr.	None
	10. Work Unit No. 505-90-01

9. Performing Organization Name and Address	11. Contract or Grant No.
Virginia Polytechnic Institute and State University Department of Engineering Mechanics Blacksburg, Virginia 24061	NAG3-172
	13. Type of Report and Period Covered Contractor Report Final

12. Sponsoring Agency Name and Address	14. Sponsoring Agency Code
National Aeronautics and Space Administration Lewis Research Center Cleveland, Ohio 44135-3191	

15. Supplementary Notes

Project Manager, Alex Vary, Structures Division, NASA Lewis Research Center. Part of this material was presented in a dissertation submitted by Michael T. Kiernan in partial fulfillment of the requirements for the degree of Doctor of Philosophy to Virginia Polytechnic Institute and State University, Blacksburg, Virginia.

16. Abstract

A basic physical explanation, a model, and comments on NDE application of the acousto-ultrasonic (AU) method for composite materials are presented. The basis of this work is a set of experiments where a sending and a receiving piezoelectric transducer were both oriented normal to the surface, at different points, on aluminum plates, various composite plates, and a tapered aluminum plate. Chapter one introduces the purpose and basic idea of the dissertation, while supporting its need. Also, general comments on the AU method are offered. The second chapter offers a literature review of areas pertinent to the dissertation, such as composite materials, wave propagation, ultrasonics, and the AU method. Special emphasis is given to theory which is used later on and past experimental results that are important to the physical understanding of the AU method. The third chapter describes the experimental set-up, procedure, and the ensuing analysis. In the fourth chapter, the experimental results are presented in both a quantitative and qualitative manner. Chapter five furnishes a physical understanding of experimental results based on elasticity solutions, Lamb wave theory, and through-the-thickness-transverse-resonance (TTR). Computer results are presented for sake of comparison. The sixth chapter discusses modeling and applications of the AU method for composite materials and the seventh chapter states general conclusions. The unique offering of this work is the physical model of the AU method for composite materials, something which has been much needed and sorely lacking. This physical understanding is possible due to the extensive set of experimental measurements, also reported in this dissertation.

17. Key Words (Suggested by Author(s))	18. Distribution Statement
Nondestructive evaluation; Nondestructive testing; Ultrasonics; Acousto-Ultrasonics; Ultrasonic wave propagation; Lamb waves; Composites; Fiber reinforced composites; Composite plates; Composite materials	Unclassified – Unlimited Subject Category 38

19. Security Classif. (of this report)	20. Security Classif. (of this page)	21. No. of pages	22. Price*
Unclassified	Unclassified	270	A11

NASA FORM 1626 OCT 86

*For sale by the National Technical Information Service, Springfield, Virginia 22161